IAEA TECDOC SERIES

IAEA-TECDOC-1780

Development of a Reference Database for Ion Beam Analysis

Report of a Coordinated Research Project on Reference Database for Ion Beam Analysis

IAEA
International Atomic Energy Agency

DEVELOPMENT OF A REFERENCE DATABASE FOR ION BEAM ANALYSIS

The following States are Members of the International Atomic Energy Agency:

AFGHANISTAN
ALBANIA
ALGERIA
ANGOLA
ANTIGUA AND BARBUDA
ARGENTINA
ARMENIA
AUSTRALIA
AUSTRIA
AZERBAIJAN
BAHAMAS
BAHRAIN
BANGLADESH
BARBADOS
BELARUS
BELGIUM
BELIZE
BENIN
BOLIVIA, PLURINATIONAL STATE OF
BOSNIA AND HERZEGOVINA
BOTSWANA
BRAZIL
BRUNEI DARUSSALAM
BULGARIA
BURKINA FASO
BURUNDI
CAMBODIA
CAMEROON
CANADA
CENTRAL AFRICAN REPUBLIC
CHAD
CHILE
CHINA
COLOMBIA
CONGO
COSTA RICA
CÔTE D'IVOIRE
CROATIA
CUBA
CYPRUS
CZECH REPUBLIC
DEMOCRATIC REPUBLIC OF THE CONGO
DENMARK
DJIBOUTI
DOMINICA
DOMINICAN REPUBLIC
ECUADOR
EGYPT
EL SALVADOR
ERITREA
ESTONIA
ETHIOPIA
FIJI
FINLAND
FRANCE
GABON
GEORGIA
GERMANY
GHANA
GREECE
GUATEMALA
GUYANA
HAITI
HOLY SEE
HONDURAS
HUNGARY
ICELAND
INDIA
INDONESIA
IRAN, ISLAMIC REPUBLIC OF
IRAQ
IRELAND
ISRAEL
ITALY
JAMAICA
JAPAN
JORDAN
KAZAKHSTAN
KENYA
KOREA, REPUBLIC OF
KUWAIT
KYRGYZSTAN
LAO PEOPLE'S DEMOCRATIC REPUBLIC
LATVIA
LEBANON
LESOTHO
LIBERIA
LIBYA
LIECHTENSTEIN
LITHUANIA
LUXEMBOURG
MADAGASCAR
MALAWI
MALAYSIA
MALI
MALTA
MARSHALL ISLANDS
MAURITANIA
MAURITIUS
MEXICO
MONACO
MONGOLIA
MONTENEGRO
MOROCCO
MOZAMBIQUE
MYANMAR
NAMIBIA
NEPAL
NETHERLANDS
NEW ZEALAND
NICARAGUA
NIGER
NIGERIA
NORWAY
OMAN
PAKISTAN
PALAU
PANAMA
PAPUA NEW GUINEA
PARAGUAY
PERU
PHILIPPINES
POLAND
PORTUGAL
QATAR
REPUBLIC OF MOLDOVA
ROMANIA
RUSSIAN FEDERATION
RWANDA
SAN MARINO
SAUDI ARABIA
SENEGAL
SERBIA
SEYCHELLES
SIERRA LEONE
SINGAPORE
SLOVAKIA
SLOVENIA
SOUTH AFRICA
SPAIN
SRI LANKA
SUDAN
SWAZILAND
SWEDEN
SWITZERLAND
SYRIAN ARAB REPUBLIC
TAJIKISTAN
THAILAND
THE FORMER YUGOSLAV REPUBLIC OF MACEDONIA
TOGO
TRINIDAD AND TOBAGO
TUNISIA
TURKEY
UGANDA
UKRAINE
UNITED ARAB EMIRATES
UNITED KINGDOM OF GREAT BRITAIN AND NORTHERN IRELAND
UNITED REPUBLIC OF TANZANIA
UNITED STATES OF AMERICA
URUGUAY
UZBEKISTAN
VANUATU
VENEZUELA, BOLIVARIAN REPUBLIC OF
VIET NAM
YEMEN
ZAMBIA
ZIMBABWE

The Agency's Statute was approved on 23 October 1956 by the Conference on the Statute of the IAEA held at United Nations Headquarters, New York; it entered into force on 29 July 1957. The Headquarters of the Agency are situated in Vienna. Its principal objective is "to accelerate and enlarge the contribution of atomic energy to peace, health and prosperity throughout the world".

IAEA-TECDOC-1780

DEVELOPMENT OF A REFERENCE DATABASE FOR ION BEAM ANALYSIS

REPORT OF A COORDINATED RESEARCH PROJECT ON REFERENCE DATABASE FOR ION BEAM ANALYSIS

INTERNATIONAL ATOMIC ENERGY AGENCY
VIENNA, 2015

COPYRIGHT NOTICE

For further information on this publication, please contact:

Nuclear Data Section
International Atomic Energy Agency
Vienna International Centre
PO Box 100
1400 Vienna, Austria
Email: Official.Mail@iaea.org

Printed by the IAEA in Austria
December 2015

IAEA Library Cataloguing in Publication Data

Development of a reference database for ion beam analysis.
— Vienna : International Atomic Energy Agency, 2015.
p. ; 30 cm. — (IAEA-TECDOC series, ISSN 1011–4289 ; no. 1780)
ISBN 978–92–0–110515–8
Includes bibliographical references.

1. Ion bombardment. 2. Stopping power (Nuclear physics). 3. Solids — Effect of radiation on. 4. Cross sections (Nuclear physics). I. International Atomic Energy Agency. II. Series.

IAEAL 15-01005

FOREWORD

Ion beam analysis (IBA) includes modern analytical techniques involving the use of energetic ion beams to probe the composition of the surface layers of solids. Major areas of application include microelectronics, cultural heritage, forensics, biology and materials sciences. The underlying science for IBA is the physics of the interactions between the ions in the beam and the atoms in the solid. Emission products from the interaction of charged particles with matter are measured, and specialized simulation and data analysis software provide information on the material composition.

Although the basic physical processes are well understood, the reliability of data interpretation is limited by the knowledge of the physical data. The primary quantities required are the stopping powers describing the slowing of the ion in the material and the cross-sections of the interactions involved. The need for reliable data on stopping powers is adequately catered for by Stopping and Range of Ions in Matter (SRIM) computer code. The situation, however, is quite different for cross-sections for nuclear reactions and non-Rutherford elastic scattering. Although there is a considerable body of published data in nuclear physics literature, examination of the unevaluated experimental data has revealed numerous discrepancies beyond the error limits reported by the authors. The lack of reliable cross-sections has been recognized by the IBA community and has been discussed at several workshops and IAEA meetings, resulting in various recommendations including the organization of a coordinated research project (CRP) on a reference database for IBA.

The main objective of the CRP was to develop a reference database for IBA that contains reliable and usable data that will be made freely available to the user community. Starting from the existing collection of data in the IAEA Ion Beam Analysis Nuclear Data Library (IBANDL), the CRP focused exclusively on the relevant nuclear cross-sections (nuclear reactions and non-Rutherford elastic scattering). During the course of the CRP, however, it was soon realized that there was also a growing demand for compilation and evaluation of nuclear reactions with gamma rays in the exit channel, which are used in the particle induced gamma ray emission technique. The recommendations led to a second CRP on the development of a reference database for particle induced gamma ray emission spectroscopy. The output of which will be published in a forthcoming IAEA publication.

The IAEA wishes to thank all the participants of the CRP for their contributions to IBANDL and to this publication. The IAEA officers responsible for this publication were D. Abriola and P. Dimitriou of the Division of Physical and Chemical Sciences.

EDITORIAL NOTE

This publication has been prepared from the original material as submitted by the contributors and has not been edited by the editorial staff of the IAEA. The views expressed remain the responsibility of the contributors and do not necessarily represent the views of the IAEA or its Member States.

Neither the IAEA nor its Member States assume any responsibility for consequences which may arise from the use of this publication. This publication does not address questions of responsibility, legal or otherwise, for acts or omissions on the part of any person.

The use of particular designations of countries or territories does not imply any judgement by the publisher, the IAEA, as to the legal status of such countries or territories, of their authorities and institutions or of the delimitation of their boundaries.

The mention of names of specific companies or products (whether or not indicated as registered) does not imply any intention to infringe proprietary rights, nor should it be construed as an endorsement or recommendation on the part of the IAEA.

The IAEA has no responsibility for the persistence or accuracy of URLs for external or third party Internet web sites referred to in this publication and does not guarantee that any content on such web sites is, or will remain, accurate or appropriate.

CONTENTS

1. INTRODUCTION 1

2. ION BEAM ANALYSIS NUCLEAR DATA LIBRARY (IBANDL) 7

2.1. General. 7
2.2. R33 format 7
2.3. File name convention 7
2.4. Ion Beam Analysis Nuclear Data Library content 8
2.5. Internal structure of IBANDL 10
2.6. EXFOR – IBANDL link 11
2.7. Statistics of IBANDL usage 11
2.8. CD version of IBANDL 13

3. MEASUREMENTS 15

3.1. Introduction 16
3.2. (p,p) measurements 16
3.2.1. D(p,p)D 16
3.2.2. T(p,p)T 17
3.2.3. He(p,p)He 18
3.2.4. ^{7}Li(p,p)^{7}Li, ^{12}C(p,p)^{12}C and ^{19}F(p,p)^{19}F 19
3.2.5. Li(p,p)Li and N(p,p)N 21
3.2.6. N(p,p)N 23
3.2.7. Al(p,p)Al 24
3.2.8. ^{23}Na(p,p)^{23}Na 25
3.2.9. K(p,p)K 26
3.3. (p,α) measurements 28
3.3.1. ^{39}K(p,α)^{36}Ar 28
3.4. (d,d) measurements 28
3.4.1. C(d,d_0)C 28
3.5. (d,p) measurements 30
3.5.1. ^{10}B(d,$p_{0,1,2,3,4\text{-}5,6}$)^{11}B 30
3.5.2. ^{11}B(d,p_0)^{12}B 32
3.5.3. ^{12}C(d,$p_{0,1,2,3}$)^{13}C 33
3.5.4. ^{14}N(d,$p_{0,1+2}$)^{15}N 35
3.5.5. ^{27}Al(d,$p_{0+1,2+3,4,5+6}$)^{28}Al 36
3.5.6. ^{28}Si(d,$p_{0,1,2,3}$)^{29}Si 37
3.5.7. ^{32}S(d,$p_{0,1,2,3,4\text{-}6,7}$)^{33}S 40
3.6. (d,α) measurements 40
3.6.1. ^{10}B(d,α)^{8}Be 40
3.6.2. ^{11}B(d,$\alpha_{0,2}$) 42
3.6.3. ^{14}N(d,$\alpha_{0,1}$)^{12}C 44
3.6.4. ^{27}Al(d, $\alpha_{0,1,2,3,4}$)^{25}Mg 45
3.7. (α,α) measurements 46
3.7.1. N(α,α)N 46

4. ASSESSMENTS 51

4.1. Introduction 51
4.2. $D(p,p_0)D$ 51
4.3. $T(p,p_0)T$ 53
4.4. $^{6}Li(p,p_0)^{6}Li$ 55
4.5. $^{7}Li(p,p_0)^{7}Li$ 63
4.6. $^{9}Be(p,p_0)^{9}Be$ 68
4.7. $^{10}B(p,p_0)^{10}B$ 71
4.8. $^{11}B(p,p_0)^{11}B$ 75
4.9. $^{12}C(p,p_0)^{12}C$ 81
4.10. $^{19}F(p,p_0)^{19}F$ 82
4.11. $^{23}Na(p,p_0)^{23}Na$ 93
4.12. $^{9}Be(\alpha,\alpha_0)^{9}Be$ 95
4.13. $^{10}B(\alpha,\alpha_0)^{10}B$ 100
4.14. $^{11}B(\alpha,\alpha_0)^{11}B$ 102
4.15. $^{12}C(\alpha,\alpha_0)^{12}C$ 105
4.16. $^{14}N(\alpha,\alpha_0)^{14}N$ 110
4.17. $D(^{4}He,D)^{4}He$ and $T(^{4}He,T)^{4}He$ 114
4.18. $D(^{3}He,p)^{4}He$ and $^{3}He(d,p)^{4}He$ 116
4.19. $^{12}C(d,p)^{13}C$ 122
4.20. $^{12}C(^{3}He,p)^{14}N$ 129
4.21. $^{16}O(d,p)^{17}O$ and $^{16}O(d,\alpha)^{14}N$ 135

5. EVALUATION 151

5.1. General.. 151
5.2. Theory… 152
5.3. The evaluated cross sections 155
5.3.1. Alpha-proton 155
5.3.2. Carbon 156
5.3.3. Nitrogen 159
5.3.4. Oxygen 160
5.3.5. Fluorine 161
5.3.6. Neon 162
5.3.7. Sodium 162
5.3.8. Magnesium 163
5.3.9. Aluminum 164
5.3.10. Silicon 164
5.3.11. Phosphorus 165
5.3.12. Sulfur 166
5.3.13. Argon 166
5.3.14. Potassium 167
5.3.15. Calcium 168
5.3.16. Titanium 168
5.4. Conclusions 169

6. BENCHMARKING CROSS-SECTION DATA 175

6.1. Introduction 175
6.1.1. Methods 176
6.1.2. Estimation of Uncertainties in the Beam Energy 177
6.2. Lithium 178
6.2.1. $^{nat}Li(p,p)^{nat}Li$ 178
6.3. Boron 179
6.3.1. $^{10}B(p,p)^{10}B$ & $^{11}B(p,p)^{11}B$ 179
6.3.2. $^{10}B(d,p_2)^{11}B$ & $^{11}B(d,\alpha_0)^{9}Be$ 182
6.4. Carbon 183
6.4.1. $^{12}C(p,p)^{12}C$ 183
6.4.2. $^{12}C(p,p)^{12}C$ 184
6.5. Nitrogen 186
6.5.1. N(p,p)N 186
6.6. Fluorine 189
6.7. Sodium 190
6.8. Aluminium 192
6.8.1. $^{27}Al(p,p)^{27}Al$ 192
6.8.2. $^{27}Al(p,\gamma)^{28}Si$ 194
6.8.3. $^{27}Al(d,p')^{28}Al$ 195
6.9. Silicon 196
6.9.1. $^{nat}Si(p,p)^{nat}Si$ 196
6.10. Titanium: $^{nat}Ti(p,p)$ 197
6.11. Magnesium 199
6.12. Conclusions 201

7. CONCLUSIONS 207

LIST OF PARTICIPANTS 209

LIST OF CONTRIBUTORS TO DRAFTING AND REVIEW 211

1. INTRODUCTION

Ion Beam Analysis (IBA) [1.1] is an analytical technique which makes substantial use of nuclear data for applications in numerous laboratories. Major areas of application include studies of solid state structure in relation to physical properties such as high temperature superconductivity, composition and growth mechanisms of thin films, and surface and interface engineering. It is also widely used in different fields of research including art and archaeology, geology, environmental studies, nuclear waste storage, etc.

IBA methods rely on our understanding of the physics of the interaction between ions and atoms in solids. Emission products from the interaction of charged particles with matter are measured and with the aid of specialized simulation and data analysis software provide information on the composition and structure of the surface layers of a sample material. Two sorts of fundamental data are needed in order to convert the measured spectra into a depth profile of the investigated elements: the stopping power is used for evaluation of the depth scale and the differential cross section is utilized to obtain the concentration. Whilst work remains to be done on accurate stopping powers, the field is largely catered for by the considerable body of work by Ziegler and co-workers, embodied in the SRIM computer code [1.2]. However, the situation with the cross sections for nuclear reactions and non-Rutherford elastic scattering was for a long time a problem that seriously limited the use of IBA. The lack of reliable cross sections was recognized by the IBA community long ago [1.3] and was discussed in several workshops at biannual IBA conferences.

Many efforts to overcome this problem were made. At first, the data were simply collected from the nuclear physics literature. Although a significant number of published data already existed, the majority of these were available only as graphs. In addition, the energy interval and angles of these data were often found to be out of the range normally used in IBA making them unsuitable for IBA. This situation forced many research groups doing IBA analytical work to measure cross sections for their own use whenever an appropriate cross section could not be found. However, such an approach has a number of limitations. Firstly, none of these works included any evaluation of the measured data: they were simply collations from the published literature. In many cases, cross sections measured by different groups would vary not only in absolute value, but even in their dependencies on projectile energy and reaction angle. Secondly, with the increasing use of computer simulation and fitting codes, the need for digital representation of cross-section data became acute. Different IBA laboratories digitized their most used data in a variety of ways, with various levels of care and accuracy. Then, in the year 2000, the IAEA organized a technical meeting to discuss the long term needs for nuclear data development [1.4], in the context of which experts advised the IAEA Nuclear Data Section (NDS) to set up a consultants meeting to evaluate data needs for IBA. The meeting took place in 2003 [1.5] and the consultants recommended starting a Coordinated Research Project (CRP) with the aim to develop a reference database for IBA and the overall objective to create a nuclear cross-section database for IBA containing reliable and usable data made freely available to the user community. As a first step, the Ion Beam Analysis Data Library (IBANDL), containing most of the available experimental data relevant to IBA, was established at the IAEA Nuclear Data Section web server (www-nds.iaea.org/ibandl/) in the year 2004. Although IBANDL made available allthe previously collected data in a uniform style, it was still very incomplete and far from satisfying the needs of the community. To address the problem in full, the IAEA held the CRP entitled Development of a Reference Database for Ion Beam Analysis from 2005 to 2010. The overall objectiveof the CRP was to produce a nuclear reaction cross section database containing

recommended data of relevance to IBA, by (i) compiling all the information scattered in the literature and performing critical assessment of the compiled data, (ii) measuring cross-section data when there were no data available or where unresolved discrepancies existed, (iii) evaluating the experimental cross sections, (iv) incorporating all of the measured and evaluated data into the database, and (v) making them available to the IBA community through IBANDL. In all the activities listed from (i) to (v), the focus was on IBA relevant data, namely, differential cross section data rather than total ones and data for elements of natural abundance rather than for separated isotopes.

The work started with the identification of the most urgent problems in nuclear data for IBA. Various IBA techniques are important for analytical purposes. Among those, the CRP focussed on Elastic Backscattering Spectroscopy (EBS) which is the natural extension of Rutherford Backscattering Spectroscopy (RBS) as the beam energy is increased and Nuclear Reaction Analysis (NRA). The application of EBS at elevated energies has advantages such as the increase of both the analysing depth and the elastic scattering cross sections for light nuclei. NRA has often better selectivity than other IBA methods and is especially convenient in depth profiling of light elements. Considering these two techniques, it is safe to assume that priority should be given to differential cross sections for proton and ^{4}He non-Rutherford elastic scattering from nuclei with $A < 40$. The energy range for the data can be estimated as corresponding to accelerators capable of generating proton beams up to 4 MeV and alpha particle beams of up to 6 MeV like the widespread 2 MV Tandetron can do. Because the registered signal depends linearly on the atomic concentration and on the cross section it is obvious that the concentration can only be determined as well as the cross section is known and, consequently, the precise knowledge of the cross sections is required.

The main source of cross-section data is, of course, experiment. Many differential cross sections relevant to IBA were measured in the course of the CRP implementation. The elements for the measurements were selected on the basis of analyzing the previously acquired data, (also) taking into account the availability of targets. The great variety of facilities at the disposal of different CRP participating groups made it possible to cover a wide interval of angles and a vast energy range. In view of significant drawbacks in deriving cross sections from thick target yield, it was decided to use thin targets. Participating laboratories unified their approach with the view to avoid the usual pitfalls and all measurements were made with surface barrier detectors using electrostatic accelerators. The energy precision was better than 0.1%. The following factors were taken into account when estimating the experimental uncertainty budget: target thickness, current integration, the statistics of the counting rates of peak areas for registered particles, solid angle, and dead time. The uncertainties of the detector angular settings were minimized to the point of being negligible. When possible, the cross sections were normalized to the Rutherford backscattering cross section to eliminate the uncertainties due to dead time, solid angle and improper charge measurement. In some cases the normalization was made against previously published results of the measurements intended to determine precise absolute cross section. All measurements were made for angles in the backward hemisphere as is needed for IBA. The energy step was adjusted to reproduce the cross-section structure in all details. Measured cross sections were uploaded into IBANDL.

In addition to the cross-section measurements, benchmark experiments were performed within this CRP. A benchmark is an integral experiment which measures the spectrum from a well characterized uniform thick target. A simulation code is then used with one cross-section dataset as input (be it evaluated or measured) and the result is compared with the experimental

benchmark, thus demsontrating how good the input cross section is to predict thick target results. This is similar to nuclear reactor physics where microscopic neutron data are validated by comparing calculated integral reactor characteristics such as neutron flux with results of direct measurements. The idea of benchmarking is to verify the validity of the data for the purpose they are intended for through their use in a typical application. Such validation depends on the availability of tested simulation codes and valid stopping powers. Within this CRP, the SIMNRA [1.6] or Data Furnace [1.7] simulation codes and SRIM-2003 [1.2] stopping powers were adopted to simulate particle spectra that correspond to a given cross section. If the simulation of a bulk sample spectrum fits, then the cross section is valid. If the simulation does not fit, then all possible reasons for this disagreement should be expored, including the stopping power data, the energy loss straggling model used in the calculations, problems in treating multiple and plural scattering, inaccuracies in the interpolation of the cross-section values or insufficiently small step width for adequate representation of the excitation function fine structure. Thus, the benchmark failure may indicate more complex problems than inaccurate cross sections and additional efforts are needed to resolve the problem. However, it is clear that in such a case the cross section cannot be recommended for use in IBA.

Whilst it should, in principle, be possible to derive cross sections from thick target yield, it is evident that even using advanced inversion techniques, the derived cross section is inferior to those obtained from thin targets. Indeed, the thick target yield $Y(x)$ from the depth x is a convolution of the cross section $\sigma(x)$ corresponding to that depth with a response function $R(x, x')$ which includes all broadening effects:

$$Y(x) = k\int \sigma(x')R(x, x')dx' + N(x), \qquad (1.1)$$

where k is a normalisation constant and $N(x)$ stands for a background, including statistical effects which are inevitable in any measurement. Whatever method is applied to derive the cross-section function from thick target spectrum, it is a deconvolution in its essence. Different mathematical methods have been developed for resolving such ill-conditioned problems. For example, when Bayesian inference is applied, a presupposed cross-section function is successively modified with the aim to reproduce experimental data. The cross-section function at a previous step is regarded as a priori information for a succeeding step. The procedure is repeated many times until some extent of agreement is achieved. Thus, a new cross-section function is derived. Although direct calculations of $Y(x)$ are made at each step of the procedure, they remain a solution of the ill-conditioned inversion problem which means that the result of the inversion depends discontinuously upon the initial data. On the other hand, when a measured thick target spectrum is used for benchmarking, it is compared with calculations which produce a simulated spectrum by convoluting an input cross section with the response function. Thus, the cross-section measurement using thick target spectrum and benchmarking are mutually inverse operations which make use of the same initial data (thick target spectrum) in a different way and for different purposes.

The compilation of the cross-section data found in the literature and those obtained in new measurements in the database is only the first step towards establishing a reliable basis for computer assisted IBA. Subsequent analysis of the compiled data has revealed numerous discrepancies in the experimental cross-section values that extend beyond the quoted uncertainties. Quite often the differential cross sections are measured at one selected scattering angle and therefore they may be directly used only in the same geometry. For

historical reasons, charged-particle detectors are fixed in different laboratories at angles that vary from approximately 130° to 180°. However, the cross section may depend strongly on the scattering angle. Fortunately, the mechanisms of nuclear reactions that are relevant to IBA applications, are generally well known and appropriate theoretical models have been developed to reproduce experimental results using adjustable parameters. The process of analyzing experimentally measured cross-section data, combining them with nuclear model calculations and attempting to extract the true value of a cross section is referred to in the nuclear data community as 'evaluation' [1.8]. Generally, an evaluation should rely as far as possible on experimental data. But when these data are insufficient, incoherent and sparse then nuclear reaction models are used to calculate cross sections and one tries to take advantage of the internal coherence of the models to obtain the best estimate of the cross section. Although we cannot obtain sufficiently accurate cross-section data when the calculations are based simply on first principles, a particular cross section can, as a rule, be reliably represented by models by properly adjusting the model parameters. Thus, nuclear models are a powerful tool for the evaluation of data on the basis of a critical analysis of the available experimental results within the limits of theoretical constraints. Nuclear data evaluation is a routine procedure in preparing neutron data for different applications. It was also successfully extended to charged-particle cross sections (see [1.9] and references therein). Theevaluation of the cross sections using on appropriate nuclear models was found to be the only way to resolve the problem of nuclear data for IBA. In order to provide recommended cross sections, a standard procedure for theevaluation of the experimental cross sections was employed based on the critical analysis of the available experimental information and the parameterization of the data within a physical model. One main advantage of such an approach is that cross sections can be predicted over the entire range of scattering angles on the basis of the nuclear model.

The need for recommended cross sections arises from the fact that cross section data used in IBA are not only sparse and insufficient but often inconsistent. An established procedure for the elaboration of the recommended cross section does not exist. Actually, evaluated cross sections are usually regarded as recommended. However, to evaluate all data of interest for IBA was beyond the capability of this CRP. Only the most needed data have been evaluated, while for the rest of the data, recommendations based on assessments and on the results of benchmark experiments, were made.

In this context, what is meant by assessment is the careful and detailed analysis of the available information for a particular measured cross section, with the aim of ascertaining its reliability and accuracy. In particular, completeness of the data contained in IBANDL was verified through a thorough literature search. Mistakes found in the compiled cross sections were corrected and gaps in energy and angle intervals were identified. Inconsistencies found in the available experimental data were analyzed by studying the experimental details. Possible sources of unaccounted errors were looked for. Cases for which new measurements were needed were pointed out. The obtained results were used as a basis for elaboration of the recommended cross sections.

The different steps taken during the CRP – compilation and new measurements, evaluations, benchmarks and elaboration of recommended cross sections are discussed in the following sections. The order of these steps is not necessarily sequential, since in many cases several iterations and re-analyses appeared necessary.

REFERENCES

[1.1] NASTASI, M.A., WANG, Y. (Eds), Handbook of Modern Ion Beam Materials Analysis, 2nd edn, Materials Research Society, 2009.

[1.2] ZIEGLER, J.F., www.SRIM.org; Nucl. Instrum. Methods Phys. Res. B **219-220** (2004) 1027.

[1.3] VICKRIDGE, I.C., A workshop on cross-section databases for IBA, Nucl. Instrum. Methods Phys. Res. B **66** (1992) 303.

[1.4] MUIR, D.W., HERMAN, M., Summary Report of the Advisory Group Meeting on Long-Term Needs for Nuclear Data Development, IAEA Report INDC(NDS)-423, IAEA, Vienna, 2000.

[1.5] VICKRIDGE, I.C., SCHWERER, O., Report of IAEA Technical Meeting on Database of Evaluated Cross Sections for Ion Beam Analysis, IAEA Report INDC(NDS)-449, IAEA, Vienna, 2003.

[1.6] MAYER, M., SIMNRA User's Guide, Technical Report IPP9/113, Max-Planck-Institut für Plasmaphysik, Garching, Germany (1997); MAYER, M., SIMNRA, a simulation program for the analysis of NRA, RBS and ERDA, AIP Conference Proceedings **475** (1999) 541; MAYER, M., Ion beam analysis of rough thin films, Nucl. Instrum. Methods Phys. Res. B **194** (2002) 177.

[1.7] BARRADAS, N.P., JEYNES, C., WEBB, R.P., Appl. Phys. Lett. **71** (1997) 291; BARRADAS, N.P., MARRIOTT, P.K., JEYNES, C., WEBB, R.P., Nucl. Instrum. Methods Phys. Res. B **136-138** (1998) 1157; JEYNES, C., BARRADAS, N.P., MARRIOTT, P.K., BOUDREAULT, G., JENKIN, M., WENDLER, E., WEBB, R.P., J. Phys. D: Appl. Phys. **36** (2003) R97.

[1.8] HERMAN, M., TRKOV, A. (Eds), ENDF-6 Formats Manual, Brookhaven National Laboratory, Upton, NY, USA, June 2009.

[1.9] GURBICH, A.F., Evaluation and Calculation of Elastic Scattering Cross Sections for Ion Beam Analysis, in: R.C. Haight, M.B. Chadwick, T. Kawano, P. Talou (Eds), Nuclear Data for Science and Technology, AIP Conf. Proc. 769, Melville, New York, 2005, p. 1670.

2. ION BEAM ANALYSIS NUCLEAR DATA LIBRARY (IBANDL)

2.1. GENERAL

IBANDL (Ion Beam Analysis Nuclear Data Library) was established at the IAEA Nuclear Data Section (NDS) server (www-nds.iaea.org/ibandl/) following recommendations of the IAEA Technical Meeting entitled Database of Evaluated Cross Sections for Ion Beam Analysis held in 2003 [2.1]. Its official start was announced in April 2004 by publication in ION, the discussion journal for the Ion Beam Community (www.kfki.hu/~ionhp/ion/journal.htm). At that time, data relevant to IBA, i.e. cross sections for scattering and reactions for light-charged projectiles with an energy not exceeding ~10 MeV were not within the IAEA scope of activities. Consequently the IAEA experimental database EXFOR contained the time practically no relevant data. To begin with, the data from SigmaBase (still available at the time of writing this report at www.mfa.kfki.hu/sigmabase/- however this site no longer exists) and NRABASE [2.2] were combined within an advanced design by converting NRABASE files into R33 format [2.3] and by converting the cross sections presented in NRABASE in a centre of mass reference frame into a laboratory one. The contents of the SigmaBase and NRABASE were compared and overlapping files identified. After that, SigmaBase and NRABASE were merged. A new design was developed to present the information in the most convenient way for IBA practitioners. Finally, this combined data base IBANDL (Ion Beam Analysis Nuclear Data Library) was made available to the public on the NDS web site at http://www-nds.iaea.org/ibandl/.

2.2. R33 FORMAT

All the IBANDL data are stored in R33 format [2.3]. The ASCII R33 format was proposed in 1991 for the communication and compilation of IBA cross-section data and was several times updated since then. A current version of the format description is available at www-nds.iaea.org/ibandl/r33.html. A special R33 manager was developed by one of the CRP participants and some codes used in IBA for spectra processing were adapted to this format. The R33 format was developed *ab ovo* with no relation to EXFOR. There are several principal differences between EXFOR and IBANDL. In EXFOR, data are compiled as they are published whereas in IBANDL, angles and cross sections are always presented in the laboratory frame of reference. Excited nucleus states are referred by numbers in IBANDL and by excitation energies in EXFOR. In addition, the R33 files include some information not normally included in EXFOR (e.g., reaction Q values); but on the other hand, EXFOR contains a lot of additional information (such as on the measurement method and other textual information) which is not included in IBANDL.

2.3. FILE NAME CONVENTION

The IBANDL data file names are assigned according to the following convention previously developed for NRABASE. The first one or two letters denote a chemical symbol of the element in the conventional notation with exception for phosphorus denoted as "pr". They are followed by a figure that is the last digit of the isotope atomic number, the “n” letter being used for the natural composition. For example, for A=109 silver isotope this part of the name is “ag9”, for sulphur of the natural abundance it is “sn” etc. The next two places in the name are occupied by projectile and outgoing particle symbols. The following codes are used: p – proton, d – deuteron, h – 3He, a – 4He, i - 6Li, l – 7Li. The next is a figure that denotes a state of the residual nucleus. Zero is used for the ground state, “1” for the first excited state, etc. The rest of the name serves to make the file name unique and consists usually from one or two letters.

2.4. ION BEAM ANALYSIS NUCLEAR DATA LIBRARY CONTENT

Since its establishment in 2004, the number of data files in IBANDL has increased from 440 to more than 1500. This fast increase clearly results from the coordinated activity undertaken in the course of the CRP (see Fig. 2.1). The complete list of reactions and literature references for newly prepared data can be found in the updates section of IBANDL.

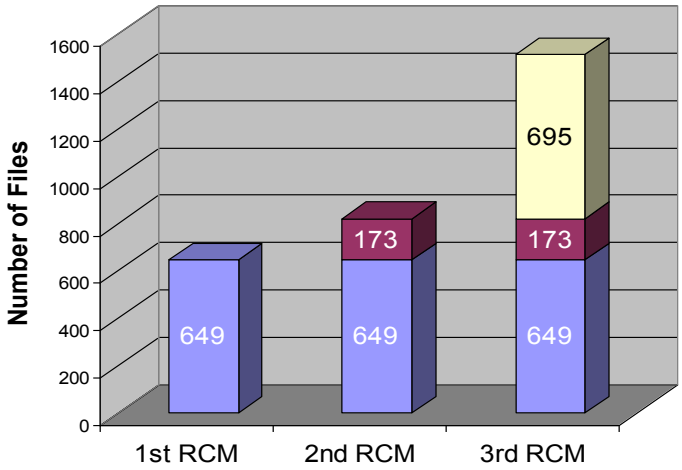

FIG. 2.1. Number of files in IBANDL.

IBANDL is being filled both with results of new measurements and with cross sections found in the literature. The data published only in graphical form are digitized using a precise technique which is standard at IAEA NDS. Their reliability was verified by comparison of the digitized data with tabulated ones for several cases when data were presented in the literature both in graphical and tabular forms. An example of such a comparison is presented in Fig. 2.2.

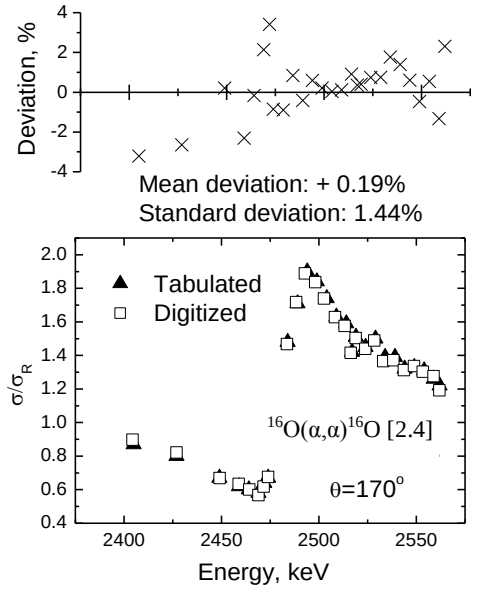

FIG. 2.2. The verification of the digitizing procedure by the comparison of the digitized and tabular data.

It was proven that the technique was accurate within 2─5 per cent depending on the quality of the published figure. Thus the additional uncertainty caused by digitizing has the same value as the usual experimental uncertainty.

Now, after the completion of the CRP (2010), IBANDL contains most (but still not all) of the available experimental nuclear cross sections relevant to IBA and much of the data on PIGE (Particle Induced Gamma-ray Emission: including d-PIGE – deuteron PIGE). All entries are supplied with a reference to the data source. The current content of IBANDL is shown in Figs. 2.3 – 2.5.

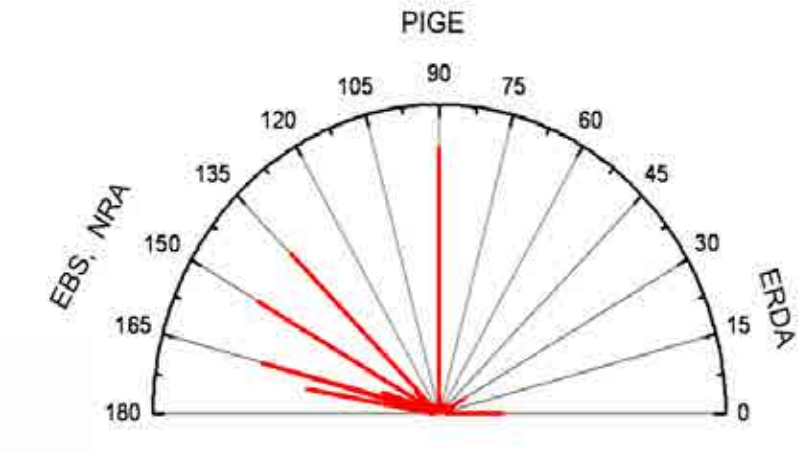

FIG. 2.3. The distribution of the IBANDL data on angle (year 2010).

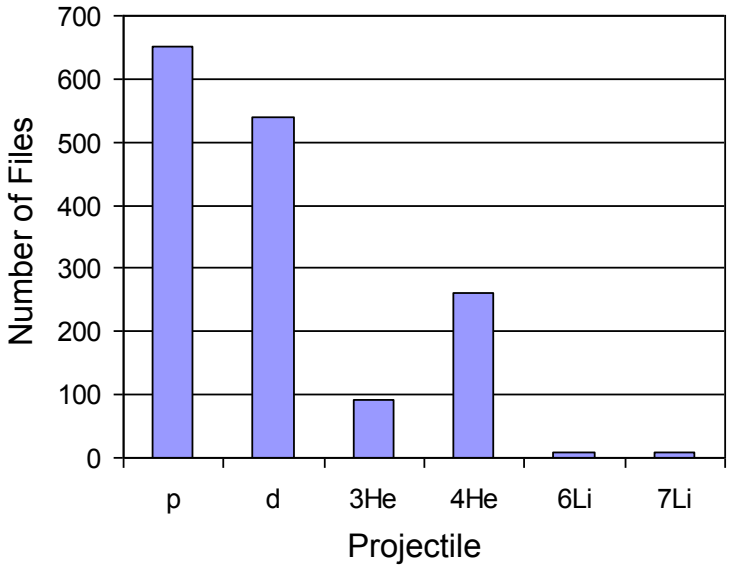

FIG. 2.4. Distribution of IBANDL files on projectile (year 2010).

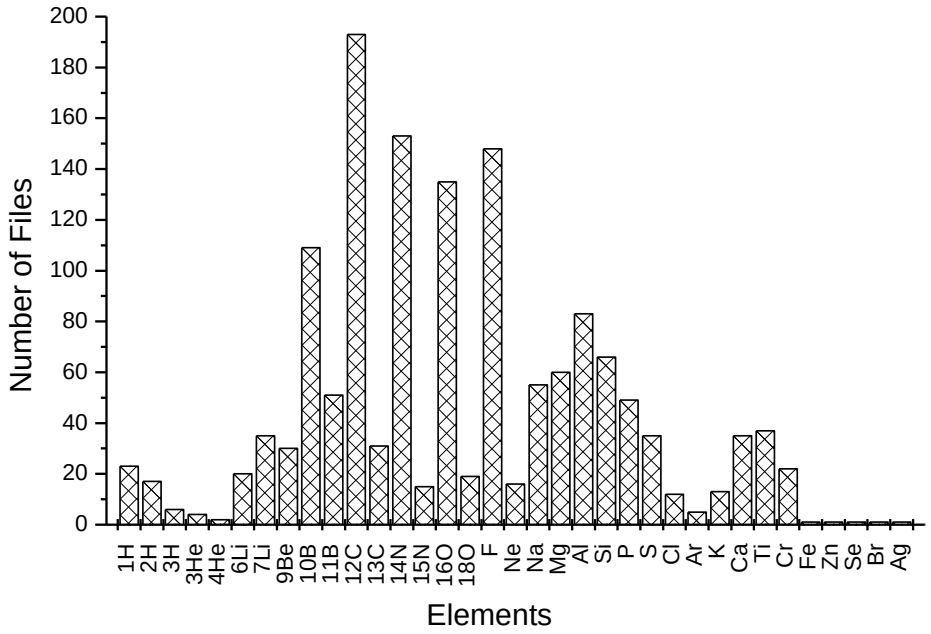

FIG. 2.5. Distribution of IBANDL files on element (year 2010).

2.5. INTERNAL STRUCTURE OF IBANDL

The IBANDL data library is located at the NDS server (www-nds.iaea.org). The folder "data2" contains all data files sorted into subfolders on the basis of the target plus projectile combination. The IBANDL functionality is provided by Perl scripts which are located in the cgi-bin folder at the server. Requested data are retrieved from the library dynamically. A table of data files is created by the "create_m.cgi" script which searches for requested data in the corresponding folder. A search pattern is constructed in "menu1.html" page by a JavaScript from the "target + projectile" part of the file name. It is passed to the "create_m.cgi" script upon pressing an "Ibandl" button in the left frame. Plots are drawn "on the fly" by the "draw2.pl" script. The script uses the gd.pm Perl module. The graphics design makes it possible to compare different data sets by superposition in the same plot using an overlay mode. The JavaScript image cropper user interface (jsCropperUI-1.2.1) allows the user to select a range of interest using an interface with the same features and styling as found in commercial image editing software.

To give members of the IBA community the possibility to share their data files, the IBANDL site provides a template which makes it easy to upload new data files, even for an inexperienced user. For computer security reasons, files uploaded by external users are stored in the "Upload" folder by means of the "fup.cgi" script. To make them available to the public they have to be checked, renamed according to the name convention and manually relocated to the appropriate subfolder.

Access to the SigmaCalc calculator which produces evaluated cross sections is arranged directly from IBANDL. The string that links IBANDL with SigmaCalc is incorporated in the table of the files retrieved according to the search pattern. This string contains a field in which the angle value for an outgoing particle has to be typed in and a button which is used to submit the information to SigmaCalc in order to start calculations. Calculation results are

integrated in the same table of files where experimental data are presented. Thus the evaluated theoretical cross sections can be directly compared with the experimental data available in IBANDL using the overlay graphics.

2.6. EXFOR – IBANDL LINK

Although the EXFOR database (www-nds.iaea.org/exfor/) has traditionally been the main source of experimental neutron cross section data, its completeness for charged-particle data has improved considerably in recent years and, in particular, many differential data for IBA have been included. The number of IBA relevant data in EXFOR is growing very fast thanks to the work of NDS staff. The EXFOR format is used for many more data types than needed in IBANDL, and was developed to be extremely versatile, which also makes it more complicated. The comparison between IBANDL and EXFOR revealed some differences in data files corresponding to the same publication (e.g., slight discrepancies in the numerical values, different number of angles in the data files, etc., see Fig. 4.74 in the assessment chapter).

In order to provide access to EXFOR files from the IBANDL page, an additional output R33 format for EXFOR database was implemented at NDS and a corresponding button to submit the request to EXFOR data base was added in the IBANDL menu. As a result the information available in EXFOR can be presented within the IBANDL page.

After analysis of the relationship between EXFOR and IBANDL, it was recognized that data should be ideally compiled in one authoritative database, but also that the convenient interface of IBANDL and the focus of the data have been significant contributing factors to its adoption by the IBA community. In view of this, it appears desirable to maintain IBANDL in its present form. Inclusion of new EXFOR data into IBANDL may be done by manual selection of data chosen. In the long term, automatic filtering is envisaged and, ultimately, the possibility to respond to IBANDL requests directly on the fly from EXFOR. One of the drawbacks of the present implementation of the EXFOR – IBANDL link is that the data are presented in separate pages and therefore the cross sections cannot be plotted in the same figure for comparison.

2.7. STATISTICS OF IBANDL USAGE

Since its development IBANDL has shown a steadily growing number of hits (Fig. 2.6). The most wanted cross sections were identified through analysis of the IBANDL statistics. A special Perl script was written and uploaded onto the IBANDL website in order to collect information on the number of cross section retrievals for individual nuclei and reactions. The results revealed the most popular 15 cross sections, which cover more than 90% of retrievals (see Fig. 2.7).

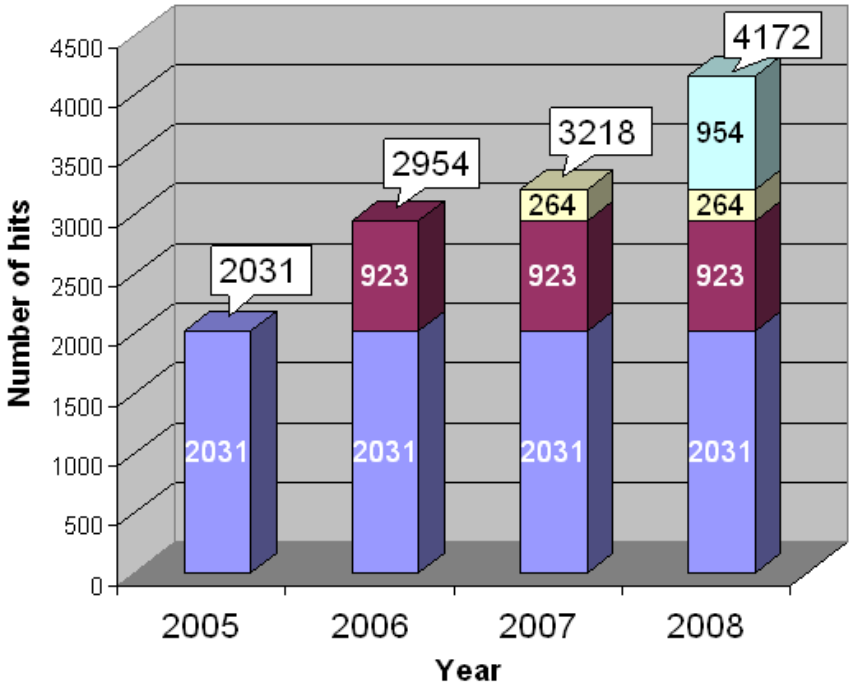

FIG. 2.6. Number of IBANDL hits per year.

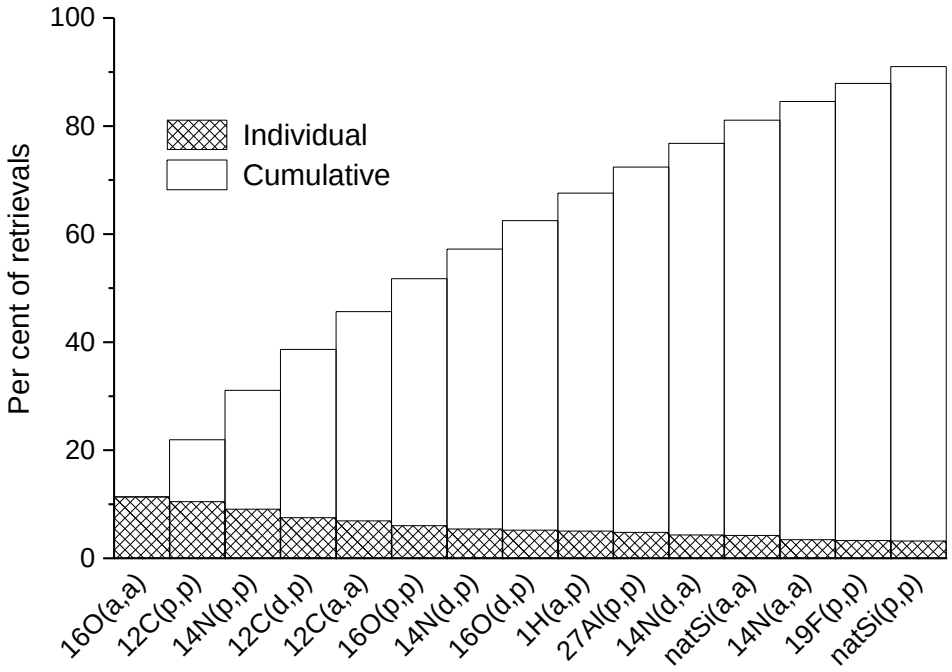

FIG. 2.7. IBANDL statistics showing the most popular retrievals.

2.8. CD VERSION OF IBANDL

A complete CD version of IBANDL was prepared in order to meet the needs of those users who have no access to the Internet or who, for some reason, prefer to have IBANDL at their personal disposal. It closely resembles the current web version both by content and data presentation including overplayed graphics and direct access to the SigmaCalc evaluated cross sections. The specialized retrieval system on the CD based on DWebPro (free license) gives users easy access to both files and plots. DWebPro is an application that makes it possible to deploy dynamic Web sites on CD. It supports server side languages including Perl used to write the scripts which provide the IBANDL functionality. The only feature that is absent in the CD version of IBANDL is the access to EXFOR.

REFERENCES

[2.1] VICKRIDGE, I.C., SCHWERER, O., Report of IAEA Technical Meeting on Database of Evaluated Cross Sections for Ion Beam Analysis, IAEA Report INDC(NDS)-449, IAEA, Vienna, 2003.

[2.2] GURBICH, A.F., IGNATYUK, A.V., Cross Section Data Base for Ion Beam Analysis, in: Reffo, G., Ventura, A., Grandy, C. (Eds), Nuclear Data for Science and Technology, AIP Conf. Proc. 59, SIF, Bologna, 1997, p. 1740.

[2.3] VICKRIDGE, I.C., Proposed ASCII Format for Communication of Reaction Cross Sections in the IBA Community, DSIR Physical Sciences Report 33, Lower Hutt, New Zealand, 1991.

[2.4] LEAVITT, J.A., MCINTYRE JR., L.C., ASHBAUGH, M.D., et al., Cross sections for 170.5° backscattering of ^{4}He from oxygen for ^{4}He energies between 1.8 and 5.0 MeV, Nucl. Instrum. Methods Phys. Res. B **44** (1990) 260.

3. MEASUREMENTS

Table 3.1 shows the reactions studied in this chapter, all energies, angles and cross sections are given in the laboratory system.

Table 3.1. LIST OF MEASUREMENTS

Nucleus/ Element	Reaction	Energy range (MeV)	Angles
D	D(p,p)D	1.8 – 3.2	155°, 165°
T	T(p,p)T	1.4 – 3.4	165°
He	He(p,p)He	1.6 – 3.6	165°
^{7}Li	^{7}Li(p,p)^{7}Li	3.0 – 7.2	150°
Li	Li(p,p)Li	1.0 – 2.2	140°, 160°
^{12}C	^{12}C(p,p)^{12}C	3.0 – 7.2	150°
N	N(p,p)N	0.7 – 2.4	110°,125°,140°,160°
N	N(p,p)N	2.4 – 5.0	118°,150°,165°
^{19}F	^{19}F(p,p)^{19}F	3.0 – 7.2	150°
^{23}Na	^{23}Na(p,p)^{23}Na	2.2 – 5.2	150°
Al	Al(p,p)Al	2.4 – 5.0	118°,150°,165°
K	K(p,p)K	3.0 – 5.0	140°,150°,160°,170°
^{39}K	^{39}K(p,α)^{36}Ar	3.0 – 5.0	140°,150°,160°,170°
C	C(d,d_0)C	0.9 – 2.0	145°,150°,155°,160°,165°,170°
^{10}B	^{10}B(d,$p_{0,1,2,3,4\text{-}5,6}$)^{11}B	0.9 – 2.0	135°,140°,145°,150°,160°,165°,170°
^{11}B	^{11}B(d,p_0)^{12}B	0.9 – 1.2	140°, 150°,160°,170°
^{12}C	^{12}C(d,p_0)^{13}C	0.9 – 2.0	135°,140°,145°,150°,155°,160°,165°,170°
^{12}C	^{12}C(d,$p_{1,2,3}$)^{13}C	0.9 – 2.0	145°,150°,155°,160°,165°,170°
^{14}N	^{14}N(d,p_0,p_{1+2})^{15}N	0.7 – 2.1	150°
^{27}Al	^{27}Al(d,$p_{0+1,2+3,4,5+6}$)^{28}Al	1.3 – 2.3	150°
^{28}Si	^{28}Si(d,$p_{0,1,2,3}$)^{29}Si	1.5 – 2.0	145°,150°,155°,160°,165°,170°
^{32}S	^{32}S(d,$p_{0,1,2,3,4\text{-}6,7}$)^{33}S	2.0 – 2.6	140°,150°,160°,170°
^{10}B	^{10}B(d,α)^{8}Be	0.9 – 2.0	135°,140°,145°,150°,155°,160°,165°,170°
^{11}B	^{11}B(d,$\alpha_{0,2}$)	0.9 – 1.2	140°,150°,160°,170°
^{14}N	^{14}N(d,$\alpha_{0,1}$)^{12}C	0.7 – 2.2	150°
^{27}Al	^{27}Al(d,$\alpha_{0,1,2,3,4}$)^{25}Mg	1.5 – 2.4	150°
N	N(α,α)N	2.5 – 4.0	118°,150°,165°

3.1. INTRODUCTION

One of the most important goals of the present CRP was to improve existing experimental cross section database by performing new cross section measurements. New measurements were especially important in cases where no data previously exist or where unresolved discrepancies between already measured data needed clarification. At the beginning it was important to unify the approach for measurements among CRP participants from different Laboratories in order to minimize potential mistakes during cross section measurements. When possible, thin targets were selected to avoid problems related with cross section extraction from thick target yields. Accelerator energy was calibrated using well known resonant reactions such as $^{27}Al(p,\gamma)^{28}Si$ at 992 keV, $^{19}F(p,\alpha\gamma)^{16}O$ at 872 keV and neutron threshold reactions such as $^{7}Li(p,n)^{7}Be$ at 1880.6 keV. All measurements were done using solid state particle detectors positioned at backward angles. For estimating the experimental uncertainty the following factors were considered: the counting statistics of peak areas, thickness of the target, current integration, detector solid angle and dead time. Uncertainties of the detector angular settings were made to be negligible. When possible, normalization to Rutherford cross sections was done in order to remove uncertainties due to dead time, improper charge collection and solid angle. The energy step for cross section measurements was adjusted according to complexity of excitation function to cover all details in it.

In this Chapter all measurements done in the framework of the present CRP are summarized and given in more detail. All energies, angles and cross sections are given in the laboratory system. Performed measurements are divided according to the projectile used to (p,p), (p,α), (d,d), (d,p), (d,α) and (α,α) measurements. Obtained excitation functions are given in the graphical form. Tabulated values are uploaded onto IBANDL (http://www-nds.iaea.org/ibandl/). Most of the data are published in Nucl. Instrum. Methods Phys. Res. B, and a complete set of references is given at the end of the Chapter. Table 3.1 shows the list of measurements.

3.2. (p,p) MEASUREMENTS

3.2.1. D(p,p)D

Data are published in [3.1]. The proton beam with energies from 1.8 to 3.2 MeV was provided by the NEC 9SDH-2 2 × 3 MV tandem accelerator at Fudan University. The scattered protons were detected at 155° and 165°, and the Au/Si surface barrier detector was put on a movable frame, which could be shifted along a circle orbit, so that the detection angle θ can be changed in the experiment. The accelerator energy scale was calibrated by using both nuclear resonance reactions of $^{27}Al(p,\gamma)^{28}Si$ at 992 keV and $^{19}F(p,\alpha\gamma)^{16}O$ at 872 keV. The beam energy has a precision better than ± 6 keV and an energy spread of around 1 keV. The beam was confined to a diameter of 0.6 mm and the beam currents were limited to 40 nA to protect the target from overheating which could cause the deuterium degassing from the sample.

A sample for cross-section measurements consists of three layers of metal films and was made by means of a DC magnetron sputtering method. A layer of ~5 nm tantalum film was sputtered on 7 μm Al substrate, which was taken as the ion dose reference. Ti film with ~50 nm thickness was deposited onto the Ta film subsequently as the deuterium storage layer, and then about 5 nm Ni was deposited onto the Ti film as the anti-oxidation layer. The areal density of Ta was measured with RBS using 4.0 MeV ^{4}He ions. The areal density of D in the target was measured with ERD analysis with 6 MeV ^{16}O ions. This was done by simultaneously employing two detectors, one was used to detect the deuterium particles

recoiled from the target at the angle of 30°, and the other was used to measure the ^{16}O particles scattered from the target at the angle of 165°.

The area of the deuterium peak could be measured accurately with the uncertainty less than 2%.The background signals under the tantalum peak were very low and negligible. The uncertainty of Rutherford cross section σ_{Ta} associated with uncertainties from the scattering angle (± 1°) and the proton beam energy (± 6 keV) is less than 1%. Thus, the total uncertainty associated with the measured cross section is less than 7.5%.

Excitation functions for D(p,p)D are presented in Fig. 3.1 for (a) 155° and (b) 165°.

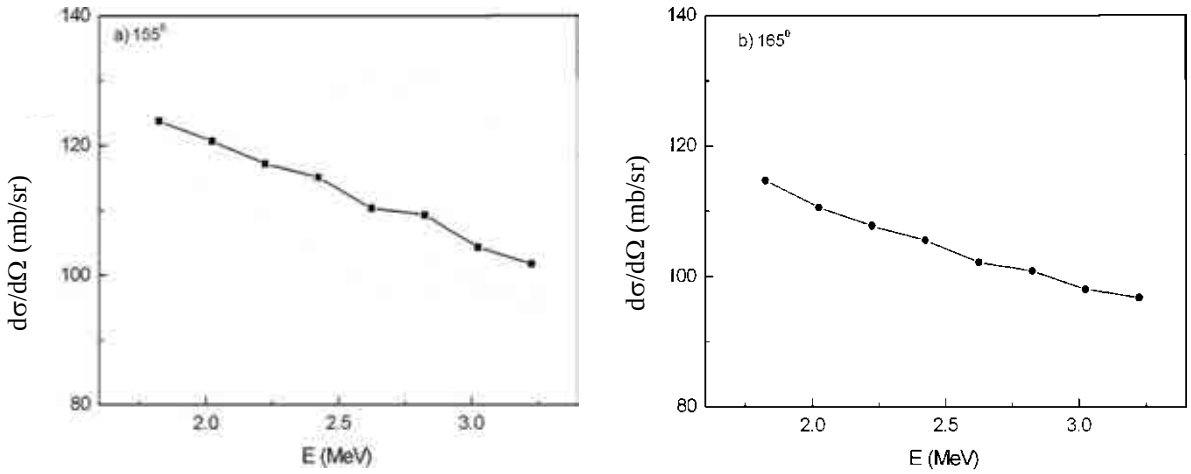

FIG. 3.1. Excitation functions for D(p,p)D at (a) 155° and (b) 165°.

3.2.2. T(p,p)T

Proton beam was provided by the NEC 9SDH-2 2 × 3 MV tandem accelerator at Fudan University. The accelerator energy was calibrated by $^{27}Al(p,\gamma)^{28}Si$ at 992 keV and $^{19}F(p,\alpha\gamma)^{16}O$ at 872 keV reactions. The energy precision was better than ± 6 keV and the energy spread was ~1 keV.

A particle detector was placed at 165° subtending solid angle of 1.87×10^{-3} sr, set by a defining slit of 3×4 mm. The detector angular resolution was 1°. The particle detector energy resolution was 12 keV for protons. The diameter of the incident beam was 0.6 mm and the current on the target was limited to 40 nA. The measurements were done in the energy range from 1.4 to 3.4 MeV in steps of 200 keV. The typical accumulated charge per measurement was 20 μC. The Pd/TiTx/Al sample prepared by a conventional hydrogenation method was used for the measurements. The target was very stable under a beam of 40 nA and average tritium losses were less than 0.2% during 20 μC runs.

The amount of tritium in the target was measured by ERD analysis using a beam of 6 MeV ^{16}O ions. This was done by simultaneously employing two detectors, one to detect the T and H recoils at a recoil angle of 30°, and the other to measure the backscattering yield of the incident ^{16}O particles at a scattering angle of 165°. The peak area of the backscattered signal of Pd was used as an ion dose calibration for the ERD measurement. An areal density of 1.62×10^{17} at/cm^2 was achieved using this tritiation process. The uncertainty associated with the determination of absolute tritium concentration was less than 5%. It was also found that virtually no tritium migrated into the Al foil.

The uncertainties in peak area determination resulted from statistical uncertainties and background subtraction uncertainties in the determination of T and Pd peak areas, are typically ± 2–3%, and in all cases less than ± 4%. The uncertainty of $\sigma_{Pd,Ruth}$ associated with uncertainties in the scattering angle (± 1°) and the proton beam energy (± 6 keV) is less than 0.96% in the measured energy region. The measuring uncertainty of the areal density $(N_t)_{Pd}$ is less than 4%. Thus, the total uncertainty associated with the measured cross section is less than 7.5%.

Data are published in [3.2]. T(p,p)T excitation function is presented in Fig. 3.2.

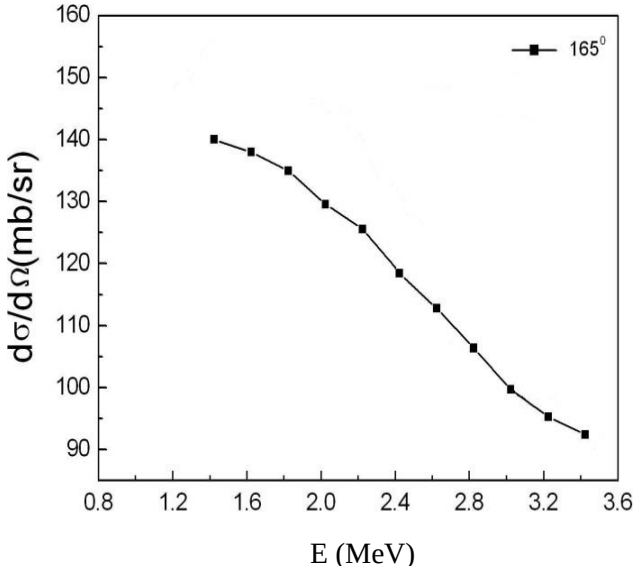

FIG. 3.2. T(p,p)T excitation function at 165°.

3.2.3. He(p,p)He

The incident proton beams used in these cross-section measurements, in the energy range from 1.6 to 3.6 MeV, were provided by the NEC 9SDH-2 2 × 3MV tandem accelerator at Fudan University. Accelerator energy calibration and experimental setup are the same as in 3.2.2.

Steps in the proton beam energy of 100 keV were taken in the energy range of 1.6─3.0 MeV and 200 keV between 3.0 and 3.6 MeV. The accumulated charge per energy interval was usually 20 μC. It was found that the Ag/TiHe$_x$ target was very stable under bombardment by 30 nanoampere proton beams and no helium losses were observed during 20 μC runs.

The target was produced by growing Ti film by DC magnetron sputtering in a mixture of working gases containing helium and argon. The helium content in the Ti film can be controlled by adjusting the ratio of the helium and argon fluxes i.e. Q_{He}/Q_{Ar} where Q_{He} and Q_{Ar} are the respective fluxes. The gases used to create the atmosphere for the DC discharge were a mixture of 99.99% purity argon and 99.99% purity helium. During the deposition, the sputtering current was about 0.32 A and the concurrent discharge voltage was about 240 V. A uniform Ti – He film with 5.3×10^{17} atoms/cm^2 Ti atoms and 1.87×10^{17} atoms/cm^2 He atoms was sputtered onto a 7 μm Al foil. Following this an Ag overlayer of 3.3×10^{16} atoms/cm^2 was deposited on the Ti film in order to prepare an Ag/TiHe$_x$/Al target for the cross-section measurements. The Ag film is important as it is used as an internal ion dose reference and also can prevent titanium from oxidizing. The reason why the thin Al foil was chosen for the

backing material was to obtain as low a background as possible in the spectral region of the helium signal.

The amount of helium in the target was measured by elastic recoil detection analysis (ERDA) using a beam of 6.8 MeV ^{12}C ions. This was done by simultaneously employing two detectors, one to detect the He recoils at a recoil angle of 30° and the other to measure the backscattered yield of the incident ^{12}C particles at a scattering angle of 165°. The peak area of the backscattered signal of Ag was also used as an ion dose calibration for the ERD measurement. Thus, the uncertainty associated with the determination of absolute helium concentration was less than 5%.

The uncertainties in A_{Ag} and A_{He} result from statistical uncertainties and background subtraction uncertainties in the determination of Ag and He peak areas and they are typically ± 2–3%. The uncertainty in $\sigma_{Ag,Ruth}$ associated with uncertainties in the scattering angle (± 1°) and the proton beam energy (± 6 keV) is less than ± 1% in the measured energy region. The uncertainty from measuring the areal density $(Nt)_{Ag}$ is less than 4%. Thus, the total uncertainty associated with the measured cross section is about 7.3%. Results are published in [3.3].

The excitation function for He(p,p)He at the angle of 165° is presented in Fig. 3.3.

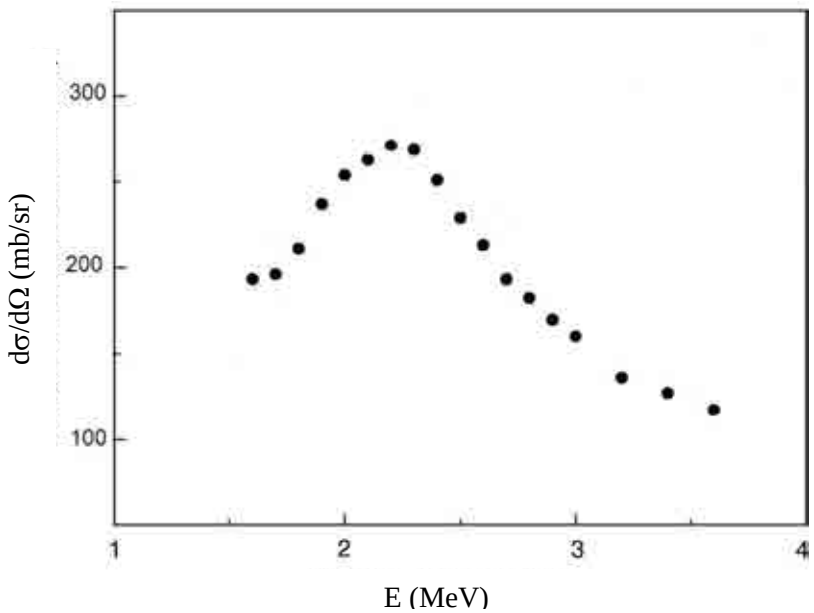

FIG. 3.3. He(p,p)He excitation function at 165°.

3.2.4. $^{7}Li(p,p)^{7}Li$, $^{12}C(p,p)^{12}C$ and $^{19}F(p,p)^{19}F$

A proton beam in the energy range of 3.0─7.2 MeV at 25 keV steps was delivered by the HVEE 5 MV Tandetron accelerator at the CMAM in Madrid. The accelerator energy was calibrated by using resonances in alpha article scattering from ^{12}C, ^{14}N, ^{16}O and ^{28}Si and in the (p,γ) reaction on ^{27}Al. The precision in the energy was better than 0.1%. Beam was collimated to dimensions of 3.0 × 3.0 mm^2. Particle detector of 50 mm^2 area, 500 μm thickness and 12 keV FWHM energy resolution, was placed at 150° (lab). Detector solid angle was defined by a 2.1 × 8.2 mm^2 rectangular collimator placed at 82.8 mm from the target. Solid angle was 2.51 msr and the spread in the scattering angle due to geometrical effects was 1.5°.

A thin LiF target (~50 μg/cm^2) was evaporated on a self-supporting C target (~30 μg/cm^2) and further coated with a thin Au layer (~20 μg/cm^2) for beam dose normalization. Proton beam was kept in the range 10–40 nA, depending on beam energy, in order to keep the count rate low enough to have negligible pile-up effects (< 0.5%). Each measurement was allowed to continue until obtaining at least 2000 counts in all the elastic scattering peaks.

The contributions to the uncertainty in the cross-section value are: ± 1.0% (from Rutherford cross section on Au), ± 1.0% (area density ratio, except ± 0.5% for carbon). If these 'non-statistical' contributions are added linearly to the statistical uncertainties from the peak areas, the following conservative estimates are obtained for the uncertainties of the absolute cross sections, at all the beam energies: ± 5.0% for proton elastic scattering on ^{19}F, ± 3.5% for proton on ^{12}C and ± 4.0% for proton on ^{7}Li. Data are published in [3.4].

^{7}Li(p,p)^{7}Li, ^{12}C(p,p)^{12}C and ^{19}F(p,p)^{19}F excitation function are plotted in Figs 3.4–3.6, respectively.

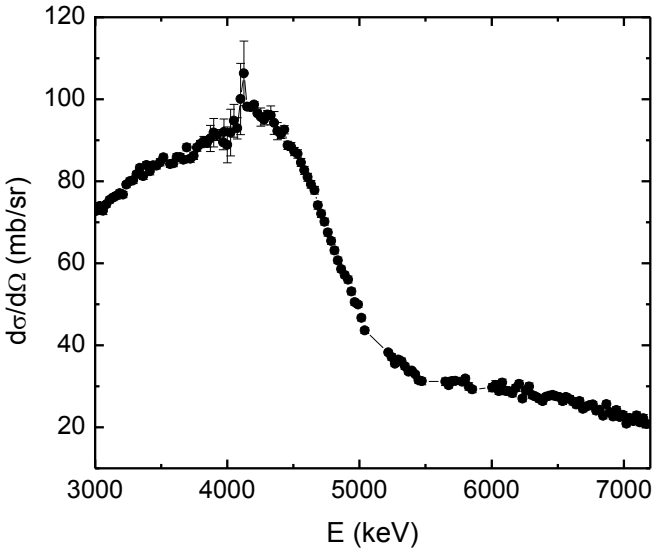

FIG. 3.4. Excitation function for ^{7}Li(p,p)^{7}Li at 150°.

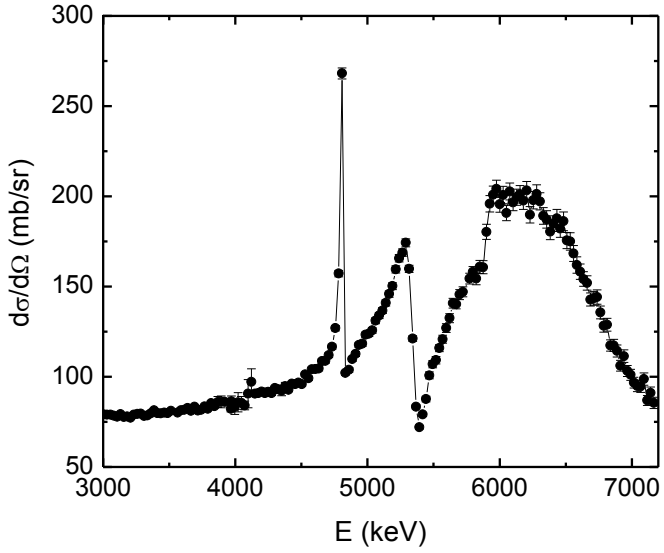

FIG. 3.5. Excitation function for $^{12}C(p,p)^{12}C$ at 150°.

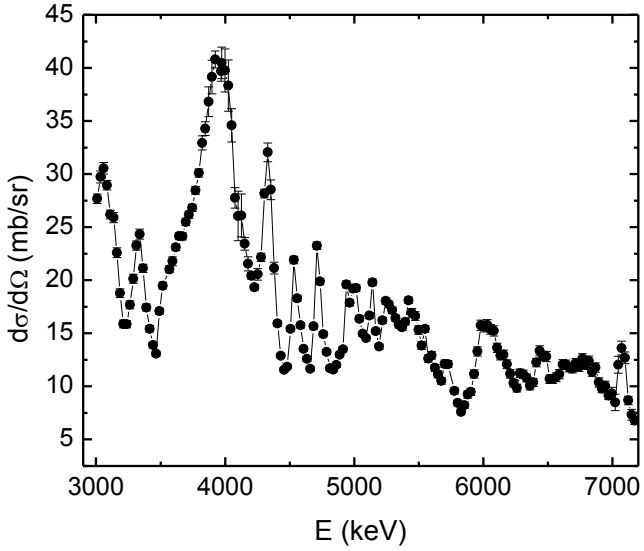

FIG. 3.6. Excitation function for $^{19}F(p,p)^{19}F$ at 150°.

3.2.5. Li(p,p)Li and N(p,p)N

Experiments were performed with the 2.5 MV Van de Graaff accelerator at the Nuclear and Technological Institute in Lisbon. Appropriate samples for cross-section measurements were prepared or acquired and their composition determined by He-RBS. Detection of scattered particles was done by a fixed Si surface barrier detector located at 160º scattering angle in Cornell geometry and a movable detector positioned at chosen scattering angles, in IBM geometry. Proton beam energy was calibrated using the resonances of the reaction $^{19}F(p,\alpha\gamma)^{16}O$ at 872, 935, 1375 and 1691 keV. $N(p,p_0)N$ cross sections were measured in the

700─2400 keV energy range and for scattering angles of 160º, 140º, 125º and 110º using the standard thin film technique.

Three samples were used for the determination of the Li(p,p_0)Li cross section. The first sample was a LiF single crystal implanted with 300 keV Ar^{2+} ions to a fluence of 6.06×10^{15} at/cm2. The implantation allowed the formation of a damaged surface layer, thus minimizing channelling effects during the measurements. To further avoid any channelling effects, the measurements were performed with the sample tilted to 5º and in permanent rotation along the azimuthal axis. A thin Au layer was deposited over the LiF to act as an internal standard during the Li cross section measurements. The exact areal density of Au was determined from an ^{4}He-RBS spectrum acquired at 2 MeV and 160º. The areal density of Au was thus determined to be $(62.0 \pm 1.2)\times10^{15}$ at/cm^2. The second sample was a pellet of LiCl anhydrous powder of 99% purity. No internal standard was used in this sample. The product $\Omega \times Q$ was adjusted using the Cl surface yield. The third and final sample was a Y-cut congruent LiNbO3 single crystal grown by the Czochralski method. No internal standard was used in this sample. The product $\Omega \times Q$ was adjusted using the Nb surface yield. To avoid any channelling effects, the measurements were performed with the sample tilted to 5º and in permanent rotation along the azimuthal axis.

To measure the Li cross sections using a thick sample (LiF single crystal implanted with 300 keV Ar^{2+} over which a $(62.0 \pm 1.2)\times10^{15}$ at/cm^2 Au layer was deposited) 15 proton spectra were acquired at 140º and 160º scattering angles for different beam energies in the 999–2200 keV interval. Given the light element composition of the sample, the Li signal is clearly visible in all spectra. However, the F presence is an additional complication due to the fact that its elastic scattering cross section is non- Rutherford and (p,p′γ) reactions are present. The Li cross section was calculated by transforming the yield at each channel into a cross-section value. However, given the fact the Li signal is superimposed on the F signal, we first determined an apparent F cross section using the same point by point procedure, but restricting the analysis to the surface channels of the F signal. Li(p,p)Li excitation functions are shown in Figs 3.7a and 3.7b.

The sample used was an AlN thin film reactive sputter deposited over a vitreous carbon substrate. A thin Au layer was deposited over the AlN to act as an internal standard. Experiments were made in the energy range 700 keV ≤ Ep ≤ 2400 keV, with minimum steps of 5 keV near the resonances, and 30 keV in other regions of the cross section. N(p,p)N excitation functions are given in Fig. 3.8a-d.

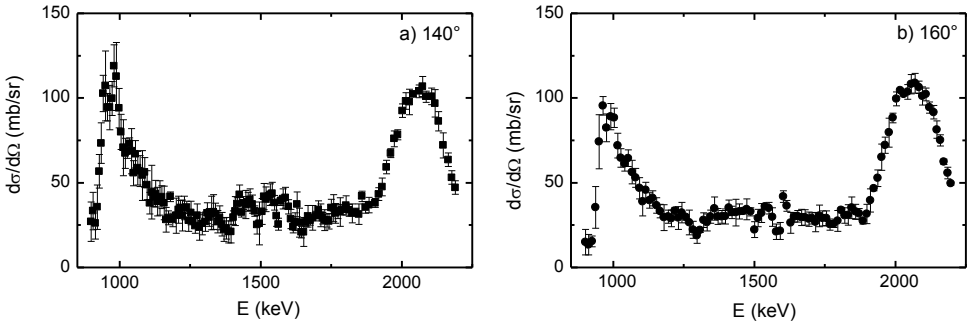

FIG. 3.7. Excitation functions for Li(p,p)Li at (a) 140º and (b) 160º.

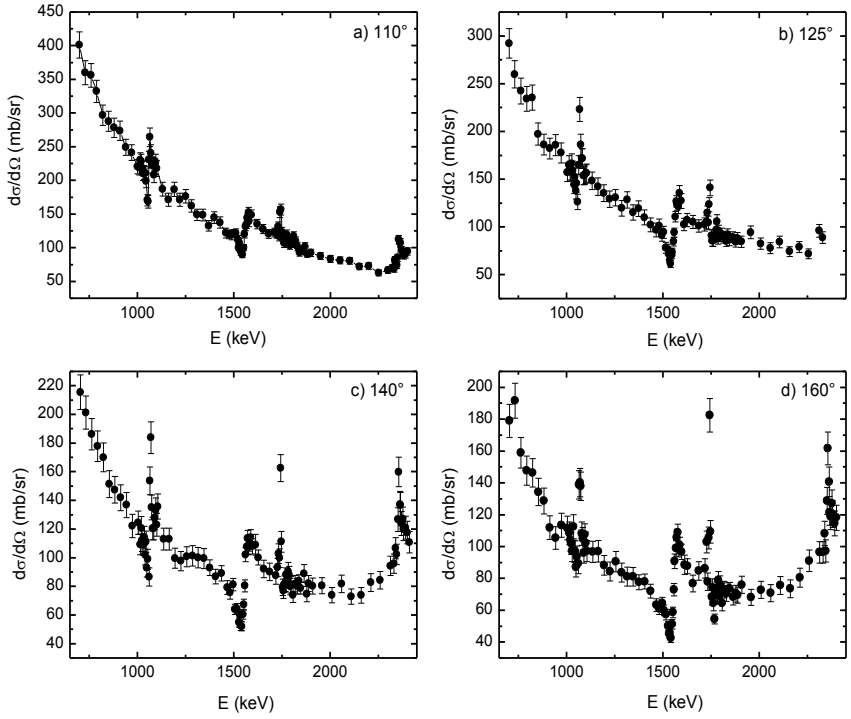

FIG. 3.8. Excitation functions for N(p,p)N at (a) 110º, (b) 125º,(c) 140º and (d) 160º.

3.2.6. N(p,p)N

Measurements were performed using proton beams from the 6.0 MV Tandem Van de Graaff accelerator at the Ruđer Bošković Institute in Zagreb. The excitation function of the $^{14}N(p,p)^{14}N$ was measured between 2.4 and 5.0 MeV with a minimum step of 10 keV where the cross section varied rapidly and 25 keV elsewhere.

Thin AlN film (~150 nm) reactive sputter deposited on vitreous graphite substrate was used. 6 nm thick Au layer was evaporated onto the target for normalization purposes. The accelerated proton beam was directed normally to the target surface with Au layer facing the beam. Measurements were performed with the proton beam in the energy interval from 2.4 to 5 MeV and with energy steps between 10 and 25 keV. Three particle detectors positioned at 118°, 150° and 165°, with a 2.5 msr solid angle each, were used to detect backscattered protons from the target. The energy resolution of the detectors was ~12 keV. Beam current was kept below 10 nA during the experiment.

The uncertainty in the measured cross sections is calculated to be less than 6% for energies below 4.6 MeV and between 6% and 8% for energies from 4.6 and 5 MeV for 165° and 150°. For 118° the relative uncertainty was below 5% for all energies. The following factors were taken into consideration for estimating the uncertainty: the counting statistics of the peak areas and the systematic error in determining the N_{Au}/N_N ratio. Uncertainties due to dead time, solid angle and improper charge measurement are eliminated with the normalization to

backscattering protons from gold. Errors of the detector angular settings were estimated to be negligible.

Data are published in [3.5]. Excitation functions are displayed in Fig. 3.9.

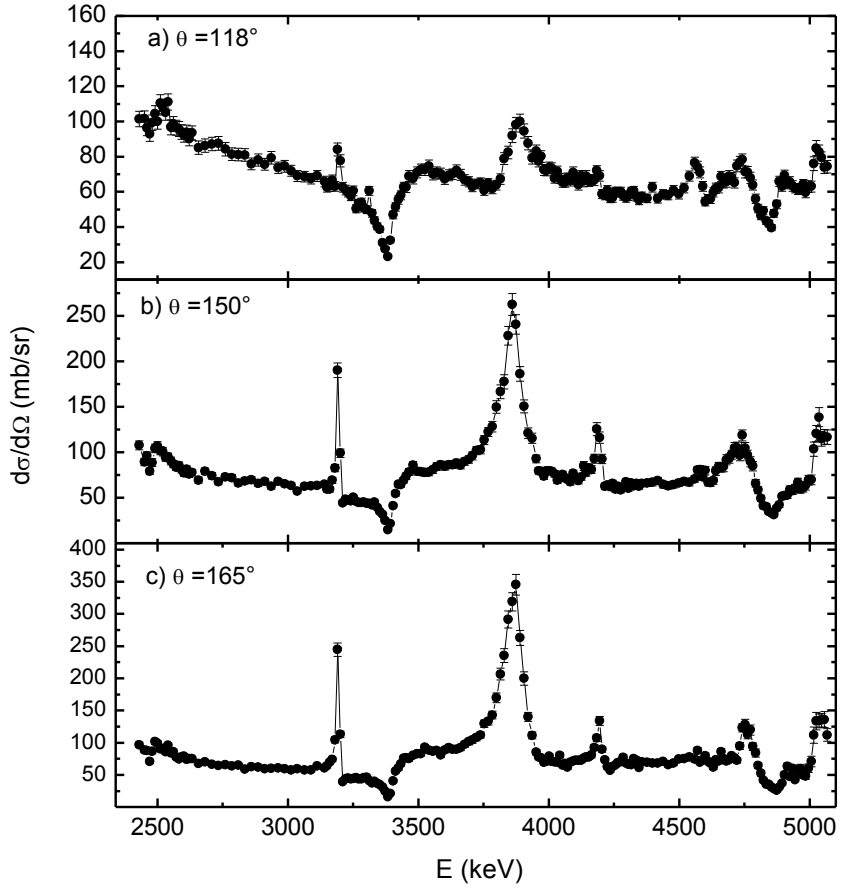

FIG. 3.9. Excitation functions for N(p,p)N at (a) 118°, (b) 150° and (c) 165°.

3.2.7. Al(p,p)Al

Measurements were done with protons from the 6.0 MV Tandem Van de Graaff accelerator at the Ruđer Bošković Institute in Zagreb. Energy calibration of analyzing 90° magnet was made using narrow resonances ^{27}Al(p, γ)^{28}Si at 991.88 keV and neutron threshold reaction ^{7}Li(p, n)^{7}Be at 1880.6 keV. Secondary calibration points ^{16}O(p, p)^{16}O at 3.47 MeV and ^{12}C(p, p)^{12}C at 4.808 MeV were used to check calibration. Energy spread of the beam was 0.1%.

Same experimental setup and target as for 3.2.6. Results are published in [3.6].

Excitation functions for elastic scattering of protons from Al at three different scattering angles are displayed in Fig. 3.10a-c.

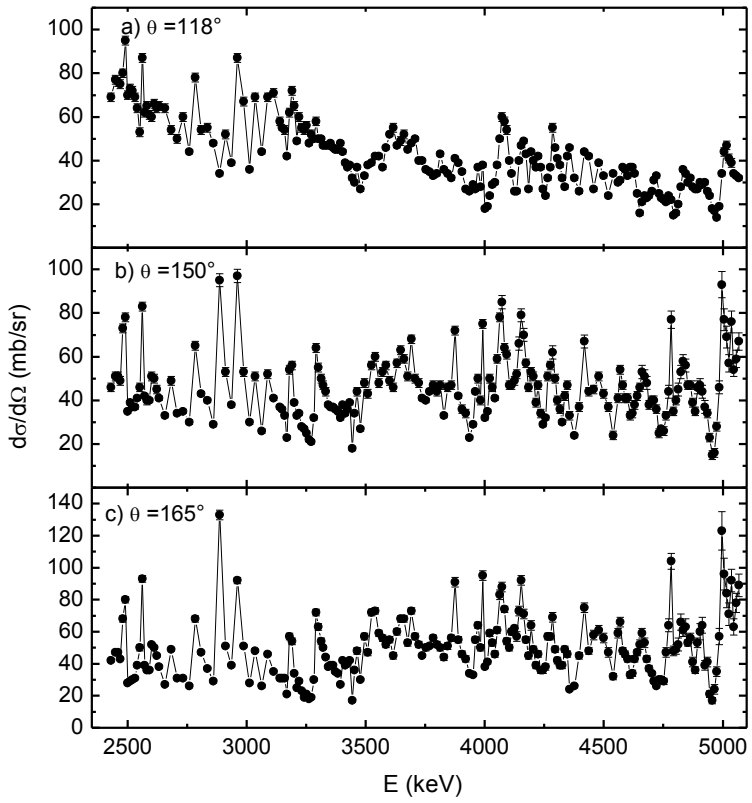

FIG. 3.10. Excitation functions for Al(p,p)Al at (a) 118°, (b) 150° and (c) 165°.

3.2.8. ^{23}Na(p,p)^{23}Na

The experimental work was conducted at the 5 MV Tandetron accelerator at the CMAM (Centro de Microanálisis de Materiales) in Madrid. The measurements were performed at proton energies from 2.2 to 5.2 MeV with steps ranging from 20 to 5 keV. The accelerator energy was calibrated using resonances in alpha particle elastic scattering from ^{12}C, ^{14}N, ^{16}O and ^{28}Si and in the (p,γ) reaction on ^{27}Al; after the calibration the bombarding energy is known to be better than ± 0.1%. The proton beam on the target was 2 × 2 mm^2.

The target was 63 μg/cm^2 NaBr evaporated on a thin C foil (about 30 μg/cm^2). The proton energy loss in the NaBr film was about 5 to 3 keV. Spectra were measured by a particle detector (50 mm^2 area, 500 μm thickness and 12 keV FWHM energy resolution) placed at 150° (Ω = 2.51 ± 0.04 msr). The spread in the scattering angle due to beam size on the target and detector finite aperture was 1.2°. The current was collected in a Faraday cup biased at +190 V, strongly inhibiting the escape of secondary electrons. During the measurements proton beam currents were in the range 20─40 nA, in order to keep the count rate low enough to reduce pile-up effects. Dead time corrections were negligible (< 0.5%).

The uncertainty contributions in the absolute differential cross section are: peak area < 1.0%, Rutherford cross section for Br 1.1%, stoichiometric ratio 2.0%, Na areal density 5.0%, particle detector solid angle 1.6% and number of incident protons 1.0%. By adding the systematic contributions to the statistical uncertainties from the peak areas, an overall uncertainty better than ± 6.0% can be estimated.

The excitation function is displayed in Fig. 3.11. Results are published in [3.7].

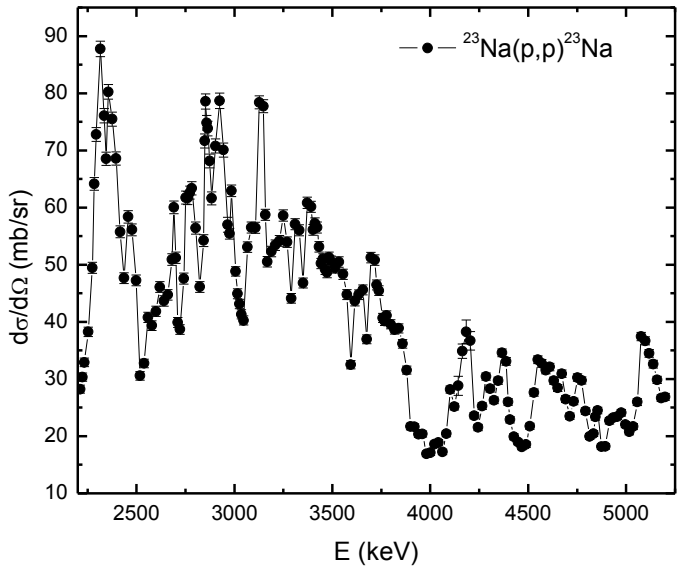

FIG. 3.11. Excitation function for ^{23}Na(p,p)^{23}Na at 150°.

3.2.9. K(p,p)K

The experiments were performed using the proton beam of the 5.5 MV TN11 Tandem Accelerator of N.C.S.R. "Demokritos", Athens, Greece. The protons, accelerated to $E_{p,lab}$=3000─5000 keV, in steps of 25 keV, were led to a cylindrical scattering chamber of large dimensions (R ~ 30 cm). The final ion energy of the proton beam (energy offset ~2.5 keV) was determined by nuclear magnetic resonance measurements (NMR) with an estimated ripple of ~0.1─0.15%, as verified by the 991.89 keV resonance of the ^{27}Al(p,γ) reaction at the beginning and at the end of the experiment, using a HPGe detector.

The detection system consisted of four Si surface barrier detectors (Thickness: 300 to 1000 μm; set at 10° intervals) along with the corresponding electronics. The spectra from all four detectors were simultaneously recorded and the procedure was repeated for every $E_{p,lab}$. The beam spot size was 2.5 × 2.5 mm^2, while the current on target did not exceed 10 nA during all measurements. Two liquid nitrogen traps were set on both ends of the goniometer in order to reduce the carbon build-up on the target, while the vacuum was kept constant, as low as ~5×10^{-7} Torr. After every ~10 steps in beam energy, the beam spot position was slightly changed in order to avoid excessive carbon buildup and/or target deterioration (mainly through heating). The target was placed at a distance of ~9 cm from the detectors. Orthogonal slits (~4.5×10 mm^2) were placed in front of the detectors in order to reduce the angular uncertainty (~ ± 1.5^o), while allowing an adequate effective solid angle to be subtended by the detectors.

The target was created as follows: A highly pure (> 99.9%) minimal quantity of dehydrated potassium fluoride (K: 19.6 ± 1.3 μg/cm^2) was evaporated on a thin (~10 μg/cm^2) carbon (accelerator, stripping) foil. The target was subsequently covered by an ultrathin evaporated Au layer (10.7 ± 0.7 μg/cm^2), which served a multitude of purposes: (a) By forming a protective layer and thus, by diminishing the absorption of humidity through air contact, it improved the mechanical stability of the target, (b) it acted as a stabilizer against fluorine evaporation and corresponding target deterioration during the irradiation and (c) it was used

for normalization purposes, as will be analyzed in the following section. The Au/K ratio was determined by XRF measurements, which also revealed a non-negligible bromine contamination. The XRF analysis was performed using the in─house developed portable milli-beam XRF spectrometer of N.C.S.R. "Demokritos". The results were verified by p-RBS, analyzing multiple spectra taken at $E_{p,lab}$=1─1.5 MeV (with an energy step of 0.1 MeV), using the same experimental setup for absolute measurements. For the corresponding analysis, SIMNRA (v. 6.04) was used along with EBS data from IBANDL, following Sigmacalc calculations, in order to determine the fluorine concentration as well as the oxygen contamination and the carbon foil thickness. XRF and p-RBS results for the critical Au/K ratio agreed with an accuracy better than 5%.

The statistical uncertainties did not exceed 1─2%, while the overall experimental uncertainty was dominated by the error in the determination of the Nt_{Au}/Nt_K ratio, which was of the order of ~10%, including mainly the uncertainties in the Q (accumulated charge) × Ω (solid angle covered by the detector) product, and in the adopted stopping power values [3.8] as well as the deviations between the obtained XRF and p-RBS results. The total experimental uncertainty was calculated following standard error propagation formulas.

Data are presented in [3.9]. Excitation functions for K(p,p)K for (a) 140°, (b) 150°, (c) 160° and (d) 170° are shown in Fig 3.12.

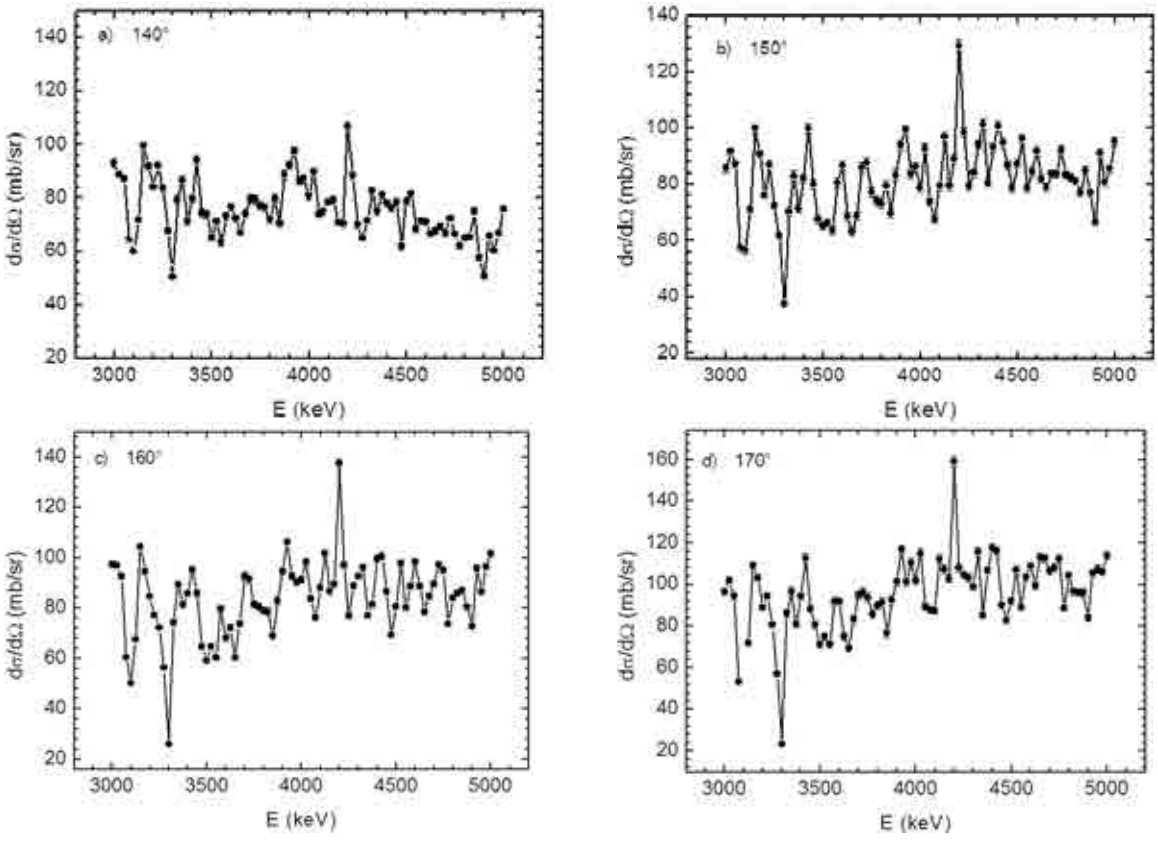

FIG. 3.12. Excitation functions for K(p,p)K at (a) 140°, (b) 150°, (c) 160° and (d) 170°.

3.3. (p,α) MEASUREMENTS

3.3.1. ^{39}K(p,α)^{36}Ar

The details of the measurement are given in 3.2.9. Data are published in [3.9]. Excitation functions for ^{39}K(p,α)^{36}Ar are shown on Fig. 3.13.

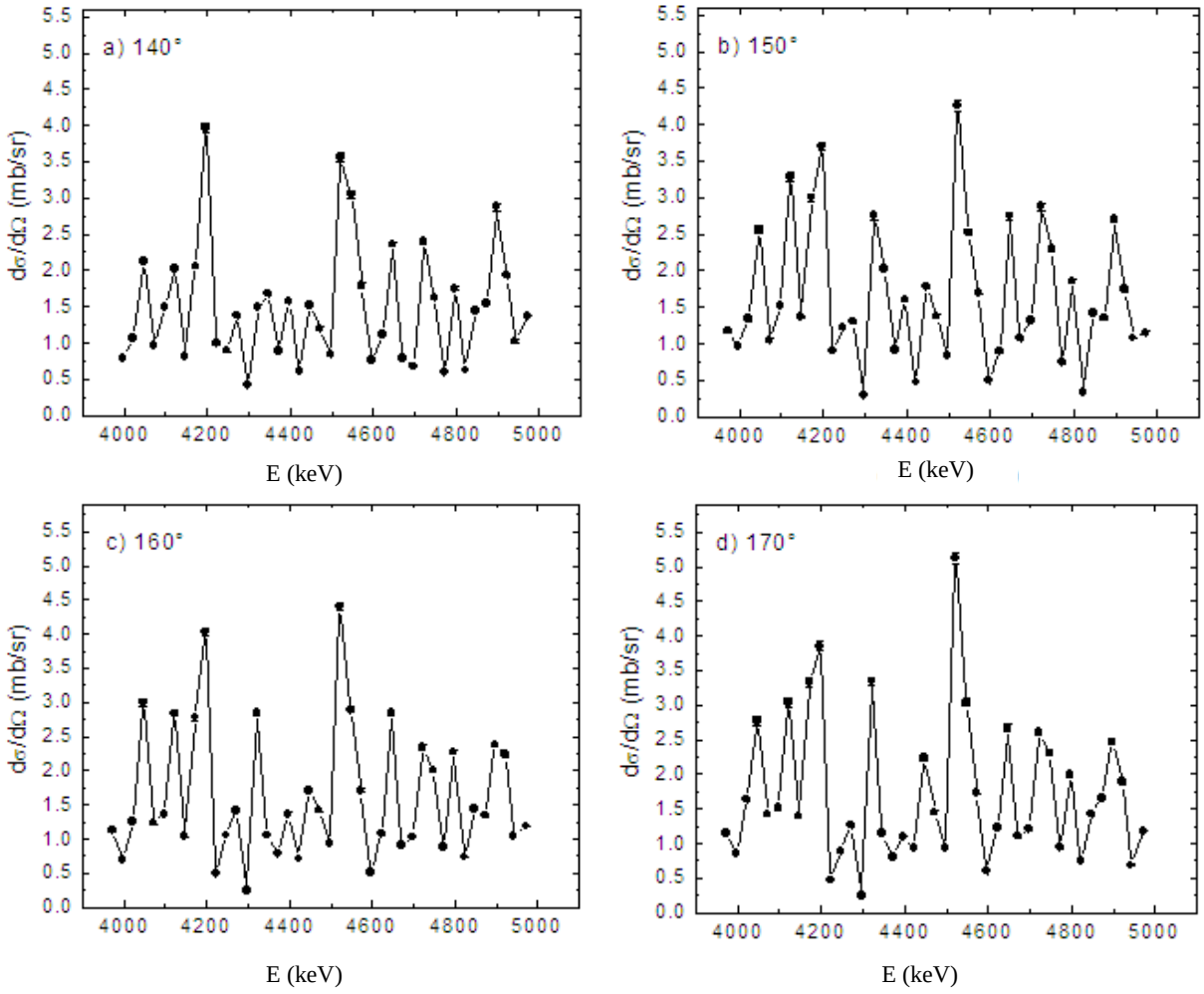

FIG. 3.13. Excitation functions for ^{39}K(p,α)^{36}Ar at (a) 140°, (b) 150°, (c) 160° and (d) 170°.

3.4. (d,d) MEASUREMENTS

3.4.1. C(d,d$_0$)C

The experiments were performed at NCSR "Demokritos", Athens, Greece, using 5.5 MV TN11 Tandem Accelerator. The deuterons were accelerated to E_d = 900–2000 keV in steps of 25 keV. The final ion energy was determined via nuclear magnetic resonance (NMR) probe with an estimated ripple of 1.6 keV, and a maximum offset of less than 0.5 keV, as verified using the 872.11 keV resonance of the ^{19}F(p, αγ) reaction at the beginning and at the end of the experiment. The maximum uncertainty in the determination of E_d was thus estimated to be ~2 keV.

The detection system consisted of five (300–2000 μm) Si surface barrier detectors (4 rotating, set at 10° intervals, and 1 fixed at 160° as monitor) along with the corresponding electronics.

The spectra from all detectors were simultaneously recorded and the procedure was repeated by turning the four Si detectors by 5° for every $E_{d,lab}$. The beam spot size was approximately 3 × 3 mm^2. The current on target did not exceed 100 nA. The high-purity (99.9%) thin carbon foils (98.9% ^{12}C–1.1% ^{13}C) were used as targets with the nominal thickness of ~1×10^{18} at/cm^2. Targets were placed at a distance of ~27 cm from the detectors. No absorber foils or slits were placed in front of the detectors. The solid angle subtended by the detectors as well as their energy resolution were determined via a triple 81.1 *n*Ci, $^{241}Am/^{239}Pu/^{244}Cm$ α-source, along with RBS data from high purity thick gold and aluminum foils. The subtended solid angle ranged between 3.6×10^{-4} and 1.5×10^{-3} sr. The total estimated uncertainty in the Q×Ω product did not exceed 4.3% in the least favorable case. A long Faraday cup was implemented for the charge collection, while voltage suppression (300 V) was employed in front of the collimator set and on target. Two liquid nitrogen traps were set on both ends of the goniometer in order to reduce the carbon build-up on the targets, while the vacuum was kept constant ~5×10^{-7} Torr.

The main source of uncertainty in the absolute cross-section measurements was the variation in the target thickness due to carbon buildup and/or sputtering. The statistical uncertainty was kept below 2% in all cases. Thus, the overall uncertainty in the absolute differential cross-section measurements varied between 6 and 22% depending mainly on the target.

Excitation functions for C(d, d_0)C between 145° and 170° are given in Figs. 3.14a─f. Data are published in [3.10].

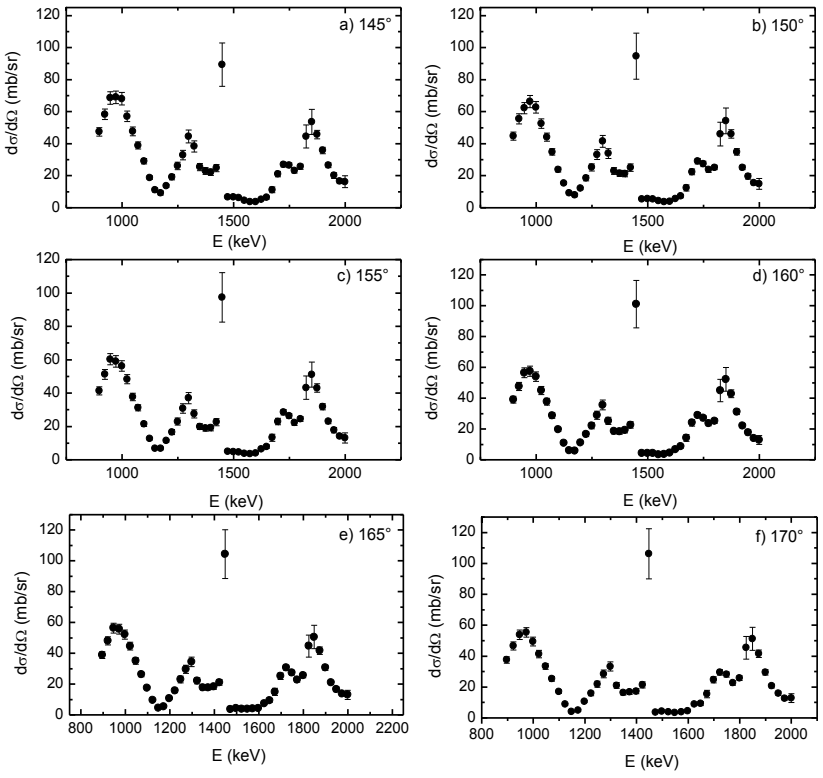

FIG. 3.14. (a─f) Excitation functions for C(d,d_0)C between 145° and 170.°

3.5. (d,p) MEASUREMENTS

3.5.1. $^{10}B(d,p_{0,1,2,3,4\text{-}5,6})^{11}B$

The experiments were performed using 5.5 MV TN11 Tandem Accelerator of N.C.S.R. "Demokritos", Athens, Greece. The deuterons were accelerated to E_d = 900–2000 keV in steps of 25 keV. Accelerator energy calibration and experimental setup are the same as described in 3.4.1.

A highly pure (> 98%), isotopically enriched (94.6%) ^{10}B target deposited on thick Ta backing was used for the experiments. The thickness of the target was 10.2 μg/cm^2 (± 10%). The target was placed at a distance of 8.5 cm from the detectors. 50 μm Kapton was used to stop elastically scattered deuterons. Additionally, orthogonal slits (4.5×10 mm^2) were placed in front of the detectors in order to reduce the angular uncertainty (± 1.5°).

The total estimated uncertainty for the product Q×Ω varied between 4─7%. The statistical uncertainty also varied between 1─5%, with the (d,p_3) being the least favorable case in the energy interval studied (mainly due to the high-induced background at low energies). The uncertainties vary between 11% and 16% and include uncertainties in the product Q × Ω, in the target thickness, in peak integration and statistical uncertainties. The main source of uncertainty is related to the determination of the ^{10}B content in the isotopically enriched target. Results are published in [3.11]. Excitation functions are displayed in Fig. 3.15a─g.

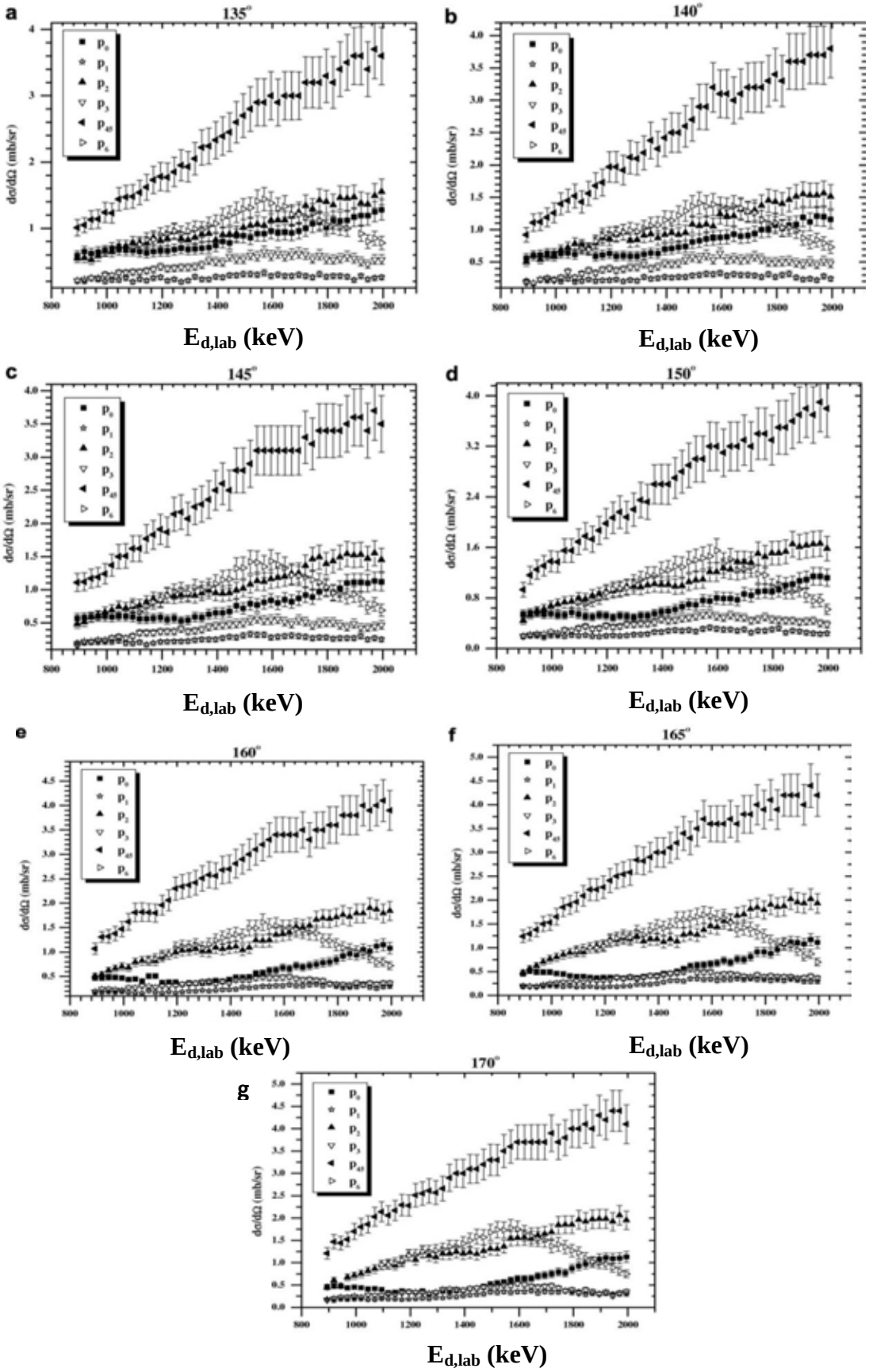

FIG. 3.15. (a─g) Excitation functions for $^{10}B(d,p_{0,1,2,3,4\text{-}5,6})^{11}B$ reactions at 135°, 140°, 145°, 150°, 160°, 165° and 170°, respectively.

3.5.2. $^{11}B(d,p_0)^{12}B$

The experiments were performed using the deuteron beam of the 5.5 MV TN11 Tandem Accelerator of N.C.S.R. "Demokritos", Athens, Greece. The deuterons, accelerated to E_d = 900─1200 keV, in steps of 25 keV, were led to a scattering chamber of large dimensions. For the charge measurements (charge collection and subsequent current integration) the whole chamber was electrically isolated from the beam line and voltage suppression of ~300 V was applied on both the collimator set and on the target. Experimental setup is described in all details in 3.4.1.

The total estimated uncertainty for the product Q × Ω varied between ~3─5%. A highly pure (> 99.9%) thin natural boron target deposited on a 6 μm Al substrate (Goodfellows microfoil) was used for the experiments. The specified thickness of the target was 0.1 μm at 20% accuracy. The actual target thickness was found to be much lower (157×10^{15} at/cm^2 ± 10%) using d-RBS, ^{12}C RBS and $^{10}B(d,p_2)$. The combined uncertainties varying between ~11─14%, the main source of uncertainty was undoubtedly the determination of the target thickness. Results are published in [3.12].

Excitation functions are shown in Fig. 3.16a─d.

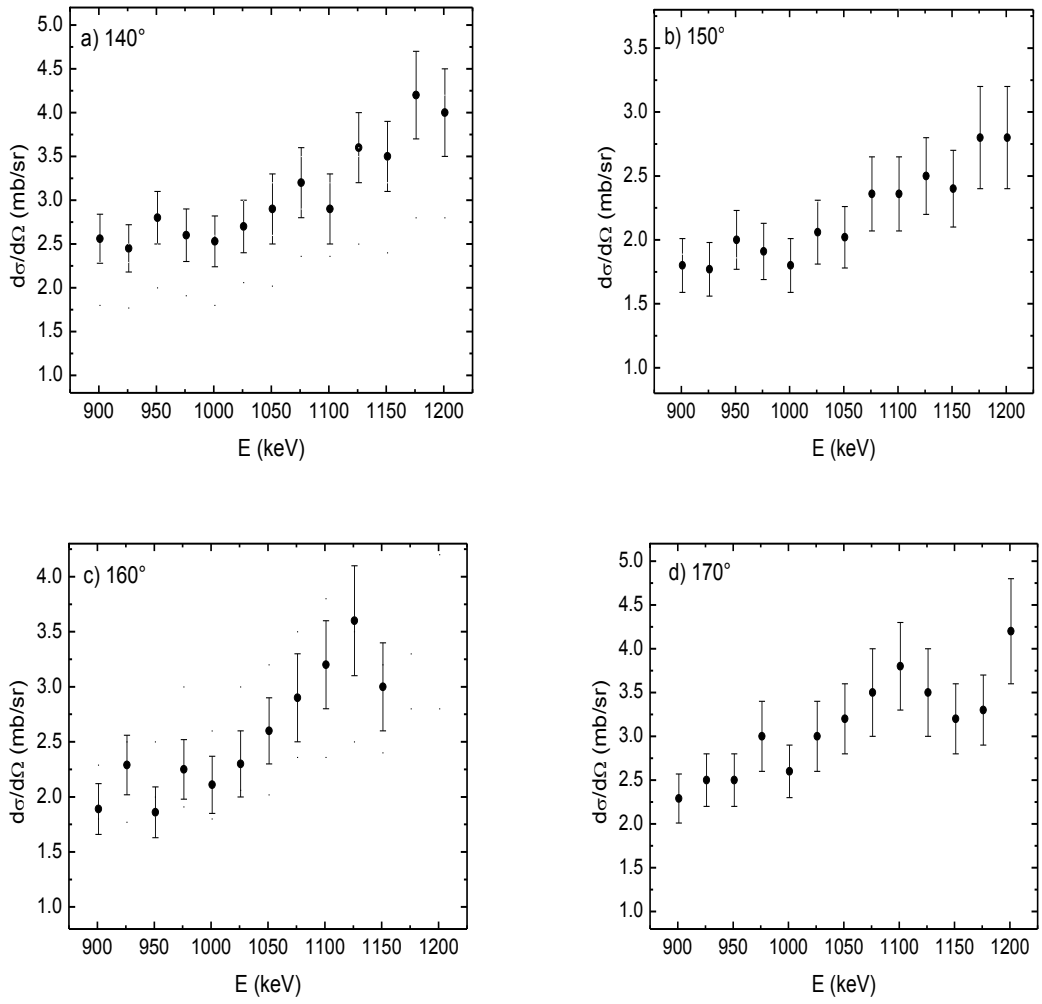

FIG. 3.16. Excitation functions for the $^{11}B(d,p_0)$ reaction at (a) 140°, (b) 150°, (c) 160° and (d) 170°.

3.5.3. $^{12}C(d,p_{0,1,2,3})^{13}C$

Details of the experimental setup are explained in 3.4.1. Several high-purity (99.9%) self-supported natural carbon foils (98.9% ^{12}C–1.1% ^{13}C) were used as targets, having a nominal thickness of ~1×10^{18} at/cm^2. The targets were placed at a distance of ~27 cm from the detectors. No absorber foils or slits were placed in front of the detectors. The main source of uncertainty in the absolute differential cross section measurements is the variation of the target thickness, primarily due to carbon build-up. This uncertainty is critical in the study of the $^{12}C(d,p_{1,2,3})$ reactions, because it does not only contribute to the uncertainty in the energy of the incoming beam, but directly affects the obtained experimental yield. The total estimated uncertainty for the product $Q\times\Omega$ did not exceed 4.3% in the least favourable case. The statistical uncertainty was below 1% for p_0 and for p_1,p_2,p_3 varied, ranging between 1% and 10%, with the (d,p_3) being the least favourable case in the studied energy interval. The oxygen contamination of the samples due to their manufacturing process was practically negligible (1–3 at %). A long Faraday cup was implemented for the charge collection, while voltage suppression (300 V) was employed in front of the collimator set and on target. Two liquid nitrogen traps were set on both ends of the goniometer in order to reduce the carbon build-up on the targets. The overall uncertainty in the absolute differential cross-section measurements varied between 6% and 22% depending mainly on the target.

Excitation functions for $^{12}C(d,p_0)^{13}C$ reaction between 135° and 170° are given in Fig. 3.17a─h and for $^{12}C(d,p_{1,2,3})^{13}C$ between 145° and 170° are given in Fig 3.18a─f. Results for $^{12}C(d,p_0)$ are published in [3.13] and for $^{12}C(d,p_{1,2,3})$ in [3.14].

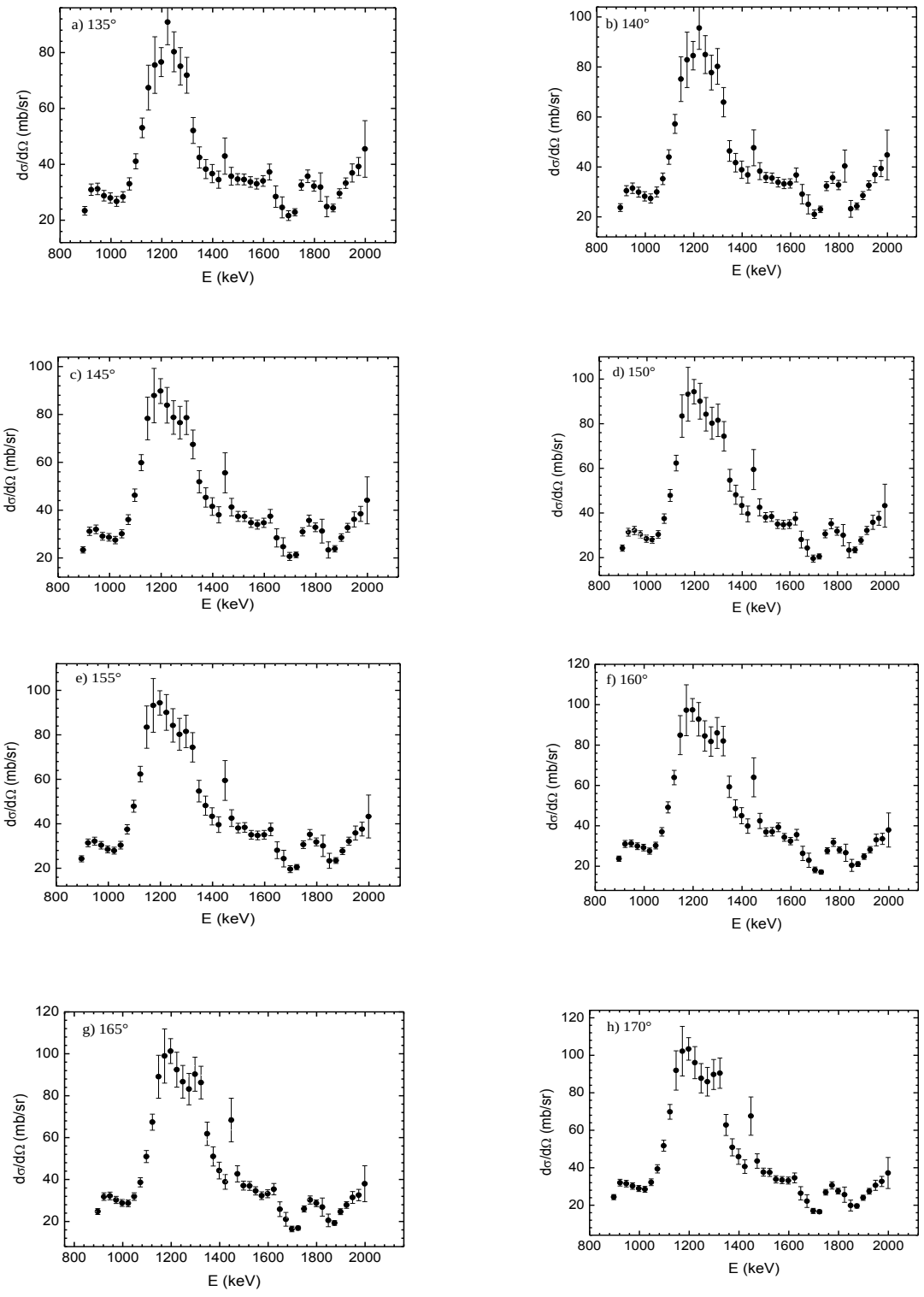

FIG. 3.17. (a─h) Excitation functions for the $^{12}C(d,p_0)^{13}C$ reaction between 135° and 170°.

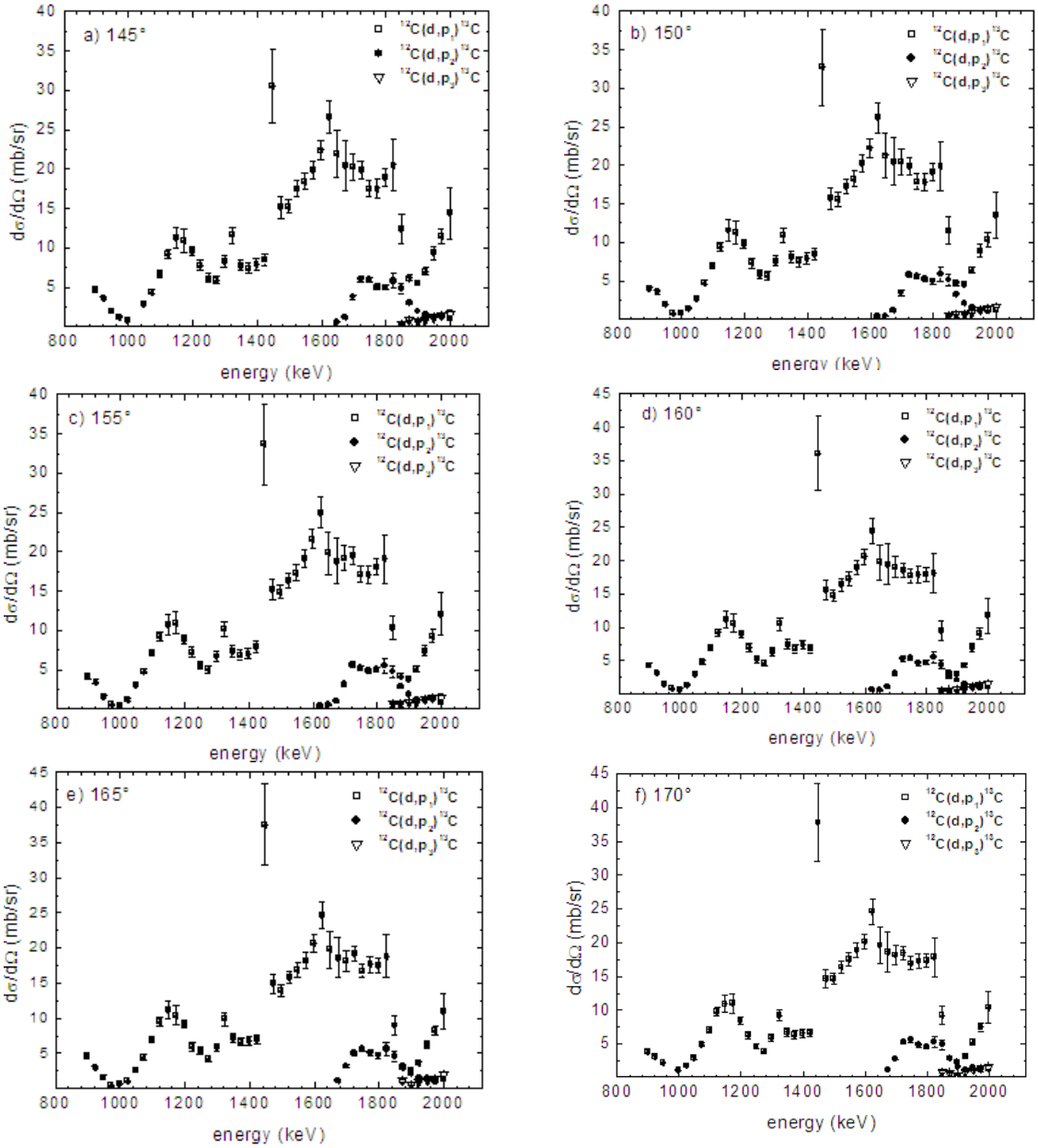

FIG. 3.18. (a–f) Excitation functions for the $^{12}C(d,p_{1,2,3})^{13}C$ reactions between 145° and 170°.

3.5.4. $^{14}N(d,p_{0,1+2})^{15}N$

The ion beam from the IPPE EG-2.5 Van de Graaff accelerator was employed with an energy resolution estimated to be 0.1%. The energy calibration of the accelerator was made using the $^{27}Al(p,\gamma)$ resonance at 991.9 keV and the $^{7}Li(p,n)$ reaction threshold at 1880.4 keV. The beam was collimated to form a 2 mm spot on the target. The target was prepared by vacuum evaporation of adenine ($C_5H_5N_5$) on ~0.3 mg/cm^2 thick silver backing. The number of nitrogen atoms in the target was estimated to be ~1.4×10^{18} cm^{-2}. A particle detector of 500 μm depletion depth at nominal voltage was placed at a distance of 63 ± 1 mm from the beam spot to measure (d,p) and (d,α) spectra. The solid angle subtended by the detector was equal to 7.61 ± 0.34 msr. It was calculated from the measurement of the distance between the beam spot on the target and the detector entrance aperture diameter, which was equal to 6.20 ± 0.1 mm. In the (d,p_0) reaction measurements, the detector was covered with a 300 μm thick

aluminum foil in order to reduce the energy of registered protons so that their range in the detector did not exceed the depletion depth.

The uncertainties in the dependence of the cross sections on energy originated mainly from the counting statistics and on the evaluation of the area under peaks. These uncertainties were estimated not to exceed 5% in total. The normalization of the measured excitation functions was made against the values obtained for incident deuterons of 972 keV as described in [3.15]. Data are published in [3.16].

The excitation functions for the $^{14}N(d,p)^{15}N$ reaction at 150° are given in Fig. 3.19.

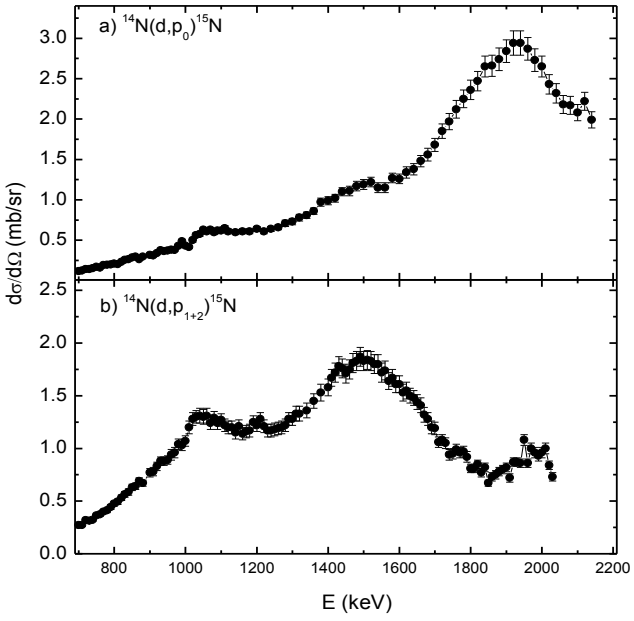

FIG. 3.19. The excitation functions for the $^{14}N(d,p)^{15}N$ reaction at 150°.

3.5.5. $^{27}Al(d,p_{0+1,2+3,4,5+6})^{28}Al$

The ion beam from the IPPE EG-2.5 Van de Graff accelerator was employed with an energy resolution estimated to be 0.1%. The energy calibration of the accelerator was made using the $^{27}Al(p,\gamma)$ resonance at 991.9 keV and the $^{7}Li(p,n)$ reaction threshold at 1880.4 keV. The obtained calibration constant at two energy points appeared to be the same within 0.07%. Since this figure was less than the accuracy of the calibration procedure, no dependence of the calibration constant on energy was assumed and an average value obtained for the two points was used. The beam was collimated to form a 2 mm spot on the target. A surface barrier detector of 700 μm depletion depth at nominal voltage was placed at a distance of 63 ± 1 mm from the beam spot ($\Omega = 7.61 \pm 0.34$ msr). In the (d,p) reaction measurements the detector was covered with a 40 μm thick aluminum foil in order to suppress elastically scattered deuterons and alpha particles from (d,α) reactions. The collected charge Q was in the range of 80–160 μC depending on the beam energy and the beam current was kept between 50 nA and 70 nA.

The target used in the measurements was a self-supporting aluminum foil ~0.6 μm thick. Its thickness was determined to be $(3665 \pm 55)\times10^{15}$ at/cm^2 by resonance profiling using 991.9 keV (p,γ) resonance. The absolute uncertainty in the measured cross sections was estimated to be below 6.0% with contributions: current integration 2%, solid angle 4.5%, target thickness 1.5% and peak statistics from 1─3%. The excitation functions for ^{27}Al(d,p$_{0\text{-}6}$)^{28}Al at 150° are given in Fig. 3.20. Data are published in [3.17].

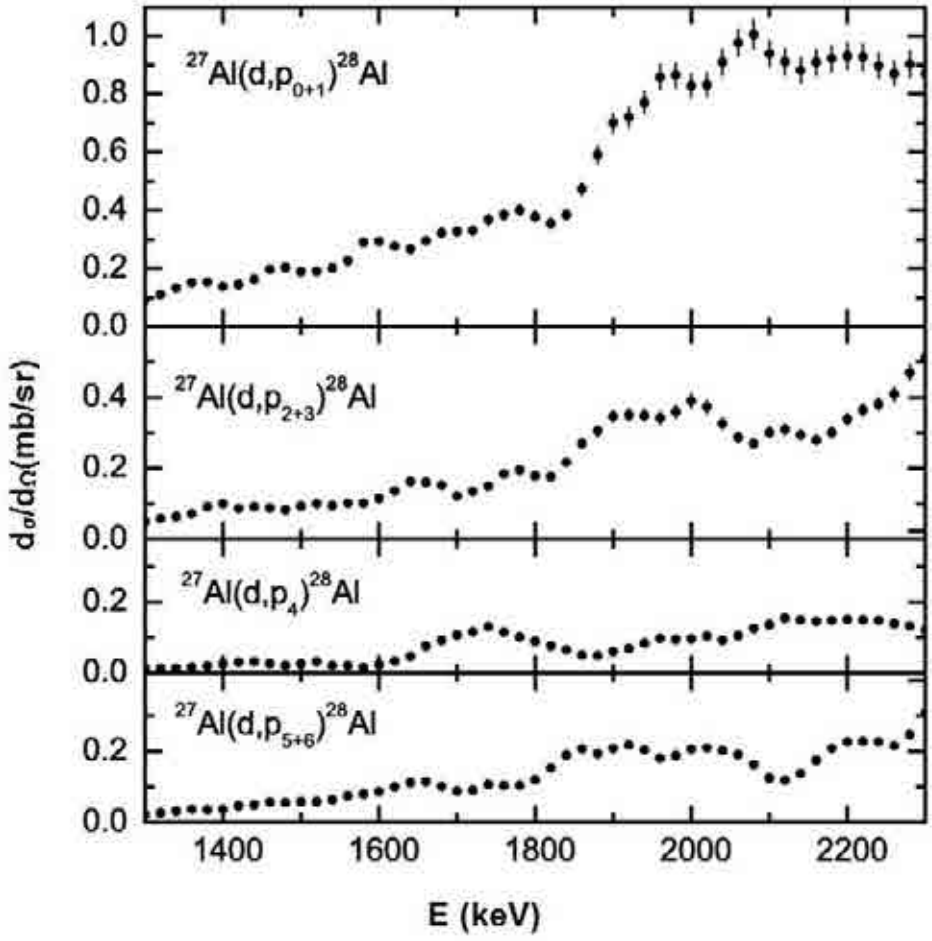

FIG. 3.20. The excitation functions for the ^{27}Al(d,p$_{0\text{-}6}$)^{28}Al reaction at 150°. Reproduced courtesy of Elsevier [3.17].

3.5.6. ^{28}Si(d,p$_{0,1,2,3}$)^{29}Si

The experiments were performed using the deuteron beam of the 5.5 MV TN11 Tandem Accelerator of N.C.S.R. "Demokritos", Athens, Greece. The deuterons, accelerated to Ed,lab = 1500─2000 keV in rough steps of ~50 keV, were led to a scattering chamber of large dimensions. For the charge measurements (charge collection and subsequent current integration) a long Faraday cup was implemented, while voltage suppression of ~300 V was applied on the collimator set, on the target and on the Faraday cup itself.

The detection system consisted of three Si surface barrier detectors (1000─2000 μm) along with the corresponding electronics. The spectra from all the three detectors were

simultaneously recorded and the procedure was repeated by turning the detectors by 5° for every E_d. No absorber foil was used. Due to the small size of the target, the collimator size was severely reduced, and thus the beam spot size was 1.5 × 1.5 mm^2, while the current on target did not exceed 100 nA during all measurements.

The target was placed at a distance of ~9 cm from the detectors. The total estimated uncertainty for the product Q×Ω varied between ~3─5%. The target used was an ultra thin, high-purity silicon nitrite membrane, having a nominal thickness of 75 nm (Silson). This self-supporting target (by the surrounding Si window) had a square shape, with an area of 5 x 5 mm^2. The combined uncertainties, varying between ~4─7% (for different levels), included uncertainties in the Q-ratio, in peak integration, as well as, statistical uncertainties, and corresponded to ± 1σ accuracy.

Data are published in [3.18]. The excitation functions for $^{28}Si(d,p\ p_{0,1,2,3})^{29}Si$ are given in Fig. 3.21.

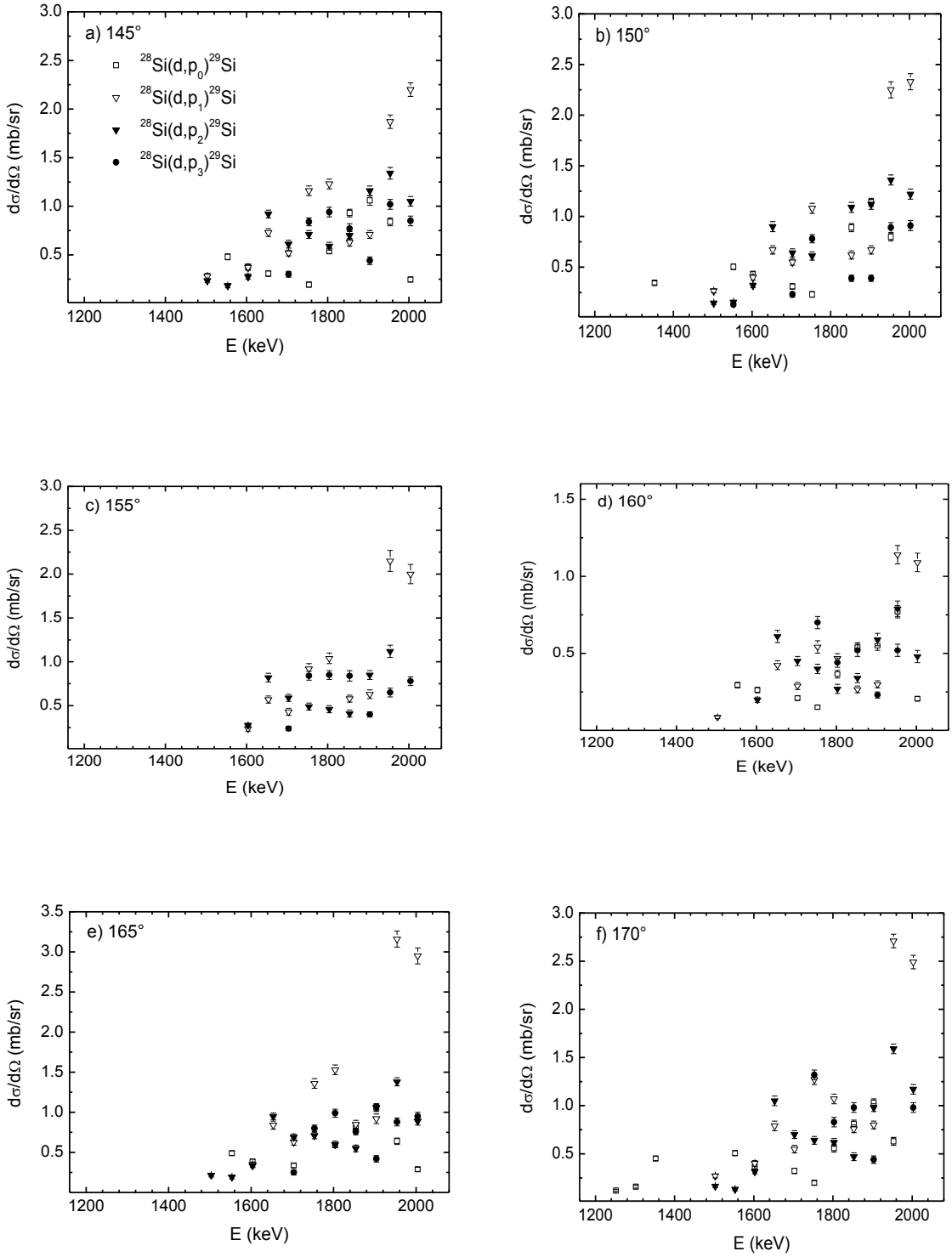

FIG. 3.21. Excitation functions for $^{28}Si(d,p_{0,1,2,3})^{29}Si$ reaction.

3.5.7. $^{32}S(d,p_{0,1,2,3,4-6,7})^{33}S$

The deuteron beams used were delivered by the 5.5 MV TN11 Tandem Accelerator of NCSR ‘‘Demokritos”, Athens, Greece. The energy of the deuterons ranged from E_{lab} = 1975 to 2600 keV in steps of 25 keV. The final energy of the deuterons was measured by nuclear magnetic resonance with an accuracy of ± 2 keV. The beam was led onto the target through a collimator of 2 mm diameter placed about 45 cm before the target, yielding a beam spot of 3 × 3 mm^2. At both the target and the collimator a suppression voltage of 300 V was applied. In front and behind the scattering chamber, a set of two liquid nitrogen traps was used, in order to reduce the carbon built up on the target.

The detection apparatus consisted of five SSB detectors. Four of them with thicknesses ranging from 1000 to 2000 μm were placed at angles from 140° to 170° in steps of 10°, and at a distance of 9 cm from the target. In front of each of these detectors an orthogonal tantalum slit was placed defining thus the measured angles with an accuracy of 0.1°. Additionally, a Kapton foil of 50 μm thickness was mounted in front of the slits and was used as an absorber for the deuterons elastically scattered by the target, enabling beam currents up to 100 nA. The fifth detector was mounted at 120° with a circular tantalum aperture in front and was used in order to detect the elastically backscattered deuterons from the target for each energy step.

The energy calibration of the detectors was made using a triple α – source (^{241}Am, ^{239}Pu, ^{244}Cm) of known activity. The same source was also used in order to measure the solid angle Ω sustained from each of the detectors. The accumulated charge Q of the beam was measured at two beam energies (900 and 1500 keV) by detecting the deuterons which were elastically scattered by a thick aluminum target. At these energies the backscattering is purely Rutherford and thus the number of scattered deuterons is proportional to the product Q × Ω.

A thin self-supported target, which was prepared by evaporating TiS_2 powder onto a carbon foil of 10 μg/cm^2 was used. On top of this target, a thin Ta layer was evaporated in order to ensure the thermal stability of the target. The exact thickness of the layer was determined by d-RBS and was found to be 3.09×10^{17} at/cm^2 consisting of 42% of natural S and 58% of Ti.

Data are published in [3.19]. The excitation functions for $^{32}S(d,p_{0,1,2,3,4–6,7})^{33}S$ reactions at (a) 140°, (b) 150°, (c) 160° and (d) 170° are given in Fig. 3.22.

3.6. (d,α) MEASUREMENTS

3.6.1. $^{10}B(d,\alpha)^{8}Be$

The experiments were performed using the deuteron beam of the 5.5 MV TN11 Tandem Accelerator of N.C.S.R. ‘‘Demokritos’’, Athens, Greece. $^{10}B(d,\alpha_0)$ reaction has been studied in the projectile energy region $E_{d,lab}$ = 900–2000 keV (in steps of 25 keV) and for detector angles 135─170° (in steps of 5°), using the ^{10}B isotopically enriched target. Details of the experimental setup are presented in detail in 3.4.1.

The uncertainty varied between ~11% and 14%, including uncertainties in the product Q × Ω, in the target thickness and in peak integration as well as statistical uncertainties to ±1σ accuracy. This work is published in [3.20]. Excitation functions for $^{10}B(d,\alpha_0)^{8}Be$ reaction at (a) 135°, (b) 140°, (c) 145°, (d) 150°, (e) 155°, (f) 160°, (g) 165° and (h) 170° are given in Fig. 3.23a─h, respectively.

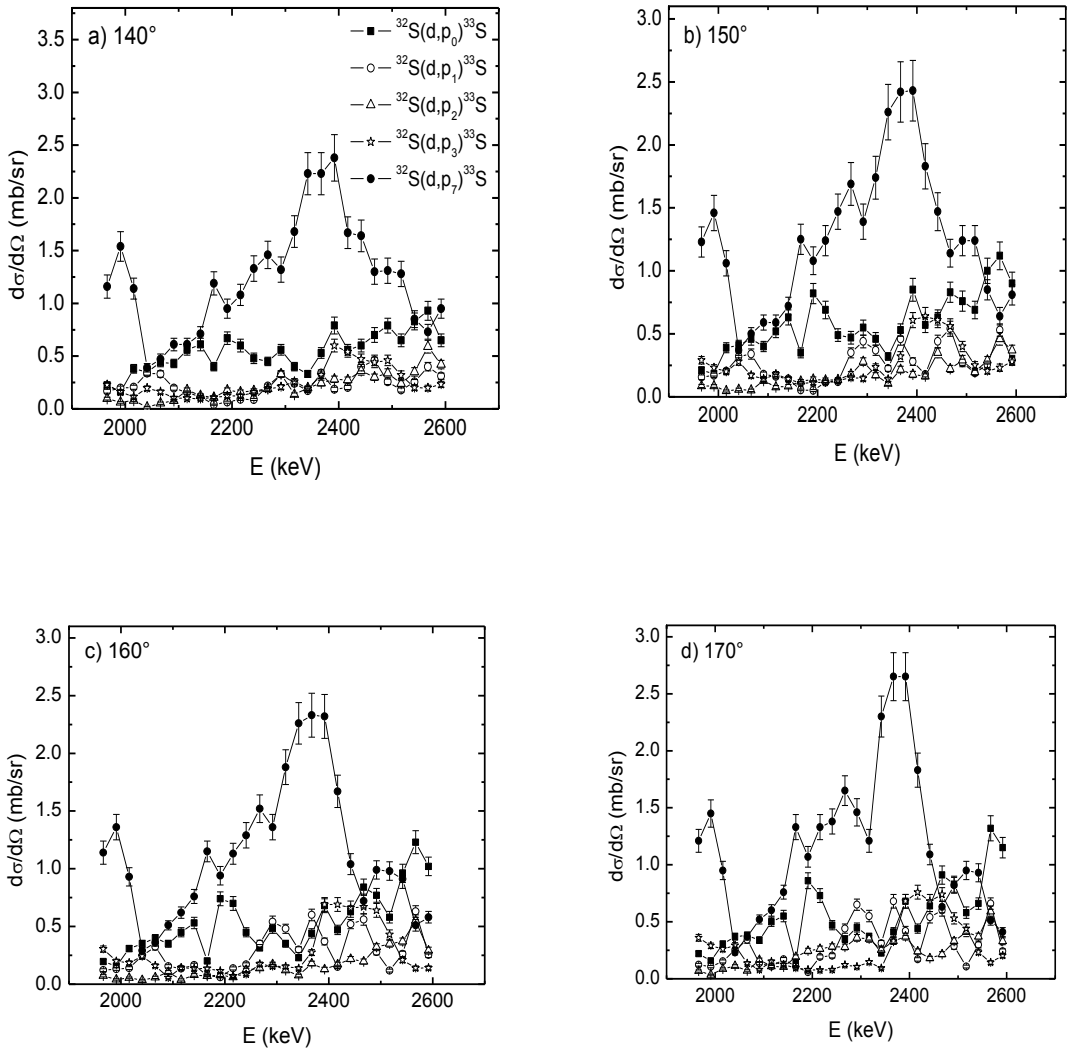

FIG. 3.22. Excitation functions for $^{32}S(d,p_{0,1,2,3,7})^{33}S$ reactions at (a) 140°, (b) 150°, (c) 160° and (d) 170°.

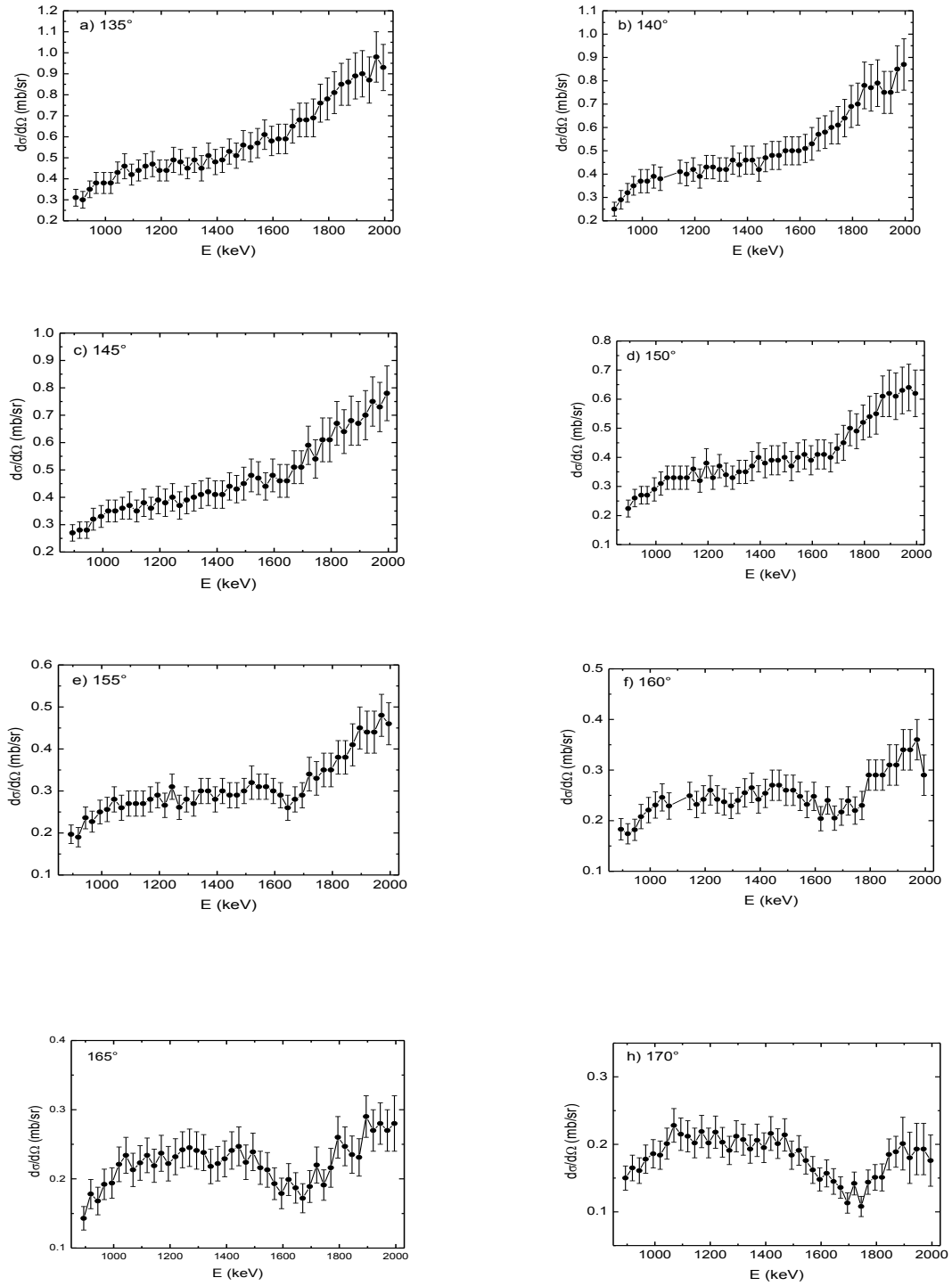

FIG. 3.23. Excitation functions for the $^{10}B(d,\alpha_0)^8Be$ reaction at (a) 135°, (b) 140°, (c) 145°, (d) 150°, (e) 155°, (f) 160°,(g) 165° and (h) 170°.

3.6.2. $^{11}B(d,\alpha_{0,2})$

The experiments were performed using the deuteron beam of the 5.5 MV TN11 Tandem Accelerator of N.C.S.R. "Demokritos", Athens, Greece. The deuterons, accelerated to $E_{d,lab}$ = 900─1200 keV, in steps of 25 keV, were led to a scattering chamber of large dimensions. For

the charge measurements (charge collection and subsequent current integration) the whole chamber was electrically isolated from the beam line and voltage suppression of ~300 V was applied on both the collimator set and on target.

Experimental setup is described in detail in 3.4.1. The target was placed at a distance of ~9 cm from the detectors. Orthogonal slits (~4.5×10 mm^2) were placed in front of the detectors in order to reduce the angular uncertainty (~ ± 1.5°), while allowing an adequate effective solid angle to be subtended by the detectors. The determination of the product Q×Ω was carried out by deuteron-induced Rutherford backscattering measurements (d-RBS) using high purity mechanically polished thick aluminum and gold foils as targets (d-RBS spectra taken at E_d = 0.9, 1.0, 1.1 and 1.2 MeV). The total estimated uncertainty for the product Q×Ω varied between ~3─5% (pending on the detector).

Work is published in [3.12]. Excitation functions for $^{11}B(d,\alpha_0)$ and $^{11}B(d,\alpha_2)$ reaction at (a) 140°, (b) 150°, (c) 160° and (d) 170° are displayed in Fig. 3.24 and Fig. 3.25, respectively.

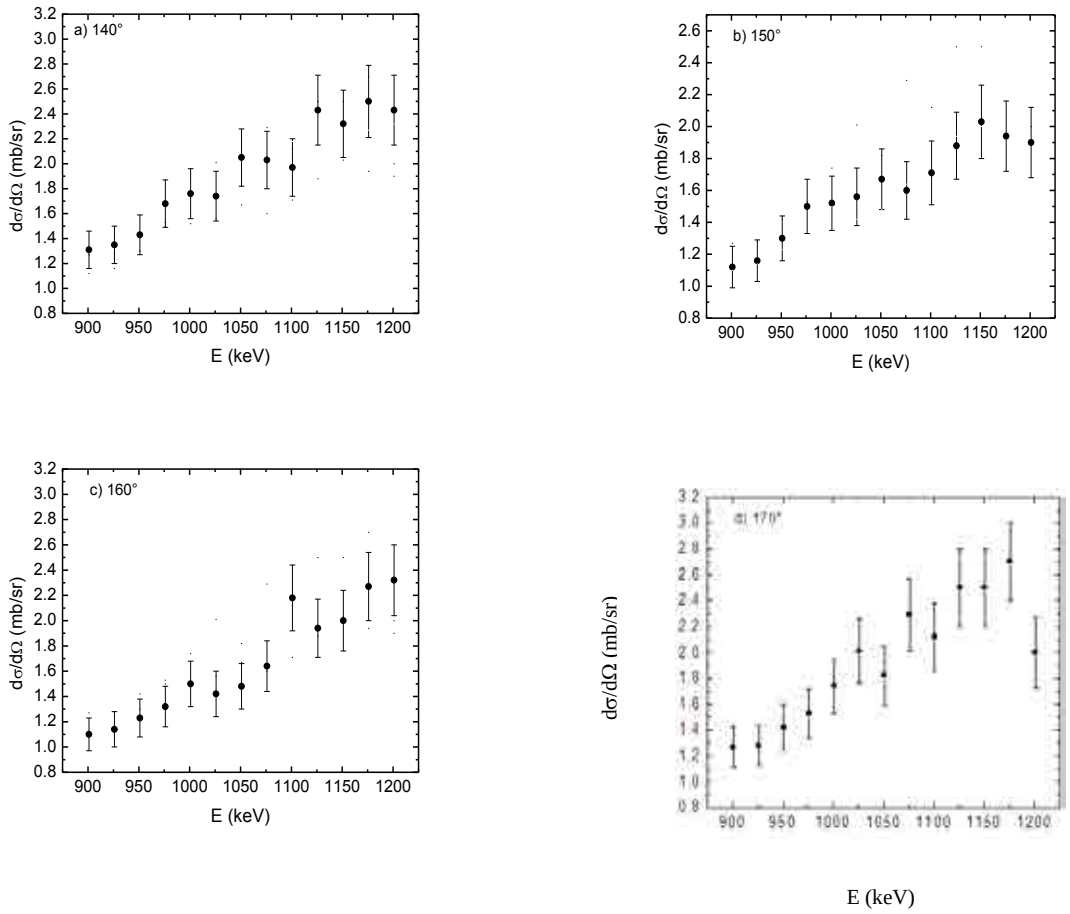

FIG. 3.24. Excitation functions for $^{11}B(d,\alpha_0)$ reaction at (a) 140°, (b) 150°, (c) 160° and (d) 170°.

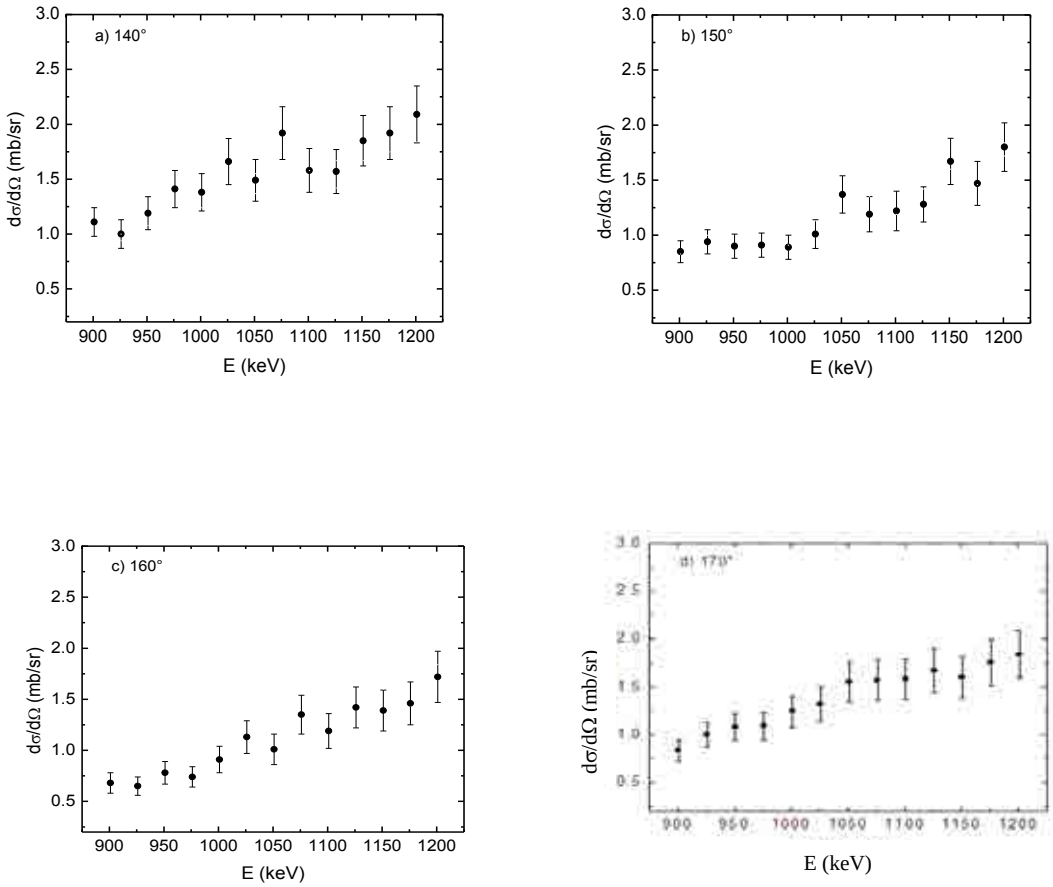

FIG. 3.25. Excitation functions for $^{11}B(d,\alpha_2)$ reactions at (a) 140°, (b) 150°, (c) 160° and (d) 170°.

3.6.3. $^{14}N(d,\alpha_{0,1})^{12}C$

The ion beam from the IPPE EG-2.5 Van de Graaff accelerator was employed with an energy resolution estimated to be 0.1%. The experimental setup is described in detail in 3.5.4.

In course of the (d,α) measurements the bias voltage was decreased so that protons corresponding to the (d,p_0) reaction deposited only a small fraction of the energy in the detector sensitive layer. In order to reduce the count rate caused by elastically scattered deuterons, the detector was covered with 17.5 μm thick aluminum foil. Thus, the alpha particle signal was registered with practically no background.

The normalization of the measured excitation functions was made against the values obtained for incident deuterons of 972 KeV as described in [3.15]. The uncertainties in the dependence of the cross sections on energy originated mainly from the counting statistics and on the evaluation of the area under peaks. These uncertainties were estimated not to exceed in total 5%.

Work is published in [3.16]. The excitation functions for the $^{14}N(d,\alpha)^{12}C$ reaction are given in Fig. 3.26.

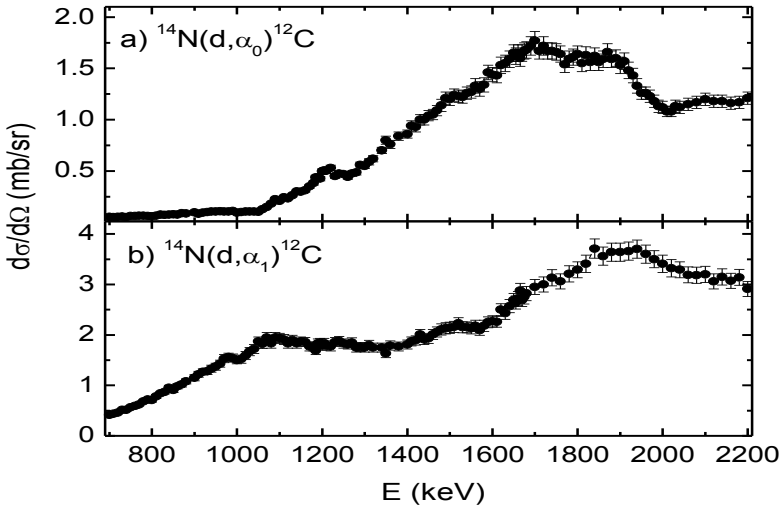

FIG. 3.26. The excitation functions for the $^{14}N(d,\alpha)^{12}C$ reaction at 150°.

3.6.4. $^{27}Al(d, \alpha_{0,1,2,3,4})^{25}Mg$

The ion beam from the IPPE EG-2.5 Van de Graaff accelerator was employed with an energy resolution estimated to be 0.1%. Experimental conditions are described in detail in 3.5.5.

In the course of the (d,α) measurements the bias voltage was reduced so that protons deposited only a small fraction of the energy in the detector sensitive layer. The scattering chamber was electrically isolated from the ground in order to collect the charge of ions impinged on the target. The collected charge Q was in the range of 80–160 μC depending on the beam energy and the beam current was kept between 50 nA and 70 nA.

The target used in the measurements was a self-supporting aluminum foil ~0.6 μm thick. Its thickness was determined by resonance profiling using 991.9 keV (p,γ) resonance and from the (d,d) spectrum measured at 1100 keV. The number of atoms N derived from the RBS experiment was equal to $(3650 \pm 90)\times10^{15}$ at/cm^2 and for PIGE it was found to be $(3680 \pm 60)\times10^{15}$ at/cm^2. The average value of N = $(3665 \pm 55)\times10^{15}$ at/cm^2 was assumed.

The absolute uncertainty in the measured cross sections was estimated to be about 6.0% (current integration: 2% - calibrated with a precise amperemeter, solid angle: 4.5% -direct geometrical measurement, target thickness: 1.5% -two independent measurements by PIGE and RBS, statistics: 1–3% ─1σ).

Work is published in [3.17]. The excitation functions for the $^{27}Al(d,\alpha)^{25}Mg$ reaction at 150° are displayed in Fig. 3.27.

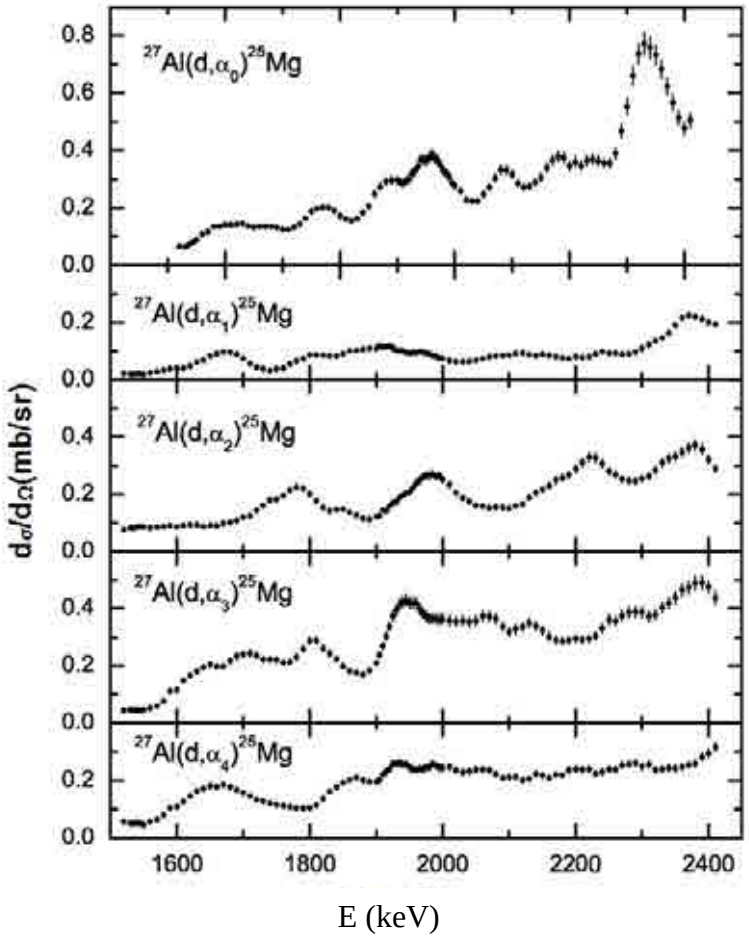

FIG. 3.27. The excitation functions for the $^{27}Al(d,\alpha)^{25}Mg$ reaction at 150°. Reproduced courtesy of Elsevier [3.17].

3.7. (α,α) MEASUREMENTS

3.7.1. N(α,α)N

Measurements were performed using alpha particle beam from the 6.0 MV Tandem Van de Graaff accelerator at the Ruđer Bošković Institute in Zagreb. The beam was extracted from the alphatros ion source. Calibration of the accelerator energy was done using narrow resonance in $^{27}Al(p,\gamma)^{28}Si$ at 991.88 keV and neutron threshold reaction $^{7}Li(p,n)^{7}Be$ at 1880.6 keV. Final energy spread of the beam was calculated to be 0.1% of the incident beam energy.

Three surface barrier detectors with a 2.5 msr solid angle were each positioned at 118°, 150° and 165°. Alphas, delimited by horizontal and vertical slits to a spot of 2 × 2 mm^2 impinged on the sample at normal incidence. The energy resolution of the detectors used was between 15─20 keV for alphas in the measured energy range. The excitation function of the $^{14}N(\alpha,\alpha)^{14}N$ was measured from 2.5 to 4.0 MeV with minimum step of 5 keV where the cross section varied rapidly and 10─30 keV elsewhere.

To avoid background and counting rate problems coming from the substrate, a thin self-supporting SiN membrane window (Spi supplies) with nominal thickness of 100 nm was selected as a target. On the top, a thin Au layer was evaporated for normalization purposes, assuming that cross sections for backscattering of alpha particles from Au are Rutherford in

the entire energy range. Target stability was monitored during the measurements by inspecting N and Au intensity ratios at 2.56 MeV a few times per day. It was found that this ratio was changing less than 2 % during the measurements.

To avoid overlap between alpha particles emitted from the $^{14}N(\alpha,\alpha)^{14}N$ reaction and protons emitted from the $^{14}N(\alpha,p_0)^{17}O$ reaction we have placed 0.9 μm thick Mylar® in front of the 150° and 165° detectors for energies higher than 3.5 MeV.

The following factors were taken into consideration for estimating the uncertainty: the counting statistics of the peak areas and the systematic error in determining the N_{Au}/N_N ratio. Uncertainties due to dead time, solid angle and improper charge measurement are eliminated with the normalization to backscattering protons from gold. Uncertainties of the detector angular settings were estimated to be negligible.

Data are published in [3.21]. Excitation functions for (a) 118°, (b) 150° and (c) 165° are presented in Fig. 3.28.

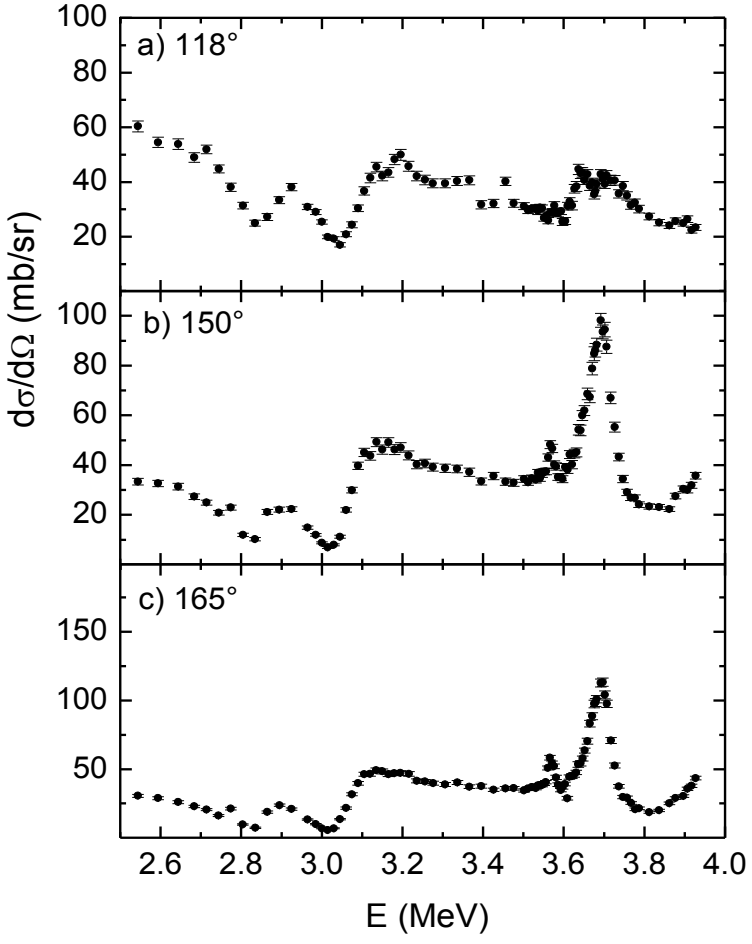

FIG. 3.28. Excitation functions for N(α,α)N at (a) 118°, (b) 150° and (c) 165°.

REFERENCES

[3.1] DING, W., SHI, L.Q., LONG, X.G. et al., Cross section for D(p,p)D elastic scattering from 1.8 to 3.2 MeV at the laboratory angles of 155° and 165°, Nucl. Instrum. Methods Phys. Res. B **267** (2009) 2341.

[3.2] XIA, X.J., DING, W., ZHANG, B., et al., Cross section for proton–tritium scattering from 1.4 to 3.4 MeV at the laboratory angle of 165°, Nucl. Instrum. Methods Phys. Res. B **266** (2008) 705.

[3.3] LU, Y.F., SHI, L.Q., HE, Z.J., et al., Elastic scattering cross section of proton from helium at the laboratory angle of 165°, Nucl. Instrum. Methods Phys. Res. B **267** (2009) 760.

[3.4] CACIOLLI, A., CHIARI, M., CLIMENT-FONT A., et al., Proton elastic scattering cross sections on F, C, Li from 3 to 7 MeV, Nucl. Instrum. Methods Phys. Res. B **249** (2006) 95.

[3.5] BOGDANOVIĆ RADOVIĆ, I., SIKETIĆ, Z., JAKŠIĆ, M., *et al.*, Measurement and parameterization of proton elastic scattering cross sections for nitrogen, J. Appl. Phys. 104 (2008) 074905.

[3.6] SIKETIĆ, Z., BOGDANOVIĆ RADOVIĆ, I., SKUKAN, N., et al., Proton elastic scattering from aluminum for 120°, 150° and 165° in the energy interval from 2.4 to 5 MeV, Nucl. Instrum. Methods Phys. Res. B **261** (2007) 414.

[3.7] CACIOLLI, A., CALZOLAI, G., CHIARI, M., et al., Proton elastic scattering and proton induced γ-ray emission cross sections on Na from 2 to 5 MeV, Nucl. Instrum. Methods Phys. Res. B **266** (2008) 1392.

[3.8] ZIEGLER, J.F., BIERSACK, J.P., ZIEGLER, M.D., SRIM – The stopping and range of ions in matter (2008) SRIM Co., ISBN 0-9654207-1-X.

[3.9] KOKKORIS, M., TSARIS, A., LAGOYANNIS, A., et al., Determination of differential cross sections for the $^{nat}K(p,p_0)$ and $^{39}K(p,\alpha_0)$ reactions in the backscattering geometry, Nucl. Instrum. Methods Phys. Res. B **268** (2010) 1797.

[3.10] KOKKORIS, M., MISAILIDES, P., KOSSIONIDES, S., et al., A detailed study of the $^{nat}C(d,d_0)$ reaction at detector angles between 145° and 170°, for the energy range $E_{d,\,lab}$ = 900–2000 keV, Nucl. Instrum. Methods Phys. Res. B **249** (2006) 81.

[3.11] KOKKORIS, M., FOTEINOU, V., PROVATAS, G., et al., A detailed study of the d + ^{10}B system for nuclear reaction analysis – Part A: The $^{10}B(d,p)^{11}B$ reaction in the energy region $E_{d,lab}$ = 900–2000 keV, Nucl. Instrum. Methods Phys. Res. B **263** (2007) 357.

[3.12] KOKKORIS, M., DIAKAKI, M., MISAELIDES, P., et al., Study of the d + ^{11}B system differential cross sections for NRA purposes, Nucl. Instrum. Methods Phys. Res. B **267** (2009) 1740.

[3.13] KOKKORIS, M., MISAELIDES, P., KOSSIONIDES, S., et al., A detailed study of the $^{12}C(d,p_0)^{13}C$ reaction at detector angles between 135° and 170°, for the energy range $E_{d,\,lab}$ = 900–2000 keV, Nucl. Instrum. Methods Phys. Res. B **249** (2006) 77.

[3.14] KOKKORIS, M., MISAELIDES, P., KONTOS, A., et al., Differential cross section measurements of the $^{12}C(d,p_{1,2,3})^{13}C$ reactions in the energy range $E_{d,lab}$ = 900–2000 keV for nuclear reaction analysis, Nucl. Instrum. Methods Phys. Res. B **254** (2007) 10.

[3.15] DAVIES, J.A., JACKMAN, T.E., PLATTNER, H., et al., Absolute calibration of $^{14}N(d,\alpha)$ and $^{14}N(d,p)$ reactions for surface absorption studies, Nucl. Instrum. Methods Phys. Res **218** (1983) 141.

[3.16] GURBICH, A., MOLODTSOV, S., Measurement of (d,p) and (d,α) differential cross sections for ^{14}N, Nucl. Instrum. Methods Phys. Res. B **266** (2008) 1206.

[3.17] GURBICH, A.F., MOLODTSOV, S., Measurement of (d,p) and (d,α) differential cross sections for aluminum, Nucl. Instrum. Methods Phys. Res. B **266** (2008) 353.

[3.18] KOKKORIS, M., MICHALAKIS, K., MISAELIDES, P., et al., Study of selected differential cross sections of the $^{28}Si(d,p_0,p_1,p_2,p_3)$ reactions for NRA purposes, Nucl. Instrum. Methods Phys. Res. B **267** (2009) 1744.

[3.19] LAGOYANNIS, A., HARISSOPULOS, S., MISAELIDES, P., et al., Differential cross-section measurements of the $^{32}S(d,p)^{33}S$ reaction for nuclear reaction analysis purposes, Nucl. Instrum. Methods Phys. Res. B **266** (2008) 2259.

[3.20] KOKKORIS, M., FOTEINOU, V., PROVATAS, G., et al., A detailed study of the d + ^{10}B system, for nuclear reaction analysis – Part B: The $^{10}B(d,\alpha_0)^8Be$ reaction in the energy region $E_{d,lab}$ = 900–2000 keV, Nucl. Instrum. Methods Phys. Res. B **263** (2007) 369.

[3.21] GURBICH, A.F., BOGDANOVIĆ RADOVIĆ, I., SIKETIĆ, Z., et al., Measurements and evaluation of the cross-section for helium elastic scattering from nitrogen, Nucl. Instrum. Methods Phys. Res. B **269** (2011) 40.

4. ASSESSMENTS

4.1. INTRODUCTION

The available experimental cross-section data sets for light elements were assessed. In a first step, the available data files were compared to the original publications and errors (if any) were corrected. In a second step, all available data sets were compared to each other, thus allowing an assessment of the reliability of different data sets. Finally, recommendations on the reliability of data sets and estimates of their accuracy were made. For a number of light elements an evaluated cross section exists, which is always recommended for quantitative analysis. However, for some light elements (especially Li, Be, B) such an evaluated cross section does not exist. For these cases recommendations on the use of existing experimental data are summarized below, as well as recommendations for extending evaluated data to higher energies.

4.2. $D(p,p_0)D$

Experimental studies on the proton-deuteron system have been published in a number of articles. EXFOR presents data from at least 45 publications. Both particles have been used as projectiles, proton scattering by deuterium and deuteron scattering by hydrogen have been measured. Again, in the case of incident deuterons, both scattered deuterons as well as recoiled protons have been detected in the experiments. The target materials employed gases or hydrogen containing non-metals, such as nylon or PET foils. Although all the published measurements claim an error in the range of ± 3─5%, the practical error may exceed these numbers due to error sources in geometry, particle detection, beam energy, gas density, and contamination, which is limited by the technological level especially for the older measurements.

Many of the experiments are of limited interest from the point of view of ion backscattering analysis, due to their high energy or because data are presented as angular distributions or the data have been taken for small scattering angles. There are, however, several publications which are potentially useful to ion beam applications. At least 14 publications present relevant cross sections [4.1 – 4.14].

In 1969, Kocher and Clegg [4.12] performed angular distribution measurements at eight energies between 1.00─10.04 MeV (Fig. 4.1).

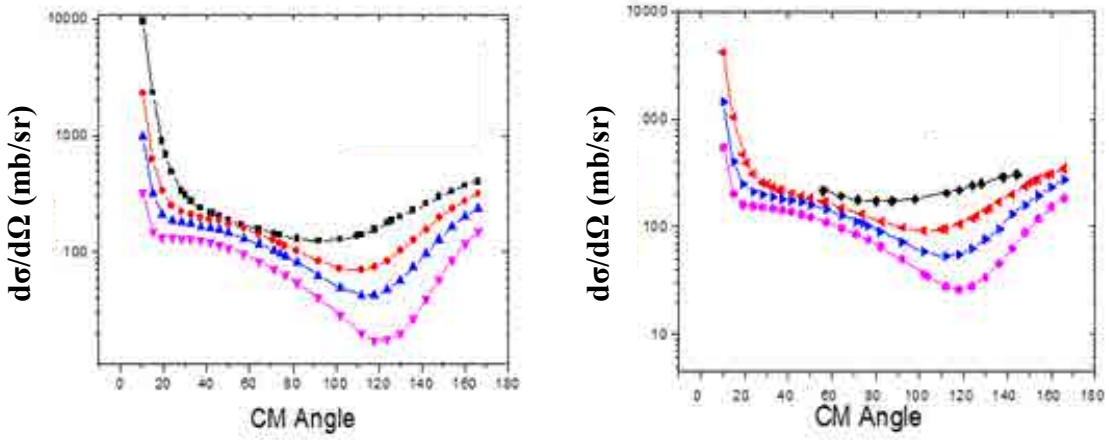

FIG. 4.1. Angular distribution of the CM cross section for elastic scattering of protons from deuterium. Left panel: 1.993 MeV (black line), 3.998 MeV (red line), 6.007 (blue line), 10.04 MeV (magenta line). Right panel: 1.000 MeV (black line), 2.995MeV (red line), 5.002 MeV (blue line), 8.025 MeV (magenta line).

Because of employing a precision gas scattering chamber with differential pumping and high resolution solid state detectors, the total maximum uncertainty can be within 2.1% and the median uncertainty for all data points is ± 0.6%. The type of uncertainty includes background subtraction in the particle yield determination (0.19%), contamination corrections (0.34%), statistical uncertainty (0.1%), gas density, G-factor and integrator calibration (0.2%), angle uncertainty (1.7%), energy uncertainty (0.98%), correction uncertainty (0.05%), and other uncertainties (0.36%).

In 1975, Langley [4.15, 4.9] used erbium deuteride films with a thickness of 800 nm deposited on kovar or alumina substrates as a solid target to measure the elastic scattering cross section for protons on deuterium. The amount of deuterium was determined by a mass spectrometric determination by outgassing of the substrate. The amount of erbium was measured by weight. The elastic scattering cross section was determined by measuring the area under the deuterium peak and the area under the erbium peak, assuming that elastic scattering of protons from erbium is Rutherford and independently measuring the loading ratio([D]/[Er]). The error associated with this measurement is ± 2% for the cross section and less than ± 0.5% for the energy.

There has been an unfortunate controversy in the data given by Langley [4.9]. The discrepancy between his two sets of values is related to the conversion between the centre-of-mass (CM) and laboratory coordinates and between absolute cross sections (in b/sr) and relative cross sections (cross section/Rutherford cross section). Langley presents the same data in mb/sr in the CM system and as relative cross sections in the laboratory system (the relative cross section is the same for both reference systems). The cross sections derived from these two data sets differ by about a factor of 4. The scattering angles are also inconsistent. The controversy has been discussed, e.g., by M. Mayer on the SIMNRA website [http://www.rzg.mpg.de/~mam/CrossSection.html].

In IBANDL, the set of relative cross-section data has been adopted as referring to a laboratory scattering angle of 151^{o}. This is similar to the figure in the Ion Beam Materials Analysis

Handbook [4.16]. SIMNRA suggests that the cross sections calculated from the absolute values by Langley (HD165_Langley.r33 in SIMNRA) should be adopted for the laboratory scattering angle of 165° (165° CM angle equals to 151° laboratory angle).

Further support for the cross sections calculated from the absolute values by Langley at the laboratory angle of 165° may be gained from comparison with other published values. Converting the CM cross sections and CM scattering angles to the laboratory system, one finds that there is good agreement between the Langley absolute values and those of Kocher and Clegg [4.12]. Kocher and Clegg quote uncertainties of the order of 1% or less for their data. Furthermore, they claim good agreement between their data and those of Refs. [4.2, 4.5, 4.6, 4.10]. These studies quote larger uncertainties, of the order of 2─5 %. A comparison of cross sections for scattering angles above 125° from various publications is presented in Fig. 4.2.

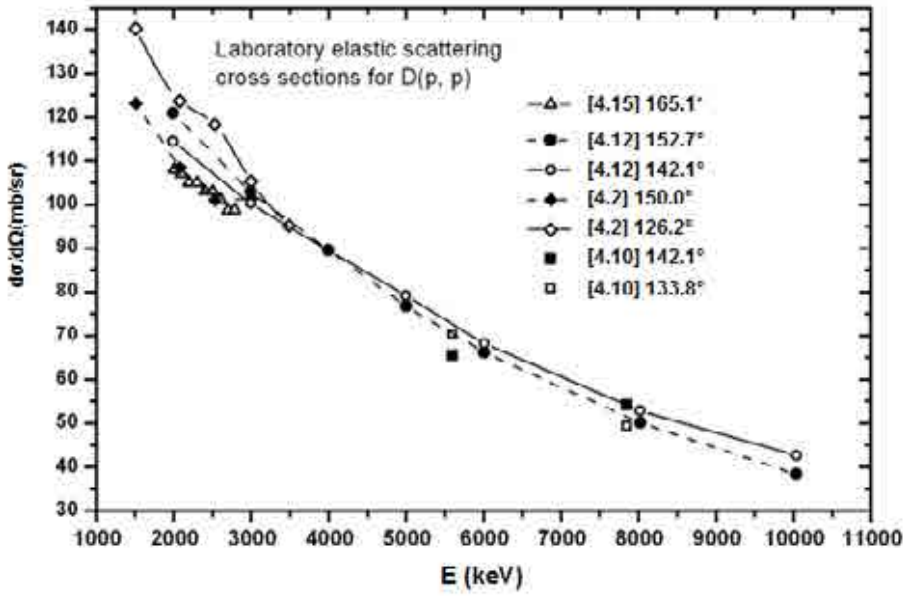

FIG. 4.2. Elastic scattering cross sections for D(p,p)D in the laboratory system for the Langley absolute data [4.15], for Kocher and Clegg [4.12], Scherr et al. [4.2] and Brolley et al [4.10]. The scattering angles refer to the laboratory frame of reference (the Langley data were approximately digitized from a graph).

Recommended data

It must be concluded that of the two Langley data sets, the one based on the relative values at 151° laboratory angle is incorrect. As long as no further data are available, the suggested cross sections for use in large-angle backscattering analysis are those of Kocher and Clegg [4.12] and the data set based on the absolute values by Langley [4.15]. The two most recent publications, by Lahlou et al. [4.13] and Huttel et al. [4.14], present a few cross-sections data points between 3.1 and 3.7 MeV and between 0.4 and 1.0 MeV for angles below 135°. These data are also in qualitative agreement with the earlier data.

4.3. $T(p,p_0)T$

As for the differential cross section for scattering of protons by tritons, Classen [4.17] performed measurements in the angular range from 41.85° to 163° in the lab system

(corresponding to 54.7° to 168.7° in the centre-of-mass system) at five energies between 2.54 and 3.5 MeV. A small volume (42 ccm) scattering chamber with an angular range of 17° to 163° was used in these measurements. It was found that the results were not valid at all angles and energies, the results being too high at the lower scattering angles. A possible reason is the presence of hydrogen contamination in the tritium. This experiment depended on the ability to measure the tritium concentration. Fig. 4.3 shows the measured cross-section data at backward scattering angles. The error estimated for the charge measurement was ± 1%. The pressure and geometry factor measurements were accurate within ± 0.5%. The error in the measurement of the hydrogen concentration was estimated to be within ± 1%, the 3% correction for the chamber characteristics, and the correction for background at high scattering angles. Due to all these reasons, the total probable error was estimated to be ± 5%.

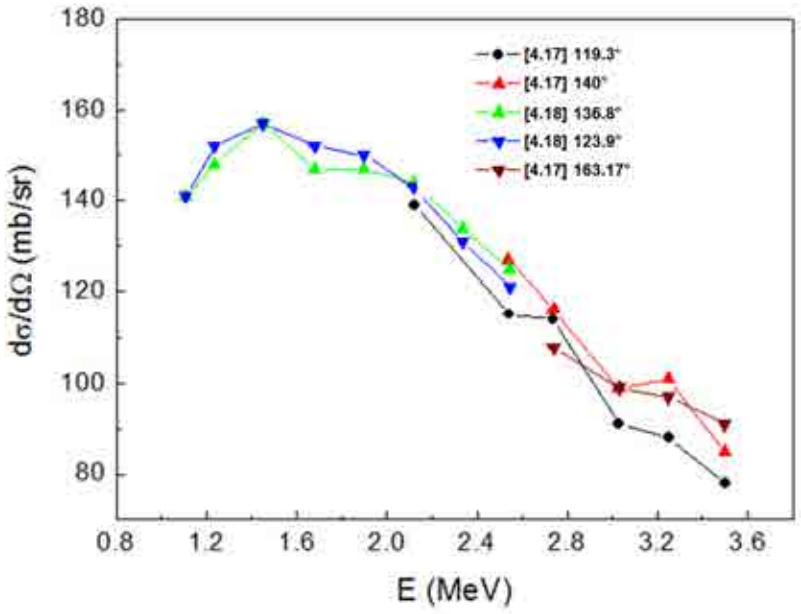

FIG. 4.3. Experimental elastic scattering cross sections for p on T at different laboratory angles.

The differential cross section for the scattering of protons by tritons at lower lab angles down to 15° and proton energies in the range from 1 to 2.55 MeV were measured by the Los Alamos group [4.18], and the measured results are also shown in Fig. 4.3. Probable errors vary between 3 and 5%. The elastic cross-section curve showed a broad peak with a maximum at about 1.4 MeV. This peak became more pronounced for larger angles, as shown in [4.18]. This particular feature in the work of Ennis and Hemmendinger [4.18] was in accordance with a theoretical prediction by Wigner [4.19].

Classen [4.17] compared their data with earlier data obtained by the Los Alamos group at 2.11 and 2.54 MeV incident proton energies [4.20], and found agreement between these data at both high and low scattering angles. But, in the region of the minimum cross section at around 100° scattering angle (c.m.), the results at 2.11 MeV and at 2.54 MeV are about 10% lower than those of the Los Alamos group [4.20]. This difference is the sum of the estimated probable error sources.

Recommended data

The data measured by Classen [4.17] at 119.3° laboratory angle seem to be relatively reliable.

4.4. $^{6}Li(p,p_0)^{6}Li$

As a first step, the data sets already existing in IBANDL [4.21–4.24] were compared with the data in the original references and several inconsistencies were found.

Firstly, the reference in IBANDL data entry no. 1 (i.e. Bashkin and Richards) is wrong (actually, it refers to the work of Warters et al. on p+^{7}Li elastic scattering): the correct one, S. Bashkin and H.T. Richards, Phys. Rev. 84 (1951) 1124, has been assigned to data entry no. 4, which is however incorrect since no such data points exist in the cited paper. Moreover, the original cross-section values from the work of Bashkin and Richards [4.21] were given in the laboratory frame of reference, while the data from IBANDL were calculated as if the original data were given in the centre-of-mass (thus the resulting data were scaled down by a factor of about 1.4); a shift of about +20 keV in the energy scale is evident too. The data available from the EXFOR nuclear database are consistent with the original ones [4.21], so in the following only the EXFOR data will be considered.

IBANDL data entry no. 2 is wrong since no data point at 1.36 MeV and 90° scattering angle exists in the original work of Warters et al. (which, as stated above, refers only to p+^{7}Li elastic scattering). Again, IBANDL data entry no. 3 is wrong as well, since no data point at 1.36 MeV and 90° scattering angle exists in the original work of McCray [4.22].

IBANDL data entry no. 6 refers to a compilation of nuclear cross sections for charged-particle-induced reactions on Li, Be and B from Kim et al. [4.23]. Actually the data presented there are McCray's tabular cross-section values at a scattering angle of 90.75° in the centre-of-mass frame of reference (laboratory angle of 81.3°). Note that from McCray's original work [4.22] the correct angle should be 90.45°, corresponding to a laboratory angle of 81.0°. Moreover, these cross-section data are shown in [4.22] in two separate figures: Fig. 3 displays them as ratios to Rutherford cross section (together with other cross-section values measured at different scattering angles), while Fig.4 presents them as absolute values. Both data sets are available in EXFOR database. In Fig. 4.4, a comparison between these three data sets (apparently referring to the same cross-section values) is shown.

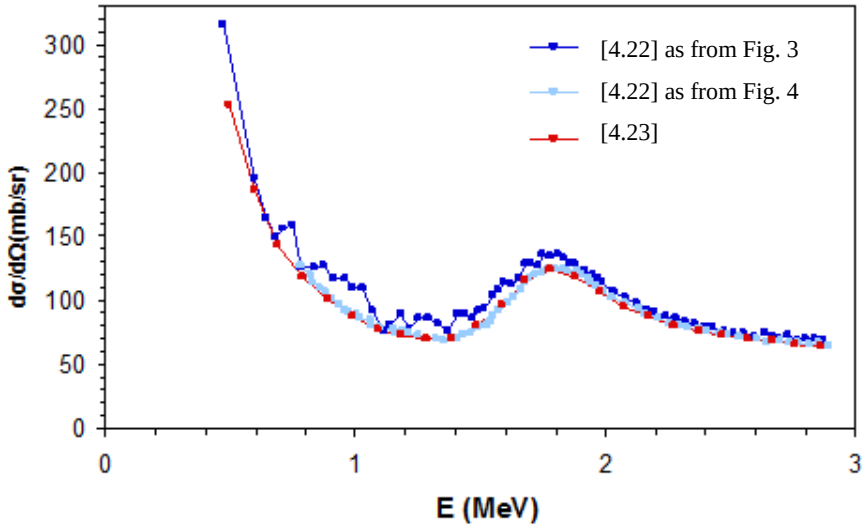

FIG. 4.4. Cross-section values of proton elastic scattering on ^{6}Li versus proton energy at sca ttering angle of 81°. All the quantities are given in the laboratory frame of reference.

From Fig. 4.4 above, the discrepancy between McCray's data taken from the two different figures, which could be attributed to the difficulty of digitizing data from Fig.3 in [4.22], is evident. The data appearing in Kim's compilation [4.23] are in excellent agreement with McCray's ones from the original Fig.4. Note that IBANDL data as compared to tabulated data from Kim [4.23] have slightly different energy values (within ± 5 keV) due to the rounding of digits and the cross-section values result in being scaled upwards by a factor 1.04, so in the following only the original data will be considered.

The second step was a thorough search in the literature and in nuclear databases for other available experimental data. Several data of interest for IBA applications (i.e. for backscattering angles in the 90°─180° range) were retrieved [4.21–4.30]. All the relevant quantities were converted to the laboratory frame of reference when necessary. Table 4.1 lists the new data sets found in the literature; these new data will be uploaded into IBANDL if deemed appropriate.

TABLE 4.1. AVAILABLE DATA IN THE LITERATURE ON $^{6}Li(p,p_0)^{6}Li$ CROSS SECTIONS

Reference	**Data source**	θ_{lab}	E_p **(MeV)**	**Target**	**Quoted uncertainties**	**Data format**
[4.21]	EXFOR	164°	1.14–3.07	Natural Li metal evaporated onto thin Ni foil	20%	Tabular
[4.22]	EXFOR	118.2° 155.8°	0.4─2.9	^{6}Li metal samples (94.5% and 99.7% purity)	3%	Tabular
[4.23]	Original paper	81.0°	0.5─2.9	─	3%	Tabular
[4.24]	EXFOR	90°	1.36	0.03 to 0.1 mg/cm^2 ^{6}LiF (95% enriched in ^{6}Li) evaporated on a C foil	15% statistical and systematic	Tabular
[4.25]	EXFOR	90°─160°	2.40─12.0	30─300 μg/cm^2 ^{6}Li (enriched to 99%) evaporated on a thin C or Ni foil.	1─15% (statistics, background subtraction, normalization)	Tabular
[4.26]	EXFOR	100.3° 116.7° 140.6° 143.8° 166.4°	1.25─5.55	99.3% enriched ^{6}Li metal evaporation on a 1000 Å Ni foil	1.5% statistical, 1% background correction	Tabular
[4.27]	EXFOR	135° 150°	1.75─10.5	─	─	Tabular
[4.28]	Original paper	95°	6.868	Enriched ^{6}LiI (99.32%), natural LiF and LiI evaporated on a Formvar backing	5%	Tabular
[4.29]	EXFOR	90°─165° (5° steps)	1.3─10.1	LiF on Ni backing, Al-^{6}Li-C, C-^{6}Li-C (50 μg/cm^2 ^{6}Li)	7.0%	Tabular
[4.30]	EXFOR	90°─160° (10° steps)	0.80─2.20 (0.1 MeV step)	C-^{6}LiF target (10 nm C and 100 nm ^{6}LiF)	0.2% statistical	Tabular

Note that an ambiguity arises from Haller's data: in Haller's original work [4.29] the cross-section values as a function of proton energy are shown in Fig. 3, where the energy is indicated as "$E_{C.M.}$". In the paper the authors show also angular distribution data for several beam energies (see Figures 5 or 7 in the original reference): in this case, it is indicated in the text that the energy is expressed in the laboratory frame of reference. Fig. 4.5 shows the comparison between cross-section values for the same scattering angle (i.e. 160° in the laboratory) as obtained from the two figures, with the energy scale converted from centre-of-mass to laboratory system for data from Fig. 3, together with the latter data without energy scale conversion. Data sources are EXFOR files.

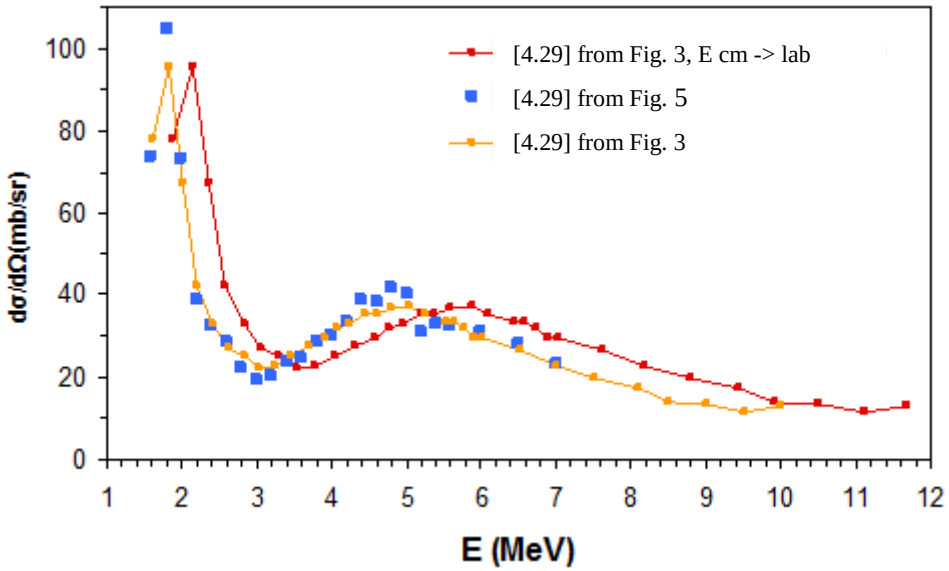

FIG. 4.5. Cross-section values of proton elastic scattering on ^{6}Li versus proton energy at scattering angle of 160°. All the quantities are given in the laboratory frame of reference.

From Fig. 4.5 above, it is evident that the agreement is better if the energy is assumed as expressed in the laboratory frame of reference even for data from Fig. 3 of [4.29]. The same result holds true by comparing data obtained at other scattering angles. Thus, in the following Haller's data will be shown with proton energy not converted.

Figures 4.6 – 4.13 present in graphical form all the cross sections listed in Table 4.1; data referring to similar scattering angles are shown together. In the graphs the proton energy and the differential cross section are given in the laboratory frame of reference, with energy units in MeV and cross-section units in mb/sr.

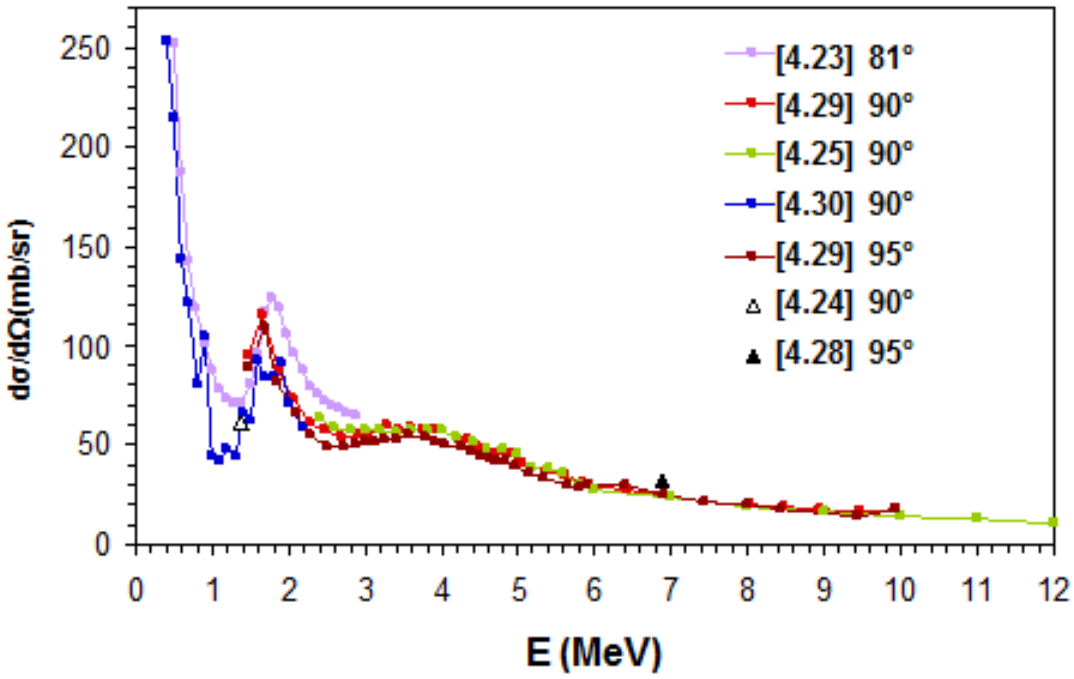

FIG. 4.6. Cross-section values of proton elastic scattering on ^{6}Li versus proton energy at scattering angles in the 81°—95° range. All the quantities are given in the laboratory frame of reference.

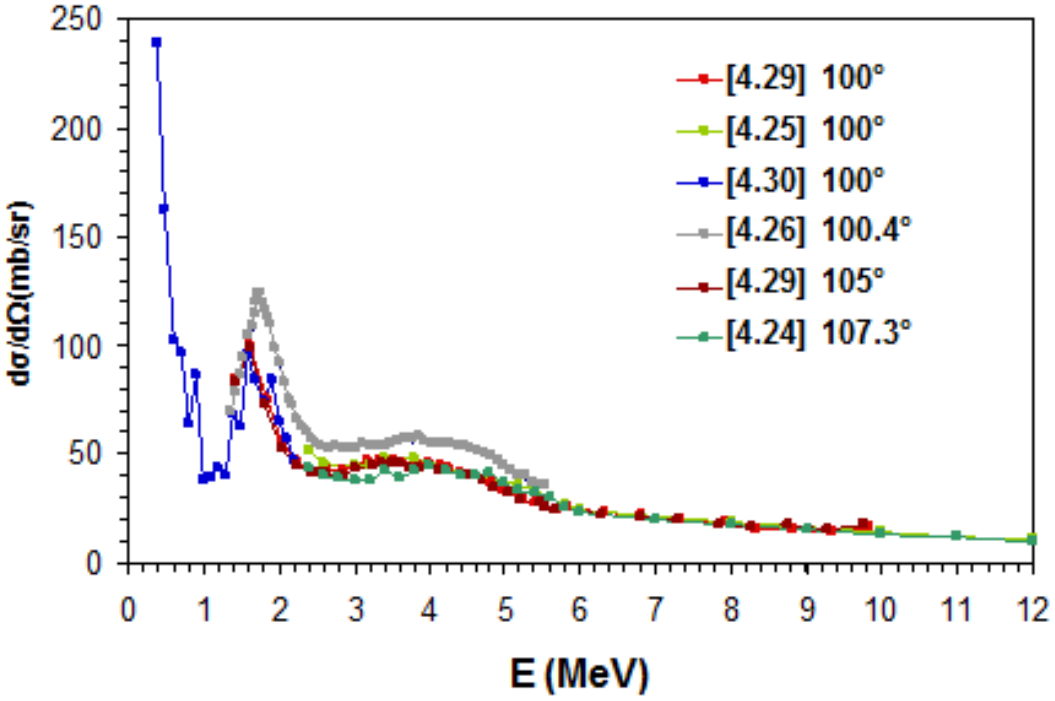

FIG. 4.7. Cross-section values of proton elastic scattering on ^{6}Li versus proton energy at scattering angles in the 100°—107° range. All the quantities are given in the laboratory frame of reference.

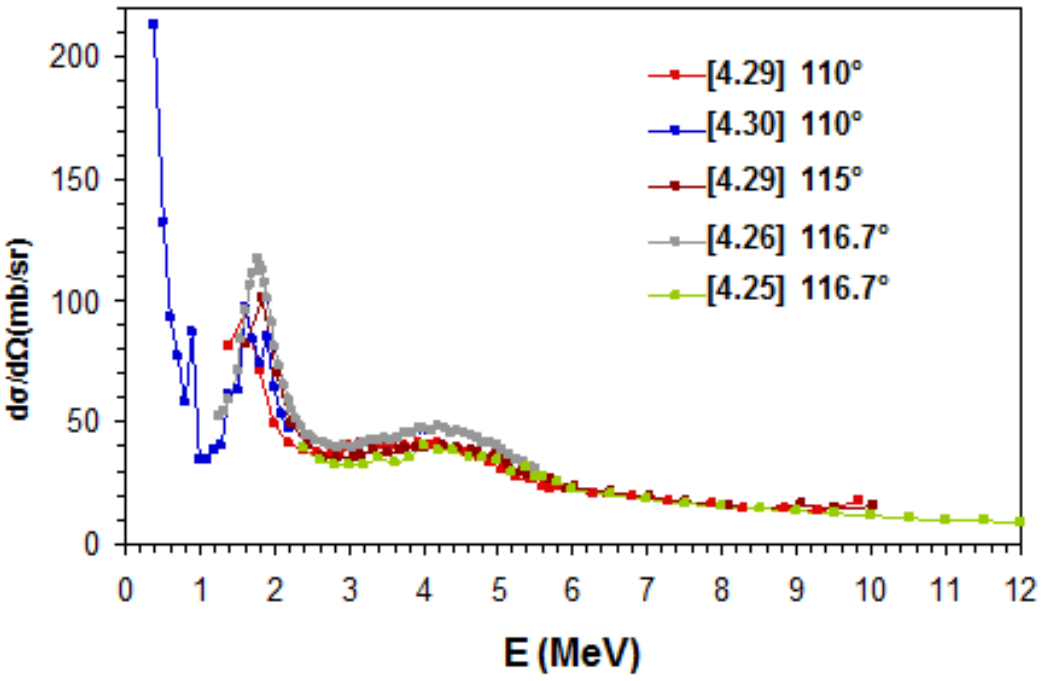

FIG. 4.8. Cross-section values of proton elastic scattering on ^{6}Li versus proton energy at scattering angles in the 110°─117° range. All the quantities are given in the laboratory frame of reference.

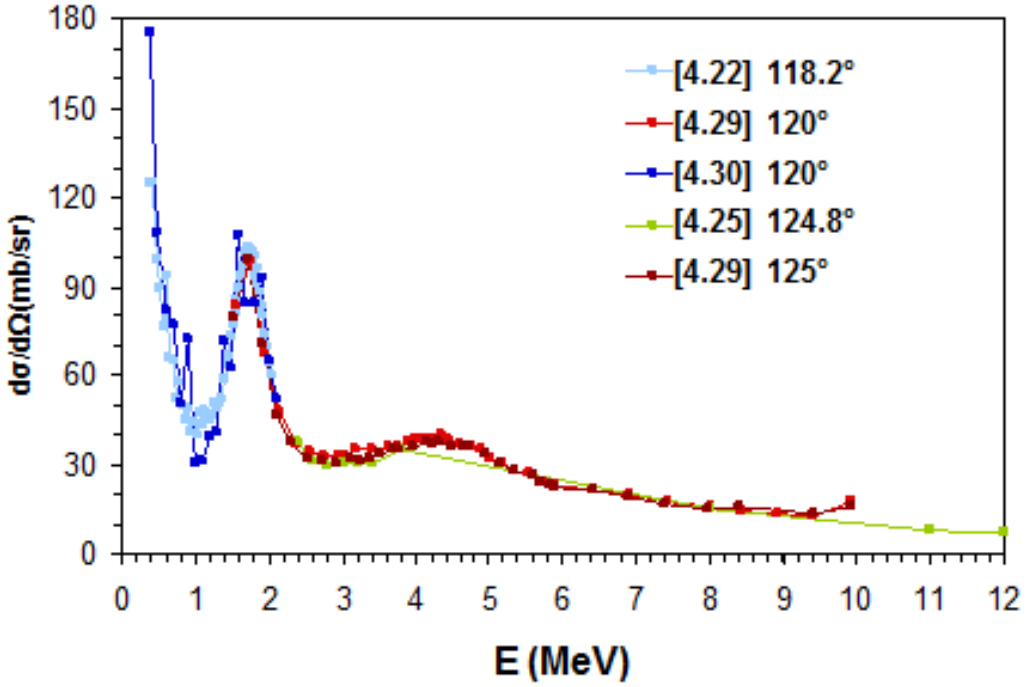

FIG. 4.9. Cross-section values of proton elastic scattering on ^{6}Li versus proton energy at scattering angles in the 118°─125° range. All the quantities are given in the laboratory frame of reference.

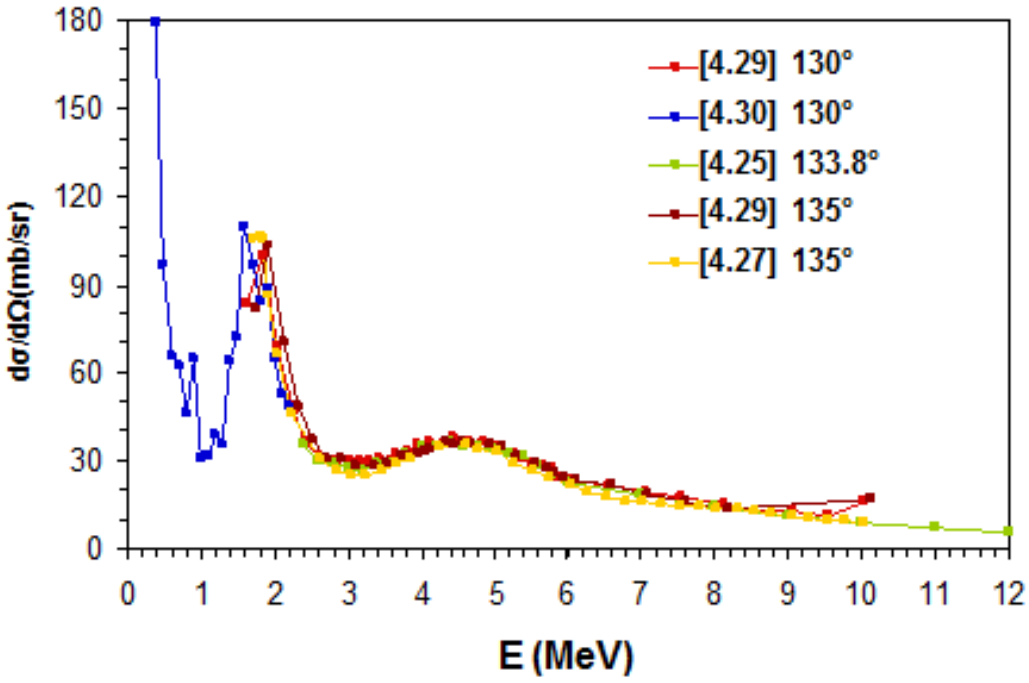

FIG. 4.10. Cross-section values of proton elastic scattering on ^{6}Li versus proton energy at scattering angles in the 130°─135° range. All the quantities are given in the laboratory frame of reference.

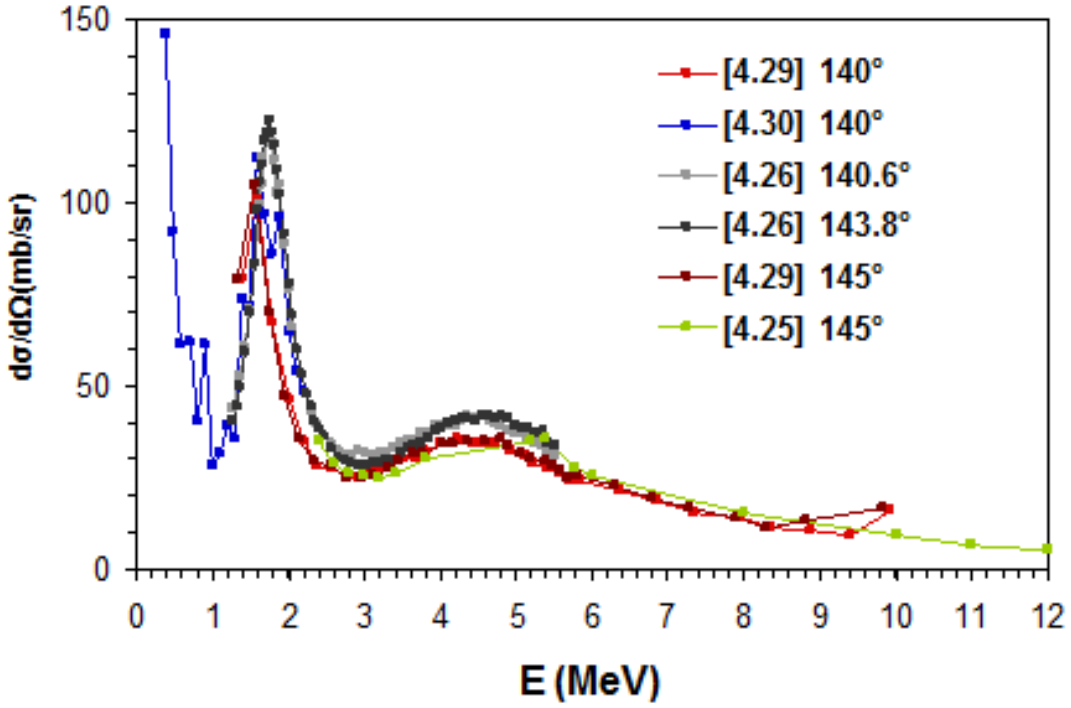

FIG. 4.11. Cross-section values of proton elastic scattering on ^{6}Li versus proton energy at scattering angles in the 140°─145° range. All the quantities are given in the laboratory frame of reference.

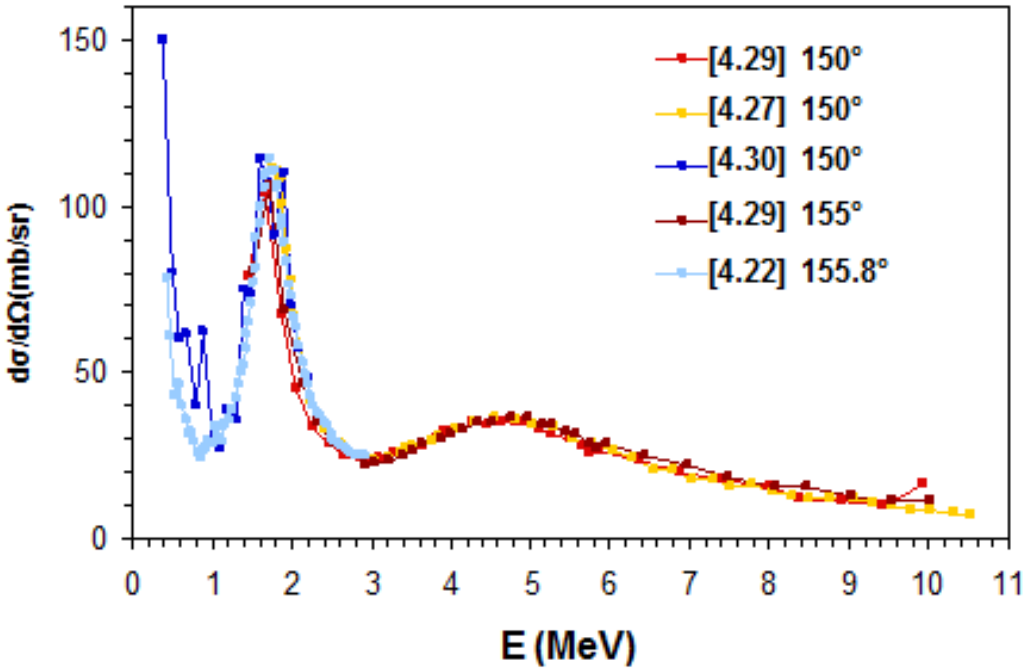

FIG. 4.12. Cross-section values of proton elastic scattering on ^{6}Li versus proton energy at scattering angles in the 150°─156° range. All the quantities are given in the laboratory frame of reference.

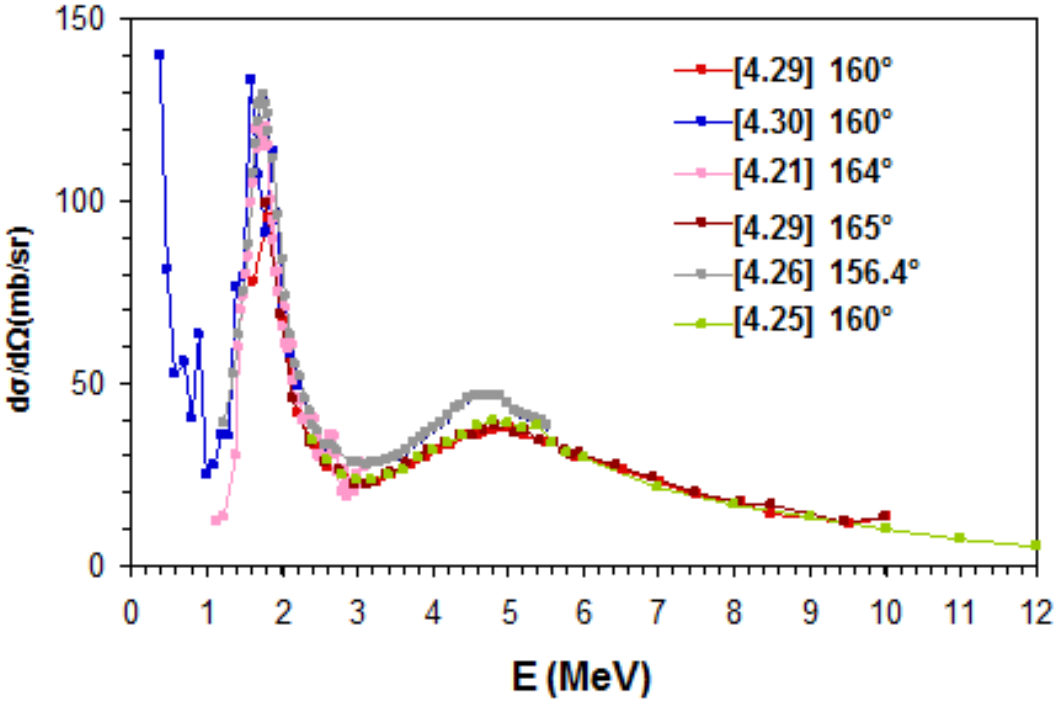

FIG. 4.13. Cross-section values of proton elastic scattering on ^{6}Li versus proton energy at scattering angles in the 160°─166° range. All the quantities are given in the laboratory frame of reference.

In general, the agreement between the data – even those referring to slightly different scattering angles – is fairly good, except in a few cases.

In particular, data from Fasoli et al. [4.26] appear systematically higher (10─15%) than the other data at similar angles [4.21, 4.27, 4.29].

Data from Haller [4.29] show discrepancies with other data with regards to the 1.8 MeV resonance for some scattering angles, especially in the resonance position (e.g. Figs 4.6, 4.7, 4.11); moreover, it should be noted that due to the large energy step employed in the measurements (about 200 keV) the shape of the resonance is hardly reproduced at all. On the contrary, Haller's data are in agreement with other data [4.25, 4.27] in the region around the broad structure at 4─5 MeV.

Data from Skill [4.30] are the only ones covering the low energy region (below 2 MeV) with high angular granularity, however they present fluctuating cross-section values that will produce corrugated spectra when implemented in simulation codes.

Recommended data
The data from [4.21, 4.22, 4.26] are recommended to be used over their respective energy ranges and scattering angles. However, note should be taken of the above comments.

4.5. $^{7}Li(p,p_0)^{7}Li$

As a first step, the data sets already existing in IBANDL [4.21, 4.31, 4.32, 4.33, 4.26, 4.24, 4.34, 4.35] were compared with the data in the original references and the agreement was good. Note that as regards the data from Bashkin and Richards [4.21], two entries exist in IBANDL: Cross-section values from entry no. 3 are taken from the original paper (where the original cross-section values are given in the laboratory frame of reference), while in entry no. 4 the data are calculated as if the original data were given in the centre-of-mass system (thus the data resulted in being scaled downwards by a factor of about 1.3). In the following only IBANDL data from entry no. 3 will be considered.

The second step was a thorough search in the literature and in nuclear databases for other available experimental data. Several data of interest for application in Ion Beam Analysis (i.e. for backscattering angles in the 90°─180° range) were retrieved [4.36, 4.31, 4.37, 4.38, 4.28, 4.39]. The data appearing in graphical form in the original references were digitized using the DataThief software [http://www.datathief.org/]. All relevant quantities were converted to the laboratory frame of reference where necessary. Table 4.2 lists the data sets found in the literature, both those already existing in IBANDL and new ones.

TABLE 4.2. AVAILABLE DATA IN THE LITERATURE ON $^{7}Li(p,p_0)^{7}Li$ CROSS SECTIONS

Reference	Data source	θ_{lab}	E_p (MeV)	Target	Quoted uncertainties	Data format
[4.21]	IBANDL	164°	0.88–3.68	Li metal evaporated upon thin Ni foil	20%	Tabular
[4.24]	IBANDL	90°	1.36	0.03 to 0.1 mg/cm^2 natural LiF evaporated on a C foil	12% statistical & systematic	Tabular
[4.26]	IBANDL	89.2° 101.5° 117.9° 134.6° 144.5° 166.2°	3.0–5.5 1.2–5.5	Isotopically enriched ^{7}Li (99.3%) evaporated on a 1000 Å Ni foil	–	Tabular
[4.28]	Original data	95.0°	6.868	Natural lithium LiI evaporated on a Formvar backing	2%	Tabular
[4.31]	IBANDL, EXFOR	102.0° 123.1° 137.9° 156.70°	0.37–1.40	Natural Li on Cu backing	5%	Tabular
[4.32]	IBANDL	90°	1.36	–	4%	Tabular
[4.33]	IBANDL	102.0° 123.1° 145.3° 164.9°	1.35–3.00	Thin lithium layer evaporated on a thin Zapon film	10%	Tabular
[4.34]	IBANDL	150°	3.0–7.2	50 µg/cm^2 LiF on 30 µg/cm^2 C, coated with 20 µg/cm^2 Au	4%	Tabular
[4.35]	IBANDL	118.05°	1.2–3.6	–	–	Tabular
[4.36]	EXFOR	137.8°	0.28–1.40	Li evaporated on Be foil	20%	Tabular
[4.37]	EXFOR	123.1° 145.4° 163.9°	2.36–12.1	Thin isotopically enriched ^{7}Li (99.97%) layer evaporated on a thin Formvar film	15%	Tabular
[4.38]	EXFOR	90° 120° 140°	2.58–10.6	Enriched ^{7}Li (99.99%, 150 µg/cm^2) evaporated onto 45 µg/cm^2 Ni backings	–	Tabular
[4.39]	Original data	140° 160°	0.8–2.2	LiF single crystal implanted with 300 keV Ar^{2+}, coated with $62 \cdot 10^{15}$ at/cm^2 Au	–	Tabular

Figures 4.14 – 4.18 present in graphical form all the cross sections listed in Table 4.2, except for data from [4.35] since they are given in arbitrary units; data referring to similar scattering angles are shown together. In the graphs the proton energies and the differential cross sections are given in the laboratory frame of reference, with energy units in MeV and cross-section units in mb/sr.

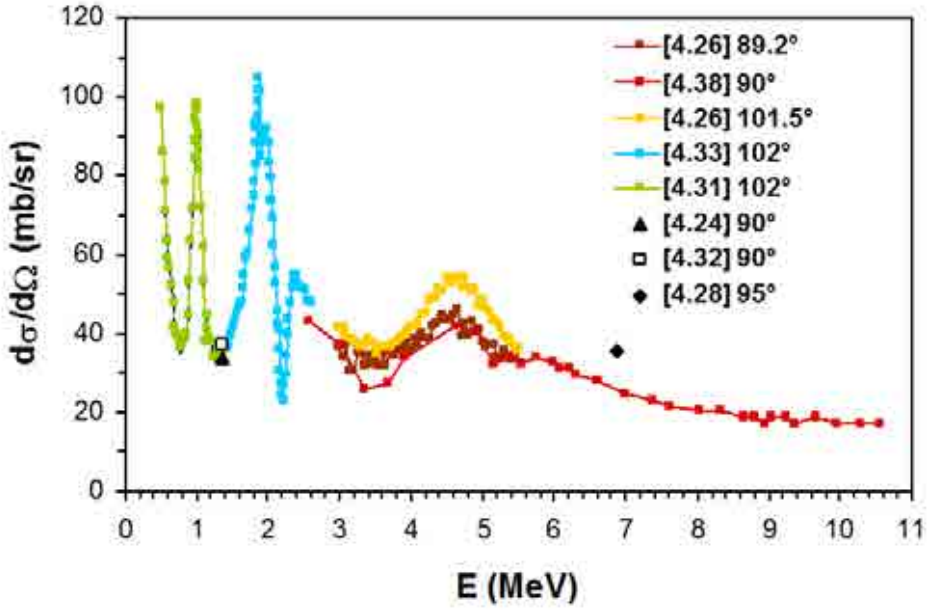

FIG. 4.14. Cross-section values of proton elastic scattering on ^{7}Li versus proton energy at scattering angles in the 90°─102° range. All the quantities are given in the laboratory frame of reference.

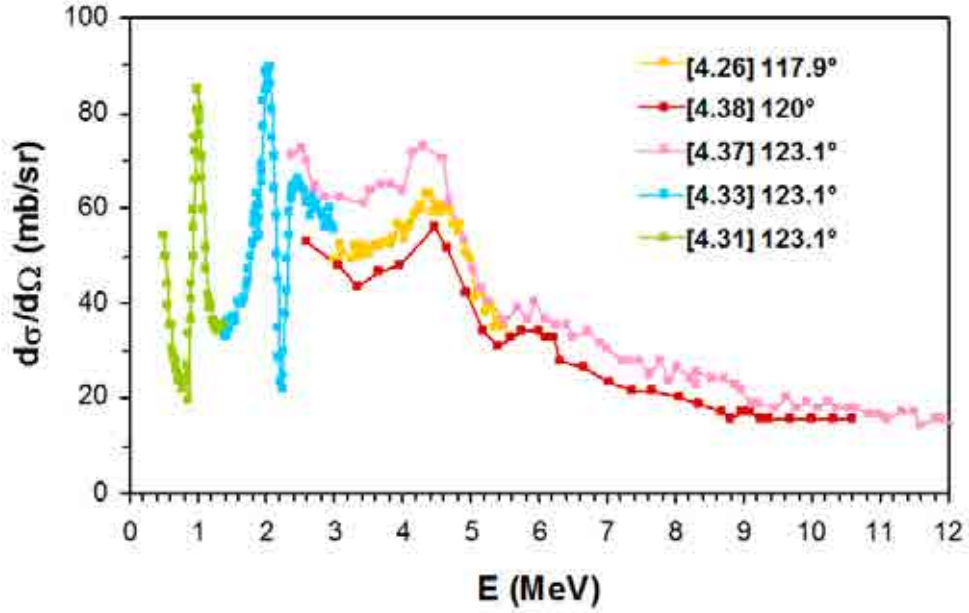

FIG. 4.15. Cross-section values of proton elastic scattering on ^{7}Li versus proton energy at scattering angles in the 118°─123° range. All the quantities are given in the laboratory frame of reference.

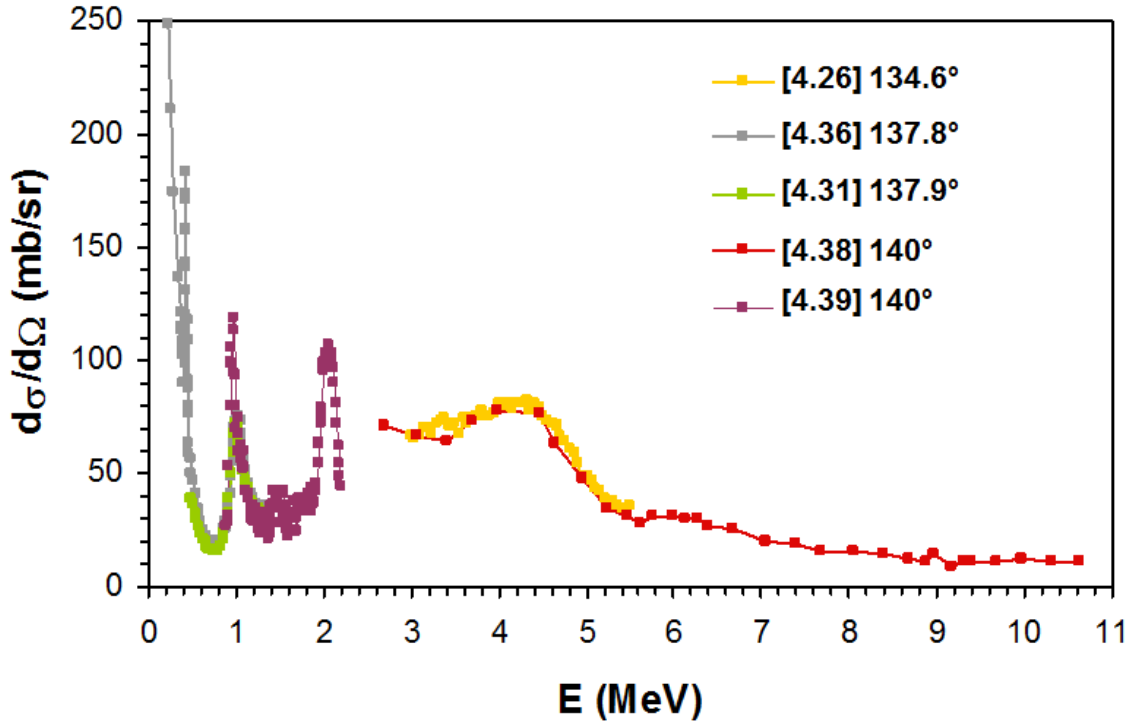

FIG. 4.16. Cross-section values of proton elastic scattering on ^{7}Li versus proton energy at scattering angles in the 134°—140° range. All the quantities are given in the laboratory frame of reference.

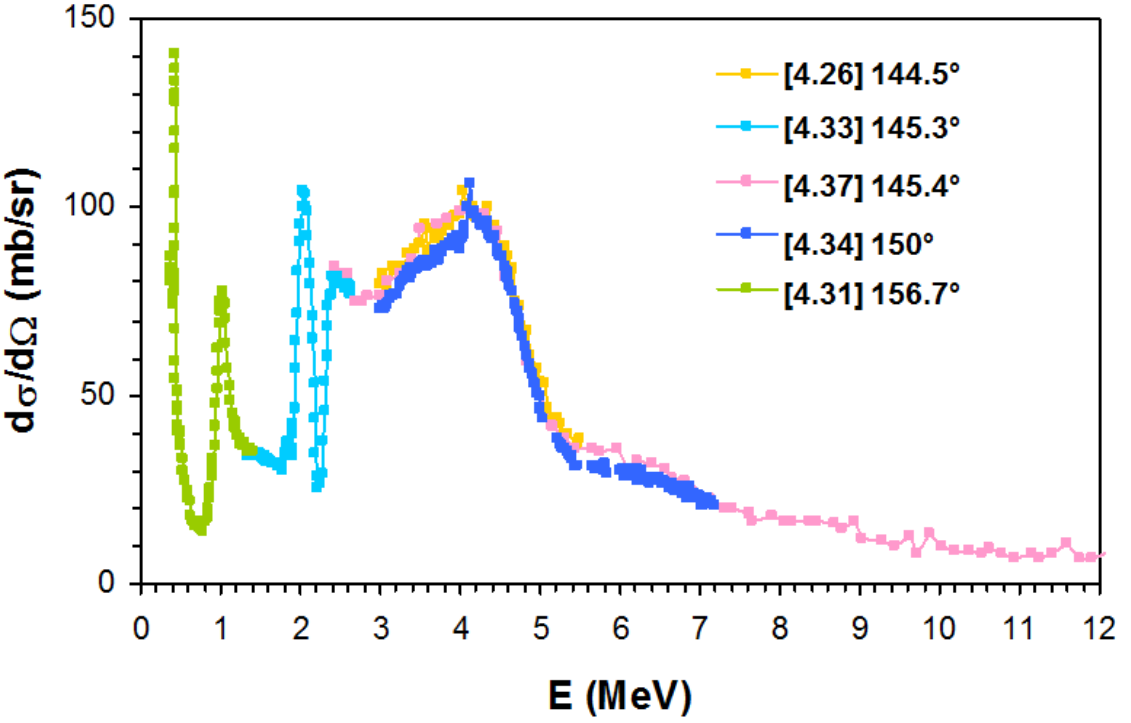

FIG. 4.17. Cross-section values of proton elastic scattering on ^{7}Li versus proton energy at scattering angles in the 145°—157° range. All the quantities are given in the laboratory frame of reference.

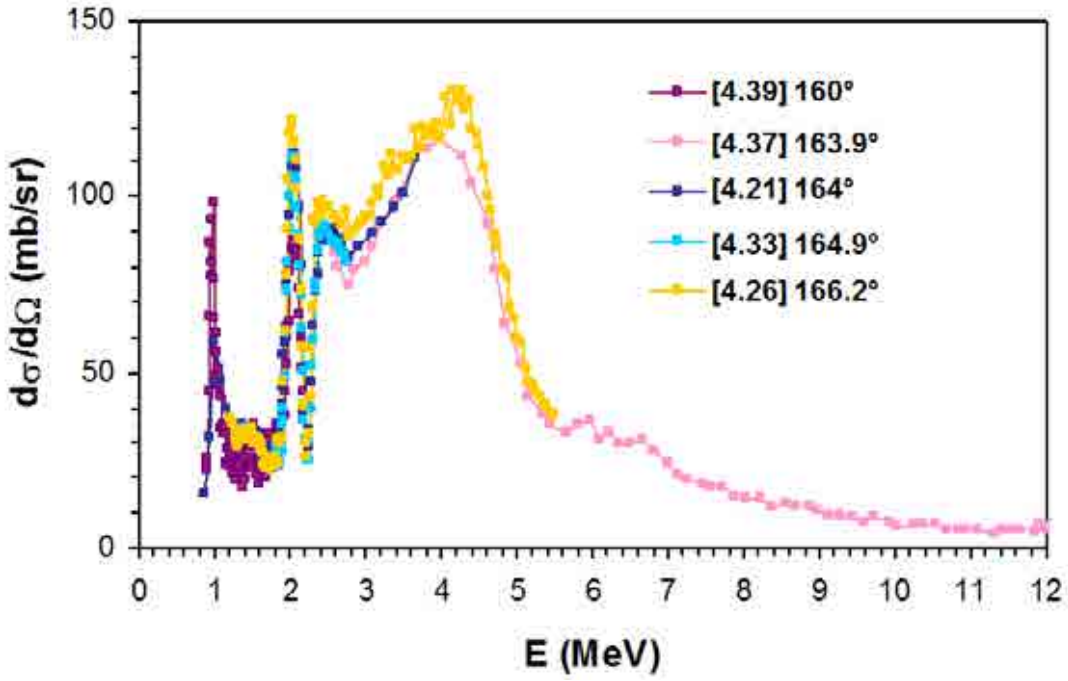

FIG. 4.18. Cross-section values of proton elastic scattering on ^{7}Li versus proton energy at scattering angles in the 160°─166° range. All the quantities are given in the laboratory frame of reference.

In general, the agreement between the data – even those referring to slightly different scattering angles – is fairly good, except in a few cases.

In particular, data from Kilian [4.38] appear systematically lower (10─15%) than the other data at similar angles [4.33, 4.26].

From Fig.4.15 a disagreement appears between data from Malmberg [4.33] and Gleyvod [4.37] at a scattering angle of 123°: cross-section values from [4.37] are about 10% higher than those from [4.33]; however, this systematic disagreement is within the experimental uncertainties quoted in Malmberg's and Gleyvod's works, 10% and 15% respectively.

From Fig.4.16, and Fig.4.18 as well, it appears that the position of the resonance peak at 1.03 MeV as obtained from the data of L. Ramos Wahl [4.39] is shifted by 50─60 keV to lower energy with respect to the other data [4.36, 4.31] and [4.21], respectively; the peak is also narrower and at its maximum the cross-section value is about 75% higher than other data [4.36, 4.31].

In Fig.4.18, the cross-section value at the maximum of the 2.05 MeV resonance peak from L. Ramos Wahl [4.39] is 20% lower as compared to the one from both Bashkin and Richards [4.21] and Malmberg [4.33]. A similar disagreement is obtained when comparing the same data from L. Ramos Wahl [4.39] to those from Malmberg [4.33] at a scattering angle of 145.3°, instead of 164.9°. Again in Fig.4.18, with respect to the peaks in the cross section at 2.05 MeV and 2.5 MeV data from Fasoli [4.26] are 10% higher than those from Bashkin and Richards [4.21] and Malmberg [4.33], anyway this difference falls within the experimental uncertainties quoted in the latter two works, 20% and 10% respectively.

Recommended data
The data from [4.36], [4.31], [4.33], [4.26] and [4.34] are recommended to be used over their respective energy ranges and scattering angles.

The data from Kilian [4.38] appear systematically lower (10─15%) than the other data at similar angles [4.33, 4.26]. At a scattering angle of 123° the cross-section values from [4.37] are about 10% higher than those from [4.33], which is within the experimental uncertainties quoted in the papers.

The position of the resonance peak at 1.03 MeV as obtained from the data of L. Ramos Wahl [4.39] is shifted by 50─60 keV to lower energy with respect to the other data [4.36, 4.21, 4.31]; the peak is also narrower and higher than other data [4.36, 4.31]. The cross-section value of the maximum of the 2.05 MeV resonance peak from L. Ramos Wahl [4.39] is 20% lower as compared to the one from both Bashkin [4.21] and Malmberg [4.33]. A similar disagreement is obtained when comparing the same data from L. Ramos Wahl [4.39] to those from Malmberg [4.33] at a scattering angle of 145.3°. The peaks in the cross section at 2.05 MeV and 2.5 MeV from Fasoli [4.26] are 10% higher than those from Bashkin [4.21] and Malmberg [4.33], which falls within the experimental uncertainties quoted in the latter two works.

4.6. $^{9}Be(p,p_0)^{9}Be$

The cross-section data for the Leavitt [4.40], Liu [4.41] and Mozer [4.42] measurements at about 160─170° are shown in Figs. 4.19 – 4.21. Liu performed his measurements in a wide energy range (from 0.2 to over 3 MeV), while Mozer and Leavitt performed measurements only in a narrower energy range (Mozer 0.2─1.7 MeV, Leavitt 2.4─2.7 MeV). Mozer's and Liu's data agree within about 5% within the whole energy range where both data are available. Liu's cross-section values approach the Rutherford cross section at energies below about 0.2 MeV. Only for the cross-section minimum at about 1.08 MeV some discrepancy between Liu and Mozer is observed, see Fig. 4.20. For the broad resonance at about 2.53 MeV Leavitt and Liu show qualitative agreement. However, the energy of the resonance is shifted by about 30 keV and the cross section in the maximum disagrees by about 30%, see Fig. 4.21.

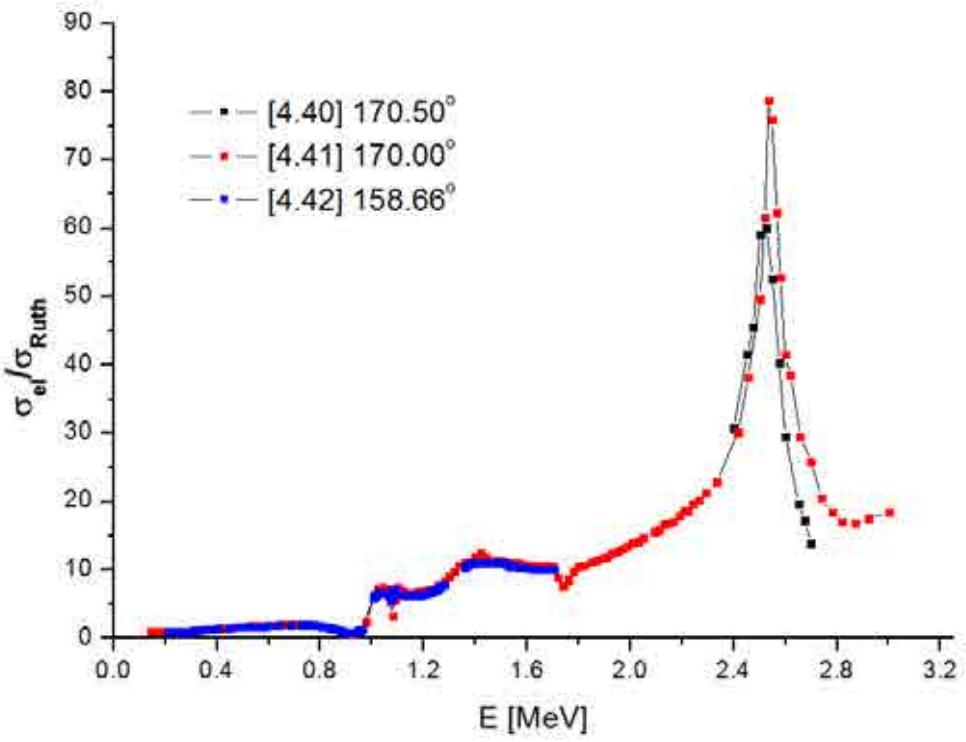

FIG. 4.19. Comparison of Leavitt [4.40], Liu [4.41] and Mozer [4.42] for $^{9}Be(p,p_0)$ at about 160─170°.

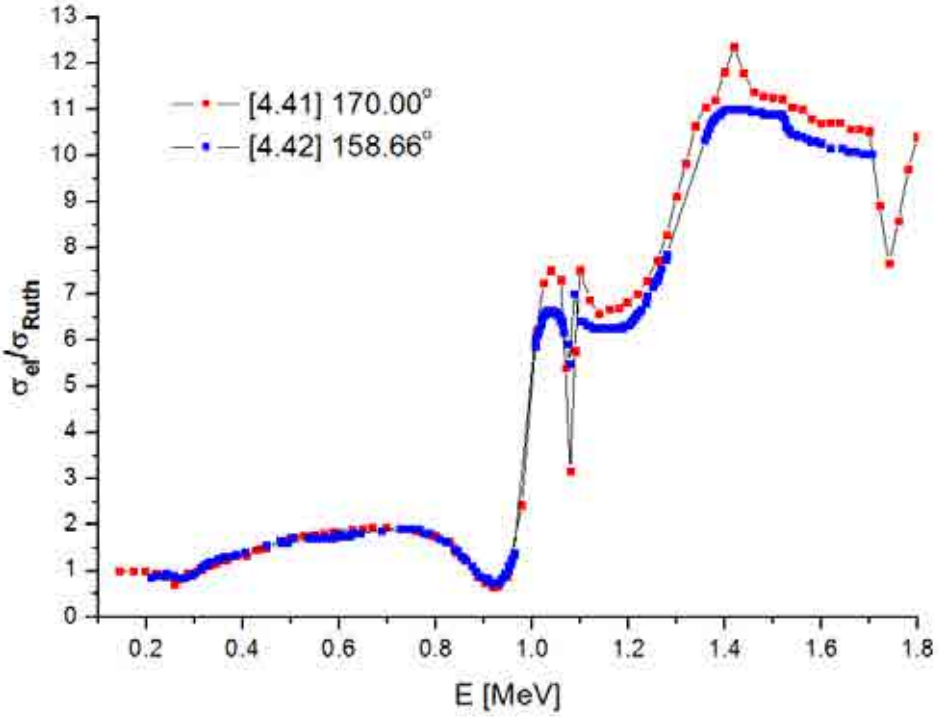

FIG. 4.20. Comparison of Liu [4.41] and Mozer [4.42] for $^{9}Be(p,p_0)$ at about 160─170°.

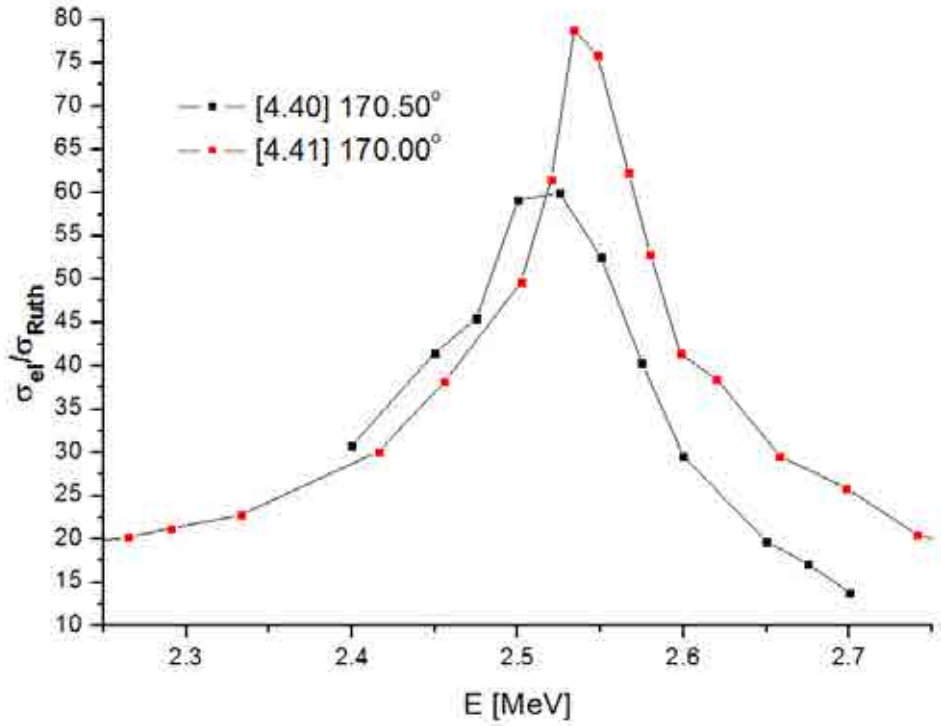

FIG. 4.21. Comparison of Leavitt [4.40], Liu [4.41] for $^{9}Be(p,p_0)$ at about 170°.

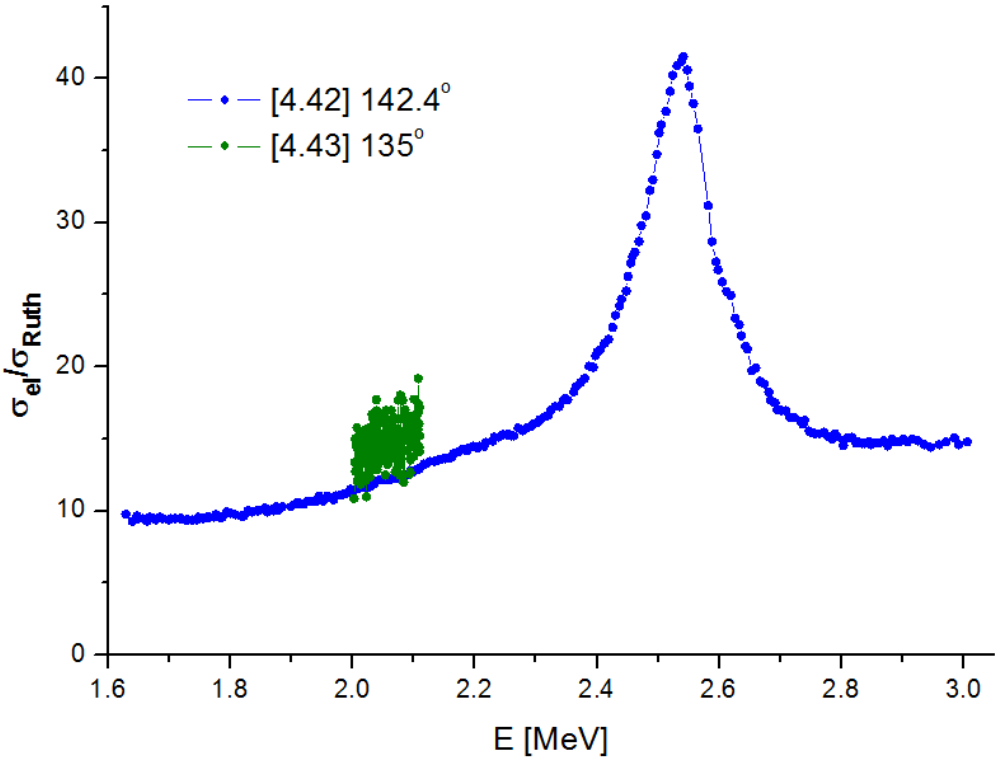

FIG. 4.22. Comparison of Mozer [4.42] and Siksin [4.43] for $^{9}Be(p,p_0)$ at 135─142.4°.

A comparison of the Mozer [4.42] and Siksin [4.43] data at 135─142.2° is shown in Fig. 4.22. Siksin measured only in a very limited energy range from 2.0─2.1 MeV, and the data show a large scatter. The Mozer and Siksin data agree within about 20%, which shows that the Mozer data cannot be totally off.

Recommended data

Mozer [4.42] and Liu [4.41] show very good agreement at 158.7─170°, and the Liu and Leavitt [4.40] data are at least in qualitative agreement at 2.4─2.7 MeV. Both Liu and Mozer data therefore can be recommended, but with preference to the Liu data due to the better resolution of the resonances. Due to the good agreement with Liu and the confirmation by Siksin [4.43] (although with a rather large uncertainty of 20%), the Mozer data [4.42] can also be recommended at 142.4°. An additional confirmation at this angular range would be desirable.

4.7. $^{10}B(p,p_0)^{10}B$

The largest measurement series was performed by Chiari et al. [4.44], who compared their data with most previous data. The experimental data of Brown et al. [4.36] were not taken into account by Chiari and will be taken into special consideration here. A complete list of data can be found in Table 4.3.

Fig. 4.23 compares experimental data of Chiari et al. [4.44] with data of Overley and Whaling [4.45] at an angle of 120°. The same is done for an angle of 155° in Fig.4.24. In both cases the data of Overley andWhaling are about 20% higher than those of Chiari, which points to a systematic error.

In Fig. 4.25 the data of Chiari et al. [4.44] are compared with those of Brown et al. [4.36] in the angular range from 135° to 140°. For energies up to 1.7 MeV both measurements of Chiari are very close together, while the data of Brown are up to 10% lower. In the energy range from 1.5 to 1.7 MeV the data sets are almost consistent.

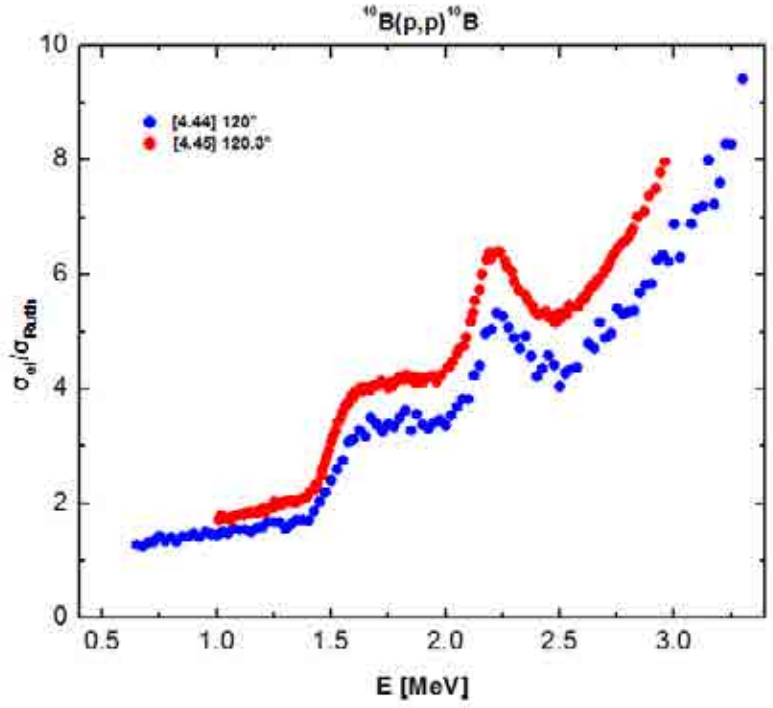

FIG. 4.23. Comparison of different experimental data for $^{10}B(p,p_0)^{10}B$ at 120°.

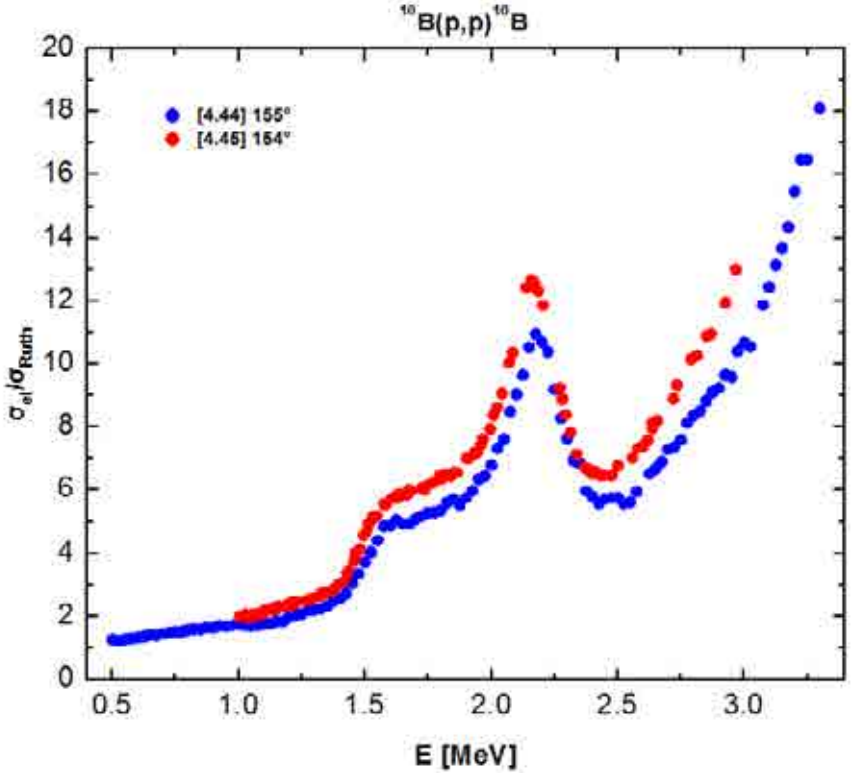

FIG. 4.24. Comparison of different experimental data for $^{10}B(p,p_0)^{10}B$ at 155°.

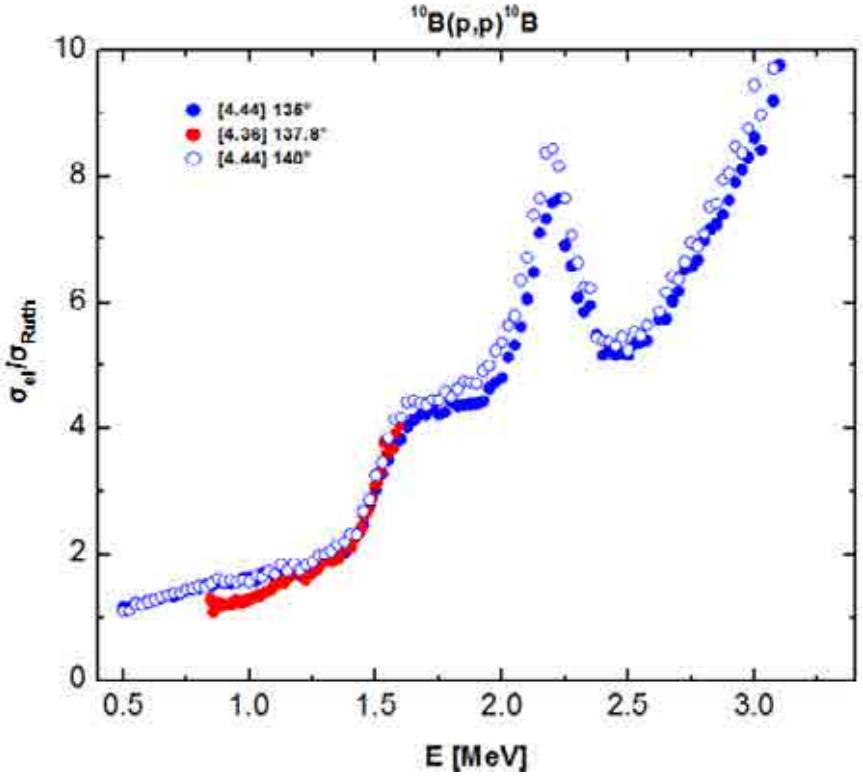

FIG. 4.25. Comparison of different experimental data for $^{10}B(p,p_0)^{10}B$ at 135°─140°.

The oldest measurements (done before 1960), i.e. Brown et al. [4.36], are 10% lower than those by Chiari et al. [4.44]. This was already observed for the $^{11}B(p,p)^{11}B$ data and might be a systematic error resulting from the inferiority of the vacuum in the 1950s and 1960s. In contrast, the data obtained by Overley and Whaling [4.45] are 15% higher than the Chiari data.

To clarify the contradiction between Chiari and Overley and Whaling, further experiments are necessary. In the meantime, Chiari's results [4.44] might be a good choice for cross-section data for the $^{10}B(p,p)^{10}B$ backscattering. The stated error is 5%. The data were provided in numeric form to IBANDL, so that no additional digitizing errors occured. A drawback is the large statistical error, which may result in corrugated spectra.

TABLE 4.3. PUBLICATIONS CONTAINING $^{10}B(p,p)^{10}B$ BACKSCATTERING DATA

Energy (MeV)	**Angle Lab (°)**	**Error**	**Format**	**Reference**	**IBANDL**	**EXFOR**
0.9─1.6	137.8	─	Graph	[4.36]	**Data missing**	A1457002
0.6─3.0	84.3	7%	Graph	[4.45]	data included	F0211002
0.6─3.1	120.3	7%	Graph	[4.45]	data included	F0211002
0.6─3.2	154	7%	Graph	[4.45]	data included	F0211002
0.5 – 2.9	various		Graph	[4.45]	Ang.distribution not suitable	F0211003
5.3─13.0	59.7	─	Graph	[4.46]	*data unsuitable too high energy*	F0156002
5.3─13.0	85.65	─	Graph	[4.46]	*data unsuitable too high energy*	F0156002
5.3─13.0	110.54	─	Graph	[4.46]	*data unsuitable too high energy*	F0156002
5.3─13.0	129.7	─	Graph	[4.46]	*data unsuitable too high energy*	F0156002
5.3─13.0	152.87	─	Graph	[4.46]	*data unsuitable too high energy*	F0156002
5.0─16.5	65	─	Graph	[4.47]	*data unsuitable too high energy*	F0093001
5.0─16.5	85	─	Graph	[4.47]	*data unsuitable too high energy*	F0093001
5.0─16.5	90	─	Graph	[4.47]	*data unsuitable too high energy*	F0093001
5.0─16.5	115	─	Graph	[4.47]	*data unsuitable too high energy*	F0093001
5.0─16.5	135	─	Graph	[4.47]	*data unsuitable too high energy*	F0093001
5.0─16.5	155	─	Graph	[4.47]	*data unsuitable too high energy*	F0093001
5.4─7.5	150	─	Graph	[4.47]	*data unsuitable too high energy*	F0093001
0.5─3.3	100	5%	─*	[4.48]	data included	
0.5─3.3	105	5%	─*	[4.44]	data included	O0922002
0.5─3.3	110	5%	Graph*	[4.44]	data included	O0922002
0.5─3.3	115	5%	─*	[4.44]	data included	O0922002
0.5─3.3	120	5%	─*	[4.44]	data included	O0922002
0.5─3.3	125	5%	─*	[4.44]	data included	O0922002
0.5─3.3	130	5%	─*	[4.44]	data included	O0922002
0.5─3.3	135	5%	Graph*	[4.44]	data included	O0922002
0.5─3.3	140	5%	─*	[4.44]	data included	O0922002
0.5─3.3	145	5%	─*	[4.44]	data included	O0922002
0.5─3.3	150	5%	Graph*	[4.44]	data included	O0922002
0.5─3.3	155	5%	─*	[4.44]	data included	O0922002
0.5─3.3	160	5%	─*	[4.44]	data included	O0922002
0.5─3.3	165	5%	─*	[4.44]	data included	O0922002
0.5─3.3	170	5%	Graph & Table*	[4.44]	data included	O0922002

*data provided in numerical form by Chiari.

Recommended data

Currently Chiari's results [4.44] are the best choice for cross-section data for $^{10}B(p,p)^{10}B$ backscattering. These data are available from 105° to 170° scattering angle from 0.5–3.3 MeV. The stated absolute error is 5%. Drawback is the statistical error of the individual data points, which may result in corrugated spectra. Further experiments are necessary to clarify the contradiction between Chiari [4.44] and Overley and Whaling [4.45].

4.8. $^{11}B(p,p_0)^{11}B$

The largest measurement series was done by Chiari et al. [4.44], which allows us to compare all previous data with their measurements. A complete list can be found in Table 4.4.

The data from Mashkarov et al. [4.49] and Dejneko et al. [4.50] at about 120° are compared in Fig. 4.26. Both data sets are from the same group, but published in different papers. The Mashkarov data were published in the laboratory system. According to the original publication, the Dejneko cross-section data are in the laboratory system, while the scattering angle is given in the centre-of-mass system and is 124° (which converts to 119.4° lab angle). This results in a disagreement of both data sets, as can be seen in the upper panel of Fig. 4.26. Assuming the Dejneko data actually are in the centre-of-mass system results in a much better agreement with the Mashkarov data, as can be seen in the lower panel of Fig. 4.26. It is therefore assumed that the original publication of Dejneko is erroneous, and the data are in the centre-of-mass and not in the laboratory system.

A comparison of the measurements at 120° is shown in Fig. 4.27. The Mashkarov [4.49] and Chiari [4.44] data agree very well. There is also good agreement with the Dejneko [4.50] data, if we assume that the published data are in the centre-of-mass system (see above). The angles 150° and 155° are shown in Fig. 4.28. Symon's and Treacy's data [4.51] agree with Chiari's data [4.44] over most of the energy range, but the dip at 3.1 MeV is missing. This is probably due to the relatively large energy step of 0.1 MeV. Tautfest's and Rubin's measurement [4.52] is 10% lower than Chiari's.

Fig. 4.29 compares measurements by Chiari et al. [4.44], Mayer et al. [4.53], and Segel et al. [4.54] at angles between 160° and 165°. Mayer's data have the same shape as Chiari's data, but are consistently about 20% higher. This indicates a problem with the absolute cross-section values, while the individual data points are in agreement with each other. Segel's data are consistent with Chiari's data up to 2 MeV, but at higher energies large discrepancies occur. The minima and maxima are at the same energies, but Segel's data cannot be scaled to Chiari's or Mayer's.

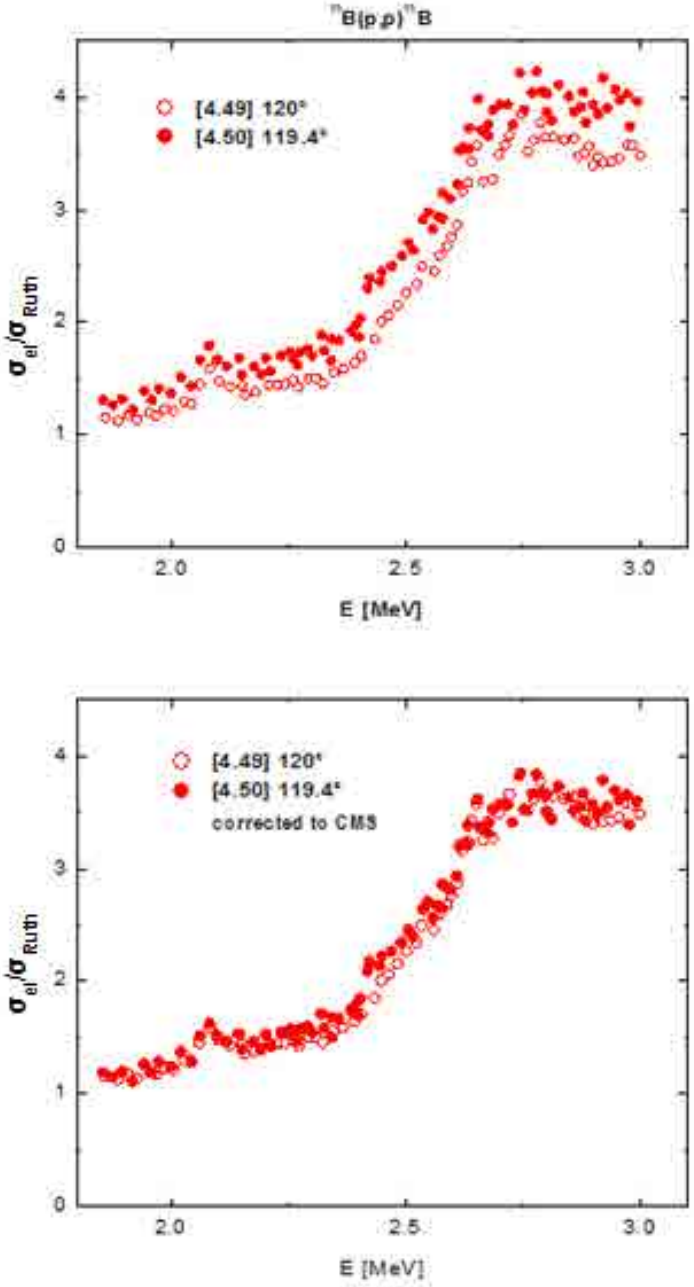

FIG. 4.26. Comparison of the Mashkarov [4.49] and Dejneko [4.50] data for $^{11}B(p,p_0)^{11}B$ at about 120°. The upper figure shows the data as published, the lower figure assumes that the Dejneko data are in the centre-of-mass system (CMS) and have been erroneously assigned to the laboratory system in the original publication.

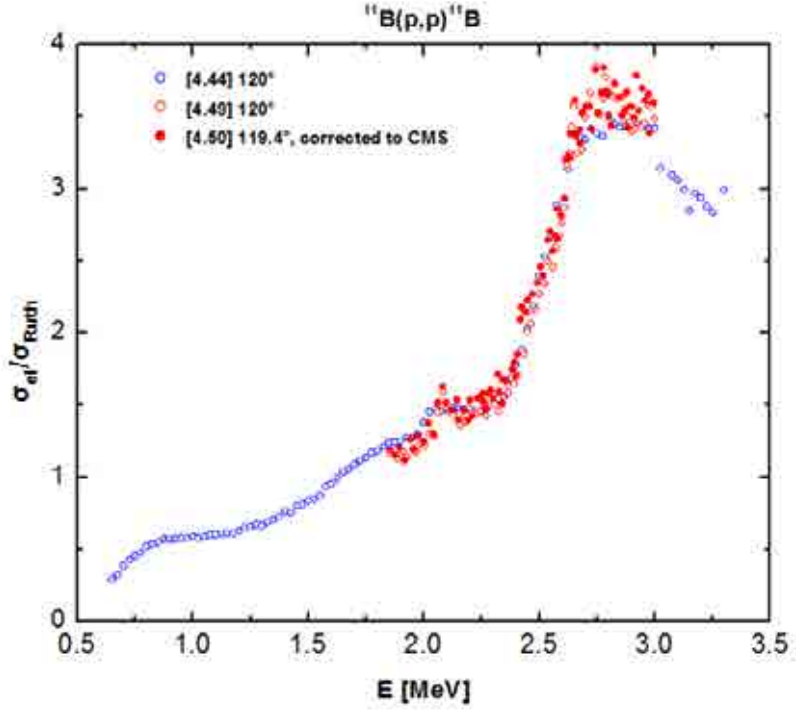

FIG. 4.27. Comparison of different experimental data for $^{11}B(p,p_0)^{11}B$ at 120°.

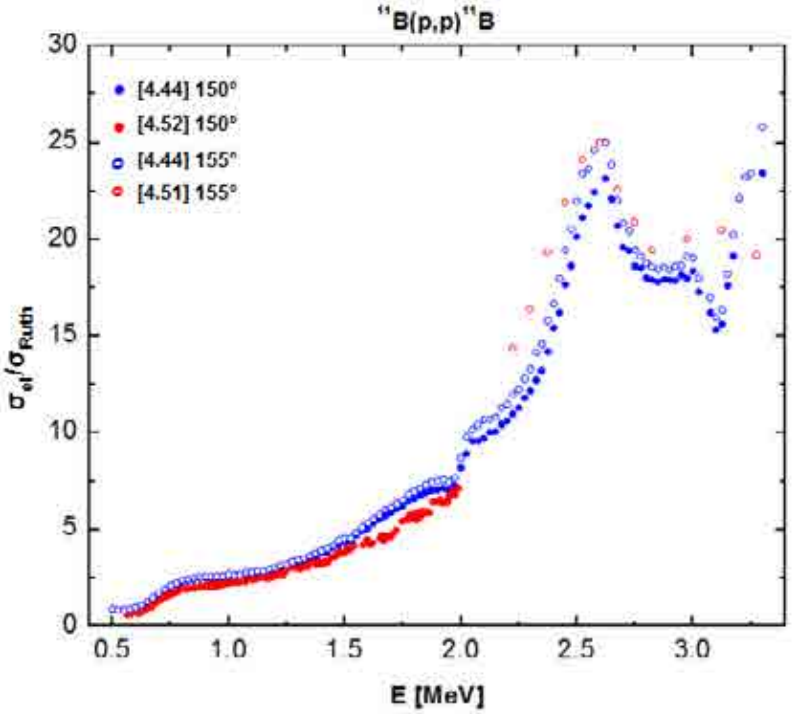

FIG. 4.28. Comparison of different experimental data for $^{11}B(p,p_0)^{11}B$ at 150° and 155°.

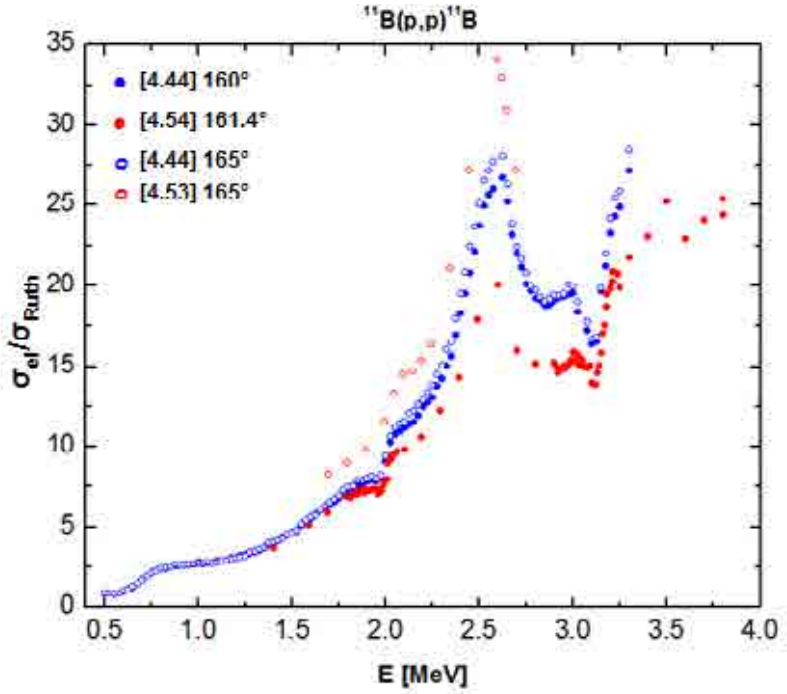

FIG. 4.29. Comparison of different experimental data for $^{11}B(p,p_0)^{11}B$ at 160°─165°.

Generally, it can be concluded that all measurements show the same main features in the data, but the different measurements are up to 20% apart from each other.

The oldest measurements (data measured before 1960), i.e. Tautfest and Rubin [4.52], are 10% lower than the measurements done by Chiari et al. [4.44]. The same observation was made for the $^{10}B(p,p)^{10}B$ backscattering data. This might hint to some systematic error, probably connected with the inferiority of the vacuum. In contrast, the data taken by Mayer et al. [4.53] are 20% higher than those from Chiari. In this connection Chiari observed that "these discrepancies are essentially systematic, even though there is not a well-defined trend" [4.44].

The Chiari data are in very good agreement with the Mashkarov [4.49] and Dejneko data [4.50] at 120° and lie between all available data at 150─165°. Although further measurements are desirable, especially in order to resolve the conflict between Chiari and Mayer, Chiari's results are probably a good basis for cross-section data for $^{11}B(p,p)^{11}B$ backscattering. The reported error of 5% make them suitable. The data were provided in numeric form to IBANDL, so that no additional digitizing errors occurred. A drawback is the large statistical error, which may result in corrugated spectra.

TABLE 4.4. PUBLICATIONS WITH $^{11}B(p,p)^{11}B$ BACKSCATTERING DATA

Energy (MeV)	**Lab Angle (°)**	**Error**	**Data**	**Ref.**	**IBANDL**	**EXFOR**	**Action**
0.6─2.0	150	─	Graph	[4.52]	data included	C0847002	
2.2─3.2	155	─	Graph	[4.51]	data included	─	
1.0─3.8	89	─	Graph	[4.54]	data unsuitable for RBS due to angle	F0332008	Data converted from EXFOR to IBANDL
1.0─3.8	161.4	─	Graph	[4.54]	data included	F0332008	
5.4─7.5	150	─	Graph	[4.48]	data unsuitable for RBS due to high energy	F0288003	
0.1─1.2	37.5	─	Graph	[4.55]	data unsuitable for RBS due to angle	A0413006	
1.7─2.7	165	7%	Graph &Table**	[4.53]	data included	O0864003	
0.5─3.3	100	5%	─*	[4.44]	data included	O0922003	
0.5─3.3	105	5%	─*	[4.44]	data included	O0922003	
0.5─3.3	110	5%	Graph*	[4.44]	data included	O0922003	
0.5─3.3	115	5%	─*	[4.44]	data included	O0922003	
0.5─3.3	120	5%	─*	[4.44]	data included	O0922003	

TABLE 4.4. (CONT')

Energy (MeV)	Lab Angle (°)	Error	Data	Ref.	IBANDL	EXFOR	Action
0.5─3.3	125	5%	─*	[4.44]	data included	O0922003	
0.5─3.3	130	5%	─*	[4.44]	data included	O0922003	
0.5─3.3	135	5%	Graph*	[4.44]	data included	O0922003	
0.5─3.3	140	5%	─*	[4.44]	data included	O0922003	
0.5─3.3	145	5%	─*	[4.44]	data included	O0922003	
0.5─3.3	150	5%	Graph*	[4.44]	data included	O0922003	
0.5─3.3	155	5%	─*	[4.44]	data included	O0922003	
0.5─3.3	160	5%	─*	[4.44]	data included	O0922003	
0.5─3.3	165	5%	─*	[4.44]	data included	O0922003	
0.5─3.3	170	5%	Graph & Table*	[4.44]	data included	O0922003	
1.9─3.0	120			[4.49]	**Data missing**	F0349003	Data converted from EXFOR to IBANDL
1.9─3.0	120			[4.50]	**Data missing**	F0285002	Data converted from EXFOR to IBANDL assuming that original data were in CM system
1.8─4.1	137.2			[4.56]	data unsuitable due to arbitrary units	F0136003	

*data provided in numeric form by M. Chiari.
**data provided in numeric form by M. Mayer.

Recommended data

The data of Chiari [4.44] are in very good agreement with the Mashkarov [4.49] and Dejneko data [4.50] at 120° and lie between all available data at 150─165°. They are therefore a good basis for cross-section data for $^{11}B(p,p)^{11}B$ backscattering. These data are available from 100° to 170° scattering angle from 0.5–3.3 MeV. The stated absolute error is 5%. A drawback is the statistical error of the individual data points, which may result in corrugated spectra. Further measurements are desirable, especially in order to resolve the conflict between Chiari [4.44] and Mayer [4.50].

4.9. $^{12}C(p,p_0)^{12}C$

IBANDL (on 01/02/2008) reported only three datasets for $^{12}C(p,p)$ differential cross sections in the energy region from 3.5–5 MeV.

Tosaki data were transferred from the original publication [4.57] to IBANDL without the errors.

The second dataset reported in IBANDL is from Jackson et al. [4.58]. They reported cross sections from 400 keV up to 4360 keV for several c.m. scattering angles 169.2°, 148.9°, 127.8° and 106.4° that corresponds to 168.2°, 146.3°, 123.8° and 101.7° lab angles. Differential cross sections are reported only in graphical form and in c.m. system. Data for 168.2° and 146.2° are present in IBANDL. For two other angles 123.8° and 101.7° data can be found in EXFOR (in R33 format). For all angles, EXFOR data were transferred to c.m. system as reported in the original publication and compared with figures from the original publication. It was found that digitized data from EXFOR are in agreement with data published in the original publication.

The third dataset reported in IBANDL is the recently published data set from Caciolli et al. [4.34]. They report proton cross sections on F, C and Li from 3 to 7 MeV and for the 150° scattering angle. Data are presented only in graphical form and have been uploaded to IBANDL by the authors.

Except those three datasets, two other works where found in EXFOR. In the first, Reich et al. [4.59] report c.m. differential cross sections (barn/sr) for following c.m. scattering angles: 54.7°, 90°, 125.3°, 131.4°, 137°, 140.8°, 149.4° and 164° which corresponds to laboratory angles of 51°, 85°, 121°, 128°, 134°, 137°, 147° and 163°. For 85° there are three different graphs with three different cross-section curves with overlapping energy region as can be seen in Fig. 4.31. The same is done for 51° where three data bases with overlapping energy region can be found in original publication. For 121° two data bases exist as can be seen on Fig. 4.32. In the original publication data are presented only in the graphical form. All data are digitized and can be found in EXFOR database. R33 files from EXFOR were compared with data from the original publication and errors were detected only in three files. At the angle of 85° (lab) in the energy region from 4113─4991 keV, the cross-section value for 4956 keV differed from the value in the original paper and was removed. The same was done for 121° (lab) in the energy region from 4114─4923 keV where the cross-section value at 4780 keV differs from the published value. Also for 85° (lab) in the 1593─5562 keV region, the cross-section value at 4814 keV was not reported in the original publication and was removed.

In the work of Swint et al. [4.60], cross sections for elastic scattering of protons from carbon are measured for laboratory angles of 25.5°, 85.2°, 105.2°, 121.2°, 137.5° and 159.5° for incident energies from 4.7 to 12.8 MeV. For two angles (85° and 105°) a comparison of R33 files generated from digitized EXFOR data with data from original publications have shown that a few points do not belong to the original graphs and so these have been removed from the R33 files.

Experimental data from different publications for the same scattering angles are shown in Figs. 4.30–4.33. In Fig. 4.30, data for 138° from Ref. [4.59] and [4.60] are compared. It can be seen that data from [4.60] are slightly lower but also the position and intensity of 4800 keV resonance are shifted comparing to data from [4.59]. For 85°, Fig. 4.31 shows that in [4.59] there are 3 data groups which overlap in the region from 4600 to 5000 keV and also differ in cross-section values and position of cross-section anomaly around 4800 keV. Data from [4.60] are shifted by about 20 keV towards lower energies compared to data from [4.59]. Similar 20 keV shift toward lower energies and difference in intensity around 4800 keV can be seen if we compare the cross section for 121° from [4.59] and [4.60]. Beyond this resonance region the two datasets are in good agreement. Around 150° we can compare data from three publications. As can be seen from Fig.4.33 they are in very good agreement except for the height of 4800 keV resonance.

As a conclusion, there are five available publications about $^{12}C(p,p)^{12}C$ scattering in the energy range from 3500–5000 keV. Available data from three old publications [4.58, 4.59, 4.60] are given only in graphical form. Major part of those data is not yet included in IBANDL but is included in EXFOR and is already digitized.

Recommended data
An evaluated cross section exists in SigmaCalc for energies from 0.4 to 4.5 MeV and all angles. This evaluated cross section is recommended for all quantitative analysis.

4.10. $^{19}F(p,p_0)^{19}F$

As a first step, the data sets already existing in IBANDL [4.61, 4.24, 4.62, 4.63, 4.64, 4.65, 4.66, 4.67, 4.34, 4.68] were compared with the data in the original references showing good agreement.

As a second step a thorough search in the literature and in nuclear databases for other available experimental data was performed. Several data of interest for applications in Ion Beam Analysis (i.e. for backscattering angles in the 90°─180° range) were retrieved [4.61, 4.69, 4.70]. The data appearing in graphical form in the original references were digitized using the DataThief software [http://www.datathief.org/]. All relevant quantities were converted to the laboratory frame of reference where necessary. Table 4.6 lists the data sets found in the literature, both those already existing in IBANDL and new ones.

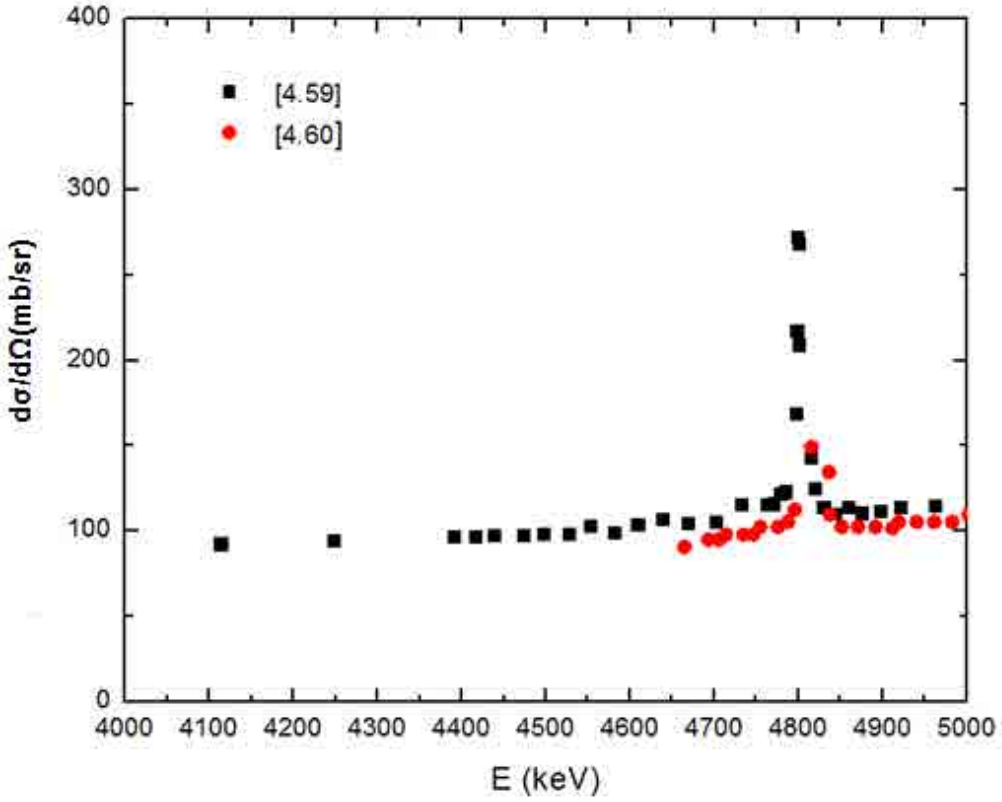

FIG. 4.30. Comparison of cross-section data from Ref. [4.59] and [4.60] for $^{12}C(p,p_0)^{12}C$ at 138°.

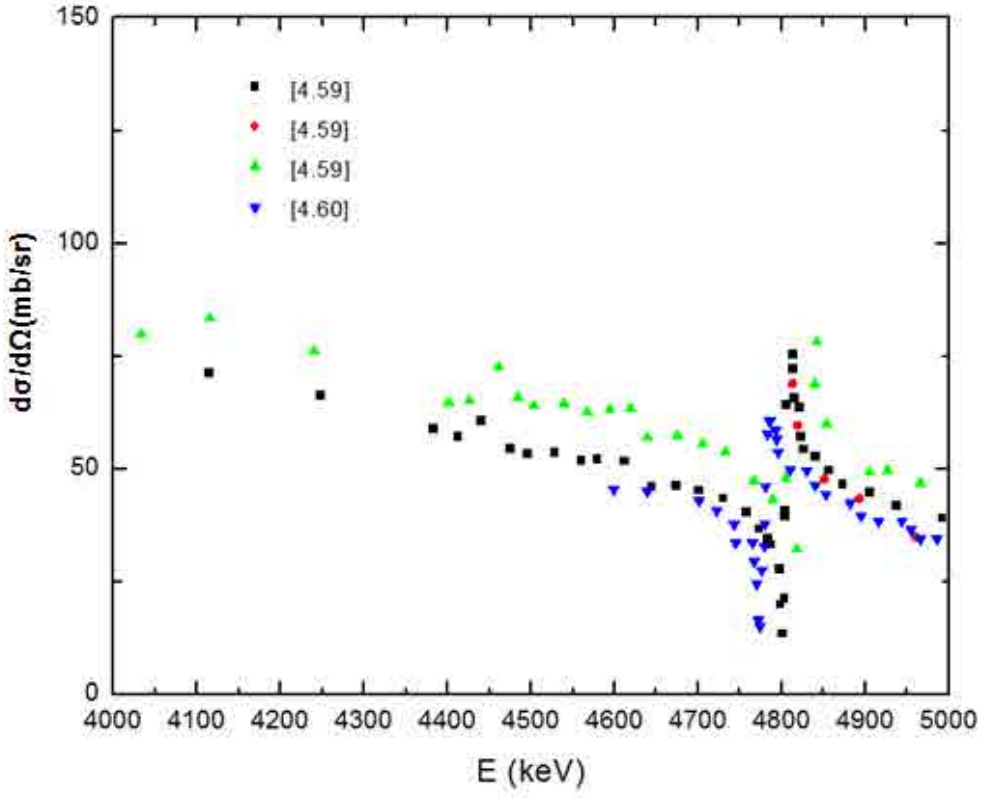

FIG. 4.31. Comparison of cross-section data from Ref. [4.59] and [4.60] for $^{12}C(p,p_0)^{12}C$ at 85°.

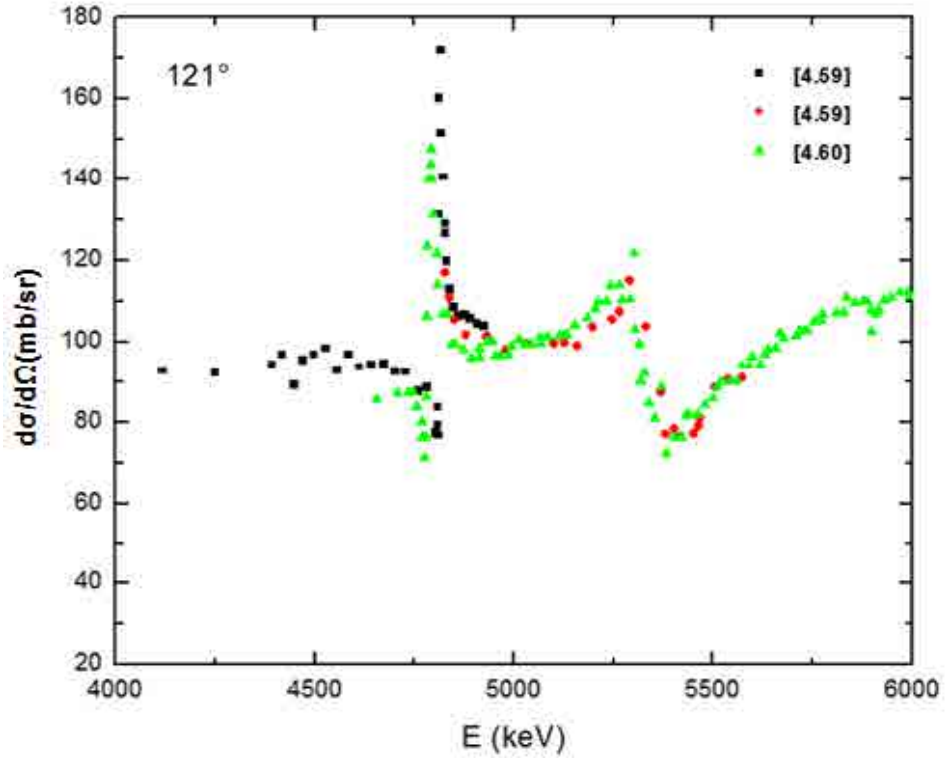

FIG. 4.32. Comparison of cross-section data from Ref. [4.59] and [4.60] for $^{12}C(p,p_0)^{12}C$ at 121°.

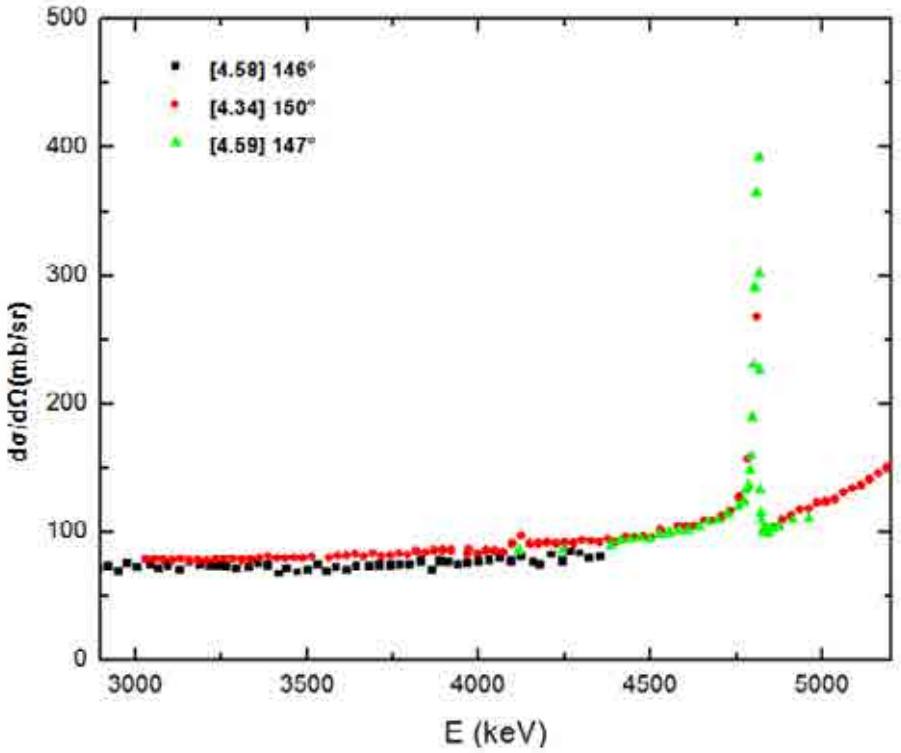

FIG. 4.33. Comparison of cross-section data from Ref. [4.58], [4.34] and [4.59] for $^{12}C(p,p_0)^{12}C$ around 150.°

TABLE 4.5. COMPARISON BETWEEN $^{12}C(p,p_0)^{12}C$ DATA FROM ORIGINAL PUBLICATIONS AND DATA PUBLISHED IN IBANDL

Angle Lab	Energy (keV)	Author	IBANDL	Action
179.2°	4000─6000	[4.57]	Data included	
168.2°	400─4360	[4.58]	Data included	
146.2°	400─4360	[4.58]	Data included	
124°	600─4360	[4.58]	Data not included	
102°	600─4360	[4.58]	Data not included	
150°	3000─7000	[4.34]	Data included	
121°	4114─4923	[4.59]	Data not included	EXFOR data are in agreement with data published in original publication except crosssection value at 4.78 MeV which is removed
138°	4113─4963	[4.59]	Data not included	
51°	4117─4965	[4.59]	Data unsuitable for RBS due to the angle	
85°	4113─4991	[4.59]	Data unsuitable for RBS due to the angle	EXFOR data are in agreement with data published in original publication except cross-section value at 4.956 MeV which is removed
128°	4624─4964	[4.59]	Data not included	
134°	4628─4967	[4.59]	Data not included	
147°	4117─4962	[4.59]	Data not included	
51°	4807─5554	[4.59]	Data unsuitable for RBS due to the angle	

TABLE 4.5. (CONT'D)

Angle Lab	Energy (keV)	Author	IBANDL	Action
121°	4827─5573	[4.59]	Data not included	
85°	4813─5549	[4.59]	Data unsuitable for RBS due to the angle	
163°	4818─5591	[4.59]	Data not included	
51°	1560─5645	[4.59]	Data unsuitable for RBS due to the angle	
85°	1593─5562	[4.59]	Data unsuitable for RBS due to the angle	EXFOR data are in agreement with data published in original publication except for cross section at 4814 keV was not in original publication and was removed
26°	4662─11590	[4.60]	Data unsuitable for RBS due to the angle	
85°	4599─12810	[4.60]	Data unsuitable for RBS due to the angle	
105°	4667─11590	[4.60]	Data not included	
121°	4655─12820	[4.60]	Data not included	
138°	4665─11480	[4.60]	Data not included	
159°	4707─12810	[4.60]	Data not included	

TABLE 4.6. AVAILABLE DATA IN THE LITERATURE ON $^{19}F(p,p_0)^{19}F$ CROSS SECTIONS

Reference	**Data source**	**θ_{lab}**	**E_p (MeV)**	**Target**	**Quoted uncertainties**	**Data format**
[4.61]	Original paper, IBANDL	122.8° 158.7°	0.55─1.80	Thick target LiF	6%	Graphical, Tabular
[4.61]	Original paper	97.0° 107.1° 133.8°	1.30─1.50	Thick target LiF	6%	Graphical
[4.69]	Original paper, IBANDL	122.8° 138.8° 158.7°	0.50─2.06	LiF evaporated on to a C backing	10%	Graphical, Tabular
[4.24]	IBANDL	90°	1.36	0.03 to 0.1 mg/cm^2 LiF evaporated on a C foil	10% statistical and systematic	Tabular
[4.68]	IBANDL	109.5° 123.0° 147.8° 168.0°	5.65─6.20	─	─	Tabular
[4.62]	IBANDL	135° 145°	0.65─1.80	─	─	Tabular
[4.70]	EXFOR	95.0° 123.0° 137.0°	1.80─2.68	─	─	Tabular
[4.63]	IBANDL	97.5° 110.6° 125.3° 137.8° 158.5°	1.52─2.10	C_2F_6 gas target	10%	Tabular
[4.64]	IBANDL	95.0° 122.7° 148.5° 161.1°	2.00─3.40	C_2F_6 gas target (2÷8 Torr)	10%	Tabular

TABLE 4.6. (CONT'D)

Reference	Data source	θ_{lab}	E_p (MeV)	Target	Quoted uncertainties	Data format
[4.65]	IBANDL	165°	0.85─1.01	85 μg/cm^2 LuF_3, deposited on polycarbonate film	2% statistical, 3─4% reproducibility	Tabular
[4.65]	IBANDL	153°	1.00─1.88	137.9 μg/cm^2 LiF, deposited on 38 μg/cm^2 Cu, deposited on 50 μg/cm^2 C	2% statistical, 3─4% reproducibility	Tabular
[4.66]	IBANDL	150°	2.50─4.79	158.5 μg/cm^2 CeF_3	8%	Tabular
[4.67]	IBANDL	165°	1.40─2.71	69, 45 and 78 μg/cm^2 GdF_3 on thin C foil	5%	Tabular
[4.34]	IBANDL	150°	3.0─7.2	50 μg/cm^2 LiF on 30 μ/cm^2 C, coated with 20 μ/cm^2 Au	5%	Tabular

Figures 4.34–4.39 present in graphical form all the cross sections listed in Table 4.6; data referring to similar scattering angles are shown together. In the case of data from [4.68], since they refer to quite high energy values (around 6 MeV), only the cross-section values for the scattering angle of 147.8° will be presented as they alone can be compared to other data [4.66, 4.34] obtained at a similar scattering angle and energy range. In the graphs the proton energy and the differential cross section are given in the laboratory frame of reference, with energy units in MeV and cross-section units in mb/sr.

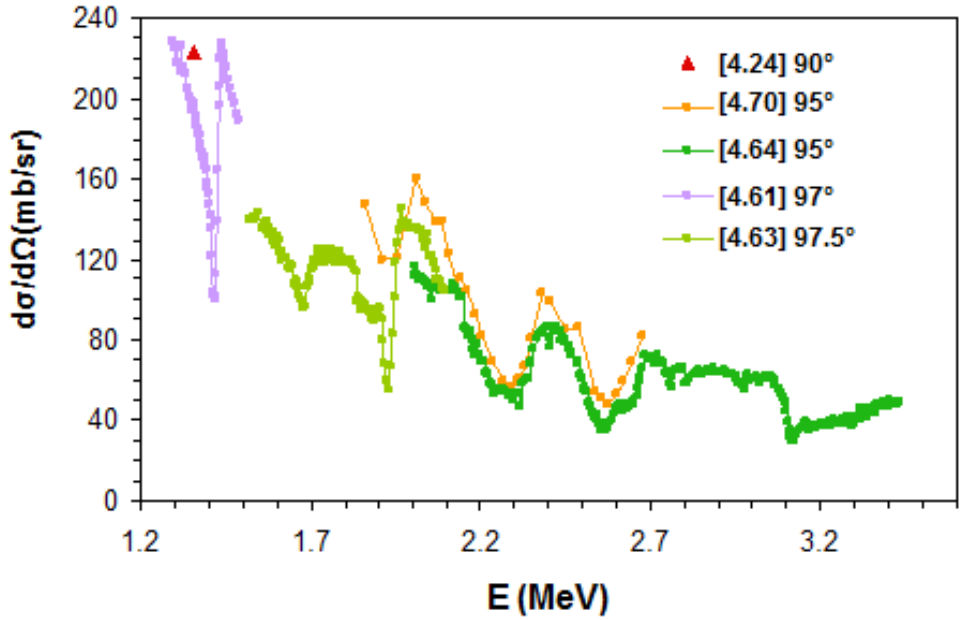

FIG. 4.34. Cross-section values of proton elastic scattering on ^{19}F versus proton energy at scattering angles in the 90°–97° range.

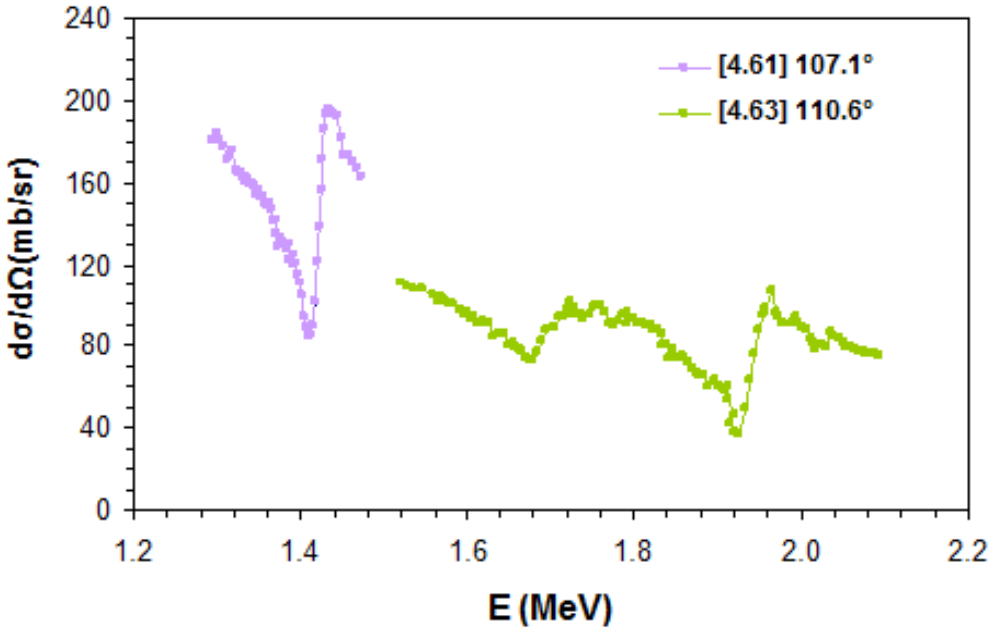

FIG. 4.35. Cross-section values of proton elastic scattering on ^{19}F versus proton energy at scattering angles in the 107°–111° range.

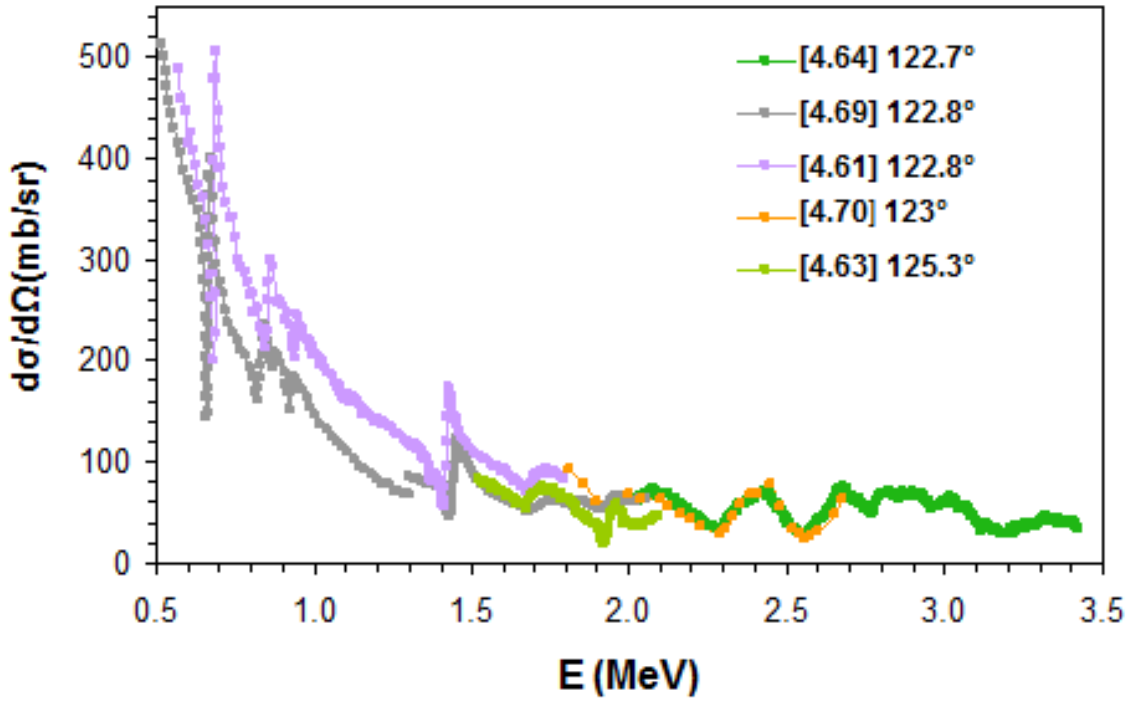

FIG. 4.36. Cross-section values of proton elastic scattering on ^{19}F versus proton energy at scattering angles in the 122°─125° range.

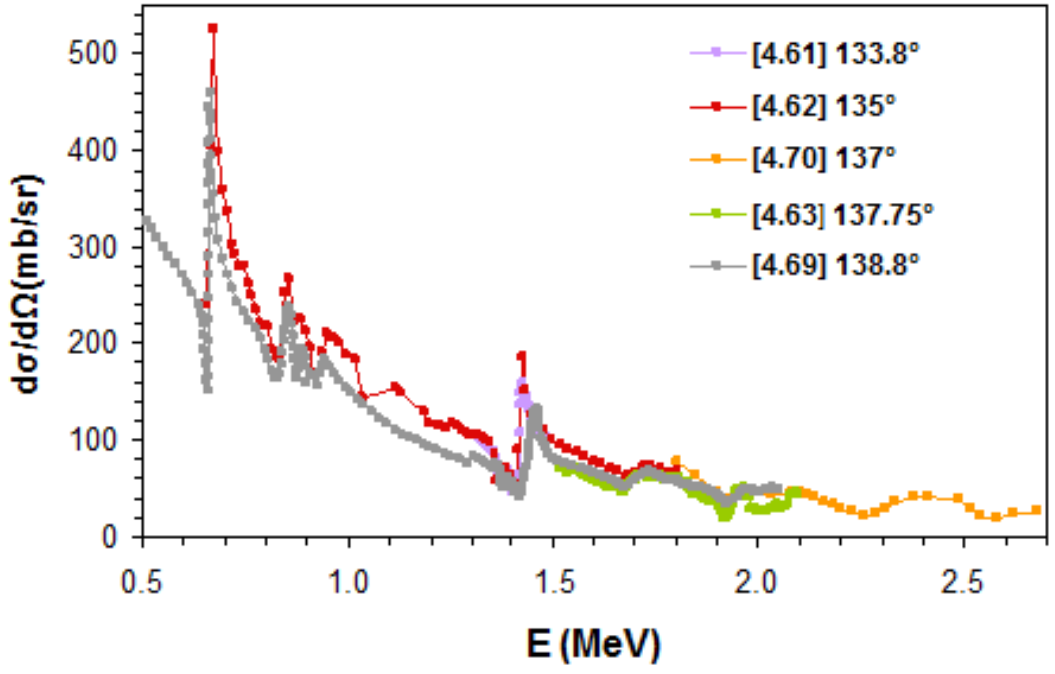

FIG. 4.37. Cross-section values of proton elastic scattering on ^{19}F versus proton energy at scattering angles in the 134°─140° range.

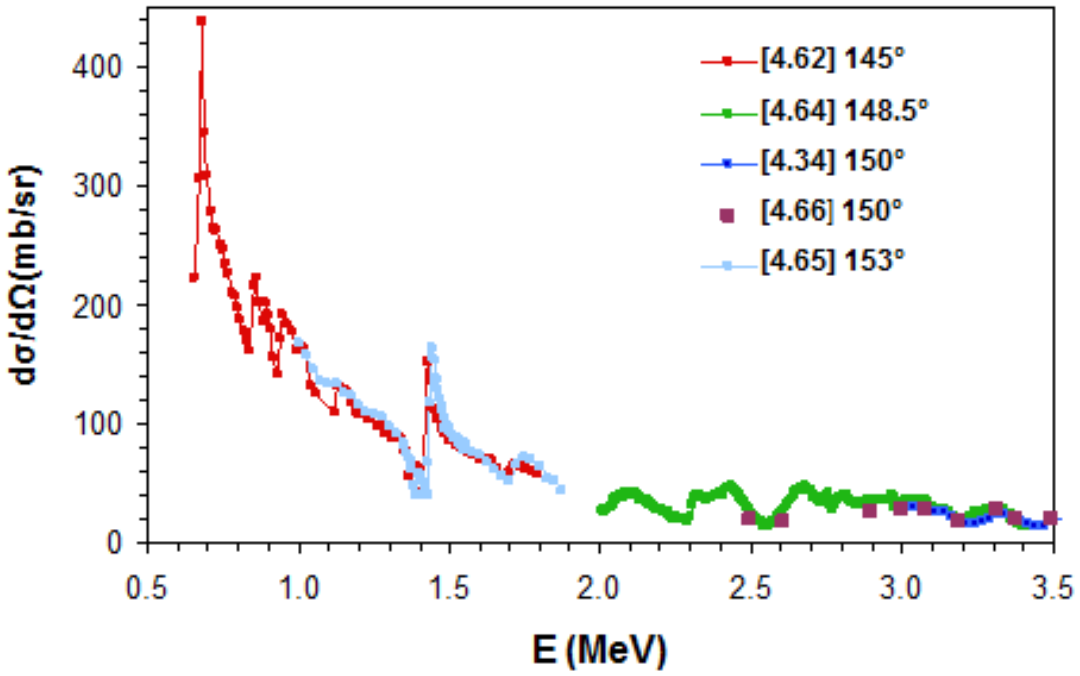

FIG. 4.38a. Cross-section values of proton elastic scattering on ^{19}F versus proton energy at scattering angles in the 145°─153° range, for proton energies lower than 3.5 MeV.

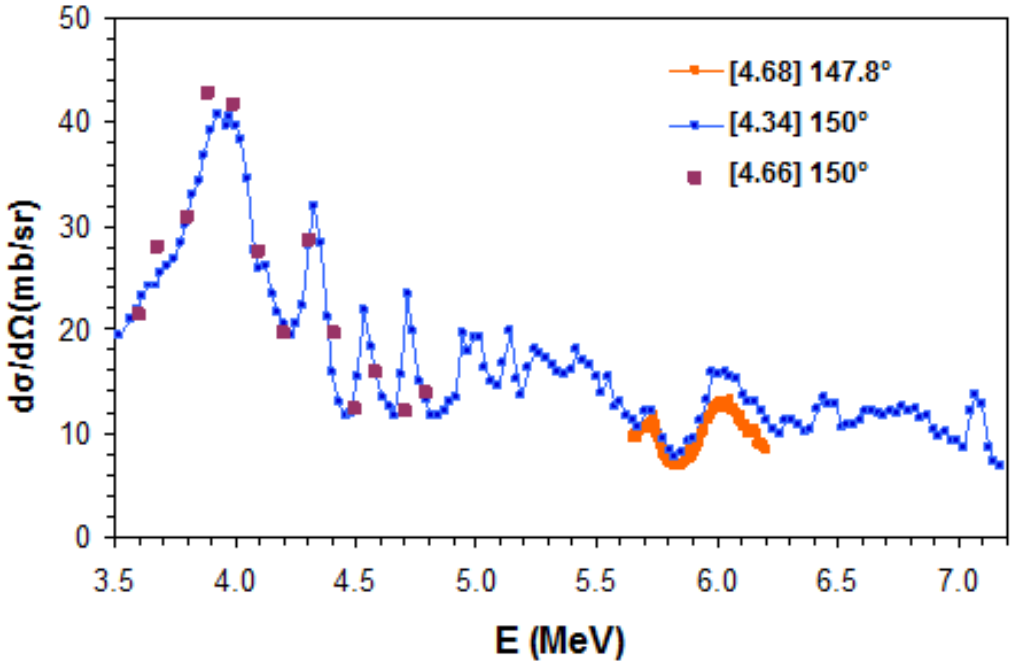

FIG. 4.38b. Cross-section values of proton elastic scattering on ^{19}F versus proton energy at scattering angles in the 148°─150° range, for proton energies between 3.5 MeV and 7.2 MeV.

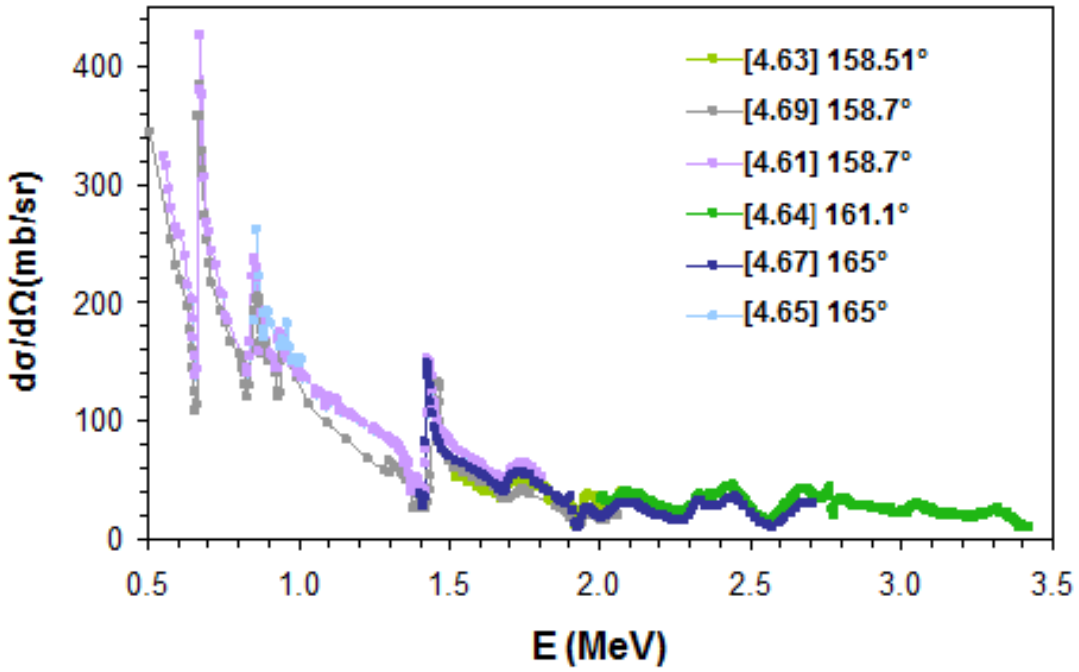

FIG. 4.39. Cross-section values of proton elastic scattering on ^{19}F versus proton energy at scattering angles in the 159°─165° range.

In general, the agreement between the data–even those referring to slightly different scattering angles–is reasonably good (within 10─15%), except in a few cases.

In particular, data taken from Ouichaoui's paper published in 1985 [4.63] concerning measurements with proton energies lower than 2 MeV, appear systematically lower (about 25─30%) than the other data at similar angles [4.61, 4.62, 4.70], whereas the data taken from Ouichaoui's 1986 publication [4.64], regarding measurements with proton energies higher than 2 MeV, appear systematically higher (about 10%, and up to 40% in just one case) than the other data at similar angles [4.70, 4.66, 4.67, 4.34] with the only exception of Cuzzocrea's data at 95° (as a matter of fact, with respect to these data, cross-section values from [4.64] are 20% lower). Moreover, the two data sets from Ouichaoui [4.63, 4.64] do not match in the overlapping energy region of 2.0–2.1 MeV.

Remarkable discrepancies appear in the data from Dearnaley [4.69] when compared to the other data [4.61, 4.62, 4.65, 4.67], especially with respect to the 1.42 MeV resonance which in addition appears to be shifted in energy; an abrupt change in the cross-section values at 1.3 MeV energy is clear too, e.g. in Figures 4.36 and 4.39 (actually, this might be an effect of the digitizing process since the cross-section curves as a function of proton energy are shown in two panels in the original reference data). For these reasons data from Dearnaley [4.69] should be used with caution.

As regards the shape and position of the 1.42 MeV resonance structure, there is a good agreement between data from Webb [4.61], Caracciolo [4.62] and Jesus [4.67], while from the data of Knox and Harmon [4.65] the position is shifted to higher energy by about 15 keV.

Recommended data

An evaluated cross section exists in SigmaCalc for proton energies up to about 1.8 MeV and is recommended. At higher energies, data from [4.70], [4.64], [4.67] and [4.34] should be

used for their respective scattering angles. Cross-section values from [4.66] appear to be reliable as well, but their sparse data points make them less suited in simulating backscattering spectra. Data from [4.69] should not be used for the aforementioned reasons and because they deviate from the evaluated cross section; for this latter reason also data from [4.63] should not be used.

4.11. $^{23}Na(p,p_0)^{23}Na$

As a first step, the data sets already existing in IBANDL were compared with the data in the original references and the agreement was good.

The second step included a thorough search in the literature and in nuclear databases for other available experimental data. Only one data set of possible interest for application in Ion Beam Analysis (i.e. for backscattering angles in the 100°─180° range) was retrieved [4.71]. Another paper [4.72] was found, however it was considered of limited interest since it focuses only on the measurement of the width of a resonance at 3.90 MeV proton energy. Table 4.7 lists the datasets found in the literature, both already existing in IBANDL and the new one.

TABLE 4.7. AVAILABLE DATA IN THE LITERATURE ON $^{23}Na(p,p_0)^{23}Na$ CROSS SECTIONS

Reference	**Data source**	**θ_{lab}**	**E_p (MeV)**	**Target**	**Quoted uncertainties**	**Data presentation**
[4.73]	IBANDL	156.5°	0.57─1.48	Metallic sodium evaporated on Nylon films	─	Tabular
[4.69]	IBANDL	123.2° 139.2° 158.9°	0.4─1.0	Na metal evaporated on a C backing	─	Tabular
[4.71]	Original paper	135°	2.25─2.50	10 μg/cm^2 Na evaporated on C foil (10 μg/cm^2)	─	Graphical; arb. units
[4.74]	IBANDL	130°	3.45─6.50	100% ^{23}Na target	─	Tabular
[4.75]	IBANDL	165°	1.08─3.50	1─3 μg/cm^2 Na evaporated on Au coated (1 μg/cm^2) C foils (5 μg/cm^2)	1─2% statistical	Tabular
[4.76]	IBANDL	150°	2.2─5.2	63 μg/cm^2 NaBr evaporated on C foil (30 μg/cm^2)	6% statistical and systematic	Tabular

Figures 4.40 and 4.41 present in graphical form all the cross sections listed in Table 4.7 (data from [4.71] are not shown since they are presented in arbitrary units); data referring to similar energy ranges are shown together. In the graphs the proton energy and the differential cross sections are given in the laboratory frame of reference, with energy units in MeV and cross-section units in mb/sr.

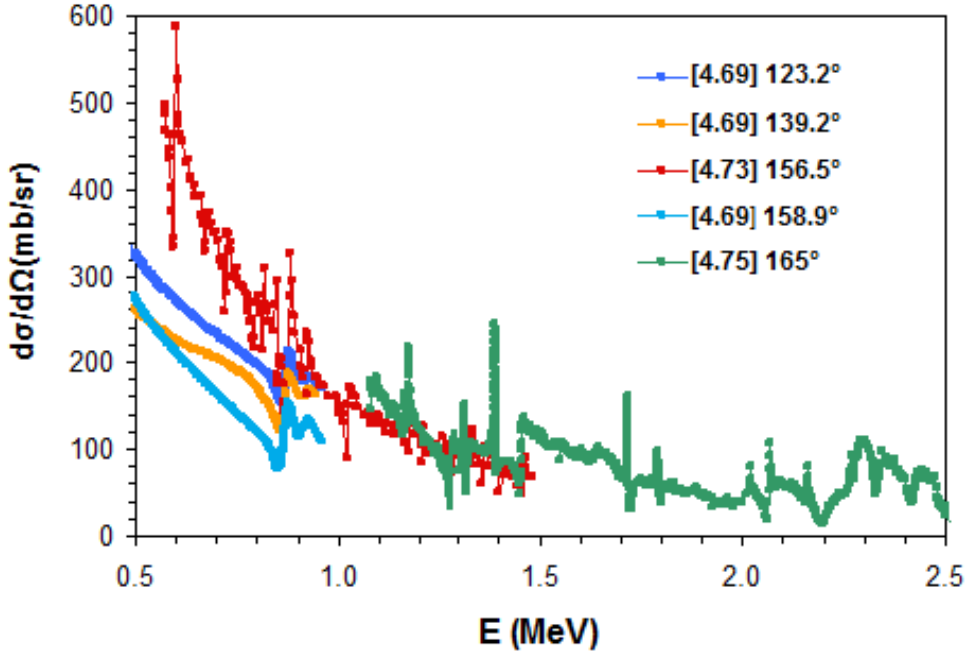

FIG. 4.40. Cross-section values of proton elastic scattering on ^{23}Na versus proton energy at different scattering angles, for energies in the 0.5─2.5 MeV range.

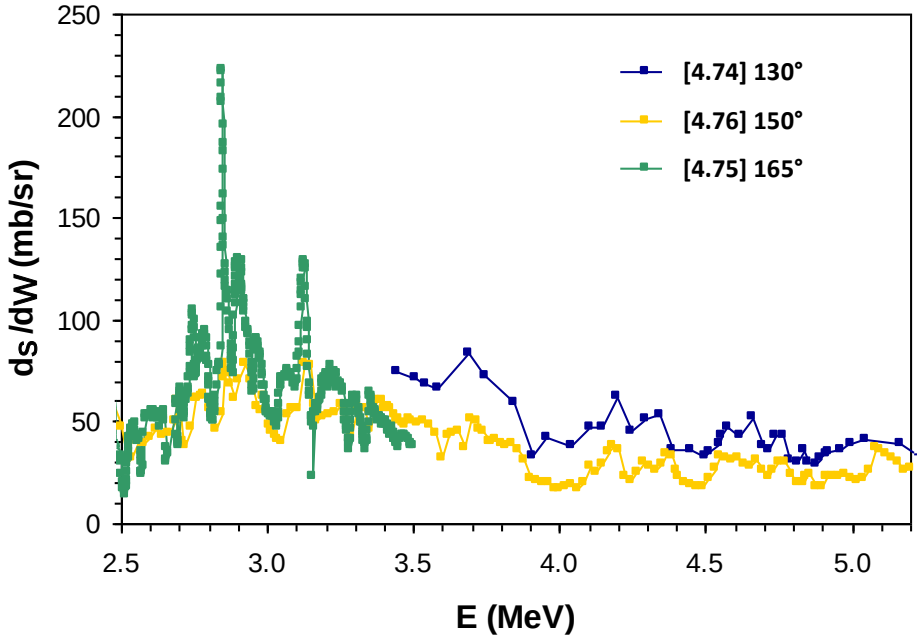

FIG. 4.41. Cross-section values of proton elastic scattering on ^{23}Na versus proton energy at different scattering angles, for energies in the 2.5─5.2 MeV range.

From Fig.4.40, a striking discrepancy is observed in the data from [4.69] referring to the scattering angle of 158.9°: these data are about a factor of 2 lower than those from [4.73] and

several resonances are missing whereas the overall agreement between data from [4.73] and [4.75] is reasonably good–keeping in mind that they refer to different scattering angles. In addition, it should be noted that the cross-section values for the three scattering angles from [4.69] are consistently lower than the Rutherford value, even at proton energies of a few hundreds keV.

From Fig.4.41, a fairly good agreement between data from [4.75] and [4.76] can be observed, taking into account that they refer to different scattering angles; however, some resonances are not well reproduced in the data from [4.76] due to the finite steps in energy of the measurement, often exceeding the proton energy loss in the target. The cross-section values from [4.74] are about 60% higher than those from [4.76] (again, the comparison is between data referring to different scattering angles) and also, in this case, the fine structure of the cross section is missed due to the sparse steps in measured energy.

Recommended data

An evaluated cross section exists in SigmaCalc for proton energies up to about 1.5 MeV and is recommended. At higher energies, data from [4.75] and [4.76] should be used.

4.12. $^{9}Be(\alpha,\alpha_0)^{9}Be$

Figs. 4.42 and 4.43 compare Taylor's [4.77] and Goss' [4.78] measurements, both done at a scattering angle of 66.05° (lab system). The measurements disagree completely, with Goss' measurement being lower than Taylor's. The data of Goss are more or less constant, while Taylor's data are rising from about 1.7 to 3 (relative to Rutherford) in this energy range.

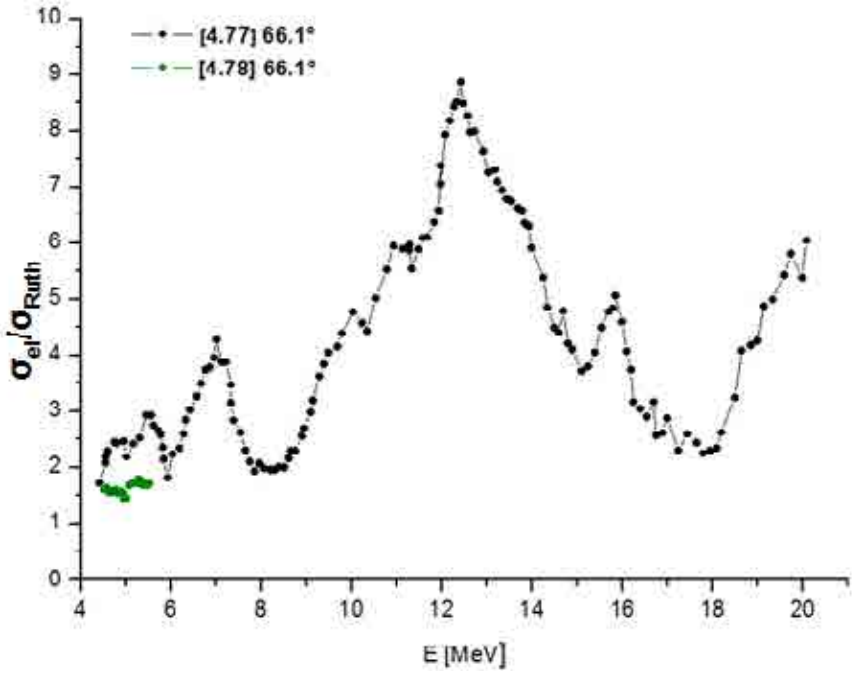

FIG. 4.42. Data comparison of Taylor [4.77] and Goss [4.78] for $^{9}Be(\alpha,\alpha_0)^{9}Be$ at 66.05°.

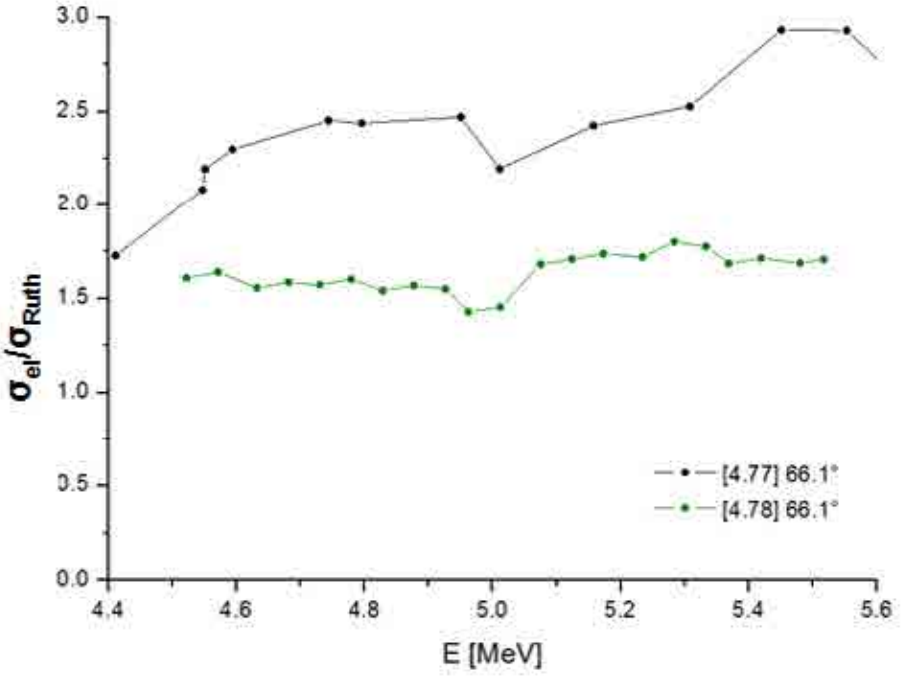

FIG. 4.43. Data comparison of Taylor [4.77] and Goss [4.78] for $^{9}Be(\alpha,\alpha_0)^{9}Be$ at 66.05°.

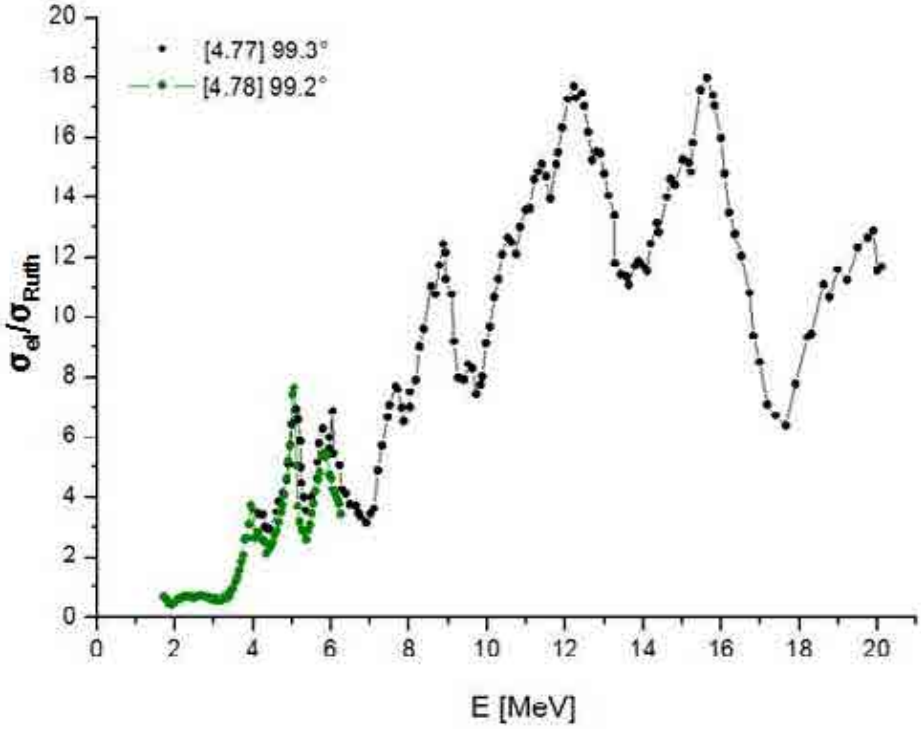

FIG. 4.44. Data comparison of Taylor [4.77] and Goss [4.78] for $^{9}Be(\alpha,\alpha_0)^{9}Be$ at 99°.

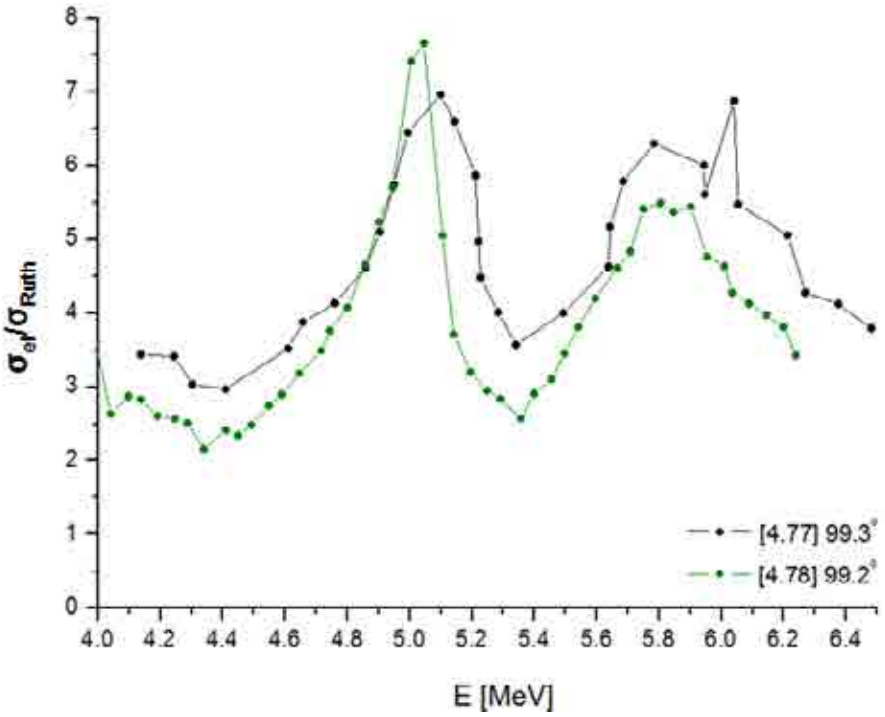

FIG. 4.45. Data comparison of Taylor [4.77] and Goss [4.78] for $^{9}Be(\alpha,\alpha_0)^{9}Be$ at 99°.

At around 99°, the shape of both curves shows some similarities, see Figs. 4.44 and 4.45, but the quantitative agreement is poor. The minima and maxima are more or less at the same energies, but the cross-section values are different. The data of Goss [4.78] are systematically lower than Taylor's [4.77] data, with the exception of the first maximum where Goss' data are higher than those of Taylor.

At around 140° data comparison is confined to Goss [4.78] and Saleh [4.79], since Taylor's measurements [4.77] were done at higher energies. The minimum in the cross section is roughly at the same energy, but Goss' data are systematically lower. The largest discrepancy is observed in the cross-section minimum, where Goss measured ~0.15 and Saleh ~0.5 (rr) – i.e. a discrepancy by a factor of about three. In the plateau region from 2.1 to 2.5 MeV the disagreement is about 20─30%. Goss' data also seem to be too low compared to Taylor's data at about 6.2─6.5 MeV.

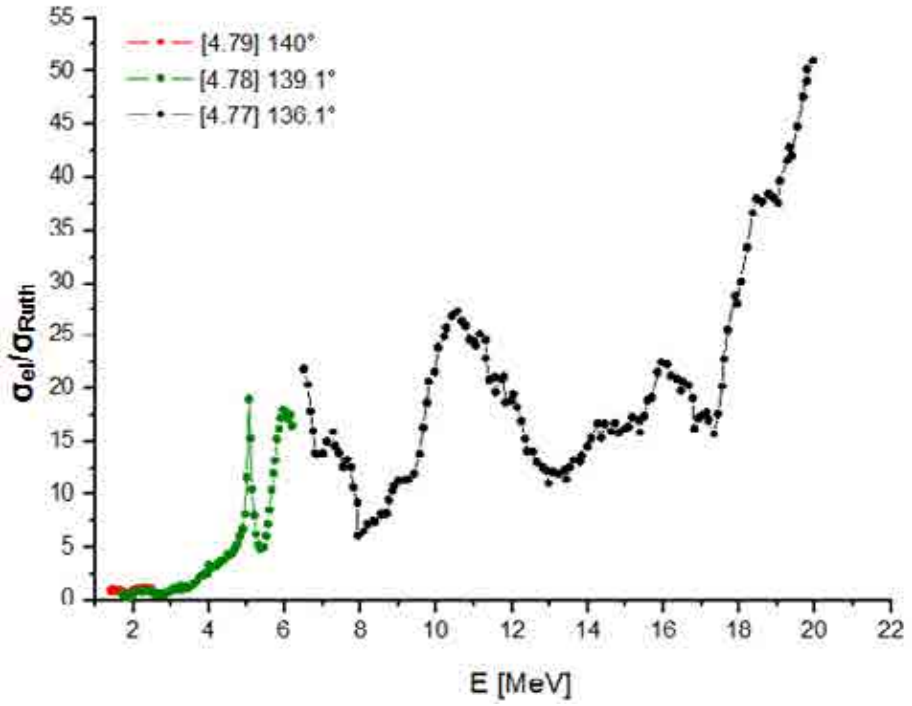

FIG. 4.46. Comparison of Taylor [4.77], Saleh [4.79], Goss [4.78] for $^{9}Be(\alpha,\alpha_0)^{9}Be$ at 136─140°.

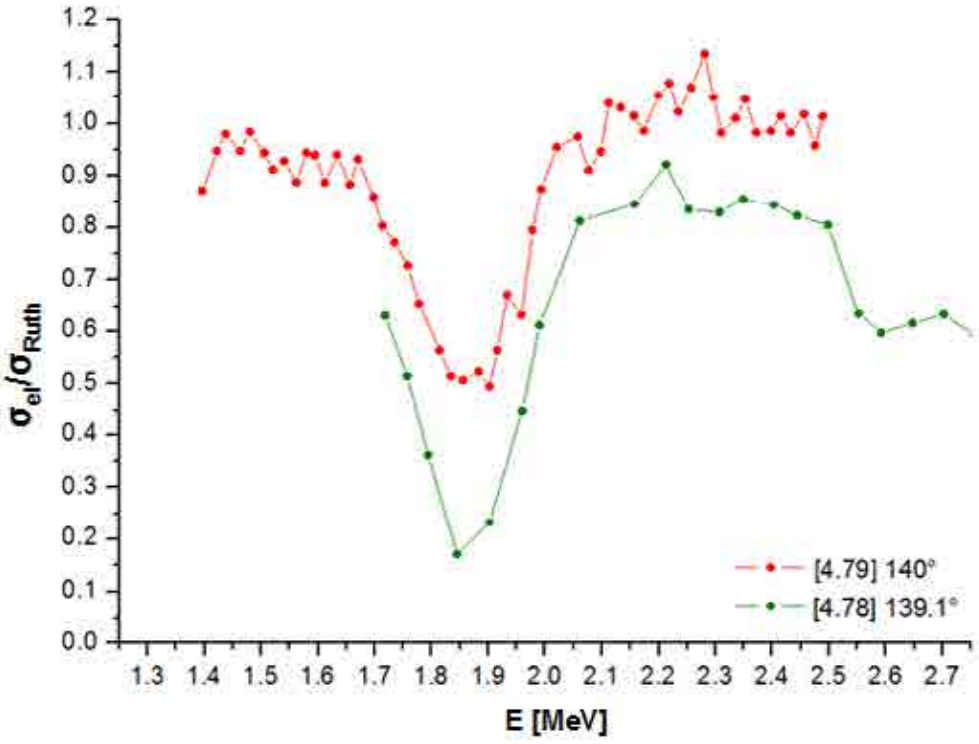

FIG. 4.47. Comparison of Saleh [4.79] and Goss [4.78] for $^{9}Be(\alpha,\alpha_0)^{9}Be$ at about 140°.

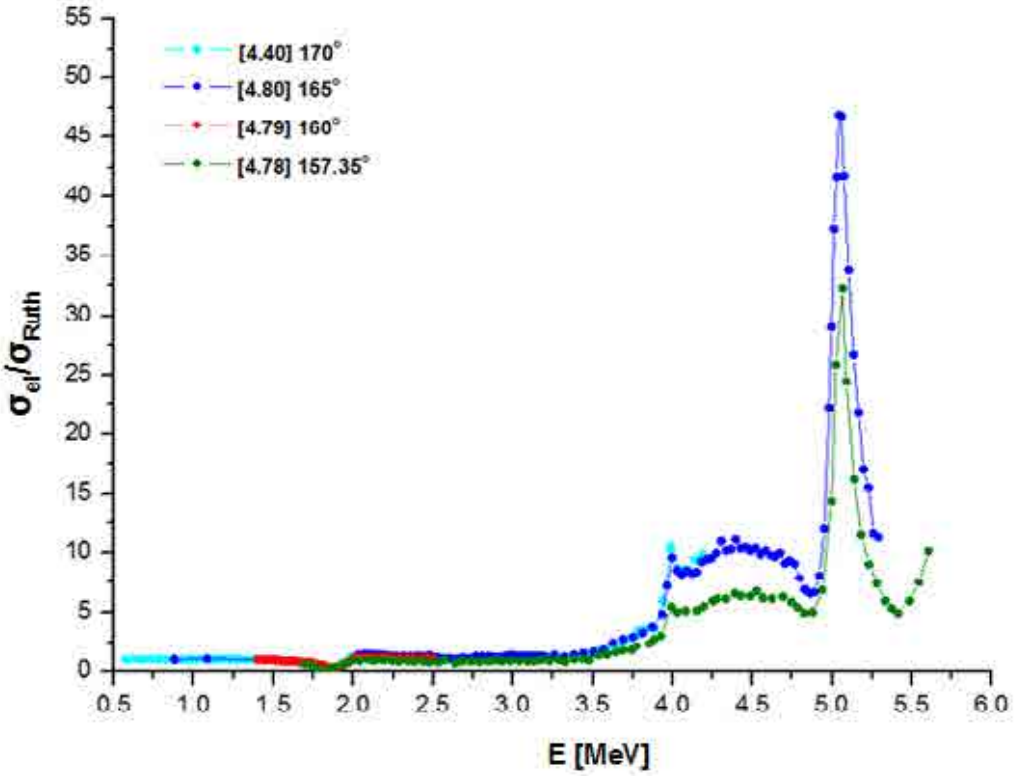

FIG. 4.48. Comparison of Leavitt [4.40], Liu [4.80], Saleh [4.79] and Goss [4.78] for $^{9}Be(\alpha,\alpha_0)^{9}Be$ at 157─170°.

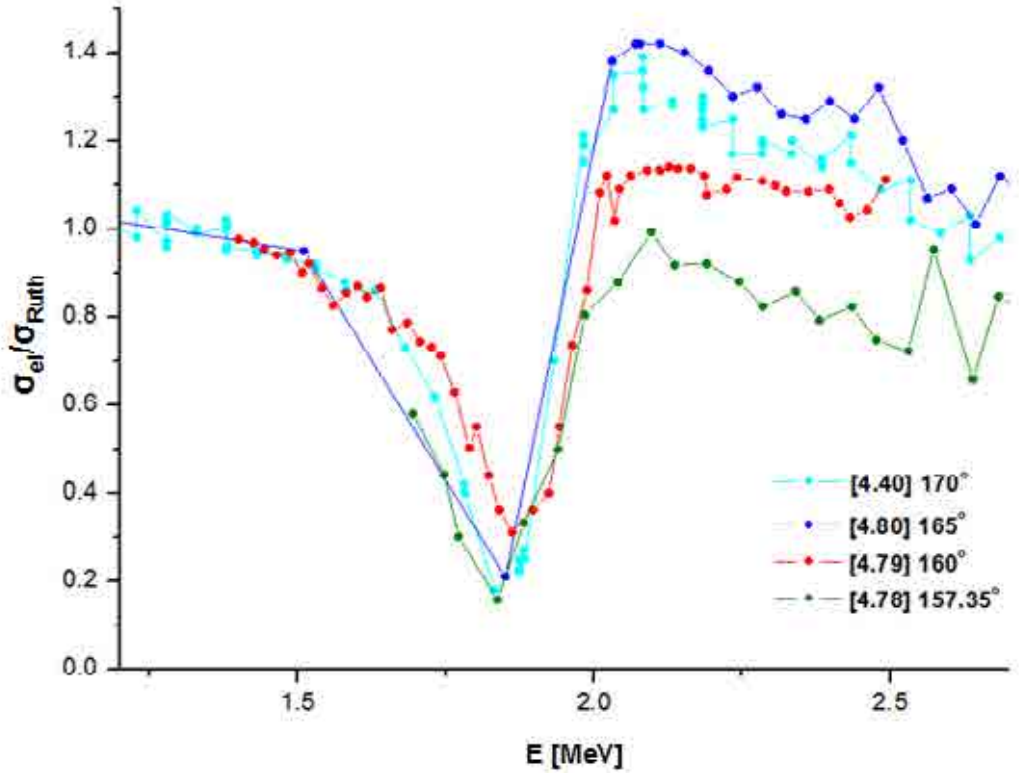

FIG. 4.49. Comparison of Leavitt [4.40], Liu [4.80], Saleh [4.79] and Goss [4.78] at 157─170°.

At 157─170° four different data sets are available, see Figs. 4.48 and 4.49. The position of the cross─section minimum at about 1.85 MeV is close within about 30 keV between all four data sets, see Fig. 4.49. Liu [4.80] and Goss [4.78] agree on the position of the cross─section maximum at 5.05─5.07 MeV. Leavitt [4.40] and Liu [4.80] show a better than 10% agreement of the cross sections over the whole energy range, while the data by Goss [4.78] are always systematically too low. Saleh [4.79] shows some agreement with Leavitt and Liu. The Leavitt and Liu data approach the Rutherford cross section at energies below about 1.5 MeV.

Recommendation:
Leavitt's data [4.40] for 170° and Liu's data [4.80] for 165° show agreement within 10% or better, and the use of their data is recommended. At smaller scattering angles the data show larger discrepancies, so that a recommendation cannot be given. The positions of the cross-section minima and maxima agree within about 30 keV. The data by Goss [4.78] are systematically lower than all other data and should not be used.

4.13. $^{10}B(\alpha,\alpha_0)^{10}B$

Only three authors have measured cross sections for alpha backscattering from ^{10}B. Their publications have been examined. Only one of these measurements was found in IBANDL. All other suitable data have been taken from EXFOR and were submitted to IBANDL. A complete list can be found in Table 4.8 below.

The existing cross-section data for α-backscattering from ^{10}B are very scarce. A comparison of the data from Mo et al. [4.81] and McIntyre et al. [4.82] is shown in Fig. 4.50. The shape of the curves is similar, but the quantitative agreement is poor. The data were recorded at slightly different angles. The angular dependence at two different energies is shown in Fig. 4.51. Although there is some angular dependence, it seems improbable that the difference between Mo [4.81] and McIntyre [4.82] can be explained by the different scattering angles. The data of McIntyre approach the Rutherford cross section at low energies. Additional experimental data are necessary in order to clarify the differences between the data.

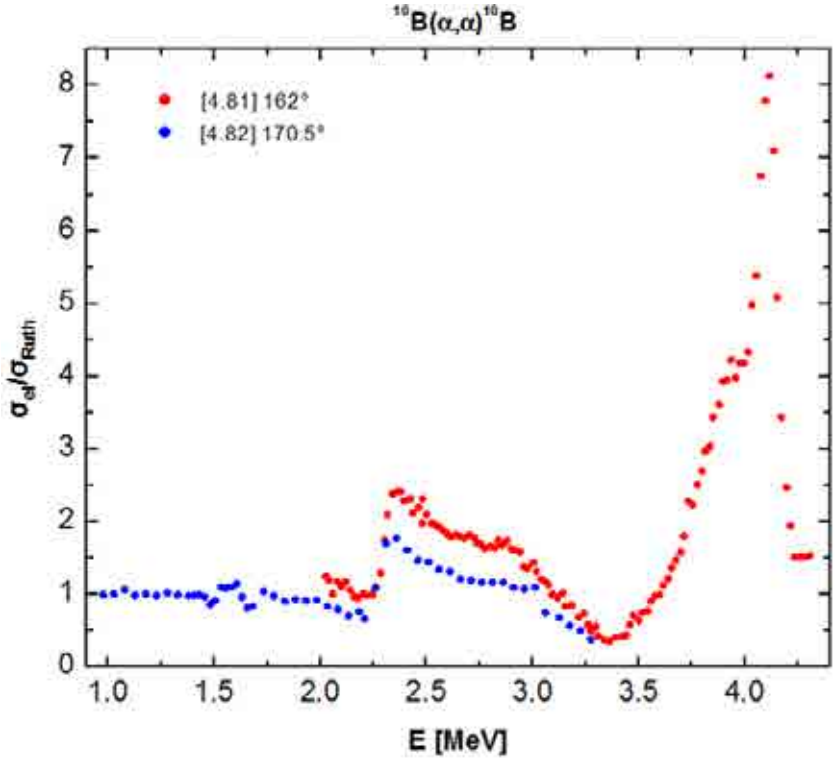

FIG. 4.50. Comparison of the data by Mo [4.81] and McIntyre [4.82] for $^{10}B(\alpha,\alpha_0)^{10}B$ at 162° and 170.5° scattering angle.

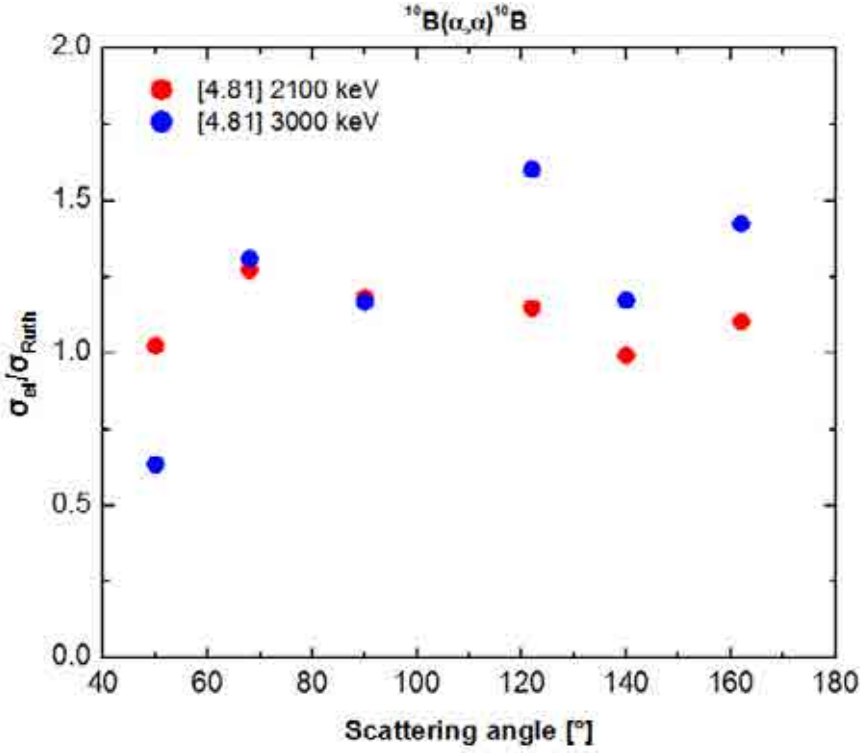

FIG. 4.51. Angular dependence of the cross section for $^{10}B(\alpha,\alpha_0)^{10}B$ at 2100 and 3000 keV. From [4.81].

TABLE 4.8. PUBLICATIONS CONTAINING $^{10}B(\alpha,\alpha)^{10}B$ CROSS-SECTION DATA

Energy Range (MeV)	Lab Angle (°)	Error	Data	Ref.	IBANDL	EXFOR	Action
5.0─30.0	57.4	─	Graph	[4.83]	data unsuitable for RBS due to angle	F0220002	
2.0─4.3	50	─	Graph	[4.81]	data unsuitable for RBS due to angle	F0486002	Data converted from EXFOR to IBANDL
2.0─4.3	68	─	Graph	[4.81]	data unsuitable for RBS due to angle	F0486002	Data converted from EXFOR to IBANDL
2.0─4.3	90	─	Graph	[4.81]	**data missing**	F0486002	Data converted from EXFOR to IBANDL
2.0─4.3	122	─	Graph (2x)	[4.81]	**data missing**	F0486002	Data converted from EXFOR to IBANDL
2.0─4.3	140	─	Graph	[4.81]	**data missing**	F0486002	Data converted from EXFOR to IBANDL
2.0─4.3	162	─	Graph (2x)	[4.81]	**data missing**	F0486002	Data converted from EXFOR to IBANDL
1.0─3.3	170.5	7%	Graph	[4.82]	data included	C0090002	

Recommended data

The existing cross-section data for $^{10}B(\alpha,\alpha)^{10}B$ are very scarce and only show qualitative agreement. None of the data sets can be recommended for quantitative purposes. In order to obtain more reliable data further measurements are necessary.

4.14. $^{11}B(\alpha,\alpha_0)^{11}B$

Several authors have measured cross sections for alpha backscattering from ^{11}B. Available publications have been collected, and if not already included in IBANDL, the data have been taken from EXFOR or the articles have been submitted to the IAEA for digitization. In one case the data available at IBANDL (file b1aa0b.r33) [4.84] turned out to be incorrect, because a mistake was made in the data conversion from the centre-of-mass system to the laboratory system. A complete list can be found in Table 4.9 below.

The available data at 165°─170° are shown in Fig. 4.52. An expansion of the low energy part below 3.4 MeV is shown in Fig. 4.53. The curves have a similar shape, but the differences are up to 30%. More experimental data are necessary.

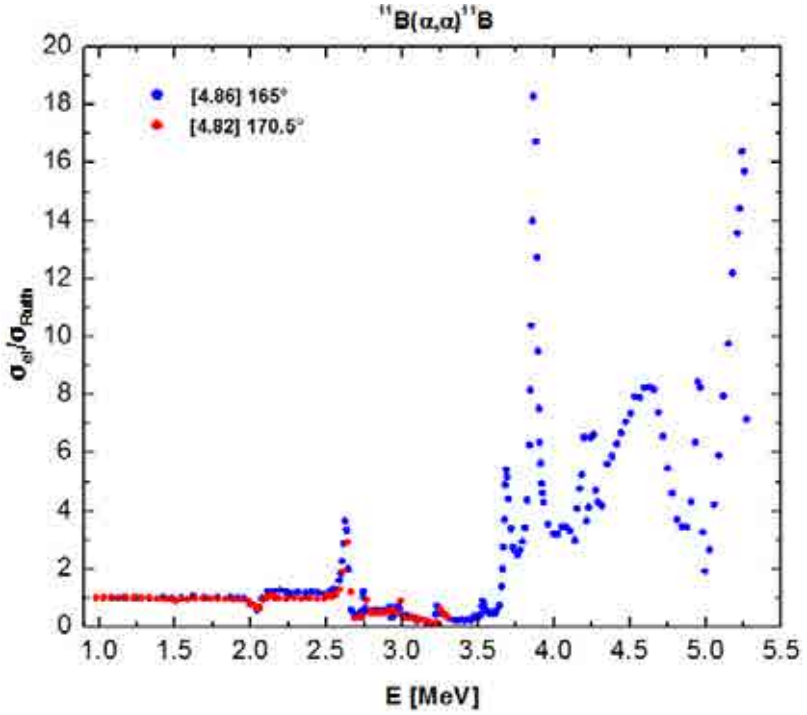

FIG. 4.52. Comparison of experimental data from Liu et al. [4.86] and McIntyre [4.82] for $^{11}B(\alpha,\alpha_0)^{11}B$ at 165° and 170.5° scattering angle.

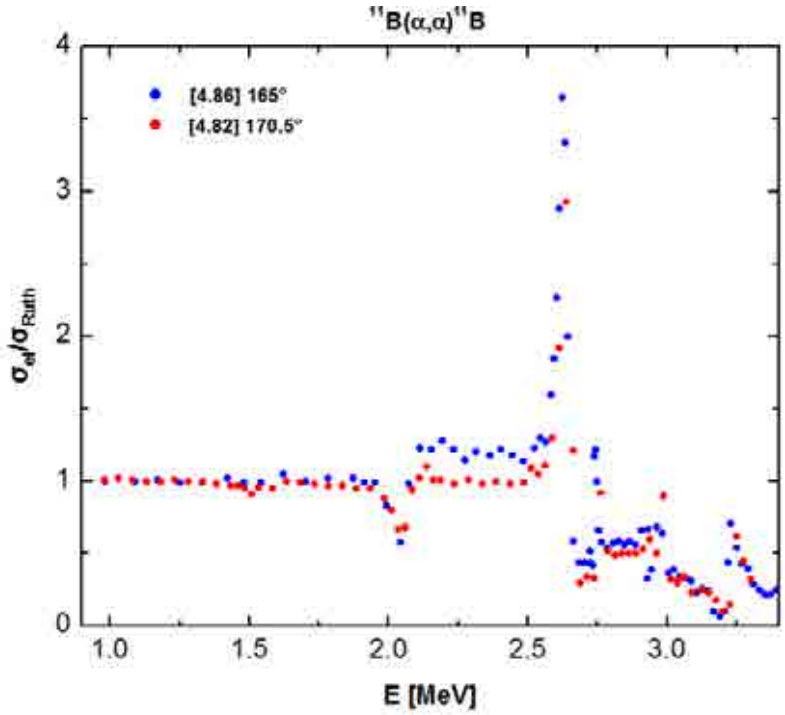

FIG. 4.53. Comparison of experimental data from Liu et al. [4.86] and McIntyre [4.82] for $^{11}B(\alpha,\alpha_0)^{11}B$ at 165° and 170.5° scattering angle below 3.4 MeV.

TABLE 4.9. PUBLICATIONS CONTAINING $^{11}B(\alpha,\alpha)^{11}B$ CROSS-SECTION DATA

Energy (MeV)	**Angle**	**Error**	**Data**	**Ref.**	**IBANDL**	**EXFOR**	**Action**
4.0─4.9	50.0	3%	Graph	[4.84]	*data unsuitable for RBS due to angle*	─	Request for digitizing submitted to IAEA
4.0─8.0	130.0	3%	Graph	[4.84]	**data missing**	─	Request for digitizing submitted to IAEA
4.0─4.9	140.0	3%	Graph	[4.84]	**data missing**	─	Request for digitizing submitted to IAEA
4.0─8.0	150.0	3%	Graph (2x)	[4.84]	**data incorrect***	C0754002**	Request for digitizing submitted to IAEA
2.1─3.9	70.4	─	Graph	[4.85]	data unsuitable for RBS due to angle	T0090002	Data converted from EXFOR to IBANDL
2.1─3.9	90.5	─	Graph	[4.85]	**data missing**	T0090002	Data converted from EXFOR to IBANDL
2.1─3.9	150.8	─	Graph	[4.85]	data included	T0090002	Data converted from EXFOR to IBANDL
1.0─3.3	170.5	7%	Graph	[4.82]	data included	C0090003	
1.0─5.3	165	2%	Graph & Table	[4.86]	**data missing**	C0887002	Data converted from EXFOR to IBANDL
2.7─3.9	Various		Graph & Table	[4.86]	Data unsuitable, angular distribution	C0887003	

*converting error in file b1aa0b.r33 (the scattering angle was 160.5° instead of 150°).
**Data incorrect due to incorrect angle, see above. The data were taken from Sigmabase.

Recommended data

The existing cross-section data for $^{11}B(\alpha,\alpha)^{11}B$ are very scarce and are only in qualitative agreement with deviations up to 30%. None of the data sets can be recommended for quantitative purposes, and further measurements are necessary in order to obtain more reliable data.

4.15. $^{12}C(\alpha,\alpha_0)^{12}C$

Comparison of data sets in IBANDL with the data of the original references showed some discrepancies which are reported in Table 4.10. It was found that only part of the data from the original publications had been digitized and transferred to the IBANDL database. For instance, IBANDL contains data from [4.87] but only for 106.7º although the original publication reports cross sections for three other lab angles 124º, 136º and 160º. Data for all angles have been digitized and are available in the EXFOR database in R33 format.

TABLE 4.10. COMPARISON BETWEEN DATA FROM ORIGINAL PUBLICATIONS AND DATA PUBLISHED IN IBANDL

Angle Lab	**Energy (keV)**	**Author**	**IBANDL**	**Action**
170º	4100─7640	[4.88]	Data included	Cross section at 5.5 MeV was missing Corrected in R33 file and uploaded to IBANDL
172º	4035─4635	[4.89]	Data included	
165º	1810─9052	[4.90]	Data included	
170.5º	1564─4976	[4.91]	Data included	
106.7º	2500─4800	[4.87]	Data included	
124º	2500─4800	[4.87]	Data not included	
136º	2500─4800	[4.87]	Data not included	
160º	2500─4800	[4.87]	Data not included	
170º	5000─9000	[4.92]	Data included	
149º	4000─13300	[4.93]	Data included	
143.9º	4000─13300	[4.93]	Data not included	
136.7º	4000─13300	[4.93]	Data not included	
125.1º	4000─13300	[4.93]	Data not included	
113.9º	4000─13300	[4.93]	Data not included	
106.8º	4000─13300	[4.93]	Data not included	
166.6º	640─1170 1910─3980	[4.94]	Data included	Digitized data available in IBANDL but from 640 – 1170 keV and from 1910 ─3980 keV
133.3º	2500─4000	[4.94]	Data included	
107.2º	2500─4000	[4.94]	Data not included	
167º	3800─7600	[4.95]	Data included	
134.3º	3800─7600	[4.95]	Data not included	
125.2º	3800─7600	[4.95]	Data not included	

TABLE 4.10. (CONT'D)

Angle Lab	Energy (keV)	Author	IBANDL	Action
104.8º	3800─7600	[4.95]	Data not included	
165°	9000─11700	[4.101]	Data not included	
107°	3540─3630	[4.102]	Data not included	
136°	3540─3630	[4.102]	Data not included	
152°	3540─3630	[4.102]	Data not included	
35 angles from 22° to 163°	1460─6560	[4.103]	Data not included	Original data not available
27° ─167° in steps of 5°.	5000 and 6000	[4.96]	Data not included	Original publication not available
170°	5000─9000	[4.92]	Data not included	Data are given as ratio-to-Rutherford
165°	5900─7100	[4.97]	Data not included	Original publication not available Data are given as ratio-to-Rutherford
167°	5040─6000	[4.98]	Data included	Original publication not available
170°	5412─5964	[4.99]	Data not included	Data in original publication are given as ratio-to-Rutherford
169°	6400─7900	[4.100]	Data included	
165°	9000─11700	[4.101]	Data not included	
107°	3540─3630	[4.102]	Data not included	
136°	3540─3630	[4.102]	Data not included	
152°	3540─3630	[4.102]	Data not included	
35 angles from 22° to 163°	1460─6560	[4.103]	Data not included	Original data not available

Ref. [4.87]: In the original publication data are only reported in graphical form. Authors report measurements with alphas in the energy range from 2.5 to 4.8 MeV. Differential cross sections were measured at the c.m. angles 70.1º, 90º, 99.3º, 109.9º, 125.3º, 140.3º, 149.5º and 166.6º. If we assume that only backscattering angles greater than 100º are of importance for the IBA community, and convert c.m. to lab angles, the cross sections reported in the original publications are available for 160º, 136º, 124º and 106.7º in the energy range from 2.5 to 4.8 MeV. Cross sections values are reported in the c.m. frame of reference. However, in IBANDL only data for 106.7º are tabulated and are in agreement with data from original publication.

Ref. [4.93]: In the original publication data are reported only in graphical form. Data are reported for c.m. angles from 30.6º up to 158.8º and laboratory energies from 4 to 13.3 MeV. Again, we are interested only in backscattering angles greater than 100º since they are the most important for IBA. Cross-section curves are plotted for 125.3º, 131.4º, 140.8º, 149.4º, 155º and 158.8º in the c.m. that corresponds to 106.8º, 113.9º, 125.1º, 136.7º, 143.9º and 149º in the lab frame, respectively. However, in IBANDL only data for 149º are tabulated.

Ref. [4.94]: In the original publication data are reported only in graphical form. Data are reported for c.m. angles from 92º, 125.5º, 147.2º and 171º that correspond to 73.7º, 107.2º, 133.3º and 166.6º lab angles. For 171º c.m. (166.6º lab), differential cross sections in the c.m. system are measured from 600–4000 keV. In IBANDL data are published for energies from 640–1170 keV and from 1910─3980 keV. For 147.2º c.m. (133.3º lab) digitized data are available in IBANDL from 2.5 to 4 MeV. This file is in agreement with data from the original publication.

Ref. [4.95]: In the original publication data are presented only in graphical form. C.M.. cross sections are presented for c.m. angles 171.2º, 147.9º, 140.8º, 123.2º and 90.0º that correspond to lab angles of 166.9º, 134.3º, 125.2º, 104.1º and 72º. Assuming only backscattering angles greater than 100º are important for the IBA community, we focus on cross-section data for 167°, 134.3º, 125.2º and 104.1º. For 167° data can be found in IBANDL and are in agreement with the original data.

There are three data sets in EXFOR [4.96], [4.92] and [4.97] and one in IBANDL [4.98] for $^{12}C(\alpha,\alpha)^{12}C$ cross sections that cannot be compared with data from original publications because the original publications are not available. In [4.96] authors have measured differential cross sections at two energies 5 and 6 MeV for scattering angles from 27° to 167° in steps of 5°. R33 files are available for downloading for angles > 100°. In [4.92] the cross-section ratio to Rutherford is reported for energies from 5─9 MeV and 170°. In [4.97] the same is reported for energies from 5.9 to 7.1 MeV and 165°.

R33 files of data from Ref. [4.99], [4.100] and [4.101] have been compared and have been found to be in agreement with data from the original publications.

Authors from ref. [4.102] reported cross sections for four lab angles 92°, 107°, 136° and 152°. In ref. [4.103] authors report angular distributions of cross sections for 35 angles in the range from θ_{lab}=22°─163°. Angular distributions have been obtained at 51 energies in the energy range from 1.466 to 6.558 MeV. It was not possible to check all original data because they are part of a PhD thesis (Plaga, R., Diploma thesis, University of Münster, 1986). Part of the data was checked in Ref. [4.103] for some energies and it was found that those data are in agreement with EXFOR generated R33 files.

Comparison of published data for different scattering angles

Around 135º, there are only three data sets that can be compared. Data from [4.104] and [4.94] are in good agreement up to 3500 keV as can be seen from Fig. 4.54. For energies higher than 3500 keV discrepancies between all three data sets exist.

Around 150º there are data from [4.93] for 149º, from [105] for 150º and from [4.103] for 148°. Data overlap in the region where a strong resonance exists. As can be seen from Fig. 4.55, two sets of data differ in both resonance position and intensity.

Around 165º there are 5 data sets available. Agreement between experimental points from [4.95], [4.103] and [4.90] is good for the resonance at ~ 4250 keV. A difference in the resonance position between data sets is about 10 keV as can be seen from Fig. 4.56. Data also differ in the height of the resonance.

Around 170° there are 6 data sets available in IBANDL. For 4275 keV three data sets can be compared, as can be seen from the magnified part of Fig. 4.57. Data from ref. [4.91] and [4.89] are in agreement concerning height as well as position of the 4275 keV resonance.

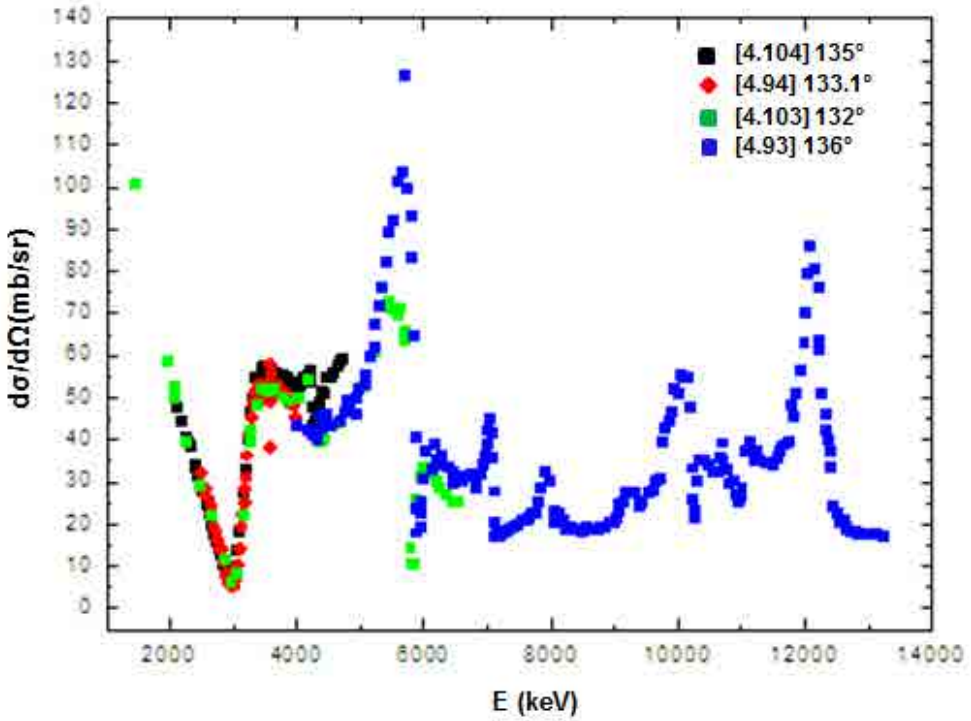

FIG. 4.54. Four sets of data from Refs [4.93], [4.94], [4.104] and [4.103] for $^{12}C(\alpha,\alpha_0)^{12}C$ at angles around 135º.

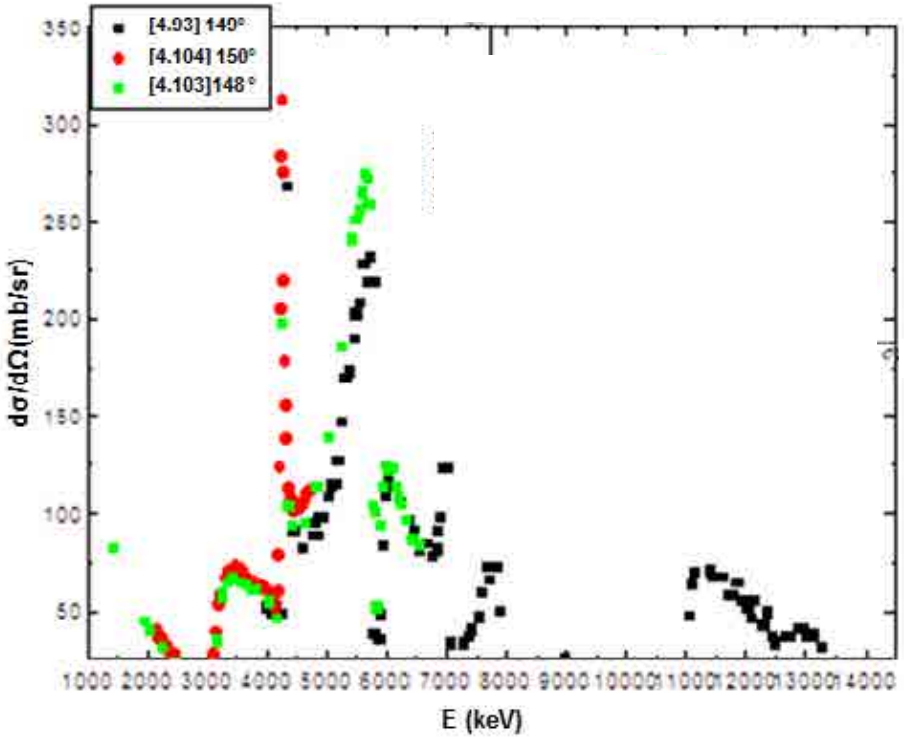

FIG. 4.55. Three sets of data for $^{12}C(\alpha,\alpha)$ differential cross sections from Refs [4.93], [4.104] and [4.103] at angles around 150º.

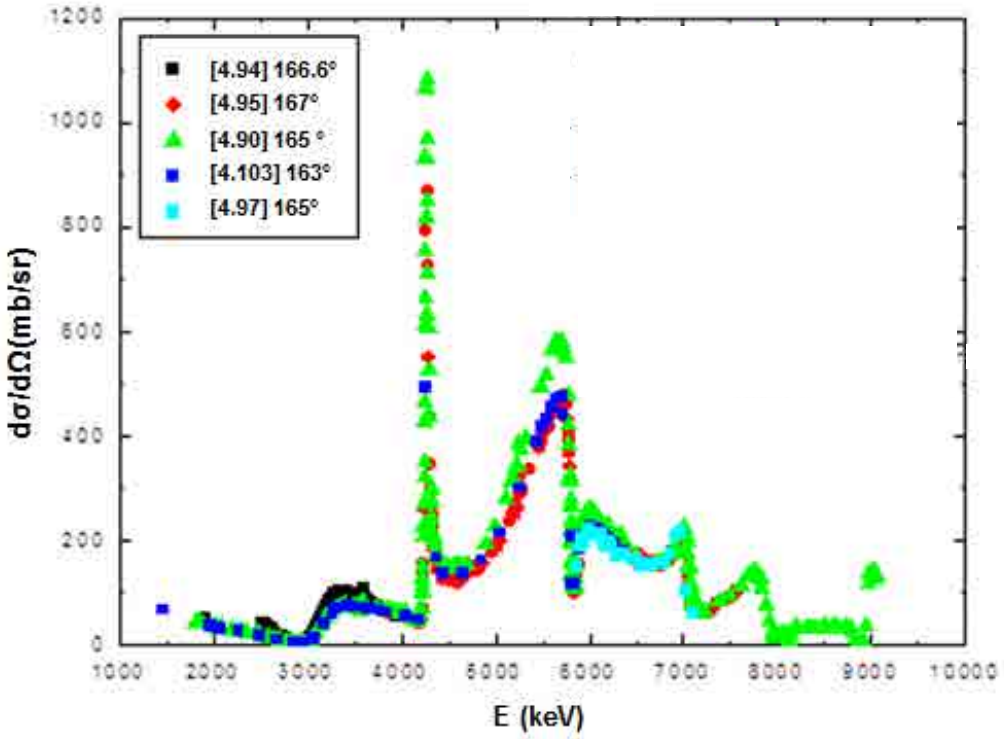

FIG. 4.56. Available data sets for $^{12}C(\alpha,\alpha)$ differential cross sections around 165º published in IBANDL.

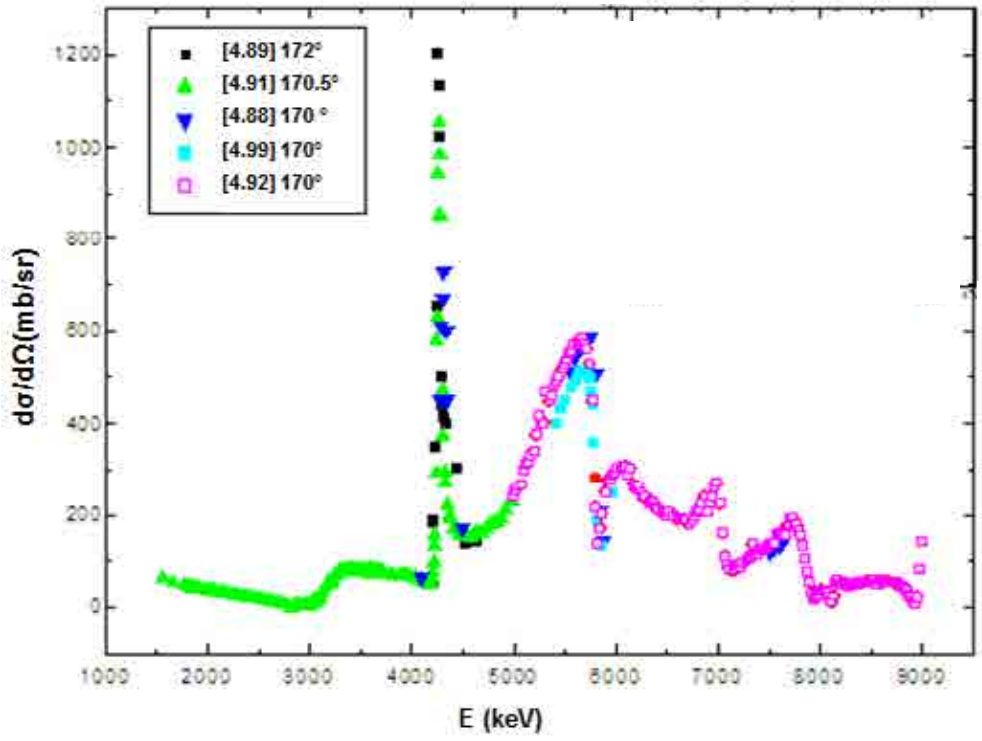

FIG. 4.57. Available data sets for $^{12}C(\alpha,\alpha)$ differential cross sections around 170º published in IBANDL.

Recommended data

An evaluated cross section exists in SigmaCalc for energies from 1.7 to 7.2 MeV and all angles. This evaluated cross section is recommended for all quantitative analysis.

4.16. $^{14}N(\alpha,\alpha_0)^{14}N$

Table 4.11 shows the list of data sets available in IBANDL. All cross-section data are shown in Figs. 4.58–4.61 in graphical form. In the graphs both the energy and the cross section are given in the laboratory frame of reference, with energy units in MeV and cross-section units in mb/sr.

TABLE 4.11. LIST OF DATA SETS AVAILABLE IN IBANDL

Nº	Reaction	Lab. Scattering Angle (°)	Energy Range (keV)	Reference
1	$N(\alpha,\alpha_0)N$	171.0°	7480─8180	[4.105]
2	$N(\alpha,\alpha_0)N$	171.0°	8980─9780	[4.105]
3	$N(\alpha,\alpha_0)N$	167.2°	2010─3840	[4.106]
4	$N(\alpha,\alpha_0)N$	167.0°	4550─6570	[4.107]
5	$N(\alpha,\alpha_0)N$	167.0°	7090─9070	[4.107]
6	$N(\alpha,\alpha_0)N$	167.0°	8700─9000	[4.107]
7	$N(\alpha,\alpha_0)N$	166.0°	920─1420	[4.108]
8	$N(\alpha,\alpha_0)N$	166.0°	1400─1920	[4.108]
9	$N(\alpha,\alpha_0)N$	166.0°	1900─2240	[4.108]
10	$N(\alpha,\alpha_0)N$	165.0°	1990─9060	[4.109]
11	$N(\alpha,\alpha_0)N$	163.7°	2680─4700	[4.110]
12	$N(\alpha,\alpha_0)N$	150.0°	3140─3770	[4.111]
13	$N(\alpha,\alpha_0)N$	109.5°	2010─3840	[4.106]
14	$N(\alpha,\alpha_0)N$	127.5°	2010─3840	[4.106]
15	$N(\alpha,\alpha_0)N$	167.2°	2010─3840	[4.106]
16	$N(\alpha,\alpha_0)N$	172.0°	5200─7500	[4.112]
17	$N(\alpha,\alpha_0)N$	177.0°	9090─9590	[4.113]
18	$N(\alpha,\alpha_0)N$	167.0°	5080─5970	[4.98]
19	$N(\alpha,\alpha_0)N$	165.0°	3420─5990	[4.114]
20	$N(\alpha,\alpha_0)N$	118.0°	2544─3927	[4.115]
21	$N(\alpha,\alpha_0)N$	150.0°	2544─3927	[4.115]
22	$N(\alpha,\alpha_0)N$	165.0°	2544─3927	[4.115]

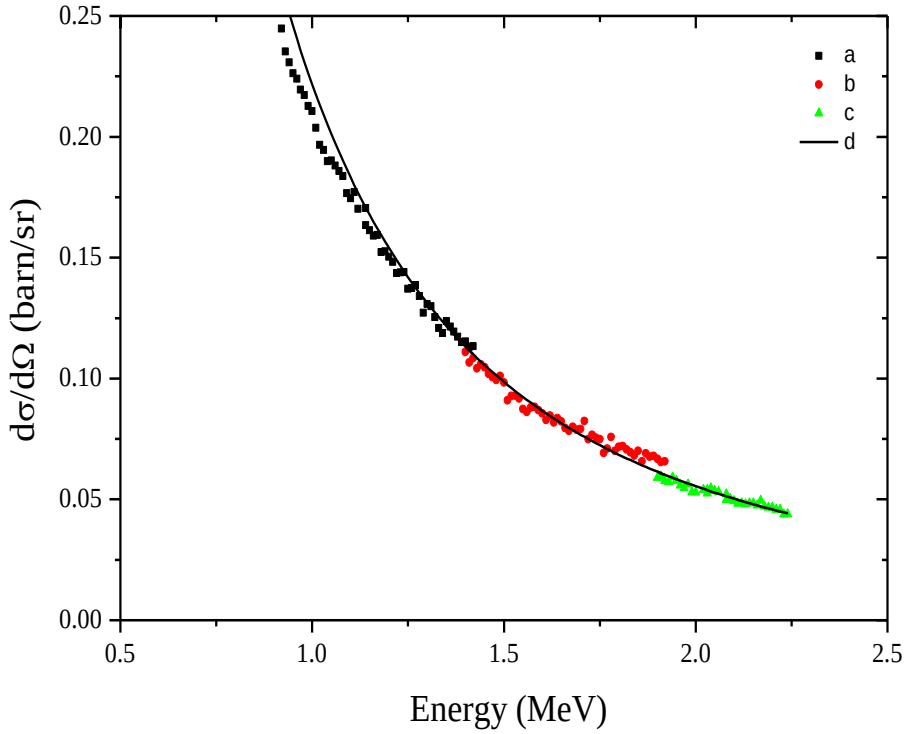

FIG. 4.58. Cross section for the N(α,α_0)N reaction measured at low energy by Silverstein et al. [4.108] at θ =166º. a, b and c are the cross section values; d is the corresponding Rutherford cross section.

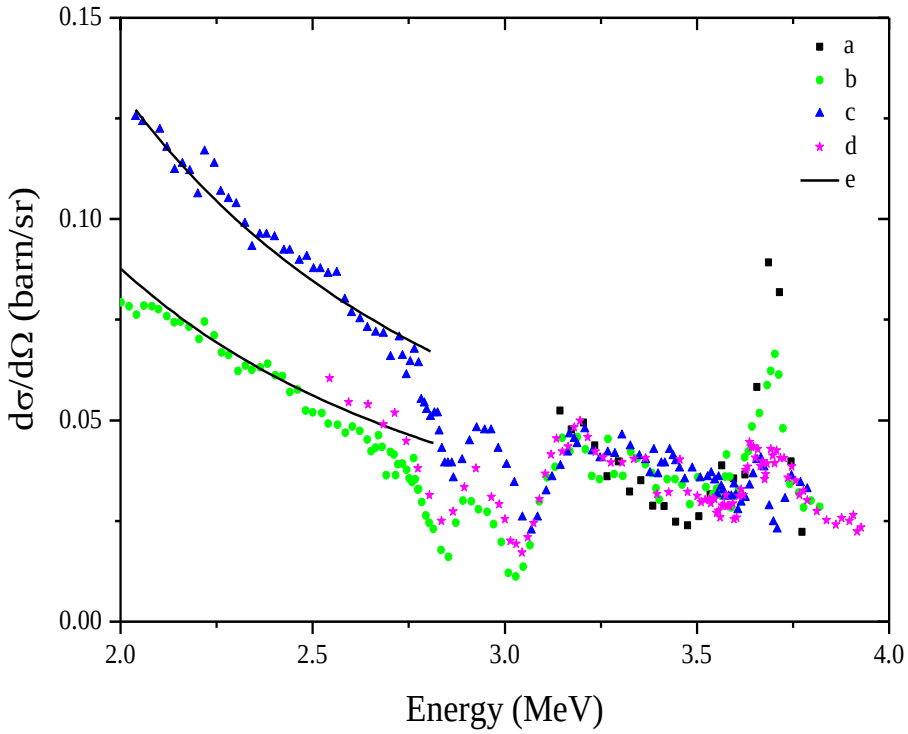

FIG. 4.59. Cross section for the N(α,α_0)N reaction at scattering angles in the 109.5º–150º range, measured for energies up to 4 MeV: (a) cross section values measured at 150º by Jiang et al. [4.111]; (b) cross section values measured at 127.5º by Herring et al. [4.106]; (c) cross section values measured at 109.5º by Herring et al. [4.106]; (d) cross section values measured at 118º by Gurbich et al. [4.115]; (e) Rutherford cross section at the same scattering angles as the Herring data.

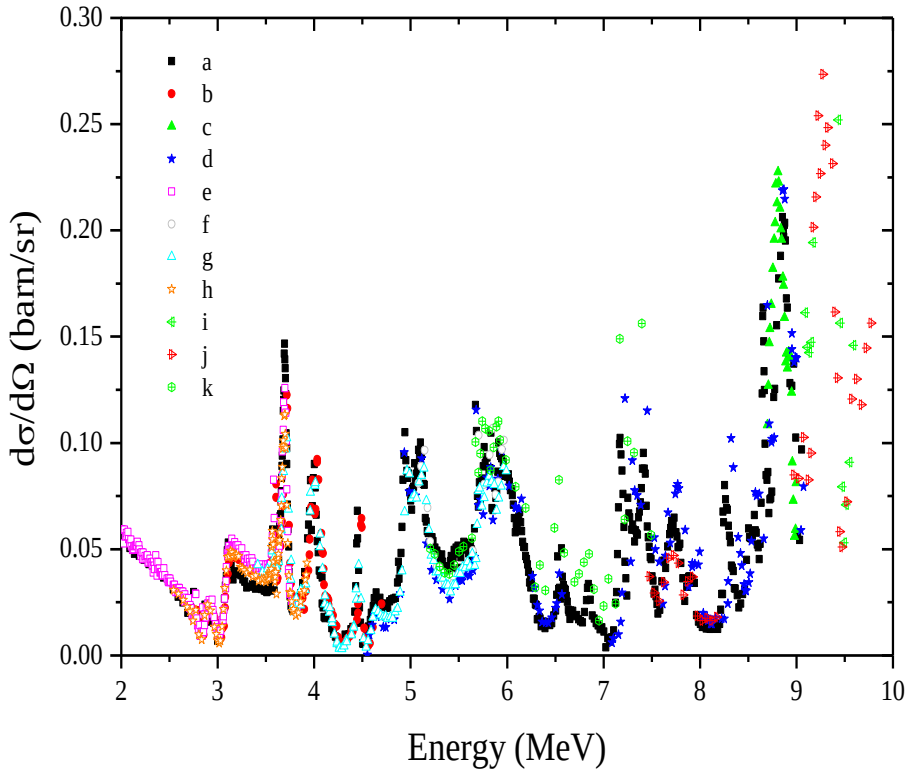

FIG. 4.60. Cross section for the N(α,α_0)N reaction at scattering angles in the 163.7º─177º range, measured for energies up to 9.75 MeV. (a) cross section values measured by Feng et al. at 165º [4.109]; (b) cross section values measured by Kashy et al. at 163.7º [4.110]; (c) cross section values measured by Foster et al. at 167º - data set # 6- [4.107]; (d) cross section values measured by Foster et al at. 167º - data set # 4 and #5- [4.107]; (e) cross section values measured by Herring et al. at 167.2º [4.106];(f) cross section values measured by Wettland et al. at 167º [4.98]; (g) cross section values measured by Terwagne et al. at 165º [4.114]; (h) cross section values measured by Gurbich et al. at 165º [4.115];(i) cross section values measured by Qiu et al at. 177º [4.113]; (j) cross section values measured by Berky et al. at 171º [4.105]; (k) cross section values measured by Artigalas et al. at 172º [4.112].

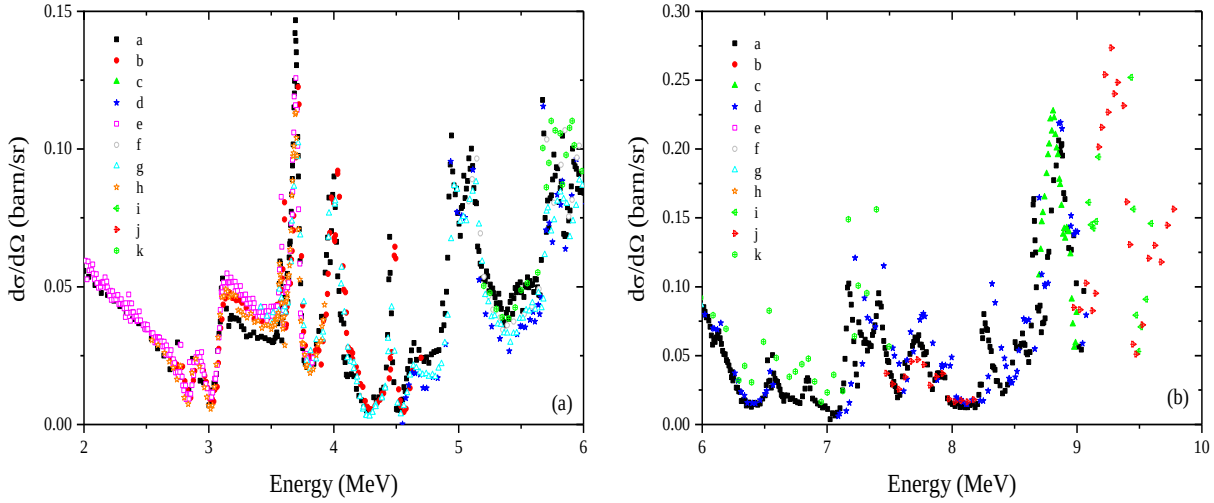

FIG. 4.61. (a) Detail of figure 4.60 in the 2─6 MeV energy range. (b) Detail of figure 4.60 in the 6─10 MeV energy range. Graph legend is the same as in Fig. 4.60.

Looking at Figs 4.58 – 4.61 it becomes clear that up to ~2.5 MeV the cross section is very close to Rutherford. Above 2.5 MeV, the cross section shows many strong resonances. The measured data reveal several discrepancies. In the following, the data sets are compared and the most consistent data sets in a certain energy and angular range are recommended for IBA use.

Considering the 163─167º angular range and the 2.5─3.8 MeV energy range the Terwagne [4.114], Kashy [4.110], Herring [4.106] and Gurbich [4.115] data show the greatest consistency, with the exception of the resonances around 3.70 and 3.57 MeV. According to Terwagne *et. al.*, the intensity of the 3.70 MeV resonance is significantly lower in the Terwagne data due to increased energy loss in their (thicker) target and due to the subtraction of the $^{14}N(\alpha,p_0)^{17}O$ contribution. Its position also appears to be shifted to higher energies in the Terwagne and Kashy data, when compared with the Feng, Herring and Gurbich data. The 3.57 MeV resonance does not even appear in the Terwagne data and its position and intensity varies in all the other data sets (Kashy, Feng, Herring and Gurbich), with the Feng (3.569 MeV) and Gurbich (3.566 MeV) data being in closer agreement. Looking at all the data sets in this energy and angular range, the Gurbich [4.115] data are the most corroborated by other measurements and should be preferred for IBA use. They should also be given greater relevance in a future evaluation.

Considering the 163─167º angular range and the 3.8─4.5 MeV energy range, three data sets exist: Terwagne [4.114], Feng [4.109] and Kashy [4.110]. As regards intensity, the Feng and Kashy data agree very well, although in the 2.5─3.8 MeV energy range, the Kashy data are ~30 keV shifted towards higher energies. The energy position of the resonances in the Terwagne data is closer to Feng's but, as discussed above, the fine structure of the resonances is lost. Thus, the preferred data set in this energy range are the Feng [4.109] data.

Considering the 163─167º angular range and the 4.5─ 6.5 MeV energy range, four data sets exist: Terwagne [4.114], Feng [4.109], Foster [4.107] and Wettland [4.98]. The Feng and Foster data agree quite well in the resonance regions although Foster's data are too low in the plateaus (it is the lowest of the four data sets). The resonances in the Terwagne data are again "smoothed" due to the effect discussed previously. In the case of Wettlands' data, the energy step is too coarse to permit the observation of some resonant structures. Thus, the preferred data set in this energy range are the Feng [4.109] data.

Considering the 163─167º angular range and the 6.5─9.5 MeV energy range, only two data sets exist: Feng's [4.109] and Foster's [4.107]. The intensity of the cross section agrees well in both data sets, but, unaccountably, Foster's data are ~50 keV shifted to higher energies, whereas, in the 4.5─6.5 MeV energy range, the resonances' energy position agreed well in the two data sets. Moreover, this energy shift decreases with increasing beam energy, until the resonance position at 8.87 MeV coincides. Given the fact that the energy position of the resonances in Feng's data is reproduced by other measurements at lower energies, Feng's data [4.109] are recommended for use in this energy interval.

Existing data at other scattering angles are too sparse and taken at scattering angles too far apart to perform an analysis similar to the one above.

Recommended data

An evaluated cross section exists in SigmaCalc for energies from 1.6 to 4.6 MeV and all angles. If available, this evaluated cross section is recommended for all quantitative analysis. Table 4.12 summarizes the recommendations for the use of experimental data. The evaluated cross section was compared with the recommended experimental cross sections in table 4.12. In the 2.5─3.8 MeV range the evaluated cross section reproduces quite closely the Gurbich

data [4.115], both at 165º and 118º scattering angle, with the notable exception of the resonance at 2.766 MeV, which is much sharper and intense in the evaluated file than in any of the measured data, recommended or otherwise. Such difference is usually related to the limited energy resolution of the experiments, since it is quite a narrow resonance. In the 3.8─4.5 MeV energy range and for scattering angles in the 163─167º range, the evaluated cross section closely follows the Kashy data [4.110], which means that the resonances appear ~30 keV shifted towards higher energies when compared with the recommend Feng data set [4.109]. The evaluated data are an important tool for the IBA analyst, especially when no experimental data exist at a particular scattering angle.

TABLE 4.12. RECOMMENDED EXPERIMENTAL CROSS SECTIONS FOR THE N(α,α_0)N REACTION FOR IBA ANALYSIS

Energy Range (MeV)	**Scattering Angle Range**	**Recommended Data**
2.5─3.8	163─167º	[4.115]
3.8─ 4.5	163─167º	[4.109]
4.5─ 6.5	163─167º	[4.109]
6.5─ 9.5	163─167º	[4.109]

4.17. D(^{4}He,D)^{4}He AND T(^{4}He,T)^{4}He

In previous works, several authors have measured the forward recoil cross sections for D(^{4}He,D)^{4}He and T(^{4}He,T)^{4}He [4.116, 4.117, 4.118, 4.119, 4.120, 4.121, 4.122]. The energy range covers 1─3 MeV and 9─11 MeV. The scattering angles are 10°, 20°, 25°, 30°, 35° and 40° for D(^{4}He,D)^{4}He, and 30° for T(^{4}He,T)^{4}He. But some disagreement among their results exists. The discrepancy mainly comes from the samples and measuring methods. For the measurement of the D(^{4}He,D)^{4}He cross section, Kellock [4.117] employed samples of 60 nm deuterated polystyrene $(C_8D_8)_n$, and used two detectors to allow the simultaneous collection of ERD and RBS spectra. Hence the deuterium differential cross section can be determined from

$$\sigma_D(E^*,\theta_D) = \frac{A_D \Omega_\alpha \sigma_C(E^*)}{A_C \Omega_D \sigma_C{}^{Ruth}(E^*)} \sigma_C{}^{Ruth}(E^*,170^0) \qquad (4.1)$$

where $\sigma_C(E^*)$ is the backscattering differential cross section for carbon at 170^0 and E^* is the mean laboratory energy of incident He^+ ions within the film. Ω_α and Ω_D are the respective solid angles of the detectors at 170º and θ_D. The above equation is independent of the amount of collected charge. The main error of the cross section comes from Ω, θ and A if the ratio of C to D is exact. However, the loss of deuterium (about 1%) due to the ion beam bombardment during each run of 20 μC is also a source of error.

Quillet [4.118] used deuterated polystyrene $(C_8D_8)_n$ to measure the deuterium differential cross section for helium energies ranging from 1─2.6 MeV at recoil angles of 10°, 20° and 30°. The cross sections were determined from the formula

$$\left(\frac{d\sigma}{d\Omega}\right) = \frac{Y(E)\cos\theta_{target}}{NQ\Omega}. \qquad (4.2)$$

When using a movable detector to measure the RBS spectrum for a Bi implanted silicon reference sample with known dose as well as the ERDA spectrum, the solid angles Ω in equation (4.2) vanishes. Thus, the total error originated from other uncertainties and was from 4 to 7%.

In 1986, Besenbacher [4.119] used a target consisting of a self-supporting 400 Å Au film, upon which 100 Å Ti was evaporated in a D atmosphere to form a $TiD_{0.8}$ layer. The D(^{4}He,D)^{4}He recoil yield was measured relative to the $D(^3He,\alpha)p$ nuclear reaction. The ^{3}He+D cross section determined by Möller and Besenbacher [4.123] has an absolute accuracy of $\pm 4\%$ for c.m. energies less than 500 keV. Since the detector solid angle is constant during the rotation around the center line, the laboratory cross section can be easily obtained from the nuclear reaction cross section as follows:

$$\left(\frac{d\sigma}{d\Omega}\right)_{lab}^{rec} = \frac{Y_{rec}}{Y_{nuc}}\frac{Q_{nuc}}{Q_{rec}}\left(\frac{d\sigma}{d\Omega}\right)_{lab}^{nuc}\left(\frac{d\Omega_{cms}}{d\Omega_{lab}}\right)^{nuc} \qquad (4.3)$$

where the last factor is the solid angle centre-of-mass to laboratory system conversion factor for the ^{3}He+D reaction. When the above statistical uncertainty of Y and Q is 2─3%, the absolute accuracy of the cross section is $\pm 5\%$, which is almost the same as that alleged by Kellock [4.117].

Sawicki [4.120] used the same measuring principle as Besenbacher [4.119] in order to measure the cross section for T(^{4}He,T) ^{4}He forward scattering. However, he employed two kinds of targets, i.e. a tritium–titanium target prepared by absorption of evaporated Ti in a T atmosphere and a tritium–silicon target fabricated by implantation. It was found that the Si-T target was much more stable than the Ti-T target. With the quoted accuracy of the cross section for the T(d,α)n reaction of 2% and all statistical uncertainties originating from Y and Q of typically $\pm 4\%$, the total error is not larger than 10%.

In recent measurements of cross sections for the D(^{4}He,D)^{4}He and T(^{4}He,T)^{4}He forward scattering, J.F. Browning et al. [4.121,4.122] used the original formula to calculate the cross section in the energy range of 911 MeV, i.e. equation (4.2). However, because they employed special methods to measure each item in the formula separately, i.e., N was measured by thermal desorption, Q by a chopper system and Ω by using a ^{238}Pu α source, the error of N, Q and Ω can be controlled in ± 2.0, ± 2.0 and ± 1.0%, respectively. So the overall uncertainty in the measured cross section is 3.2%.

For measuring the D(^{4}He,D)^{4}He cross section, the various experimental data show some discrepancies in the absolute values both within and outside of the resonance region. Fig. 4.62 shows a comparison of the experimental data at several angles. The work by Besenbacher [4.119] is the most complete, having been done over a wide range of energies and angles. Below the resonance energy, Besenbacher's values are in agreement with Kellock's [4.117] results. However, in the resonance region there is a systematic disagreement in the magnitude of the cross section, which apparently could be explained by a constant offset of ~2° in the detector angle. Kellock's results are closer to Quillet's data [4.118] in the resonance region.

Besenbacher [4.119] quotes his angular precision to be ± 2°, which would explain the discrepancy with Kellock's work. The strong dependency on the detector angle is nonetheless noteworthy, and indicates the need for special angular precision when working in the resonance region.

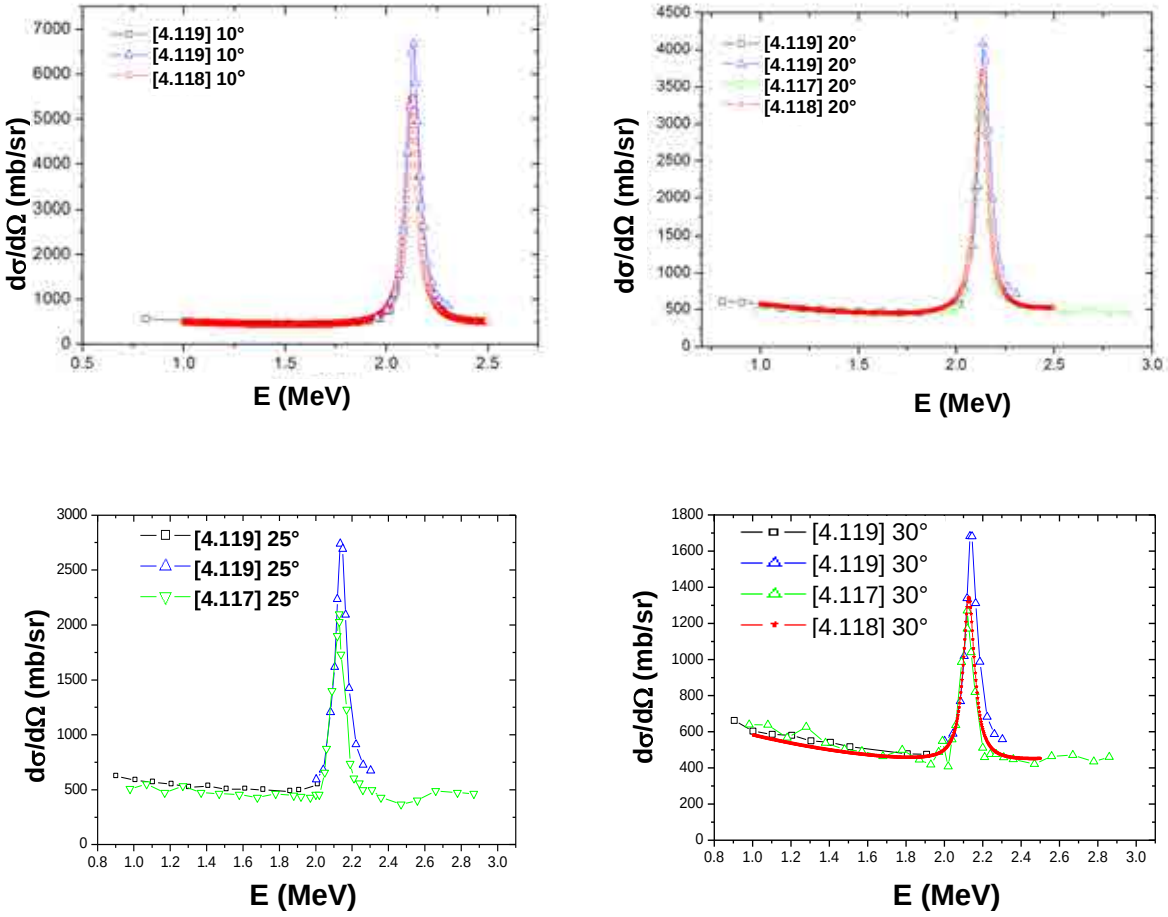

FIG. 4.62. Comparison of the D(^{4}He,D)^{4}He recoil cross section at different recoil angles.

Recommended data

For the D(^{4}He,D)^{4}He recoil cross section the data sets by Besenbacher [4.119], Quillet [4.118] and Kellog [4.117] agree within 10─15% at energies below about 2 MeV at recoil angles from 10° ─ 30°. Within the resonance region (from about 2.0 to 2.3 MeV) Besenbacher's data show disagreement with the data from Quillet and Kellog and seem to suffer from a systematic error in the recoil angle. The data sets from Quillet and Kellog show qualitative agreement for the cross section in the resonance region, but with a small shift of the position of the resonance and a difference of about 5─10% in the peak values.

4.18. D(^{3}He,p)^{4}He AND ^{3}He(d,p)^{4}He

The experimental data for the total cross section of the D(^{3}He,p)^{4}He and ^{3}He(d,p)^{4}He reaction show large discrepancies, both with respect to the absolute cross-section values and the position of the resonance, as can be seen in Fig. 4.63–4.65. The low energy data of Jarvis [4.124] are totally off, see Fig. 4.63. The data of Freier [4.125] are larger than all other data at the position of the resonance, see Fig. 4.64.

The more recent data by Möller and Besenbacher [4.123] have an accuracy of about 5%. The data by Kunz [4.126] and by Möller/Besenbacher [4.123] indicate an identical position of the resonance, but their absolute cross-section values disagree.

The total cross section was evaluated in [4.127] using R-matrix theory, the result of this evaluation is shown in Figs. 4.63–4.65 as solid line. However, because this evaluation was based on R-matrix calculations performed already in 1979, only experimental data taken before this year were taken into account, and the data by Möller and Besenbacher [4.123] and Krauss et al. [4.128] were not included. As can be seen in Fig. 4.63 and Fig. 4.65, the R-matrix result is in good agreement with the data by Krauss et al. [4.128], but systematically lower than the Möller and Besenbacher data [4.123] at the position of the resonance. Bosch and Hale suppose their evaluation to be correct to at least 10%, with the maximum uncertainty occurring near the peak of the resonance [4.127]. The parameterizations by Peres [4.129] and Duane [4.130] (dashed and dotted lines in Figs. 4.63–4.65) show larger inaccuracies in comparison to the experimental data, and their use is not recommended.

As it was shown by several authors [4.131, 4.126, 4.132], the angular distribution of the differential cross section is almost isotropic in the centre-of-mass system at incident deuteron energies below about 1 MeV (corresponding to incident ^{3}He energies below about 1.5 MeV), see Figs. 4.66 and 4.67. The deviation from isotropic is below about 2%. Therefore, in this energy range the differential cross section can be obtained at any laboratory angle by using the total cross section (for example from the evaluation of Bosch and Hale [4.127] or by using experimental data from Möller and Besenbacher [4.123]), dividing it by 4π in the centre-of-mass system, and then converting the cross section to the laboratory system.

At higher energies experimental differential cross-section data have to be used. Alimov et al. [4.133] determined the differential D(^{3}He,p)^{4}He reaction cross section at a laboratory angle of 135° for ^{3}He energies between 0.5 and 6 MeV [4.133]. The relative accuracy of the individual Alimov data points is about 3.5%. The absolute cross-section values were obtained by fitting the measured values to the Möller and Besenbacher values [4.123] in the energy range 0.55–1.2 MeV, where the absolute accuracy is about 4%.

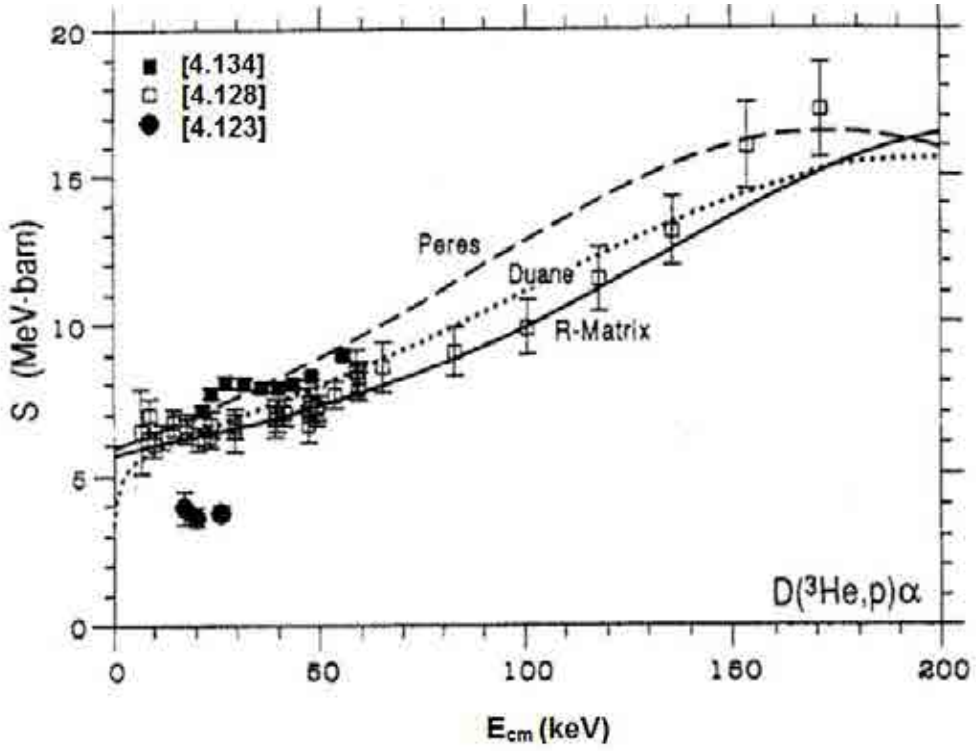

FIG. 4.63. S values for the D(^{3}He,p)^{4}He reaction as a function of the centre-of-mass energy for energies below 200 keV. The solid line is the result of the R-matrix evaluation from [4.128]. Figure taken from [4.127].

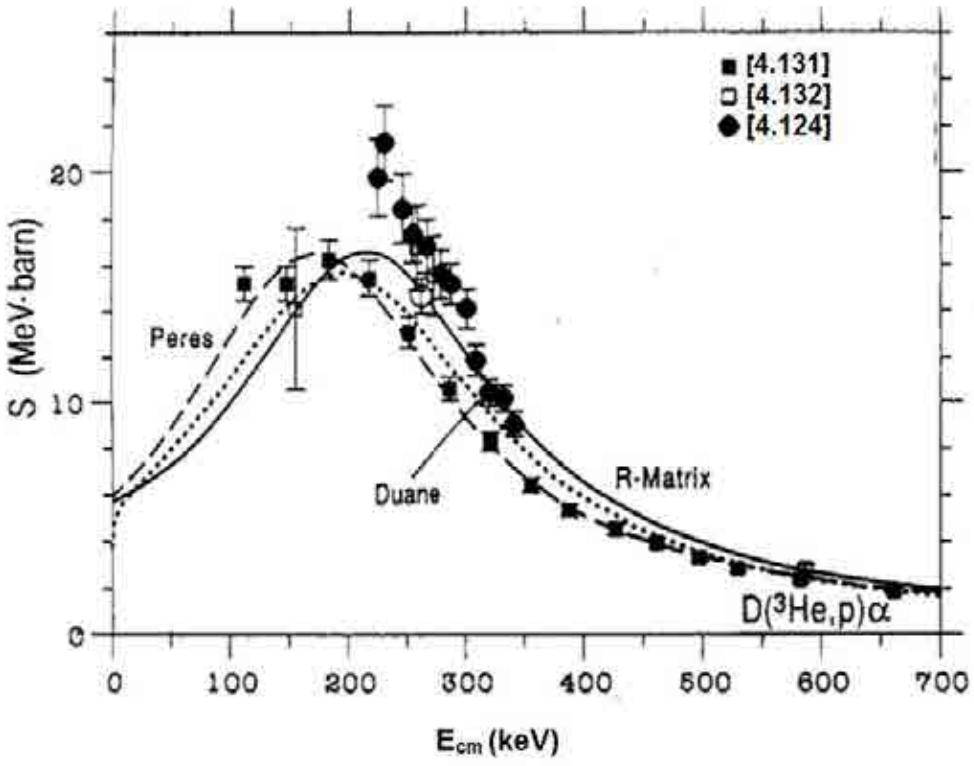

FIG. 4.64. S values for the D(^{3}He,p)^{4}He reaction as a function of the centre-of-mass energy. The solid line is the result of the R-matrix evaluation from [4.127]. Figure taken from [4.127].

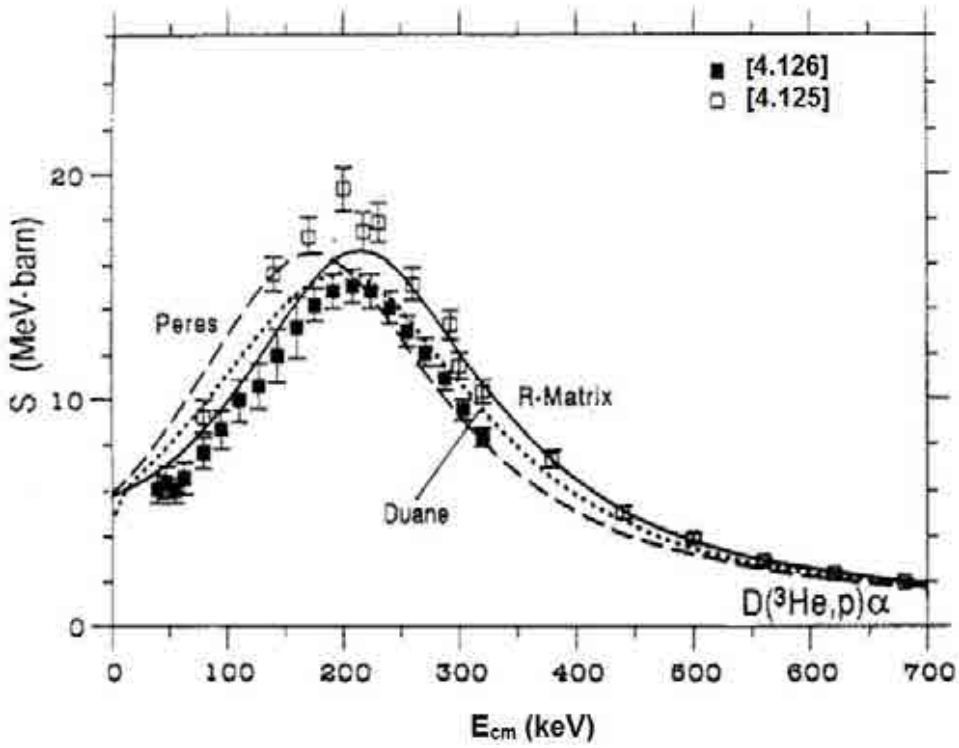

FIG. 4.65. S values for the D(^{3}He,p)^{4}He reaction as a function of the centre-of-mass energy. The solid line is the result of the R-matrix evaluation from [4.127]. Figure taken from [4.127].

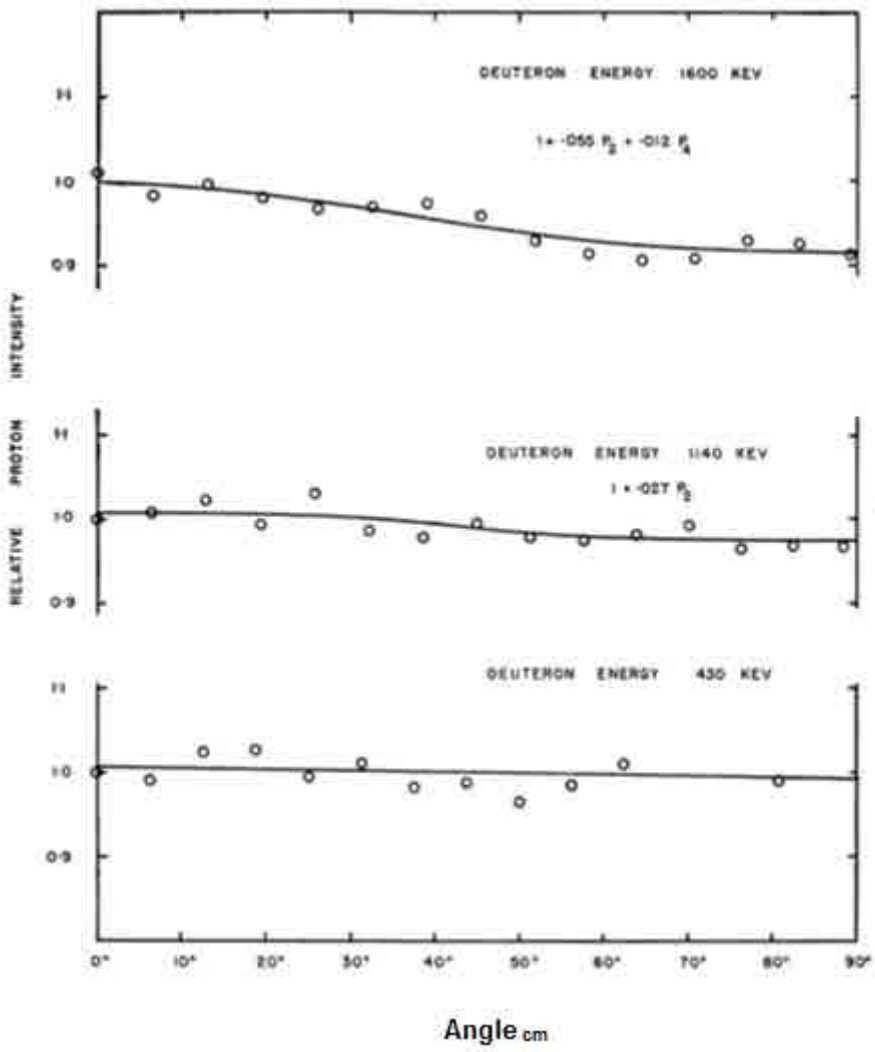

FIG. 4.66. Centre-of-mass angular distribution of protons created from the $^{3}He(d,p)\alpha$ reaction at different deuteron energies. Figure reproduced courtesy of American Physical Society [4.131].

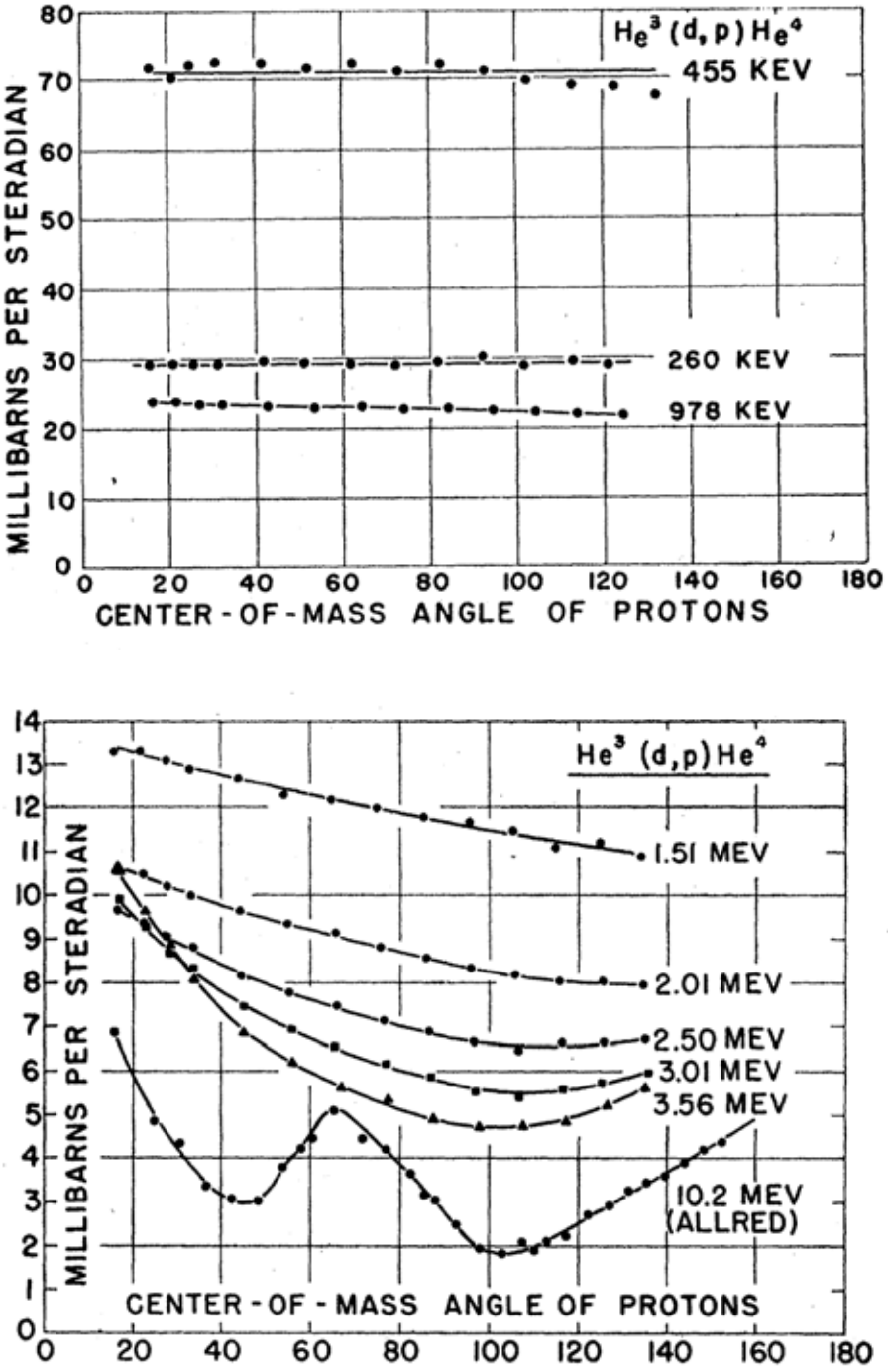

FIG. 4.67. Centre-of-mass angular distribution of protons created from the $^{3}He(d,p)\alpha$ reaction at different deuteron energies. Figure reproduced courtesy of American Physical Society [4.132].

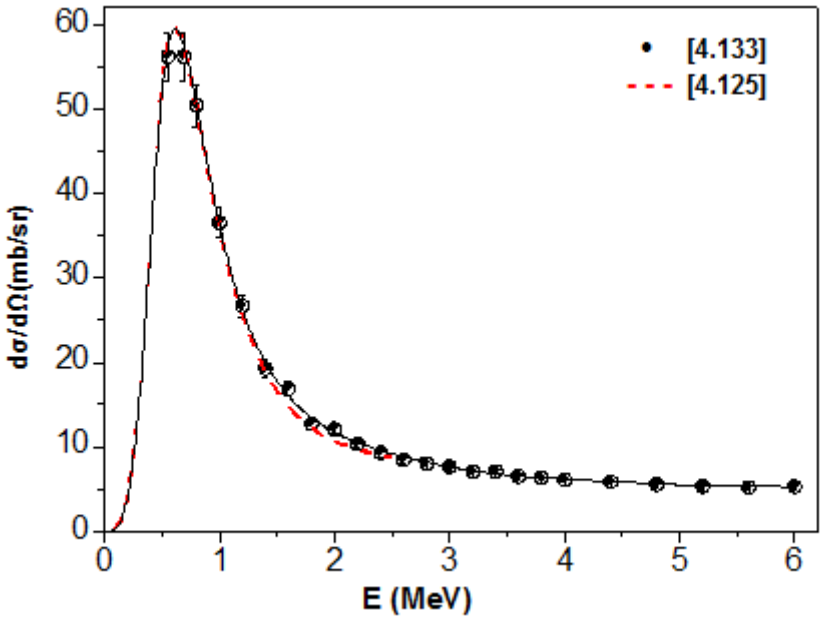

FIG. 4.68. Differential cross section of the D(^{3}He,p)^{4}He nuclear reaction at an angle of 135° in the laboratory system. Dots: experimental data from [4.133]. Solid line to guide the eyes. Dashed line: differential cross section from the fit function of Möller and Besenbacher [4.123] to the total cross section, assuming angular independence in the centre-of-mass system.

Recommended data

The total cross section of the D(^{3}He,p)^{4}He and ^{3}He(d,p)^{4}He reaction was evaluated using the R-matrix theory by Bosch and Hale [4.127] with an absolute accuracy of about 10%, and precise experimental data for the total cross section with an accuracy of about 5% were provided by Möller and Besenbacher [4.123]. [4.127] and [4.123] show reasonable agreement. The differential cross section can be obtained from the total cross section by assuming angular independence in the centre-of-mass system at incident deuteron energies below about 1 MeV, corresponding to incident ^{3}He energies below about 1.5 MeV. This introduces an additional error below about 2%. For higher energies Alimov provided reliable cross-section data for the D(^{3}He,p)α reaction up to 6 MeV at a reaction angle of 135° [4.133].

4.19. ^{12}C(d,p)^{13}C

No significant problems for the ^{12}C(d,p)^{13}C cross section were found. Recent results obtained by Kokkoris et al. [4.145] are in reasonable agreement with the data acquired many years ago. Thanks to Kokkoris' detailed measurements, the cross section for ^{12}C+d is known both for the transitions to the ground and to excited states in a sufficiently wide interval of angles. The quality of the available experimental data is illustrated by Fig. 4.69, where different data sets are compared for 165°. Some uncertainty is seen in the peak locations and in the magnitude of the broad peak near 1200 keV. A substantial discrepancy is observed only in the energy region above 1900 keV indicated by a circle. It is worth noting that for the 1200 keV peak the data obtained by Kashy et al. [4.140] and Balin et al. [4.142] are in excellent agreement (the absolute value reported by Balin et al. is 102 ± 6.7 mb/sr) whereas Kokkoris' points lie a little bit lower. The data by Phillips et al. [4.141] reproduced in the LA-2014 report are erroneously normalized (see Fig. 4.70) by a factor of about 2.

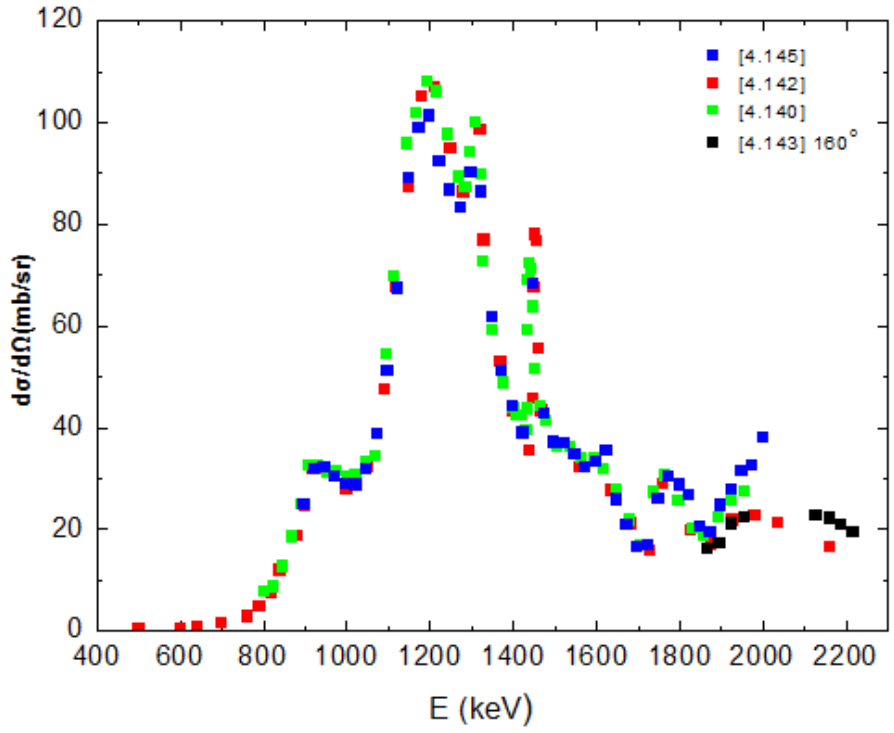

FIG. 4.69. Comparison of different experimental data for $^{12}C(d,p_0)^{13}C$ at 165°.

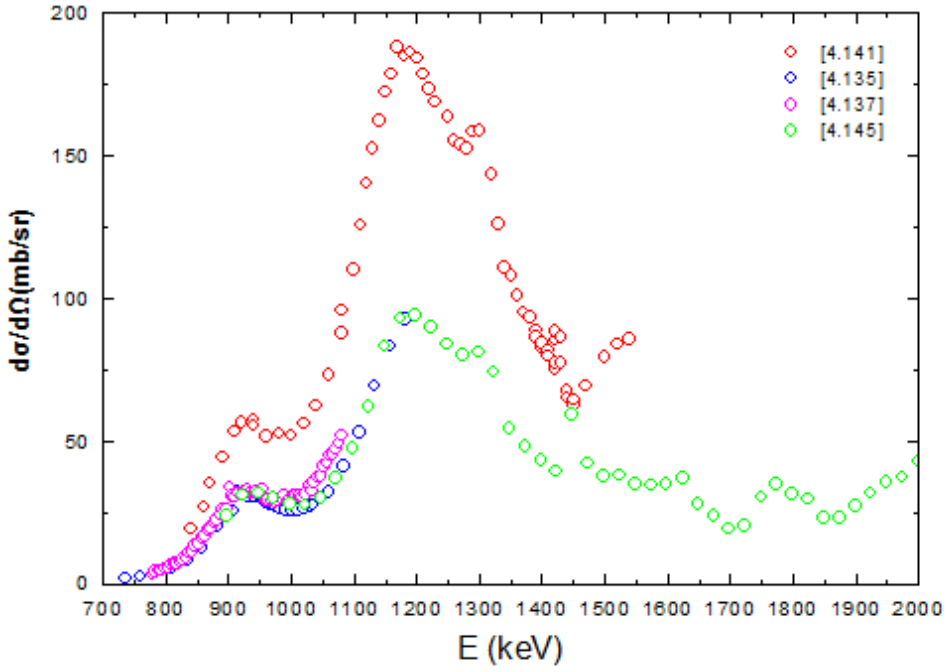

FIG. 4.70. Comparison of different experimental data for $^{12}C(d,p_0)^{13}C$ at 150°.

Special efforts were applied for the absolute calibration of the $^{12}C(d,p_0)^{13}C$ cross section at the 900─1000 keV plateau. The obtained results along with Jiang's tabulated data [4.137] are

compared in Table 4.13. Again, the agreement between the values reported by different authors is good.

TABLE 4.13. ABSOLUTE VALUES FOR THE $^{12}C(d,p_0)^{13}C$ CROSS SECTION AT 150°

Energy, keV	Cross section (mb/sr)	Target	Reference
968	29.5±1.2	Polystyrene	[4.118]
970	27.9±1.4	Frozen gas	[4.135]
970	25.5±0.8	Frozen CO_2	[4.136]
969	29.25±1.2	C/Glass	[4.137]

Only scarce information is available for the cross sections of the reaction leading to excited states of the residual nucleus. In order to make a comparison, excitation functions for the $^{12}C(d,p_1)^{13}C$ reaction were derived from the angular distributions presented in [4.138] (see Figs. 4.71–4.73). As can be seen from these figures, some discrepancy is observed in the 1700─1800 keV energy region for 145° and 150° and good agreement is observed for 165°. It should be noted that the cross-section behaviour in the vicinity of the sharp resonance at an energy slightly below 1500 keV was measured in insufficient detail.

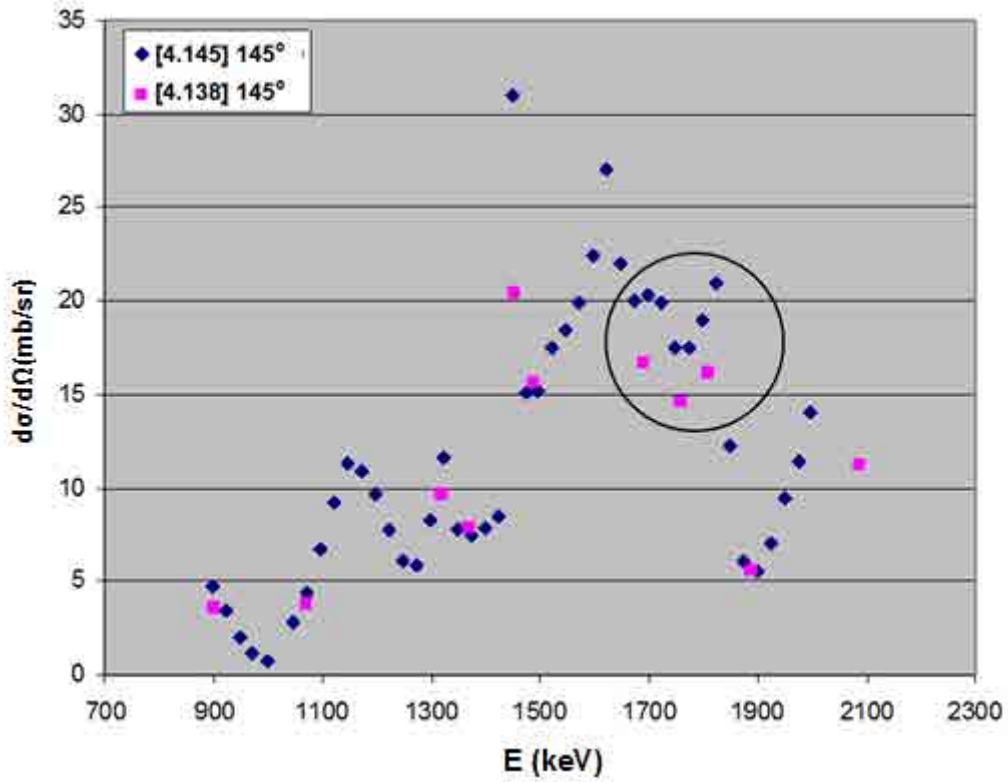

FIG. 4.71. Excitation function for the $^{12}C(d,p_1)^{13}C$ reaction at 145°.

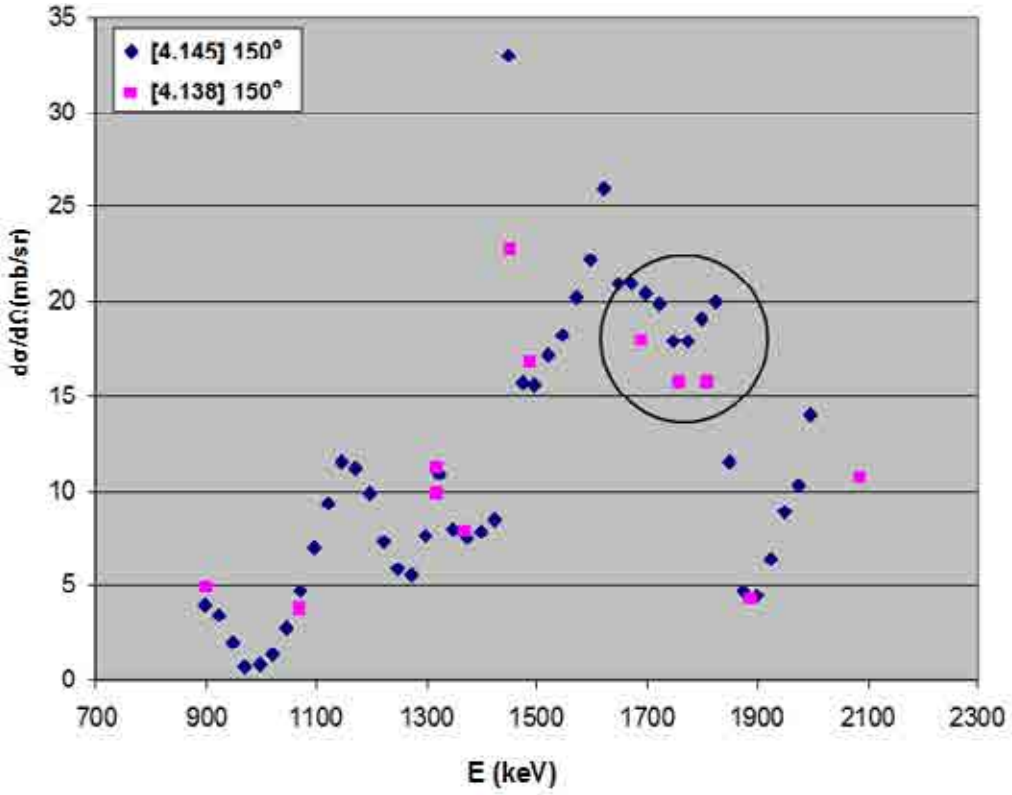

FIG. 4.72. Excitation function for the $^{12}C(d,p_1)^{13}C$ reaction at 150°.

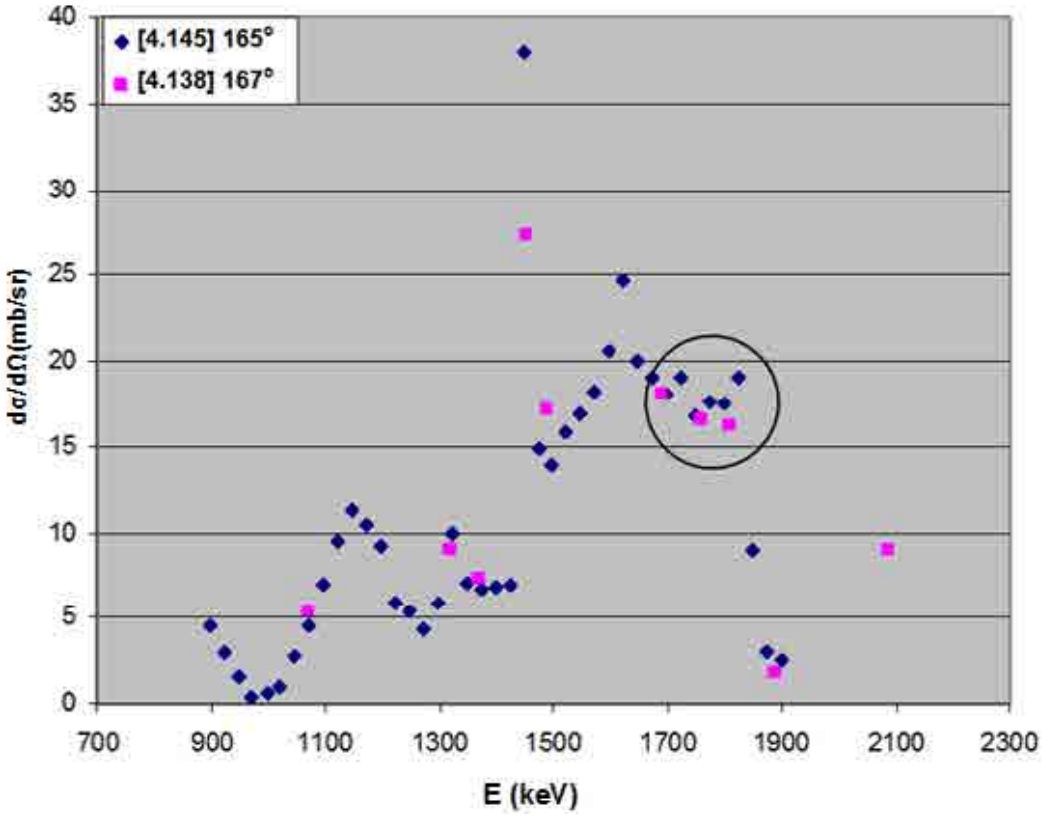

FIG. 4.73. Excitation function for the $^{12}C(d,p_1)^{13}C$ reaction around 165°.

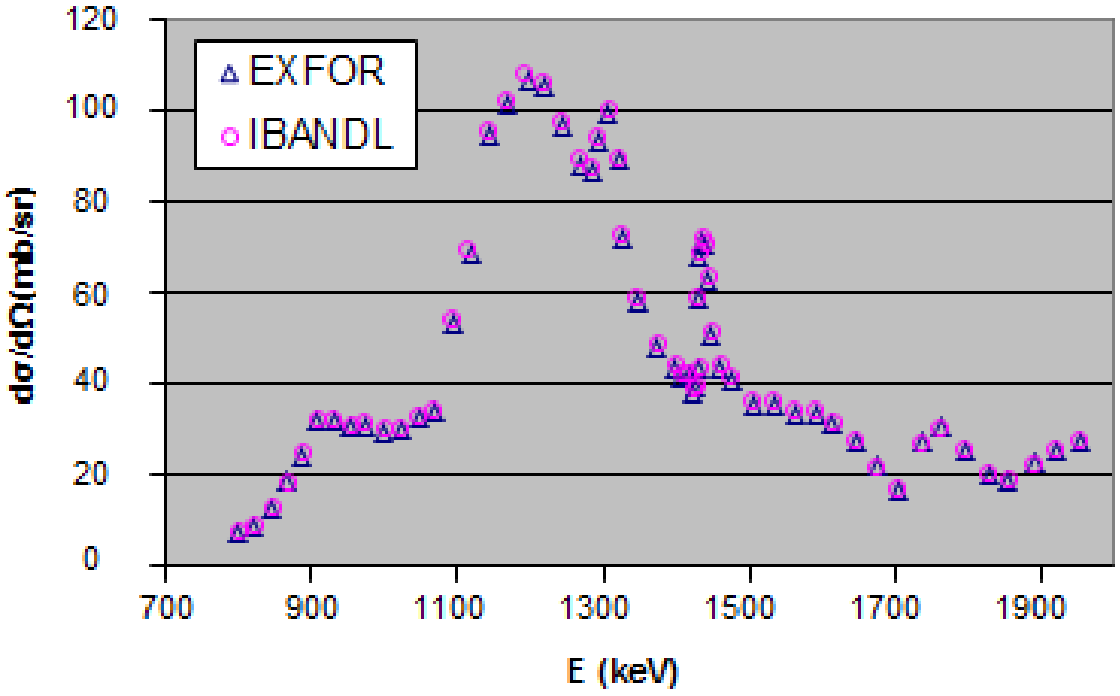

FIG. 4.74. Comparison of Kashy et al data [4.140] at 165° as *compiled in EXFOR and IBANDL.*

Cumulative information on the studied cross sections is presented in Table 4.14. The comparison of different compilations of Kashy's data [4.140] for 165° (EXFOR vs IBANDL) as shown in Fig. 4.74 demonstrates good agreement. Nevertheless, a decision should be made which of the data sets should be accepted if the data bases have identical data for the same paper.

TABLE 4.14. CUMMULATIVE INFORMATION ON THE DEUTERON INDUCED REACTIONS FOR ^{12}C

Energy (MeV)	Reaction	Target	Energy (MeV) [angular distribution]	Angle [excitation function]	Error	Data	Notes	Ref.
0.9─2.1	(d,p_1)	Thin self-supporting ^{12}C targets made from suspension of graphite in alcohol	0.9, 1.07, 1.32, 1.37, 1.452, 1.49, 1.69, 1.76, 1.809, 1.89, 2.088			Graph	EXFOR F0334002 Excitation functions for 145°, 150°, 167° derived from angular distributions are shown in Figs. 4.70 ─ 4.72	[4.138]
0.968	(d,p_0)	Polystyrene film		150	4%	Value		[4.118]
0.970	(d,p_0)	Frozen CO_2		150	2%	Value	Added to IBANDL	[4.136]
0.74─1.18	(d,p_0)	Frozen gas		150	5%	Table	Added to IBANDL	[4.135]
0.8─1.1	(d,p_0)	C/Glass		150	4%	Table, Graph	Added to IBANDL	[4.137]
0.5─3.0	(d,p_0)	Carbon foil		135	12%	Graph	Jarjis' data are presented in IBANDL	[4.139]
0.75─1.98	(d,d), (d,p_0), (d,p_1)	Carbon foil	0.92, 1.19, 1.31, 1.61, 1.76	47.6, 80.5, 158.4, 165.0	8%	Graph	Cross section for 158.4° was added to IBANDL (EXFOR 1007003). Data for (d,p_1) are presented only for 80.5°.	[4.140]
0.78─1.55	(d,p_0)	Cracking benzene vapor on silver foils	0.75, 0.91, 0.99, 1.09, 1.16, 1.286, 1.30, 1.32	0, 90, 150		Graph	Data from LA-2014 report are presented in IBANDL	[4.141]

TABLE 4.14. (CONT'D)

Energy (MeV)	Reaction	Target	Energy (MeV) [angular distribution]	Angle [excitation function]	Error	Data	Notes	Ref.
0.5─2.16	(d,p_0)	Carbon foil		165	7%	Graph	Data supplied by the authors are presented in IBANDL	[4.142]
1.87─3.51	(d,p_0)	Gas		160, 168.7	5%	Graph	Cross section for 160° was added to IBANDL (EXFOR C0993006 converted to lab.)	[4.143]
0.8─1.5	(d,p_0)	Thick target		165		Graph		[4.144]
0.9─2.0	(d,p_{0-3})	Carbon foils		145, 150, 155, 160, 165, 170		Graph, Table	Added to IBANDL	[4.145]

Recommended data

An evaluated cross section exists in SigmaCalc for the $^{12}C(d,p_0)^{13}C$ reaction at energies from 0.9 to 1.9 MeV and all angles. This evaluated cross section is recommended for all quantitative analysis.

4.20. $^{12}C(^3He,p)^{14}N$

The $^{12}C(^3He,p)^{14}N$ reaction can be used for the detection of ^{12}C if the simultaneous detection of deuterium by the $D(^3He,p)\alpha$ reaction is required or if the use of a deuterium beam and the reaction $^{12}C(d,p)^{13}C$ is not possible due to radiation protection reasons. The reactions $^{12}C(^3He,p_{0,1,2})^{14}N$ have Q values that are high enough for the protons from these reactions to be visible even in detectors with thick absorber foils, while protons from higher excited states require thinner absorber foils.

Available cross-section data for the different reactions are listed in Tables 4.15 to 4.19. The available IBANDL files were compared with the original publications. The data from [4.146] in the file c2hp0c.r33 were stored with only 2 digits, although they were given with 3 digits in the original publication. This resulted in a difference of about 1% between the published data and IBANDL. A corrected file was supplied to IBANDL. Most other files have been digitized from the published graphs, and no visible differences were found between the IBANDL files and the original publications. The data from [4.147] at 76° and from [4.148] at 30° and 7° are not in IBANDL, but can be found in EXFOR. Due to the forward reaction angle they are only of limited use for IBA. The data from [4.147] for the $^{12}C(^3He,p_3)^{14}N$ and $^{12}C(^3He,p_4)^{14}N$ reactions at 76° and 159.4° are also missing in IBANDL. However, these data are also only of limited use in IBA.

TABLE 4.15. AVAILABLE CROSS-SECTION DATA FOR THE $^{12}C(^3He,p_0)^{14}N$ REACTION

Reference	Reaction angle	Energy range (keV)	Presentation	IBANDL file
[4.147]	159.4°	1770 – 5360	Graph	c2hp0b.r33
[4.148]	150°	2010 – 5010	Graph	c2hp0i.r33
[4.148]	120°	2020 – 4950	Graph	c2hp0h.r33
[4.149]	90°	1600 – 3000	Numeric, from author	c2hp0d.r33
[4.150]	90°	1940 – 2810	Graph	c2hp0a.r33
[4.148]	90°	2010 – 5010	Graph	c2hp0g.r33
[4.146]	90°	2100 – 2420	Table	c2hp0c.r33
[4.147]	76°	1780 – 5400	Graph	–
[4.148]	60°	2000 – 5010	Graph	c2hp0f.r33
[4.148]	30°	2000 – 5000	Graph	–
[4.148]	7°	2000 – 5000	Graph	–

TABLE 4.16. AVAILABLE CROSS-SECTION DATA FOR THE $^{12}C(^{3}He,p_1)^{14}N$ REACTION

Reference	Reaction angle	Energy range (keV)	Presentation	IBANDL file
[4.149]	177.2	1960 – 2940	Numeric, from author	C2hp1c.r33
[4.147]	159.4°	1770 – 5360	Graph	c2hp1a.r33
[4.148]	150°	2010 – 5010	Graph	c2hp1i.r33
[4.148]	120°	2020 – 4950	Graph	c2hp1h.r33
[4.149]	90°	1600 – 3000	Numeric, from author	c2hp1d.r33
[4.150]	90°	1940 – 2810	Graph	c2hp1b.r33
[4.148]	90°	2010 – 5010	Graph	c2hp1g.r33
[4.146]	90°	2100 – 2420	Table	c2hp1e.r33
[4.147]	76°	1780 – 5400	Graph	—
[4.148]	60°	2000 – 5010	Graph	c2hp1f.r33
[4.148]	30°	2000 – 5000	Graph	—
[4.148]	7°	2000 – 5000	Graph	—

TABLE 4.17. AVAILABLE CROSS-SECTION DATA FOR THE $^{12}C(^{3}He,p_2)^{14}N$ REACTION

Reference	Reaction angle	Energy range (keV)	Presentation	IBANDL file
[4.149]	177.2	1960 – 2940	Numeric, from author	C2hp2c.r33
[4.147]	159.4°	1780 – 5390	Graph	c2hp2a.r33
[4.148]	150°	2000 – 5000	Graph	c2hp2h.r33
[4.148]	120°	2190 – 4990	Graph	c2hp2g.r33
[4.149]	90°	1600 – 3000	Numeric, from author	c2hp2d.r33
[4.150]	90°	1200 – 2880	Graph	c2hp2b.r33
[4.146]	90°	2100 – 2420	Table	c2hp2e.r33
[4.147]	76°	1780 – 5400	Graph	—
[4.149]	60°	2990 – 4980	Graph	c2hp2f.r33
[4.149]	30°	2000 – 5000	Graph	—
[4.149]	7°	2400 – 5000	Graph	—

TABLE 4.18. AVAILABLE CROSS-SECTION DATA FOR THE $^{12}C(^{3}He,p_3)^{14}N$ REACTION

Reference	Reaction angle	Energy range (keV)	Presentation	IBANDL file
[4.147]	159.4°	1780 – 5390	Graph	–
[4.149]	90°	1600 – 3000	Numeric, from author	c2hp3a.r33
[4.147]	76°	1780 – 5400	Graph	–

TABLE 4.19. AVAILABLE CROSS-SECTION DATA FOR THE $^{12}C(^{3}He,p_4)^{14}N$ REACTION

Reference	Reaction angle	Energy range (keV)	Presentation	IBANDL file
[4.147]	159.4°	1780 – 5390	Graph	–
[4.149]	90°	1600 – 3000	Numeric, from author	c2hp4a.r33
[4.147]	76°	1780 – 5400	Graph	–

The different data at a reaction angle of 90° are compared in Fig.4.75–4.77. The data from Tong et al. [4.146] and Terwagne et al. [4.149] are always in perfect agreement. However, because these data have been at least partly measured by the same group, the question remains whether these data sets are subject to identical systematic errors. The agreement between Tong [4.146], Terwagne [4.149], Bromley et al. [4.150] and Johnston et al. [4.148] is poor, both for the absolute cross-section values and for the energies of the resonances. The data by Bromley and Johnston are not too different, but disagree with Tong and Terwagne. The only exception are the data for the $^{12}C(^{3}He,p_2)^{14}N$ reaction, where Tong, Terwagne and Bromley lie closer together. It was speculated by Terwagne et al. [4.149] that the discrepancy with respect to the data of Bromley et al [4.150] was due to an inaccurate accelerator energy calibration by the latter. However, no proof was given for this speculation. Moreover, the data of Bromley et al [4.150] and Johnston et al [4.148] agree for the energies of the resonances, so that this speculation seems unjustified.

The cross-section data at angles in the range 150–160° from Kuan [4.147] and Johnston [4.148] are shown in Figs 4.78–4.80. The general trend of the curves is similar, but the quantitative agreement is poor.

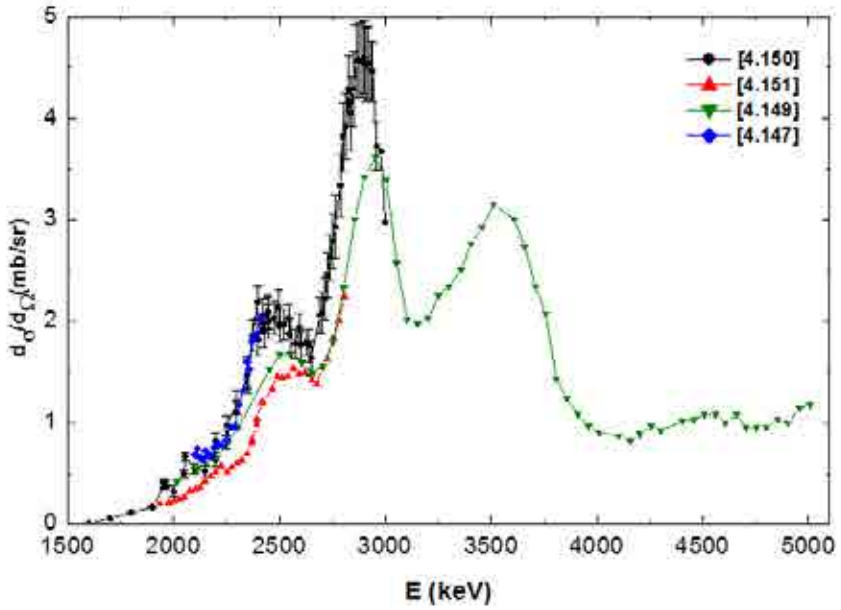

FIG. 4.75. Differential cross sections for the reaction $^{12}C(^{3}He,p_0)^{14}N$ at a reaction angle of 90°.

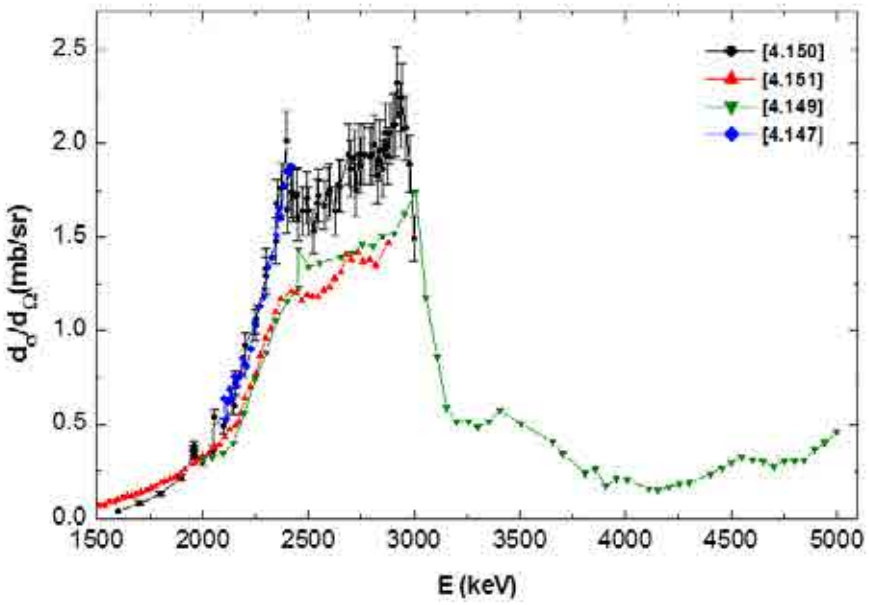

FIG. 4.76. Differential cross sections for the reaction $^{12}C(^{3}He,p_1)^{14}N$ at a reaction angle of 90°.

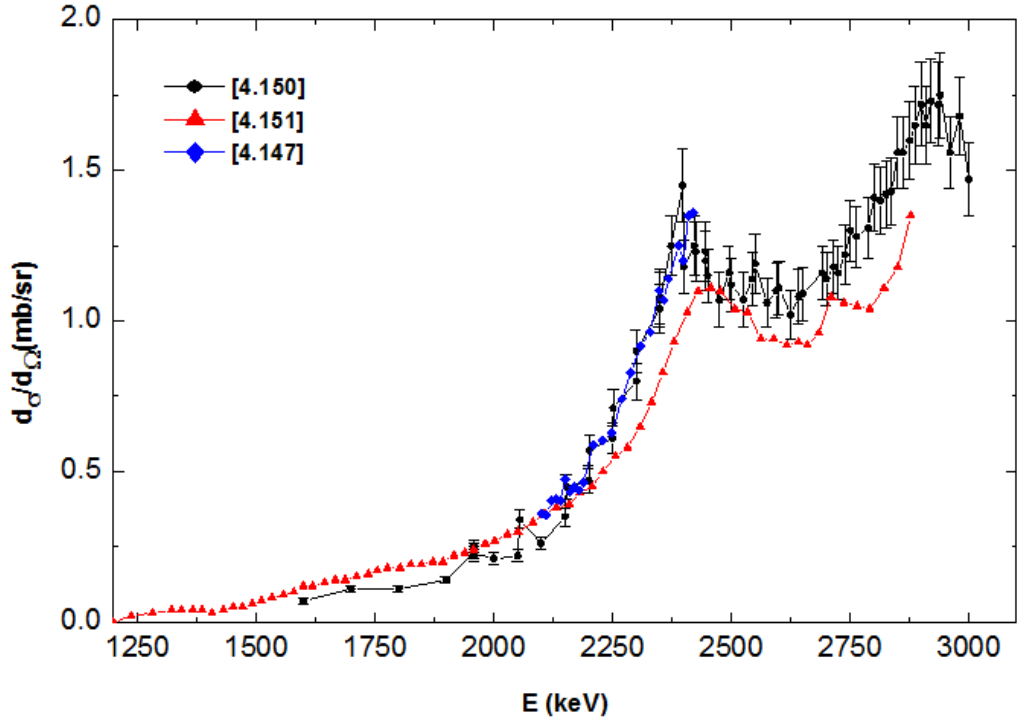

FIG. 4.77. Differential cross sections for the reaction $^{12}C(^{3}He,p_2)^{14}N$ at a reaction angle of 90°.

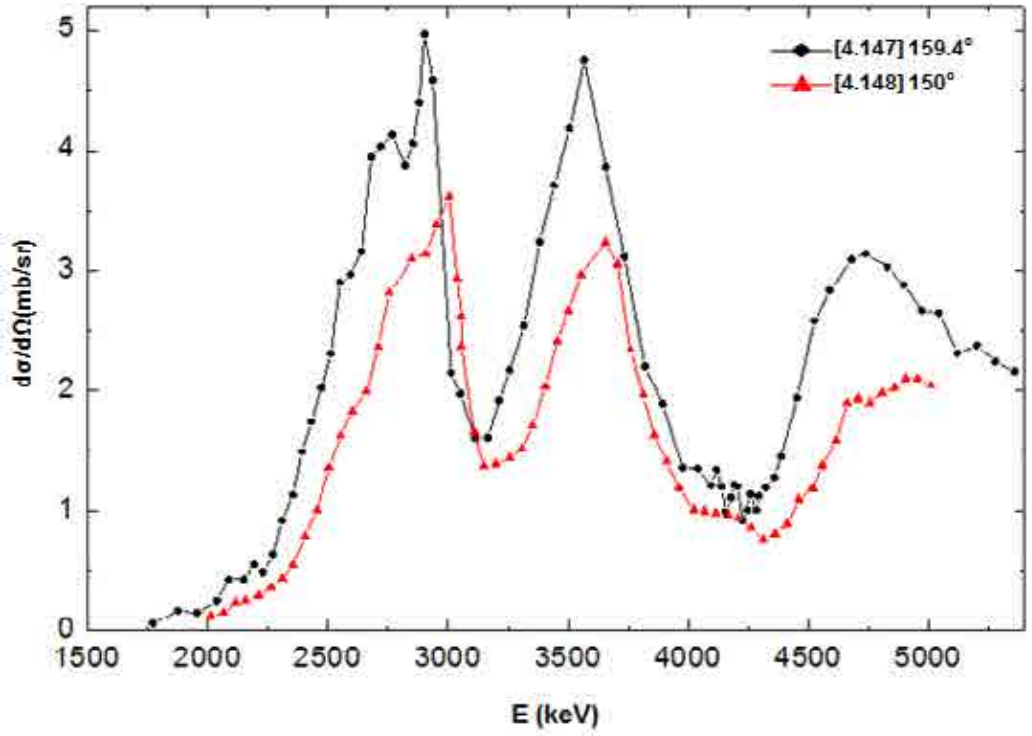

FIG. 4.78. Differential cross sections for the reaction ^{12}C ($^{3}He,p_0)^{14}N$ at reaction angles from 150° to 160°.

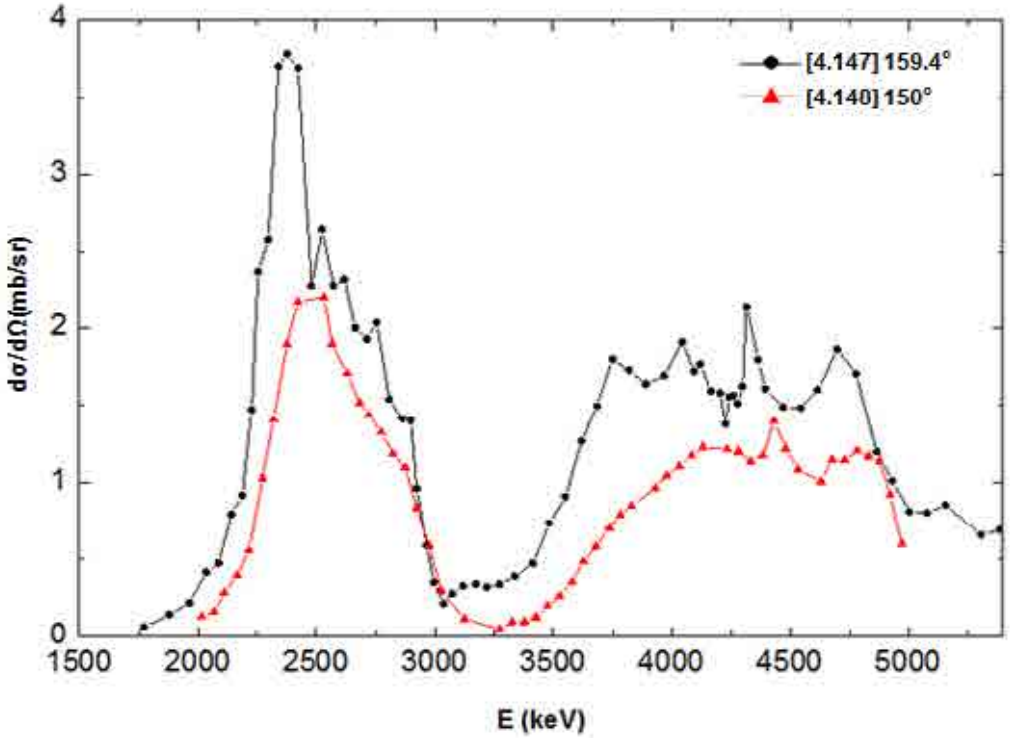

FIG. 4.79. Differential cross sections for the reaction $^{12}C(\ ^{3}He,p_1)^{14}N$ at reaction angles from 150-160°.

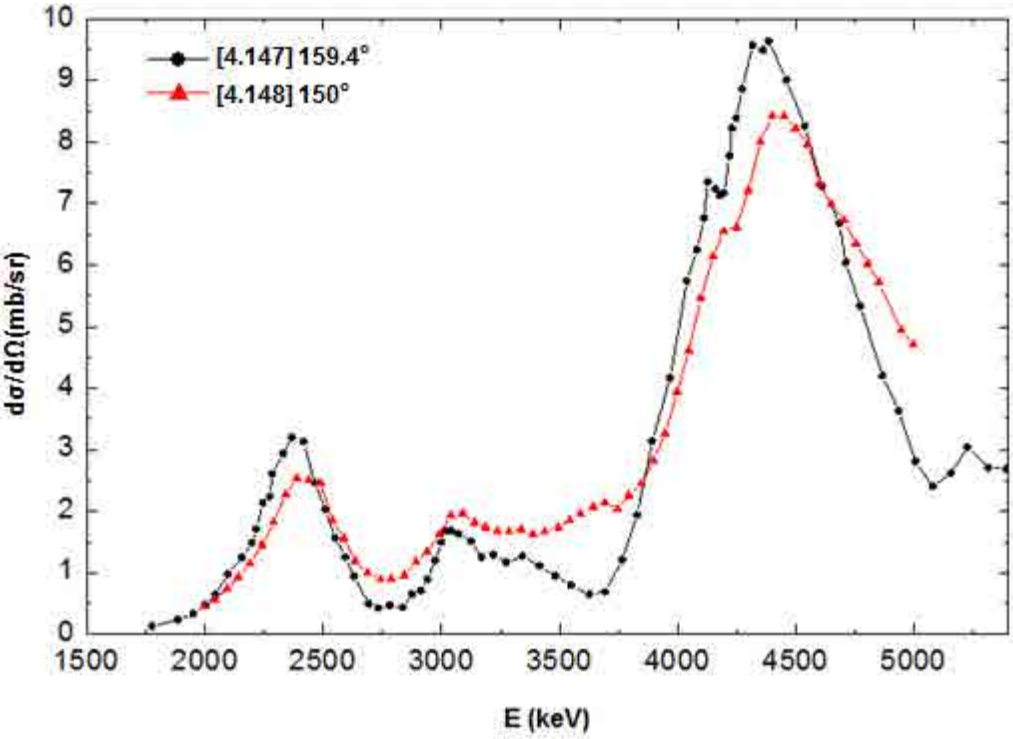

FIG. 4.80. Differential cross sections for the reaction $^{12}C(\ ^{3}He,p_2)^{14}N$ at reaction angles from 150°-160°.

Recommended data

Due to the large discrepancies of the different measurements, a recommendation cannot be given and additional measurements are necessary in order to resolve the open questions.

4.21. $^{16}O(d,p)^{17}O$ AND $^{16}O(d,\alpha)^{14}N$

The $^{16}O(d,p_1)^{17}O$ reaction is known to be very popular for oxygen analysis [4.151]. A relatively wide plateau in the 800─900 keV energy region provides favourable conditions for IBA and so the cross section in this region was measured in a number of works. Most of the results were obtained at 150° (see Fig. 4.81) and therefore additional measurements are needed in a wider interval of angles.

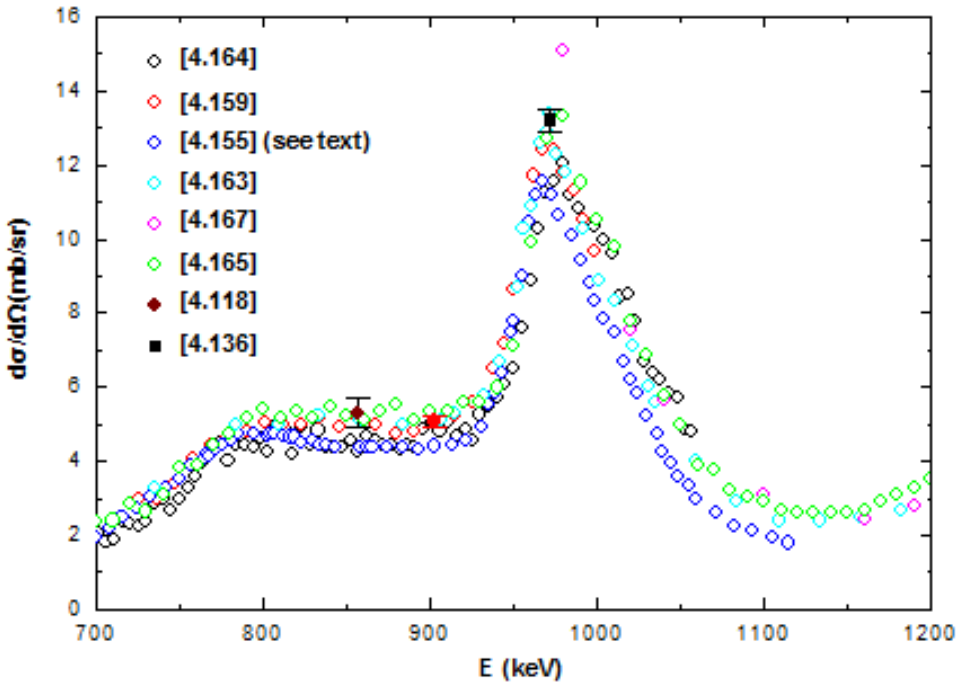

FIG. 4.81. Experimental data available for the $^{16}O(d,p_1)^{17}O$ reaction in the energy range from 700 to 1200 keV at 150°. Solid points represent the data.

An ambiguity should be noted concerning the $^{16}O(d,p_1)^{17}O$ cross section obtained by Amsel et al. and presented by the authors in graphical form in four original publications [4.152,4.153, 4.154,4.155]. There is every indication that the data are the same in all the figures. Strangely enough none of the papers contains a description of the cross-section measurements. Therefore nothing is known about the experimental conditions at which the data were obtained. The scattering angle is 165° in the laboratory frame in the figures in all the papers except for [4.152] where the scattering angle is not indicated at all. However, it is the figure from [4.152] which is reproduced in the handbooks [4.156,4.157], the cross section being attributed to an angle of 150°. This angle is mentioned in the paper [4.152], but on another occasion.

There are at least two papers [4.153, 4.158] where Amsel et al. demonstrate the application of the $^{16}O(d,p_1)^{17}O$ cross section to particular studies, with the experimental set-up being presented in the figures. The detector is fixed at 165° in both cases. Amsel's data [4.155] are compared in Fig. 4.82 with the data sets obtained for 150° [4.159] and 164°15′ [4.160] and

the agreement is much better for the 164°15′ case in the plateau region. The decrease of the cross section with increasing angle for backward angles corresponds to the angular distribution shown in Fig. 4.83.

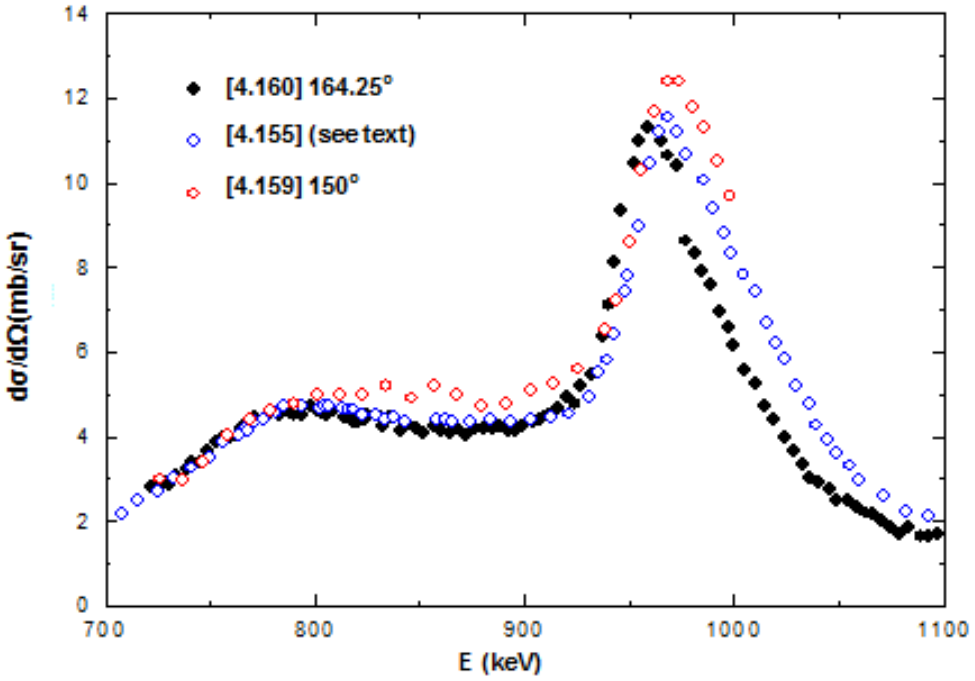

FIG. 4.82. Comparison of Amsel's data with results obtained for for the $^{16}O(d,p_1)^{17}O$ reaction at 150° and 165°.

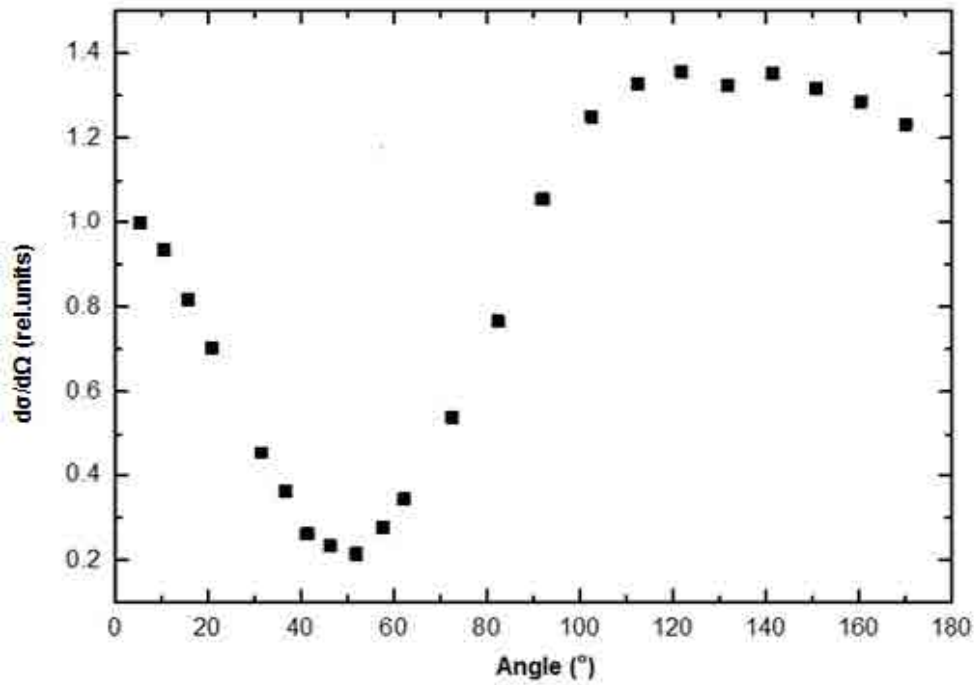

FIG. 4.83. Angular distribution for the $^{16}O(d,p_1)^{17}O$ reaction at 900 keV [4.169].

Summing up, it seems likely that the angle in the handbooks [4.156,4.157] was assigned to the data by mistake. However, Amsel tends to believe that the correct number for the scattering angle is 150° [4.161]. His reasons are derived from speculations about the preferable experimental conditions for application of the reaction rather than grounded on some notes or reminiscences concerning the cross-section measurements.

Special efforts were applied for absolute calibration of the $^{16}O(d,p_1)^{17}O$ cross section in Refs. [4.118,4.136,4.162,4.163]. The obtained results along with the absolute data from [4.159] and [4.164] published in tabular form are compared in Table 4.20.

TABLE 4.20. ABSOLUTE VALUES FOR THE $^{16}O(d,p_1)^{17}O$ CROSS SECTION

Energy (keV)	**Cross section (mb/sr)**	**Target**	**Reference**
857	5.3±0.4	Ta_2O_5	[4.118]
903	5.07±0.15	Al_2O_3	[4.159]
972	13.6±0.4	Ta_2O_5	[4.163]
972	13.3±0.4	Ta_2O_5	[4.136]
972	13.2±0.3	Ta_2O_5	[4.162]
857	4.28±0.11	SiO_2	[4.164]
969	11.22±0.45		
974	11.53±0.46		
979	12.05±0.48		

All the results, except for [4.164], are in a good agreement. As is seen from Table 4.20, the peak in the cross section [4.164] is shifted by 7 keV and the values are lower both at the plateau and for the peak. The peak to plateau ratio is 2.82 in [4.164] versus 2.57 in average for the other works.

At higher energies the data were measured at various angles and a comparison is difficult (Fig. 4.84). The significant difference between the data from [4.165] (150°) and [4.166] (142.2°) near 1.6 MeV in Fig. 4.84 can be caused by the cross-section resonance behaviour.

Only scarce information is available for the $^{16}O(d,p_0)^{17}O$ and $^{16}O(d,\alpha_0)^{14}N$ cross sections. The comparison between the $^{16}O(d,p_0)^{17}O$ data from [4.165] and [4.166] demonstrates a reasonable agreement (Fig. 4.85). Cumulative information on the studied cross sections is presented in Table 4.21. Some ambiguity should be mentioned concerning Ref. [4.160]. The conversion of the angle from the laboratory system into the centre-of-mass one depends on the energy. So it is impossible to assign the same c.m. angle to all points of the excitation function as it is done in the paper. There is no indication whether the correct c.m. angle was applied in the conversion of the measured yields into the cross section. It is worth noting that the dependence of the angle conversion rate on energy is actually small.

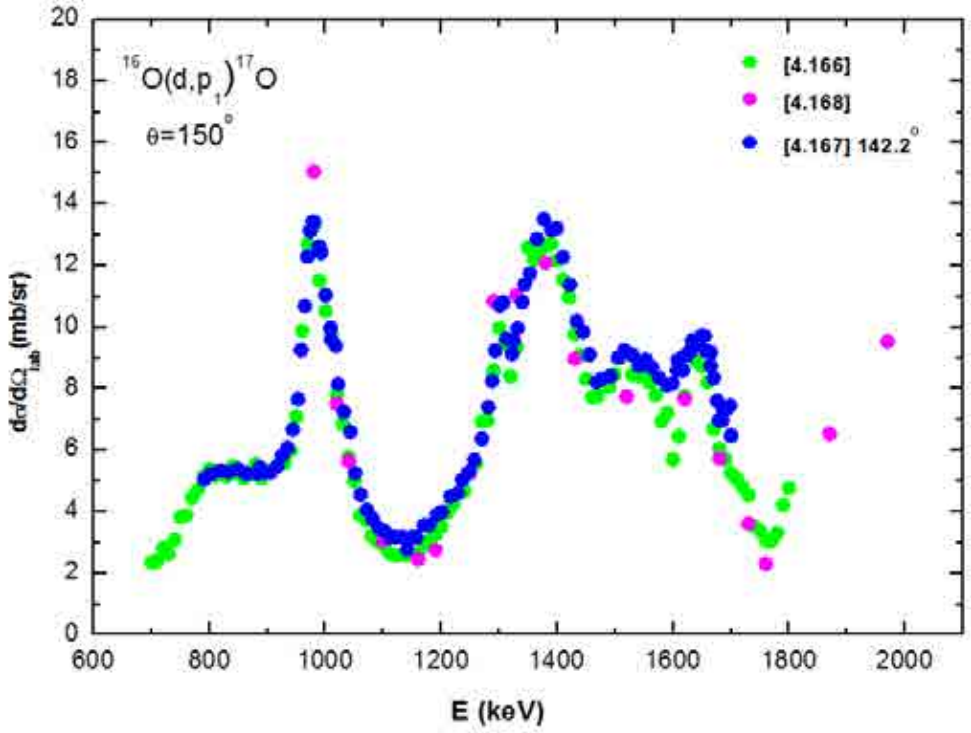

FIG. 4.84. Comparison of different data for the $^{16}O(d,p_1)^{17}O$ reaction in a wide energy range. The excitation function of [4.167] was constructed from angular distributions.

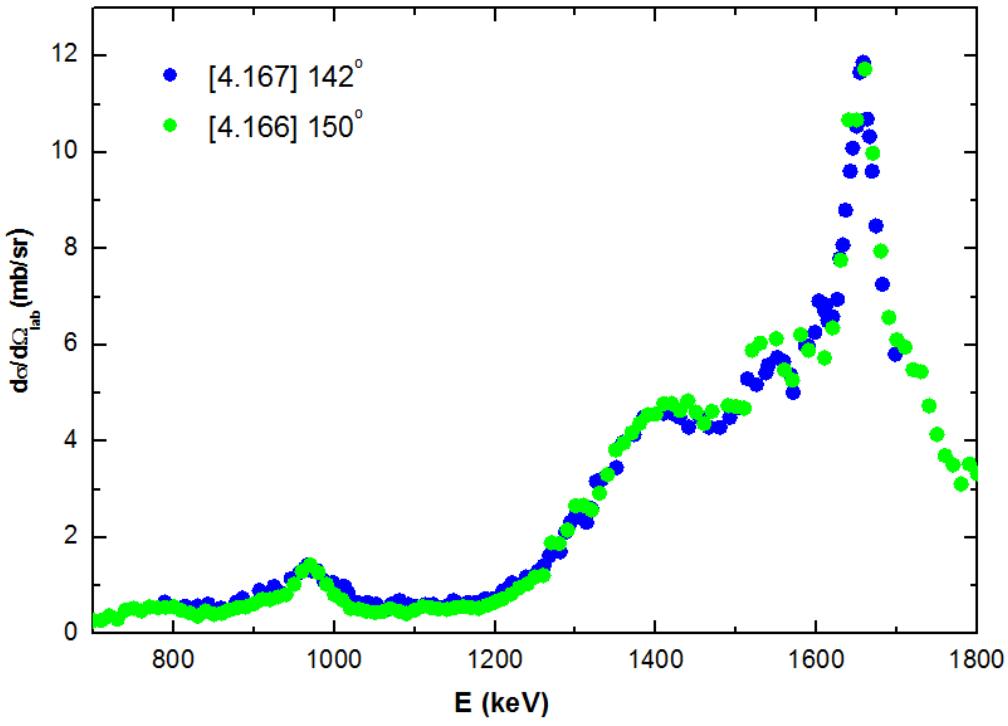

FIG. 4.85. Comparison of different data for the $^{16}O(d,p_0)^{17}O$ reaction.

TABLE 4.21. CUMULATIVE INFORMATION ON THE DEUTERON INDUCED REACTIONS FOR ^{16}O

Energy range (MeV)	Reaction	Target	Energy (MeV) [angular distribution]	Angle [excitation function]	Error	Data	Notes	Ref.
0.8─1.7	(d,p_0), (d,p_1), (d,α_0)	Gas		51.4, 66.9, 86.7, 127.7, 142.2, 164.3	5%	Graph	Added to IBANDL	[4.166]
0.7─1.0	(d,p_1)	Al_2O_3, 62.8 μg/cm^2		150	3─5%	Table		[4.159]
0.98─1.97	(d,d_0), (d,p_0), (d,p_1), (d,α_0)	Gas	0.98, 1.02, 1.04, 1.10, 1.16, 1.19, 1.25, 1.29, 1.34, 1.38, 1.43, 1.52, 1.62, 1.68, 1.73, 1.76, 1.87, 1.97, 1.02, 1.04, 1.10, 1.16, 1.19, 1.25, 1.29, 1.34, 1.38, 1.43, 1.52, 1.62, 1.68, 1.73, 1.76, 1.87, 1.97		6%	Graph	Excitation function for 150° derived from angular distributions was added to IBANDL	[4.167]
0.857	(d,p_1)	Ta_2O_5, $361\cdot10^{15}$ cm^2		150	7.5%	Value		[4.118]
0.972	(d,p_1)	Ta_2O_5		150	2%	Value	Added to IBANDL	[4.136], [4.162]
0.7─1.8	(d,p_0), (d,p_1)	Al_2O_3, 60 μg/cm^2		150	7.5%	Graph, IBANDL	Mistakes were corrected in the IBANDL files	[4.165]
0.972	(d,p_1)	Ta_2O_5		150		Value	Added to IBANDL	[4.163]
0.7─1.2	(d,p_1)	Ta_2O_5		150	5%	Table	Added to IBANDL	[4.135]
0.7─1.06	(d,p_1), (d,α_0)	SiO_2		150	4%	Table, Graph		[4.164]
0.55─0.66	(d,p_0)	Ta_2O_5		150	10%	Graph		[4.168]

TABLE 4.21. (CONT'D)

Energy range (MeV)	Reaction	Target	Energy (MeV) [angular distribution]	Angle [excitation function]	Error	Data	Notes	Ref.
0.65─2.0	(d,p_0), (d,p_1), (d,α_0)	Gas		164.25	5%	Graph	Added to IBANDL (EXFOR data converted from c.m. to lab) instead of data from NDT.	[4.160]
0.5─3.0	(d,p_0), (d,p_1), (d,α_0)	SiO_2, Ta_2O_5		135	12%	Graph	Added to IBANDL (EXFOR data) instead of Jarjis' reproduced data.	[4.139]
0.8─2.0	(d,p_0), (d,p_1), (d,α_0)	Ta_2O_5	0.900, 0.950, 0.986, 1.013, 1.040, 1.067, 1.069, 1.145, 1.206, 1.266, 1.299, 1.310, 1.385	90, 135, 165 (d, α); 10, 87, (d,p0,1)		Graph		[4.169]
0.42─1.12	(d,p_1)	Presumably Ta_2O_5		150(?), 165(?)		Graph		Amsel [4.152─155, 4.158]
0.84─1.02	(d,α_0)	SiO_2		160		Graph		[4.170]
0.76─0.95	(d,p_1), (d,α_0)	SiO_2		145		Graph		[4.171]

Recommended data

An evaluated cross section exists in SigmaCalc for the $^{16}O(d,p_0)^{17}O$ reaction at energies from 0.5 to 1.8 MeV and all angles. This evaluated cross section is recommended for all quantitative analysis.

REFERENCES

[4.1] TASCHEK, R.F., Scattering of protons by deuterium, Phys. Rev. **61** (1942) 13.

[4.2] SHERR, R., BLAIR, J.M., KRATZ, H.R., et al., Scattering of protons by deuterons, Phys. Rev. **72** (1947) 662.

[4.3] RODGERS, F.A., LEITER, H.A., KRUGER, P.G., Deuteron-proton scattering using photographic techniques, Phys. Rev. **78** (1950) 656.

[4.4] ROSEN, L., ALLRED, J.C., The scattering of 10.4-Mev deuterons by hydrogen, Phys. Rev. **82** (1951) 777.

[4.5] KARR, H.J., BONDELID, R.O., MATHER, K.B., Deuteron-proton scattering at 10.0 Mev by a coincidence method, Phys. Rev. **81** (1951) 37.

[4.6] BROWN, R.J.S., FREIER, G.D., HOLMGREN, H.D., et al., Differential cross-section measurements for the scattering of protons by deuterons, Phys. Rev. **88** (1952) 253.

[4.7] ALLRED, J.C., ARMSTRONG, A.H., BONDELID, R.O., et al., Elastic scattering of 9.7-Mev protons by deuterium and by hydrogen, Phys. Rev. **88** (1952) 433.

[4.8] MATHER, K.B., Proton-deuteron scattering at 5.1 Mev and deuteron-proton scattering at 10.2 Mev, Phys. Rev. **88** (1952) 1408.

[4.9] LANGLEY, R.A., in: Proc. Int. Conf. on Radiation Effects and Tritium Technology for Fusion Reactors (WALSON, J.S., WIFFEN, F.W., Eds), Vol. IV, 1976.

[4.10] BROLLEY, J.E., PUTNAM, T.M., ROSEN, L., et al., Hydrogen-Helium isotope elastic scattering processes at intermediate energies, Phys. Rev. **78** (1960) 1307.

[4.11] WILSON, A.S., TAYLOR, M.C., LEGG, J.C., et al., The elastic scattering of protons by Deuterium, Nucl. Phys. A **130** (1969) 130, 624.

[4.12] KOCHER, D.C., CLEGG, T.B., Cross sections for proton-deuteron scattering from 1.0 to 10.0 MeV, Nucl. Phys. A **132** (1969) 455.

[4.13] LAHLOU, F., SLOBODRIAN, R.J., BRICAULT, P., DASGUPTA, S.S., ROY, R., RIOUX, C., Variation des dephasages de la diffusion p-d pres du seuil de cassure du deuton, J. Phys. (Paris) **41** (1980) 485.

[4.14] HUTTEL, E., ARNOLD, W., BERG, H., KRAUSE, H.H., ULBRICHT, J., CLAUSNITZER, G., Differential cross sections and analyzing powers for pd elastic scattering below 1.0 MeV, Nucl. Phys. A **406** (1983) 435.

[4.15] LANGLEY, R.A., Sandia Laboratories Report SaND75-0331, 1975.

[4.16] COX, R.P., LEAVITT, J.A., MCINTYRE, L.C. Jr., in: Handbook of Modern Ion Beam Materials Analysis (TESMER, J.R., NASTASI, M., Eds), Materials Research Society (1995) 483.

[4.17] CLAASSEN, R.S. BROWN, R.J.S., FREIER, G.D., et al., The scattering of protons by tritons, Phys. Rev. **82** (1951) 589.

[4.18] ENNIS, M.E., HEMMENDINGER, A., Small-angle cross sections for the scattering of protons by tritons, Phys. Rev. **95** (1954) 772.

[4.19] WIGNER, E.P., On the behavior of cross sections near thresholds, Phys. Rev. **73** (1948) 1002.

[4.20] HEMMENDINGER, A., JARVIS, G.A., TASCHEK, R.F, Scattering of protons by tritons, Phys. Rev. **76** (1949) 1137.

[4.21] BASHKIN, S., RICHARDS, H.T., Proton bombardment of the lithium isotopes, Phys. Rev. **84** (1951) 1124.
[4.22] MCCRAY, J.A., Elastic scattering of protons from ^{6}Li nuclei, Phys. Rev. **130** (1963) 2034.
[4.23] KIM, H.J., et al., Nuclear Data Sect. A, vol. 1, no. 3-4 (1966) 211.
[4.24] LERNER, G.M., MARION, J.B., Measurement of (p,p) and (p,α) cross sections for lithium and fluorine, Nucl. Instrum. Methods **69** (1969) 115.
[4.25] HARRISON, W.D., WHITEHEAD, A.B., Elastic scattering of protons by ^{6}Li, Phys. Rev. **132** (1963) 2607.
[4.26] FASOLI, U., SILVERSTEIN, E.A., TONIOLO, D., et al., The elastic scattering of protons by ^{6}Li in the energy range (1.3-5.6) Mev, Nuovo Cimento **34** (1964) 1832.
[4.27] LAURAT, M., Centre d`Etudes Nucleaires, Saclay Reports No.3727 (1969).
[4.28] BINGHAM, H.G., ZANDER, A.R., KEMPER, K.W., et al., Elastic scattering of deuterons by ^{6}Li and ^{7}Li at 8.0-12.0 MeV, Nucl. Phys. A **173** (1971) 265.
[4.29] HALLER, M., BETZ, M., KRETSCHMER, W., et al., Elastic scattering of polarized protons by ^{6}Li (I). Optical-Model Analysis, Nucl. Phys. A **496** (1989) 189.
[4.30] SKILL, M., BAUMANN, R., KEIL, G., et al., Differential cross section and analyzing power for elastic scattering of protons on ^{6}Li below 2.2 MeV, Nucl. Phys. A **581** (1995) 93.
[4.31] WARTERS, W.D., FOWLER, W.A., LAURITSEN, C.C. et al., The elastic scattering of protons by lithium, Phys. Rev. **91** (1953) 917.
[4.32] LIBERMAN, D., 17.63 and 18.14 Mev states in ^{8}Be, Ph.D. thesis, California Institute of Technology, 1955.
[4.33] MALMBERG, P.R., Elastic scattering of protons from ^{7}Li, Phys. Rev. **101** (1956) 114.
[4.34] CACIOLLI, A., CHIARI, M., CLIMENT-FONT, A., et al., Proton elastic scattering cross-sections on F, C and Li from 3 to 7 MeV, Nucl. Instrum. Methods Phys. Res. B **249** (2006) 95.
[4.35] ANDREEV, G.B., DEINEKO, A.S., MALAKHOV, I.Y., Elastic scattering of protons by ^{7}Li, Bull. Acad. Sci. USSR, Phys. Ser. 29, 211 (1966), Izvestiya Akademii Nauk **29** (1965) 210.
[4.36] BROWN, A.B., SNYDER, C.W., FOWLER, W.A., et al., Excited states of the mirror nuclei, ^{7}Li and ^{7}Be, Phys. Rev. **82** (1951) 159.
[4.37] GLEYVOD, R., HEYDENBURG, N.P., NAQIB, I.M., Elastic and inelastic scattering of protons by ^{7}Li, Nucl. Phys. **63** (1965) 650.
[4.38] KILIAN, K., CLAUSNITZER, G., DURR, W., et al., Untersuchung der Reaktionen ^{7}Li(p,p0)^{7}Li, ^{7}Li(p,p1)^{7}Li und ^{7}Li(p,α)^{4}He mit Polarisierten Protonen der Energie 2.7 bis 10.6 MeV., Nucl. Phys. A **126** (1969) 529.
[4.39] RAMOS, A.R., BARRADAS, N.P., ALVES, E., Final Report: Measurement of proton elastic scattering cross sections for light elements – validation of a "bulk sample" method, Contract Number: 13273/R0/Regular Budget Fund, Instituto Tecnológico e Nuclear, Sacavém, Portugal, (2009).
[4.40] LEAVITT, J.A., McINTYRE JR., L.C., CHAMPLIN, R.S., et al., Quantification of beryllium in thin films using proton backscattering, Nucl. Instrum. Methods Phys. Res. B **85** (1994) 37.
[4.41] LIU, Z., WANG, R., Non-rutherford elastic scattering cross sections for 170° backscattering of 0.15-3.00 MeV protons from beryllium, Nucl. Instrum. Methods Phys. Res. B **93** (1994) 404.

[4.42] MOZER, F.S., Elastic scattering of protons by beryllium, Phys. Rev. **104** (1956) 1386.
[4.43] SIKSIN, V.S., DOMORATSKII, V.N., DONETSKOV, L.V., et al., Differential cross sections of elastic scattering of protons by Be nuclei and total cross section of the reaction ^{9}Be(p,n)^{9}B near its threshold, Sov. J. Nucl. Phys. **12**/9 (1971), Yadernaya Fizika **12** (1970) 15.
[4.44] CHIARI, M., GIUNTINI, L., MANDO, P.A., et al., Proton elastic scattering cross-section on boron from 0.5 to 3.3 MeV, Nucl. Instrum. Methods Phys. Res. B **184** (2001) 309.
[4.45] OVERLEY, J.C., WHALING, W., Highly excited states in ^{11}C. Elastic scattering of protons by ^{10}B, Phys. Rev. **128** (1962) 315.
[4.46] WATSON, B.A., SINGH, P.O., SEGEL, R.E., Optical-model analysis of nucleon scattering from 1p-shell nuclei between 10 and 50 MeV, Phys. Rev. **182** (1969) 977.
[4.47] WATSON, B.A., SEGEL, R.E., KROEPFL, J.J., et al., Inelastic scattering of protons from ^{10}B between 5 and 16.5 MeV, Phys. Rev. **187** (1969) 1351.
[4.48] HÖHN, J., KAYSER, J., PILZ, W., et al., Experimental investigation of the ^{11}B + p reaction and analysis in the frame of the continuum shell model, J. Phys. G: Nucl. Phys. **7** (1981) 803.
[4.49] MASHKAROV, Y.G., DEJNEKO, A.S., MALAKHOV, I.Y, et al., Elastic scattering of protons and the (p,α_0) reaction on ^{11}B, Bull. Acad. Sci. USSR, Phys. Ser. **39**, No.8, (1975) 143, Izv. Rossiiskoi Akademii Nauk, Ser. Fiz. **39** (1975) 1736.
[4.50] DEJNEKO, A.S., MASHKAROV, Y.G., SLABOSPICKIJ, R.P., et al., Polarization of protons scattered elastically by ^{7}Li and ^{11}B, Bull. Acad. Sci. USSR, Phys. Ser. **38**, No.8 (1974) 115, Izv. Rossiiskoi Akademii Nauk, Ser. Fiz. **38** (1974) 1694; Bull. Acad. Sci. USSR, Phys. Ser. **41**, No.10 (1977) 27, Izv. Rossiiskoi Akademii Nauk, Ser. Fiz. **41** (1977) 2018.
[4.51] SYMONS, G.D., TREACY, P.B., The ^{11}B(p,α)^{8}Be reaction and ^{12}C states between 15 and 20 MeV, Nucl. Phys. **46** (1963) 93.
[4.52] TAUTFEST, G.W., RUBIN, S., Elastic scattering of protons from ^{11}B and ^{14}N, Phys. Rev. **103** (1956) 196.
[4.53] MAYER, M., ANNEN, A., JACOB, W., et al., The ^{11}B(p,α_0)^{8}Be nuclear reaction and ^{11}B(p,p)^{11}B backscattering cross sections for analytical purposes, Nucl. Instrum. Methods Phys. Res. B **143** (1998) 244.
[4.54] SEGEL, R.E., HANNA, S.S., ALLAS, R.G., States in ^{12}C between 16.4 and 19.6 MeV, Phys. Rev. B **139** (1965) 818.
[4.55] BECKER, H.W., ROLFS, C., TRAUTVETTER, H.P., et al, Low energy cross sections for ^{11}B(p,3a), Zeitschrift für Physik A **327** (1987) 341.
[4.56] ANDREEV, G.B., DEJNEKO, A.S., MALAKHOV, I.Y., Elastic scattering of protons from ^{9}Be and ^{11}B, Bull. Acad. Sci. USSR, Phys. Ser. **27** (1964) 1282, Izv. Rossiiskoi Akademii Nauk, Ser. Fiz. **27** (1963) 1305.
[4.57] TOSAKI, M., ITO, S., MAEDA, N., Detailed analysis of the resonant backscattering spectrum for deeply penetrating protons in carbon, Nucl. Instrum. Methods Phys. Res. B **168** (2000) 543.
[4.58] JACKSON, H.L., GALONSKY, A.I., EPPLING, F.J., et al., The ^{12}C(p,p)^{12}C differential cross section, Phys. Rev. **89** (1953) 365.
[4.59] REICH, C.W., PHILLIPS, G.C., RUSSELL, J.L. Jr., Scattering of protons from ^{12}C, Phys. Rev. **104** (1956) 143.
[4.60] SWINT, J.B., BARNARD, A.C.L., CLEGG, T.B., et al., Cross sections as a function of energy for the scattering of protons from ^{12}C, Nucl. Phys. **86** (1966) 119.

[4.61] WEBB, T.S., HAGEDORN, F.B., FOWLER, W.A., et al., Elastic scattering of protons by ^{19}F, Phys. Rev. **99** (1955) 138.
[4.62] CARACCIOLO, R., CUZZOCREA, P., DE ROSA, A., et al., The 13.645 MeV state in ^{20}Ne, Lett. Nuovo Cimento **11** (1974) 33.
[4.63] OUICHAOUI, S., BEAUMEVIEILLE, H., BENDJABALLAH, N. et al., States in ^{20}Ne from ^{19}Fe(p,p) and ^{19}Fe(p,α) reactions at Esub(p) = (1.5-2.1) MeV, Nuovo Cimento A **86** (1985) 170.
[4.64] OUICHAOUI, S., BEAUMEVIEILLE, H.; BENDJABALLAH, N.; et al., T = 1 states in ^{20}Ne as compound resonances induced by the p+^{19}F reaction, Nuovo Cimento A **94** (1986) 133.
[4.65] KNOX, J.M., HARMON, J.F., Non-Rutherford elastic scattering in fluorine, Nucl. Instrum. Methods Phys. Res. **44** (1989) 40.
[4.66] BOGDANOVIĆ, I., FAZINIĆ, S., JAKŠIĆ, M., et al., Proton elastic scattering from fluorine, chlorine, zinc, selenium and bromine in the energy region from 2.5 to 4.8 MeV, Nucl. Instrum. Methods Phys. Res. **79** (1993) 524.
[4.67] JESUS, A.P., BRAIZINHA, B., CRUZ, J., et al., Influence of target thickness on resonant elastic scattering of protons by ^{19}F, Nucl. Instrum. Methods Phys. Res. B **174** (2001) 229.
[4.68] KUAN, H.M., LATSHAW, G.L., O'CONNELL, W.J., et al., Observation of the second T = 2 state of ^{20}Ne as a compound resonance in the ^{19}F + p reactions, Nucl. Phys. A **193** (1972) 497.
[4.69] DEARNALEY, G., The elastic scattering of protons by light elements, Philos. Mag. **1** (1956) 821.
[4.70] P. CUZZOCREA, DE ROSA, A., INGLIMA, G., et al., Quartet states in ^{20}Ne., Lett. Nuovo Cimento **28** (1980) 515.
[4.71] HIRATATE, Y., TAKEUCHI, Y., YAMAYA, T., et al., Some studies of the ^{23}Na+p reaction at E = 2.2 - 4.5 MeV, J. Phys. Soc. Jpn. **24** (1968) 690.
[4.72] WILKERSON, J.F., MOONEY, T.M., FAUBER, R.E., et al., Isospin-nonconserving particle decays in light nuclei, Nucl. Phys. A **549** (1992) 223.
[4.73] BAUMANN, N.P., PROSSER, F.W., Jr., , READ, W.G., et al., Elastic scattering of protons from ^{23}Na, Phys. Rev. **104** (1956) 376.
[4.74] CENJA, M., DUMA, M., HATEGAN, C., et al., The (p,n) threshold anomaly in proton elastic scattering on ^{23}Na, ^{27}Al, ^{31}P, ^{35}Cl and ^{34}S, Nucl. Phys. A **307** (1978) 65.
[4.75] VANHOY, J.R., BILPUCH, E.G., WESTERFELDT, C.R., et al., Proton resonances in ^{24}Mg from Ex = 12.7 to 15.7 MeV, Phys. Rev. C **39** (1987) 920.
[4.76] CACIOLLI, A., CALZOLAI, G., CHIARI, M., et al., Proton elastic scattering and proton induced γ-ray emission cross-sections on Na from 2 to 5 MeV, Nucl. Instrum. Methods Phys. Res. B **266** (2008) 1392.
[4.77] TAYLOR, R.B., FLETCHER, N.P., DAVIS, R.H., Elastic scattering of 4-20 MeV alpha particles by ^{9}Be, Nucl. Phys. **65** (1965) 318.
[4.78] GOSS, J.D., BLATT, S.L., PARSIGNAULT, D.R., et al., Elastic scattering of α particles by ^{9}Be and highly excited states of ^{13}C, Phys. Rev. C **7** (1973) 1837.
[4.79] SALEH, Z.A., MACHALI, F., BONDOUK, I.I., et al., Elastic scattering of α-particles on ^{9}Be, Ann. Phys. **31** (1974) 76.
[4.80] LIU, Z., ZHENG, Z., CHU, W.-K., Cross section for non-Rutherford Backscattering of α on Be, Nucl. Instrum. Methods Phys. Res. **108** (1996) 247.
[4.81] MO, T., WELLER, H.R., Energy levels of ^{14}N from the elastic scattering of α particles by ^{10}B, Phys. Rev. C **8** (1973) 972.

[4.82] McIntyre JR., L.C., LEAVITT, J.A., ASHBAUGH, M.D., et al, Cross sections for 170.5° backscattering of ^{4}He by the isotopes of boron for ^{4}He energies between 1.0 and 3.3 MeV, Nucl. Instrum. Methods Phys. Res. B **64** (1992) 457.
[4.83] DAVID, P., DEBRUS, J., MOMMSEN, H., et al., Elastic scattering of α-particles on ^{10}B for E = 5-30 MeV, Nucl. Phys. A **182** (1972) 234.
[4.84] OTT, W.R., WELLER, H.R., A study of ^{15}N by means of the ^{11}B(α,α)^{11}B reaction, Nucl. Phys. A **198** (1972) 505.
[4.85] RAMIREZ, J.J., BLUE, R.A., WELLER, H.R., Multilevel multichannel study of the structure of ^{15}N from 12- to 14-MeV excitation energy, Phys. Rev. C **5** (1972) 17.
[4.86] LIU, J.R., ZHENG, Z.S., CHU, W.K., (α,α) Cross section on ^{11}B for α-energies between 1.0 and 5.3 MeV, Nucl. Instrum. Methods Phys. Res. B **108** (1996) 1.
[4.87] C. MILLER JONES et al., The scattering of alpha particles from ^{12}C, Nucl. Phys. **37** (1962) 1.
[4.88] DAVIES, J.A., ALMEIDA, F.J.D., HAUGEN, H.K., et al., Quantitative calibration of intense (α,α) elastic scattering resonances for ^{12}C at 5.50-5.80 MeV and for ^{16}O at 7.30-7.65 MeV, Nucl. Instrum. Methods Phys. Res. B **85** (1994) 28.
[4.89] SOMATRI, R., CHAILAN, J.F., CHEVARIER, A., et al., Alpha backscattering used in stoichiometry determination of thin SiC coatings on Si(100) wafers, Nucl. Instrum. Methods Phys. Res. B **113** (1996) 284.
[4.90] FENG, Y., ZHOU, Z., ZHOU, Y., et al., Cross sections for 165° backscattering of 2.0-9.0 MeV ^{4}He from Carbon, Nucl. Instr. and Meth. B **86** (1994) 225.
[4.91] LEAVITT, J.A., McINTYRE, L.C. Jr., STOSS, P., et al., Cross sections for 170.5° backscattering of ^{4}He from Carbon for ^{4}He Energies between 1.6 and 5.0 MeV, Nucl. Instrum. Methods Phys. Res. B **40/41** (1989) 776.
[4.92] SHEN HAO, CHENG HUAN-SHENG, TANG JIA-YONG, YANG FU-JA, The study of non-Rutherford backscattering of ^{4}He from Carbon, Acta Physica Sinica **43** (1994) 1569.
[4.93] MARVIN, T.P., SINGH, P.P., Energy levels of ^{16}O between 10.0 and 17.1 MeV excitation, Nucl. Phys. A **180** (1972) 282.
[4.94] HILL, R.W., Elastic scattering of alpha-particles by carbon, Phys. Rev. **90** (1953) 845.
[4.95] BITTNER, J.W., MOFFAT, R.D., Elastic scattering of alpha particles by carbon, Phys. Rev. **96** (1954) 374.
[4.96] WANG, C.W., KIANG, G.C., KIANG, L.L., et al., The α - ^{7}Li and α - ^{12}C elastic scattering at E(α) = 5 and 6 MeV, J. Phys. Soc. Jpn. **51** (1982) 3093.
[4.97] ZHOU ZHUYING, QIU YUANXUN, ZHAO GUOQING, et al., Conf. High Energy and Heavy Ion Beams in Material Analysis, 1989, p. 183.
[4.98] WETTELAND, C.J., MAGGIORE, C.J., TESMER, J.R., et al., "Magic" energies for detecting light elements with resonant alpha particle backscattering, LA-UR-98-4867, 1998.
[4.99] BERTI, M., De SALVADOR, D., DRIGO, A.V., ^{12}C(α,α)^{12}C resonant elastic scattering at 5.7 MeV as a tool for carbon quantification in silicon-based heterostructures et al., Nucl. Instrum. Methods Phys. Res. B **143** (1998) 357.
[4.100] YONEZAWA, H., SHIKANO, K., SHIGEMATSU, T., Backscattering cross section of 5.5 to 8 Me V alpha particles from carbon, oxygen and silicon, Nucl. Instrum. Methods Phys. Res. B **88** (1994) 207.
[4.101] BANKS, J.C., WAMPLER, W.R. BROWNING, J.F,. et al., Cross sections for 165° backscattering of 8.0–11.7 MeV α from carbon, Nucl. Instrum. Methods Phys. Res. B **249** (2006) 101.

[4.102] KOVASH, M.A., LOURIE, R.W., PUGH, W., et al., Search for a doublet in ^{16}O near 9.85 MeV, Phys. Rev. C **31** (1985) 1065.
[4.103] PLAGA, R., BECKER, H.W., REDDER, A., et al., The scattering of alpha particles from ^{12}C and the ^{12}C(α,γ)^{16}O stellar reaction rate, Nucl. Phys. A **465** (1987) 291.
[4.104] BOGDANOVIĆ RADOVIĆ, I., JAKŠIĆ, M., BENKA, O., et al., Helium elastic scattering from carbon for 30° to 150° in the energy region from 2 to 4.8 MeV, Nucl. Instrum. Methods Phys. Res. B **190** (2002) 100.
[4.105] BERKY, W., STEINBAUER, U.C, BAUMANN, H., Measurement of non-Rutherford cross sections of ^{4}He Ions on ^{14}N at a laboratory backscattering angle of 171° between 7.5 and 9.8 MeV, Nucl. Instrum. Methods Phys. Res. B **192** (2002) 249.
[4.106] HERRING, D.F., CHIBA, R., GASTEN, B.R., et al., ^{14}N(α,α)^{14}N and ^{14}N(α,p)^{17}O differential cross sections, Phys. Rev. **112** (1958) 1210.
[4.107] FOSTER, L.A., TESMER, J.R., JERVIS, T.R., et. al, Non-Rutherford backscattering analysis of nitrogen content in titanium substrates, Nucl. Instrum. Methods Phys. Res. B **79** (1993) 454.
[4.108] SILVERSTEIN, E.A., SALISBURY, S.R., HARDIE, G., et al., ^{14}N + ^{4}He and ^{16}O + ^{3}He differential cross sections, Phys. Rev. **124** (1961) 868.
[4.109] FENG, Y., ZHOU, Z., ZHOU, G., et al., Cross sections for 165° backscattering of 2.0–9.0 MeV ^{4}He ions from nitrogen, Nucl. Instrum. Methods Phys. Res. B **94** (1994) 11.
[4.110] KASHY, E., MILLER, P.D., RISSER, J.R, Energy Levels in ^{18}F from the ^{14}N(α,n)^{14}N and ^{14}N(α,p)^{17}O reactions, Phys. Rev. **112** (1958) 547.
[4.111] JIANG, W., SHUTTHANANDAN, V., THEVUTHASAN, S., et al., Nitrogen analysis using energetic ion beams, Surf. Interface Anal. **37** (2005) 374.
[4.112] ARTIGALAS, H., CHEVARIER, A., CHEVARIER, N., et al., Nitrogen profiling in nitride films and nitrogen-implanted samples using the ^{14}N(α,α) and ^{14}N(α,p) reactions at 6 MeV incident energy, Nucl. Instrum. Methods Phys. Res. B **66** (1992) 237.
[4.113] QIU, Y., RICE, A.P., TOMBRELLO, T.A., Nitrogen detection by means of a broad resonance at 9.3 MeV in ^{14}N(α,α)^{14}N elastic backscattering, Nucl. Instrum. Methods Phys. Res. B **71** (1992) 324.
[4.114] TERWAGNE, G. GENARD, G., YEDJI, M., et al., Cross-section measurements of the ^{14}N(α,p)^{17}O and ^{14}N(α,α)^{14}N reactions between 3.5 and 6 MeV, J. Appl. Phys. **104** (2008) 084909.
[4.115] GURBICH, A.F., BOGDANOVIĆ RADOVIĆ, I., SIKETIĆ, Z., et al., Measurements and evaluation of the cross-section for helium elastic scattering from nitrogen, Nucl. Instrum. Methods Phys. Res. B **269** (2011) 40.
[4.116] NAGATA, S., YAMAGUCHI, S., FUJINO, Y., et al., Depth resolution and recoil cross section for analyzing hydrogen in solids using elastic recoil detection with ^{4}He beam, Nucl. Instrum. Methods Phys. Res. B **6** (1985) 533.
[4.117] KELLOCK, A.J., BAGLIN, J.E.E., Absolute cross section for D(^{4}He,D)^{4}He forward scattering, Nucl. Instrum. Methods Phys. Res. B **79** (1993) 493.
[4.118] QUILLET, V., ABEL, F., SCHOTT, M., Absolute cross section measurements for H and D elastic recoil using 1 to 2.5 MeV ^{4}He ions, and for the ^{12}C(d,p)^{13}C and ^{16}O(d,p1)^{17}O nuclear reactions, Nucl. Instrum. Methods Phys. Res. B **83** (1993) 47.
[4.119] BESENBACHER, F., STENSGAARD, I., VASE, P., Absolute cross section for recoil detection of deuterium, Nucl. Instrum. Methods Phys. Res. B **15** (1986) 459.

[4.120] SAWICKI, J.A., Measurements of the differential cross sections for recoil tritons in $^{4}He–^{3}T$ scattering at energies between 0.5 and 2.5 MeV, Nucl. Instrum. Methods Phys. Res. B **30** (1988) 459.
[4.121] BROWNING, J.F., LANGLEY, R.A., DOYLE, B.L., et al., High accuracy, high energy He-ERD analysis of H, D and T, Nucl. Instrum. Methods Phys. Res. B **161-163** (2000) 211.
[4.122] BROWNING, J.F., BANKS, J.C., WAMPLER, W.R., et al., Cross-sections for the elastic recoil of hydrogen isotopes for high energy helium ions, Nucl. Instrum. Methods Phys. Res. B **219-220** (2004) 317.
[4.123] MÖLLER, W., BESENBACHER, F., A note on the ^{3}He + D nuclear reaction cross section, Nucl. Instrum. Methods Phys. Res. **168** (1980) 111.
[4.124] JARVIS, R.G., ROAF, D., Comparison of D-T and D-^{3}He at low energies, Proc. Roy. Soc. A **218** (1953) 432.
[4.125] FREIER, G., HOLMGREN, H., Interaction between D2 and ^{3}He in the neighbourhood of the 18.6-MeV Level of ^{5}Li, Phys. Rev. **93** (1954) 825.
[4.126] KUNZ, W.E., Deuterium ^{3}He reaction, Phys. Rev. **97** (1955) 456.
[4.127] BOSCH, H.-S., HALE, G.M., Improved formulas for fusion cross-sections and thermal reactivities, Nuclear Fusion **32** (1992) 611.
[4.128] KRAUSS, A., BECKER, H.W., TRAUTVETTER, H.P., et al., Low-Energy Fusion Cross Sections of D + D and D + ^{3}He Reactions, Nucl. Phys. A **465** (1987) 150.
[4.129] PERES, A.J., Fusion cross sections and thermonuclear reaction rates, J. Appl. Phys. **50** (1979) 5569.
[4.130] DUANE, B.H., Fusion cross section theory, in: Annual Report on CTR Technology 1972 (WOLKENHAUER, W.C., Ed.), Rep. BNWL-1685, Battelle Pacific Northwest Laboratory, Richland, WA (1972).
[4.131] BONNER, T.W., CONNER J.P., LILLIE, A.P., Cross section and angular distribution of the ^{3}He (d,p)^{4}He nuclear reaction, Phys. Rev. **88** (1952) 473.
[4.132] YARNELL, J.L., LOVBERG R.H., STRATTON, W.R., Angular distribution of the reaction ^{3}He(d,p)^{4}He between 240 keV and 3.56 MeV, Phys. Rev. **90** (1953) 292.
[4.133] ALIMOV, V.KH., MAYER, M., ROTH, J., Differential cross-section of the D(^{3}He,p)^{4}He nuclear reaction and depth profiling of deuterium up to large depths, Nucl. Instrum. Methods Phys. Res. B **234** (2005) 169.
[4.134] ARNOLD, W.R., PHILIPPS, J.A., SAWYER, G.A., et al., Cross Sections for the reactions D(d,p)T, D(d,n)^{3}He, T(d,n)^{4}He, and ^{3}He(d,p)^{4}He below 120 keV, Phys. Rev. **93** (1954) 483.
[4.135] LENNARD, W.N., MASSOUMI, G.R., ALKEMADE, P.F.A., et al., Revisiting the ^{12}C(d,p)^{13}C reaction cross section using condensed gas targets, Nucl. Instrum. Methods Phys. Res. B **61** (1991) 1.
[4.136] DAVIES, J.A., NORTON, P.R., Absolute coverage measurement of adsorbed CO and D2 on platinum, Nucl. Instrum. Methods Phys. Res. **168** (1980) 611.
[4.137] JIANG, W., SHUTTHANANDAN, V., THEVUTHASAN, S., et al., Carbon analysis using energetic ion beams, Nucl. Instrum. Methods Phys. Res. B **222** (2004) 538; B **227** (2005) 450 (Erratum).
[4.138] POORE, R.V., SHEARIN, P.E., TILLEY, D.R., et al., Differential cross sections of ^{12}C(d,p)^{13}C and ^{10}B(d,p)^{11}B below E = 3.0 MeV, Nucl. Phys. A **92** (1967) 97.
[4.139] DEBRAS, G., DECONNINK, G., Light elements analysis and application to glass industry, J. Rad. Chem. **38** (1977) 193 (reproduced by JARJIS, R.A., Internal Report, Univ. of Manchester (1979)).

[4.140] KASHY, E., PERRY, R.R., RISSER, J.R., Excited States in ^{14}N from ^{12}C(d,d)^{12}C, ^{12}C(d,p$_0$)^{13}C, and ^{12}C(d,p$_1$)^{13}C, Phys. Rev. **117** (1960) 1289.
[4.141] PHILLIPS, G.C., The long-range protons from the disintegration of carbon by deuterons and a study of the competing reactions, Phys. Rev. **80** (1950) 164 (reproduced by N. Jarmie and J.D. Seagrave in Los Alamos Report LA-2014 (1957)).
[4.142] BALIN, V.G., GURBICH, A.F., SHORIN, V.S., Preprint FEI-1341, Obninsk (1982).
[4.143] McELLISTREM, M.T., JONES, K.W., CHIBA, R., Differential cross sections for ^{12}C(d,d)^{12}C and ^{12}C(d,p)^{13}C, Phys. Rev. **104** (1956) 1008.
[4.144] BARIT, I.YA., KOGAN, D.L., KUZMIN, L.E., et al. Short communications in Physics PHIAS, No.7 (1986) 29 (in Russian).
[4.145] KOKKORIS, M., MISAELIDES, P., KOSSIONIDES, S., A detailed study of the ^{12}C(d, p$_0$)^{13}C reaction at detector angles between 135° and 170°, for the energy range Ed, lab = 900–2000 keV, Nucl. Instrum. Methods Phys. Res. B **249** (2006) 77.
[4.146] TONG, S.Y., LENNARD, W.N., ALKEMADE, P.F.A., et al., Absolute surface carbon coverage determination via the ^{12}C(^{3}He,p)^{14}N reaction, Nucl. Instrum. Methods Phys. Res. B **45** (1990) 91.
[4.147] KUAN, H.-M., BONNER, T.W., RISSER, J.R., An investigation of the ^{12}C + ^{3}He reactions at bombarding energies between 1.8 and 5.4 MeV, Nuclear Physics **51** (1964) 481.
[4.148] JOHNSTON, R.L., HOLMGREN, H.D., WOLICKI, E.A., et al., Differential cross sections for the ^{12}C(^{3}He,p)^{14}N reaction, Phys. Rev. **109** (1958) 884.
[4.149] TERWAGNE, G., Cross section measurements of the reactions induced by ^{3}He particles on carbon, Nucl. Instrum. Methods Phys. Res. B **122** (1997) 1.
[4.150] BROMLEY, D.A., ALMQVIST, E., GOVE, H.E., et al., Study of some ^{3}He-induced reactions on ^{12}C, Phys. Rev. **105** (1957) 957.
[4.151] COHEN, D.D., ROSE, E.K., Analysis of oxygen by charged-particle bombardment, Nucl. Inst. and Meth. B **66** (1992) 158.
[4.152] AMSEL, G., SAMUEL, D., Microanalysis of the stable isotopes of oxygen by means of nuclear reactions, Anal. Chem. **39** (1967) 1689.
[4.153] AMSEL, G., BERNAGER, G., De GELAS, B., et al., Use of the nuclear reaction ^{16}O(d,p)^{17} to study oxygen diffusion in solids and its application to Zirconium, J. Appl. Phys. **39** (1968) 2246.
[4.154] AMSEL, G., DAVID, D., BERANGER, G., et al., Rev. Phys. Appl. **3** (1968) 373.
[4.155] AMSEL, G., NADAI, J.P., D'ARTEMARE, E., et al., Microanalysis by the direct observation of nuclear reactions using a 2 MeV Van de Graaff, Nucl. Instrum. Methods Phys. Res. **92** (1971) 481.
[4.156] MAYER, J.W., RIMINI, E. (Eds), Ion Beam Handbook for Material Analysis, Academic Press, New York, 1977.
[4.157] TESMER, J.R., NASTASI, M., (Eds), Handbook of Modern Ion Beam Materials Analysis, MRS, Pittsburg, PA, 1995.
[4.158] AMSEL, G., DAVID, D., BERANGER, G., et al., J. Nucl. Materials **29** (1969) 144.
[4.159] KARABASH, V.A. , SOSNIN, A.N., SHORIN, V.S., Voprosy At. Nauky Techn. Ser.: Yad. Const. **3** (1988) 31.
[4.160] SEILER, R.F., JONES, C.H., ANZICK, W.J., et al., The elastic scattering of deuterons by ^{16}O from 0.65 to 2.0 MeV, Nucl. Phys. **45** (1963) 647 (reproduced by H.J. Kim, W.T. Milner and F.K. McGowan Nuclear Data Tables v.A3 (1967) 123).
[4.161] AMSEL, G., private communications, 2008.

[4.162] DAVIES, J.A., JACKMAN, T.E., PLATTNER, H., et al., Absolute calibration of $^{14}N(d,\alpha)$ and $^{14}N(d,p)$ reactions for surface absorption studies, Nucl. Instrum. Methods Phys. Res. **218** (1983) 141.
[4.163] LENNARD, W.N., TONG, S.Y., MITCHEL, I.V., et al., An alternative technique for oxygen surface coverage measurements, Nucl. Instrum. Methods Phys. Res. B **43** (1989) 187.
[4.164] JIANG, W., SHUTTHANANDAN, V., THEVUTHASAN, S., et al., Oxygen analysis using energetic ion beams, Nucl. Instrum. Methods Phys. Res. B **207** (2003) 453.
[4.165] GURBICH, A.F., MOLODTSOV, S.L., Application of IBA techniques to silicon profiling in protective oxide films on a steel surface, Nucl. Instrum. Methods Phys. Res. B **226** (2004) 637.
[4.166] KIM, H.C., SEILER, R.F., HERRING, D.F., et al., Nucl. Phys. **57** (1964) 526.
[4.167] CAVALLARO, S., CUNSOLO, A., POTENZA, R., et al., ^{16}O + d Reactions at E < 2 MeV, Il Nuovo Cimento **14A** (1973) 692.
[4.168] BERTI, M., DRIGO, A.V., Simultaneous nuclear microanalysis of nitrogen and oxygen on silicon, Nucl. Instrum. Methods Phys. Res. **201** (1982) 473.
[4.169] AMSEL, G., Semiconductor detector spectroscopy of the nuclear reactions ^{16}O + d, ^{18}O + p, Ann. Phys. **9** (1964) 297.
[4.170] PICRAUX, S.T., Low-concentration oxygen depth profiling by the $^{16}O(d,\alpha)^{14}N$ reaction, Nucl. Instrum. Methods Phys. Res. **149** (1978) 289.
[4.171] TUROS, A., WIELUNSKI, L., OLENSKI, J., Phys. Stat. Sol. A **16** (1973) 211; TUROS, A., WIELUNSKI, L., BARCZ, A., Nucl. Instrum. Methods Phys. Res. **111** (1973) 605.

5. EVALUATION

5.1. GENERAL

The evaluation of cross sections for any particular reaction consists in the elaboration of the most accurate possible cross sections through incorporation of the all relevant experimental data in the framework of nuclear physics theory. These data include not only measured scattering cross sections but also other information such as nuclear spectroscopy information on the positions, spin and parity of the nuclear energy levels. The evaluation procedure consists of the following, generally established steps (Fig. 5.1). Firstly, a search of the literature and of nuclear data bases is made to compile relevant experimental data. Data published only as graphs are digitized. Then, data from different sources are compared, and the reported experimental conditions and errors assigned to the data are examined. Based on this, the apparently reliable experimental points are critically selected. Free parameters of the theoretical model, which involve appropriate physics for the given scattering process, are then fitted in the limits of reasonable physical constraints. The model calculations are finally used to produce the optimal theoretical differential cross section. Thus, the data measured under different experimental conditions at different scattering angles become incorporated into the framework of the unified theoretical approach. The final stage is to compare the calculated curves to the experimental points and analyze the revealed discrepancies. In dubious cases the measurement performed with a standard sample (benchmark) followed by spectrum simulation can help to clarify the reality. If no explanation for the revealed disagreements can be found, then a new measurement of the critical points should be made.

The outcome of the evaluation is that the required excitation functions may be calculated for any scattering angle with a reliability exceeding that for any individual measurement. Theoretical and methodological issues of the evaluation can be found in [5.1].

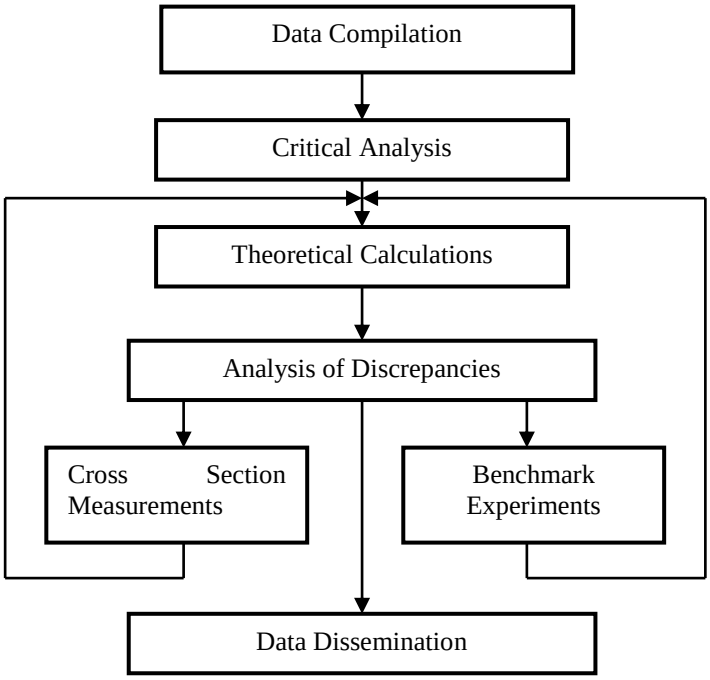

FIG. 5.1. Evaluation scheme. Reproduced courtesy of Elsevier [5.1].

5.2. THEORY

According to quantum mechanics the differential cross section for elastic scattering at the center mass angle θ is determined through an amplitude of the divergent wave $f(\theta)$ as

$$\frac{d\sigma}{d\Omega} = \left| f(\theta) \right|^2 \quad . \tag{5.1}$$

The $f(\theta)$ function can be expressed through partial wave phase shifts δ_l, which are functions of the wave number k. For a spinless charged projectile the relation for the scattering amplitude is

$$f(\theta) = f_C(\theta) + \frac{1}{2ik}\sum_{l=0}^{\infty}(2l+1)(S_l - 1)e^{2i\alpha_l} P_l(\cos\theta) \tag{5.2}$$

where $S_l = e^{2i\delta_l}$ are elements of the scattering matrix, P_l ($cos\theta$) are Legendre polynomials, $f_C(\theta)$ and α_l are amplitude and phase shifts of the Coulomb scattering respectively. Explicitly the cross section for elastic scattering for spinless particles on spinless nuclei is given by

$$\frac{d\sigma}{d\Omega} = k^{-2}\left| -\frac{1}{2}\eta \csc^2(½\theta)\exp\left(i\eta \ln \csc^2(½\theta)\right) + \sum_l (2l+1)\exp[(i(2\alpha_l + \delta_l)]\sin\delta_l \; P_l(\cos\theta)\right|^2, \tag{5.3}$$

where η is the Sommerfeld parameter $Zze^2/\hbar v$.

For protons the cross section is

$$\frac{d\sigma}{d\Omega} = \left|A(\theta)\right|^2 + \left|B(\theta)\right|^2, \tag{5.4}$$

the scattering amplitudes $A(\theta)$ and $B(\theta)$ being defined by the following relations

$$A(\theta) = f_C(\theta) + \frac{1}{2ik}\sum_{l=1}^{\infty}[(l+1)S_l^+ + lS_l^- - (2l+1)]\exp(2i\alpha_l)P_l(\cos\theta);$$

$$B(\theta) = \frac{1}{2ik}\sum_{l=0}^{\infty}(S_l^+ - S_l^-)\exp(2i\alpha_l)P_l^1(\cos\theta) \tag{5.5}$$

where $P_l^1(\cos\theta)$ are associated Legendre polynomials, S_l^+ and S_l^- are scattering matrix elements for different spin orientation.

The only unknowns in the cross-section relations are the δ_l and as soon as they are determined the cross section can be calculated. There are different phenomenological approaches to the determination of the phase shifts from experimental data. They can be found (i) by direct fitting the cross section relations (phase-shift analysis), (ii) through resolving Schrödinger equations for partial waves, with parameters of the nuclear potential being free, and (iii) in the framework of the R-matrix theory [5.2] by adjusting compound nucleus level parameters and boundary conditions.

Since the δ_l values depend on energy, the phase-shift analysis (i) is impractical for the evaluation. In case (ii) the nucleus is represented by means of a potential well, described by only a few parameters with slight if any at all dependence on energy. The potential is real if elastic scattering is the only channel and complex if absorption takes place (optical model). In the general case the potential is of the form

$$U(r) = U_C(r) + U_R(r) + iU_I(r) + U_{so}(r), \tag{5.6}$$

where U_C, U_R, U_I, and U_{so} stand for Coulomb, central real, imaginary, and spin-orbit potential respectively. The cross section calculated with this model is smooth with rather broad resonances observed only at energies when conditions for standing waves to form in the nucleus potential well are fulfilled. Narrow resonances which commonly influence the cross section for light and medium-heavy nuclei are not reproduced in the framework of the potential model. One of the ways to take resonance scattering into account is to add Breit-Wigner resonance terms to the diagonal elements of the scattering matrix. Then, for protons the element of scattering matrix has the form

$$S_l^{\pm} = \exp(2i\lambda_l^{\pm})\left[\exp(-2\mu_l^{\pm}) + \exp(2i\phi_p)\frac{i\Gamma_p}{E_0 - E - \frac{1}{2}i\Gamma}\right], \tag{5.7}$$

where $\lambda_l^{\pm} + i\mu_l^{\pm}$ is the off-resonance nuclear phase shift and the quantities E_0, Γ, and Γ_p are the energy, total width and partial elastic width, respectively. The subscript l is the relative angular momentum of the proton and the target in units of $\hbar$. The plus sign refers to the case when $J = l + ½$ and the minus sign to the case when $J = l - ½$. The quantity ϕ_p is a resonance phase shift.

In most cases of charged-particle low energy scattering the contribution of the reaction channels is negligible and so the imaginary potential is close to zero. The calculated cross section is extremely sensitive to the potential parameters as is illustrated in Fig. 5.2. It is worth noting that the differential cross section is as a rule insensitive to the spin-orbit potential which influences mainly polarization data. In the low energy region this is not the case. Because of the spin-orbit interaction the single-particle resonances split with respect to the total angular momentum as is shown in Fig. 5.3.

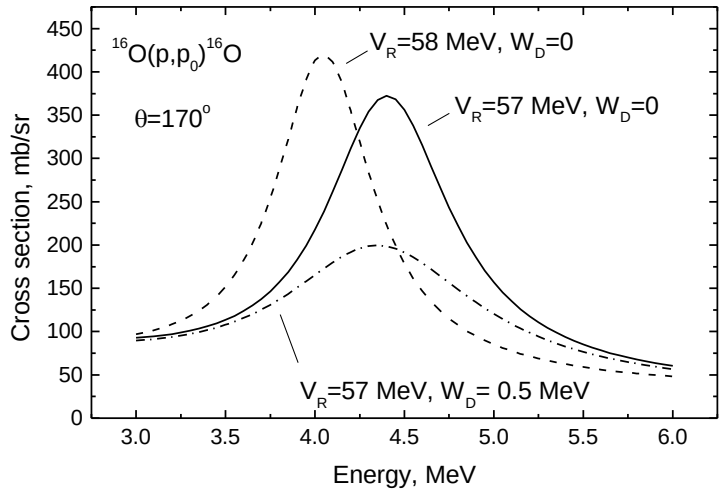

FIG. 5.2. The sensitivity of single particle resonances to the potential parameters. Reproduced courtesy of Elsevier [5.1].

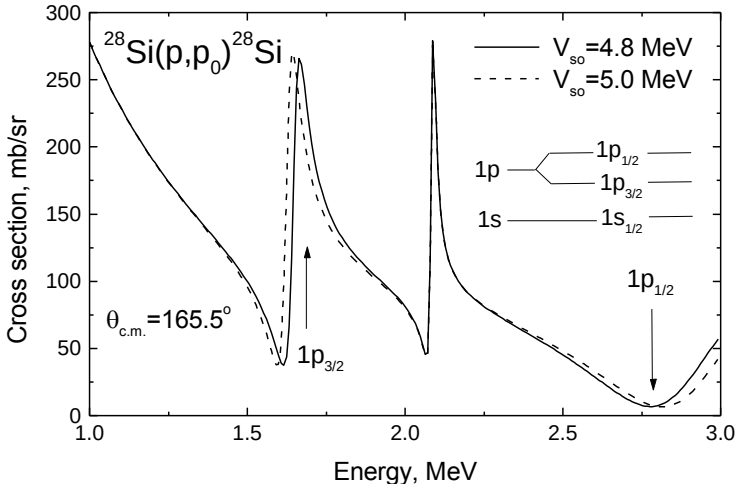

FIG. 5.3. Splitting of a single particle resonance due to the spin-orbit interaction. Reproduced courtesy of Elsevier [5.1].

When narrow resonances dominate in the cross section, the R-matrix theory is most adequate and method (iii) was applied in such cases in the present work. In order to take into account single-particle resonances in a more physical way than just adding them to the R matrix, the phase shifts calculated in framework of potential model were substituted for hard sphere ones normally used.

For the analysis of the experimental data on the (*d,p*) reactions in the deuteron energy range below 10 MeV, the distorted wave approximation or the approximation of coupled channels is usually applied. The theory of scattering for the compound systems with particle transfer is extremely complicated since it includes the many-body problem. For the characterization of the direct mechanisms of reactions which include transfers, the following assumptions are usually made. At the first stage, the interaction of the complex projectile with a mean field of the nucleus is considered and this process is interpreted in the framework of the two-particle optical potential, the excitation of the target nuclei being neglected. It is also assumed that the

ingoing and outgoing particles are of the simple structure of a molecular type that includes a skeleton and a fragment and both components do not excite during scattering. At the second stage, the process of the transfer of the fragment as a whole to (or from) a nucleus occurs and, to account for this stage, different approximations are used. All the information concerning the second stage of the scattering is contained in the form factor which is essentially dependent on the approximations made. At the third stage, the process of elastic scattering of the created new systems is considered and it is again interpreted in the framework of the optical potential. The factorization of the amplitude, i.e. its presentation as a product of the kinematical and spectroscopic factors which accounts for single-particle properties of the nucleus, is possible only provided that the target nucleus states are not excited at the first and the third stages.

In the case the interaction of deuterons with nuclei goes via a resonance at energy E_R with spin I_R and orbital momentum L_R, the amplitude of the resonance process can be written as

$$T^{\mu_b M_B}_{\mu_a M_A}(L_R I_R \pi_R) = \sum_{l_b m} Z^{\mu_b M_B}_{\mu_a M_A}(I_A, I_B, l_b) P_{l_b m}(\theta) e^{im\varphi} \delta_{m, m_a + M_A - m_b - M_B}, \tag{5.8}$$

$$\begin{aligned} Z^{\mu_b M_B}_{\mu_a M_A}(I_A, I_B, l_b) &= \sum_{J j_b} (-1)^m \sqrt{2l_b + 1} \sqrt{\frac{(l_b - m)!}{(l_b + m)!}} \Xi_{\mu_a M_A}(I_R, l_b, j_b, I_A, I_B) \times \\ &\times < l_b m s_b \mu_b \mid j_b \mu_a + M_A - M_B >< j_b \mu_a + M_A - M_B I_B M_B \mid I_R \mu_a + M_A >, \\ \Xi_{\mu_a M_A}(I_R, l_b, j_b, I_A, I_B) &= \frac{1}{k_a} \sum_{l_a j_a} \sqrt{2l_a + 1} e^{i\sigma_{l_a} + i\sigma_{l_b}} < l_a 0 s_a \mu_a \mid j_a \mu_a > \times \\ &\times < j_a \mu_a I_A M_A \mid I_R \mu_a + M_A > C^{I_R \pi_R}_{l_a j_a I_A, l_b j_b I_B}, \end{aligned} \tag{5.9}$$

where

$$C^{I_R \pi_R}_{l_a j_a I_A, l_b j_b I_B} = -e^{i\delta_{l_a j_a I_A} + i\delta_{l_b j_b I_B}} \frac{\Gamma^{1/2}_{l_a j_a I_A} \Gamma^{1/2}_{l_b j_b I_B}}{E - E_R + i\Gamma^{I_R L_R}_R / 2}. \tag{5.10}$$

Here $\Gamma^{I_R L_R}_R$ is a total resonance width, $\Gamma_{l_a j_a I_A}$ is an entrance resonance width, $\Gamma_{l_b j_b I_B}$ is an exit resonance width, δ_i denotes a phase. For several isolated resonances the amplitude is

$$T^{\mu_b M_B}_{\mu_a M_A}(res) = \sum_R T^{\mu_b M_B}_{\mu_a M_A}(L_R I_R \pi_R). \tag{5.11}$$

5.3. THE EVALUATED CROSS SECTIONS

5.3.1. Alpha-proton

The alpha-proton cross section has been studied intensively. Based on different sets of experimental data the R-matrix parameterization of the cross section was produced in [5.3].

The analysis reported in [5.4] and more recent measurements [5.5] also supported the results obtained in [5.3]. However, later it was found that the parameterization [5.3] did not reproduce the cross section adequately in the region of the broad maximum at E_{He}~8.8 MeV, and so a new search for parameters was performed [5.6]. The cross section retrieved with these parameters was assumed to be evaluated. As can be seen in Fig. 5.4, a significant discrepancy between data sets is observed in the region of the cross-section minimum. Consequently, its real value in this region is rather uncertain. It is worth noting that the dependence of the cross section on angle is not strong in the minimum whereas in the vicinity of the 8.8 MeV maximum the cross section varies by ~5% per degree around 30°. At an energy lower than ~1 MeV the cross section is close to Rutherford. The evaluated cross section is based on the 469 data points measured at different angles with both protons and alphas as projectiles. To calculate the cross sections for kinematically reversed reactions ^{1}H(α,p)^{4}He and ^{4}He(p,p)^{4}He the identity of the direct and inverse processes in the centre of mass frame of reference is utilized.

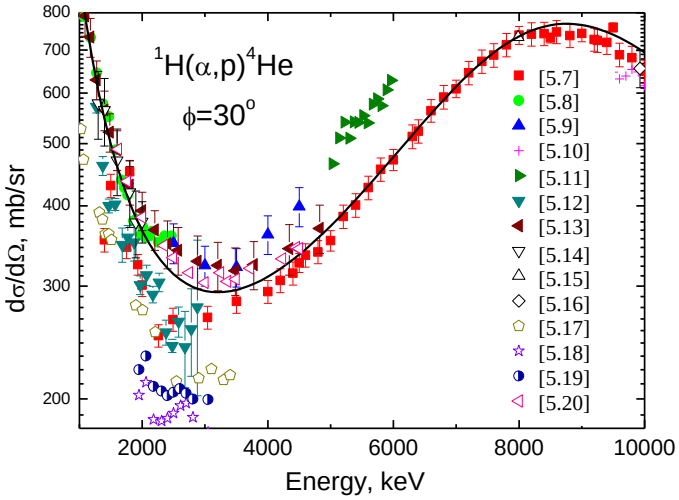

FIG. 5.4. The comparison of the evaluated cross section for α+p (solid line) with experimental data (dots). Reproduced courtesy of Elsevier [5.106].

5.3.2. Carbon

The evaluation of the cross section for proton elastic scattering in the energy range from 0.2 to 3.5 MeV was described in [5.21]. Later it was extended up to 4.5 MeV. The evaluated cross section for the scattering angle of 170° and the corresponding experimental data are presented in Fig. 5.5.

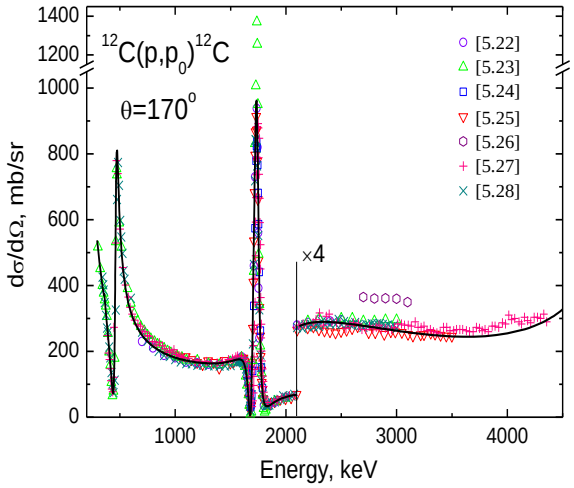

FIG. 5.5. The same as in Fig. 5.4 for $^{12}C(p,p_0)^{12}C$. Reproduced courtesy of Elsevier [5.106].

As is shown in Fig. 5.5, the cross section is non-Rutherford in a whole energy range. The comparison of the obtained results with posterior measurements was made in [5.28,5.29,5.30]. The reliability of the theoretical cross sections was proved in all the cases. The singular result of [5.23] for the cross section in the peak at $E_p \approx 1.734$ MeV (see Fig. 5.5) was not confirmed by the experiments and analysis [5.29]. The only significant difference reported in [5.30] was the position of the strong narrow resonance which was placed in the calculations at 1734 keV whereas in the last work it was found at 1726 keV. The position of this resonance used in the calculations is the adopted one taken from the compilation of F. Ajzenberg-Selove [5.31].

The evaluation of alpha elastic scattering is described in [5.32]. The energy range from Coulomb scattering up to 8 MeV is covered (Figs. 5.6–5.7).

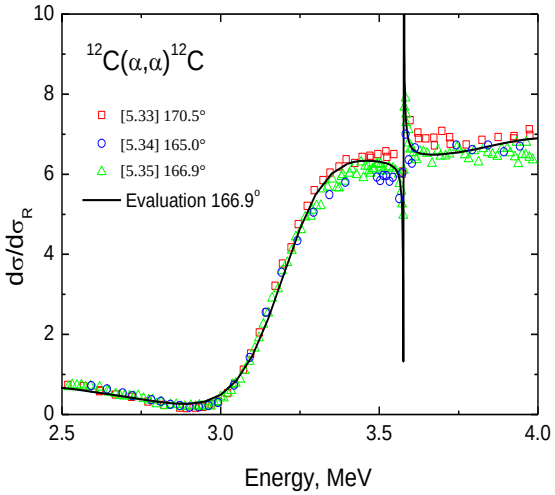

FIG. 5.6. The same as in Fig. 5.4 for $^{12}C(\alpha,\alpha_0)^{12}C$ in the energy range 2.5─4.0 MeV. Reproduced courtesy of Elsevier [5.32].

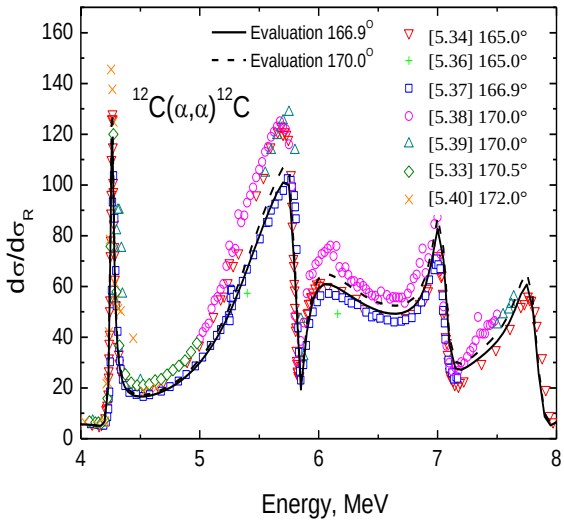

FIG. 5.7. The same as in Fig. 5.4 for $^{12}C(\alpha,\alpha_0)^{12}C$ in the energy range 4.0-8.0 MeV. Reproduced courtesy of Elsevier [5.32].

With the exception of normalization, a fair agreement is generally observed between the available sets of experimental data. The posterior measurements for α+C scattering cross sections were performed at five scattering angles (30, 45, 60, 135 and 150 degrees) in the energy range from 2.5 to 4.8 MeV [5.41]. The results are in satisfactory agreement with the theoretical calculations. The calculations show that the resonance cross section at E=4.26 MeV has strong angular dependence. Its maximal value reached at 180° exceeds the Rutherford cross section by a factor of 145 whereas the anomaly in the cross section completely vanishes at 136.1° (149.5° c.m.) where the Legendre polynomial of the forth order is equal to zero.

The available data for the elastic scattering of deuterons were analyzed in terms of the optical model and resonance reaction mechanism. The deuteron optical potential from [5.42] was used. The evaluated cross section is compared with the available experimental data [5.43, 5.44] for the scattering angle of 165° in Fig. 5.8.
The results for the $^{12}C(d,p_0)^{13}C$ cross section are shown in Fig. 5.9. There, some discrepancies in the experimental data can be seen, especially in the vicinity of resonances.

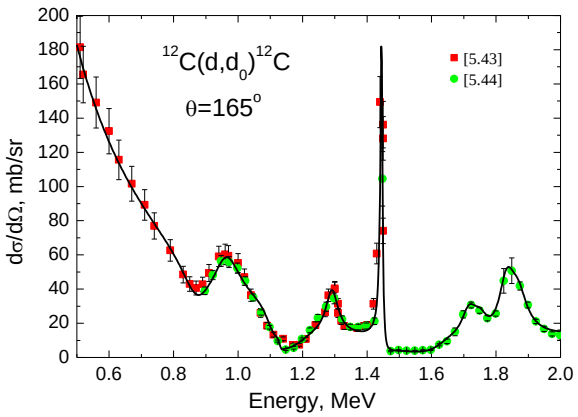

FIG. 5.8. The same as in Fig. 5.4 for $^{12}C(d,d_0)^{12}C$. Reproduced courtesy of Elsevier [5.106].

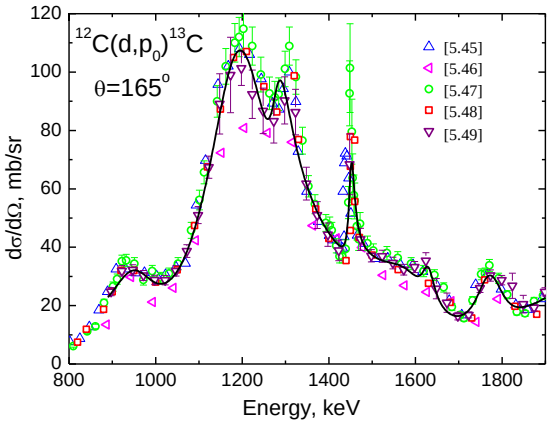

FIG. 5.9. The same as in Fig. 5.4 for $^{12}C(d,p_0)^{12}C$. Reproduced courtesy of Elsevier [5.106].

5.3.3. Nitrogen

For proton elastic scattering a satisfactory overall agreement is observed for most of the available experimental data. However, discrepancies in normalization, peak positions, and peak heights are often far beyond assigned experimental errors. The evaluated cross section in the energy range up to 3.5 MeV [5.50] is compared with experimental data for the scattering angle ~150° in Fig. 5.10.

The measured height of the resonance at 1742 keV (the resonance width ~3.5 keV) is reduced due to the insufficient energy resolution. As far as significant discrepancies exist between different sets of the experimental data theory in principle cannot reproduce all the data simultaneously. The evaluated curve gives the best possible cross sections that can be obtained by the analysis of the existing experimental points. The extension of the evaluation on the energy range up to 5 MeV [5.55] is shown in Fig. 5.11.

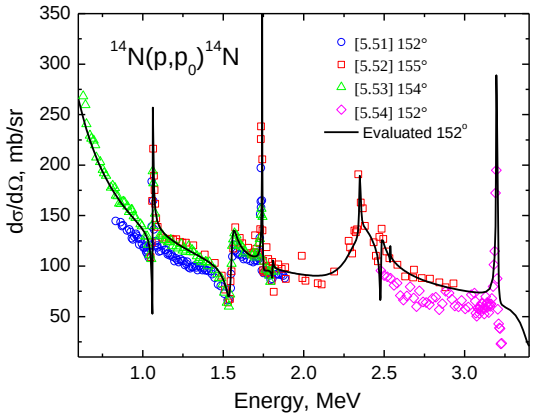

FIG. 5.10. The same as in Fig. 5.4 for $^{14}N(p,p_0)^{14}N$ in the energy range 0.6─3.4 MeV. Reproduced courtesy of Elsevier [5.106].

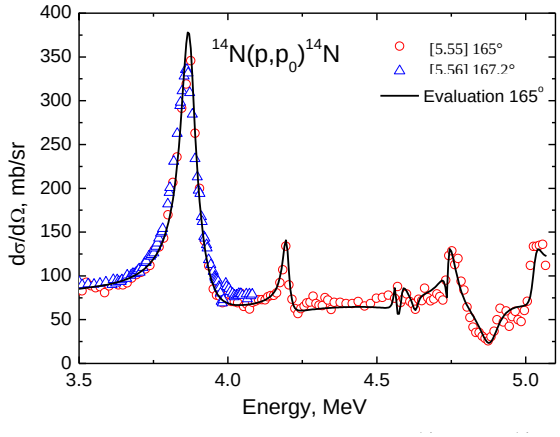

FIG. 5.11. The same as in Fig. 5.4 for $^{14}N(p,p_0)^{14}N$ in the energy range 3.5─5.0 MeV. Reproduced courtesy of Elsevier [5.106].

The comparison of the evaluated curve with the available experimental data for alpha elastic scattering at 165° is presented in Fig. 5.12 for the energy range from 2.5 to 4.6 MeV. The calculations show that the resonance structure located around 3 MeV influences the cross section even at rather low energy resulting in the deviation from Rutherford of about 3% at 2.0 MeV. It should be noted that in most of the measurements the fine structure of the cross section is not adequately reproduced.

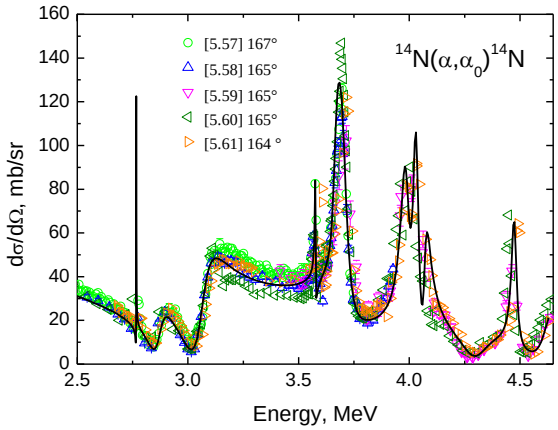

FIG. 5.12. The same as in Fig. 5.4 for $^{14}N(\alpha,\alpha_0)^{14}N$. Reproduced courtesy of Elsevier [5.106].

5.3.4. Oxygen

The evaluation of the proton elastic scattering cross section is described in [5.62]. The theoretical curve is shown together with the experimental results in Fig. 5.13. The comparison with posterior measurements [5.30] showed an excellent agreement.

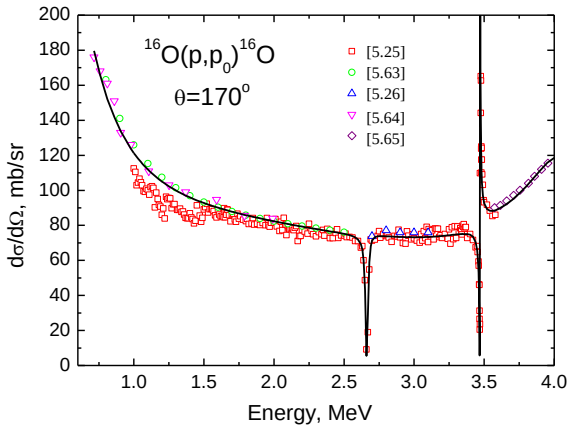

FIG. 5.13. The same as in Fig. 5.4 for $^{16}O(p,p_0)^{16}O$. Reproduced courtesy of Elsevier [5.106].

In the case of elastic scattering of alphas the most important for practice is the resonance at ~3.04 MeV. The cross section in the vicinity of this resonance was measured many times and different values in the range from 3.032 to 3.045 were reported for its location. The theoretical curve for 170° shown in Fig. 5.14 is close to the available experimental points and the only problem is the uncertainty of the resonance parameters. This problem cannot be overcome theoretically and so new precise measurements are needed. A strong angular dependence of the cross section at the resonance energy should be noted.

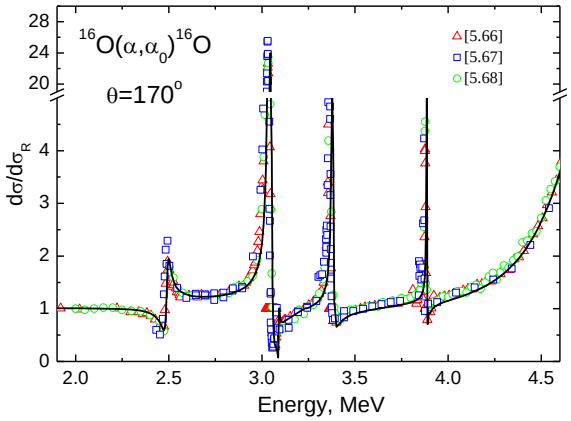

FIG. 5.14. The same as in Fig. 5.4 for $^{16}O(\alpha,\alpha_0)^{16}O$. Reproduced courtesy of Elsevier [5.106].

5.3.5. Fluorine

The experimental data for proton elastic scattering are in poor agreement (see Fig. 5.15). The evaluation was to a great extent based on the structure data for the compound nucleus ^{20}Ne. The theoretical curves for the scattering angles in the interval 159°–165° are indistinguishable and so the difference between the data sets cannot be attributed to the cross section angular dependence.

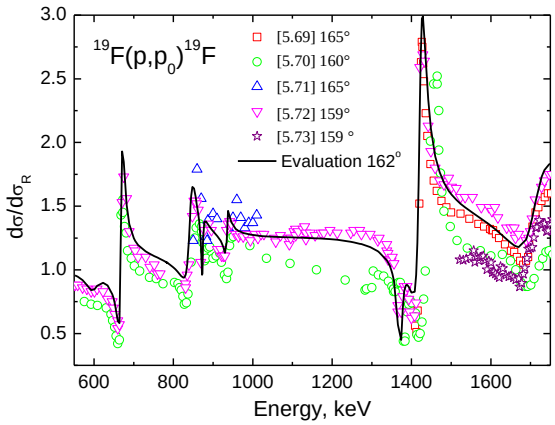

FIG. 5.15. The same as in Fig. 5.4 for $^{19}F(p,p_0)^{19}F$. Reproduced courtesy of Elsevier [5.106].

5.3.6. Neon

The experimental differential cross sections for elastic scattering of protons were found in two papers only [5.74 5.75]. Gas of natural abundance (90.92% of ^{20}Ne) was used in both cases. The available data sets are in reasonable agreement though it is evident that the cross-section structure was partly missed in [5.75] due to insufficient energy resolution. The results of the evaluation are shown in Fig. 5.16.

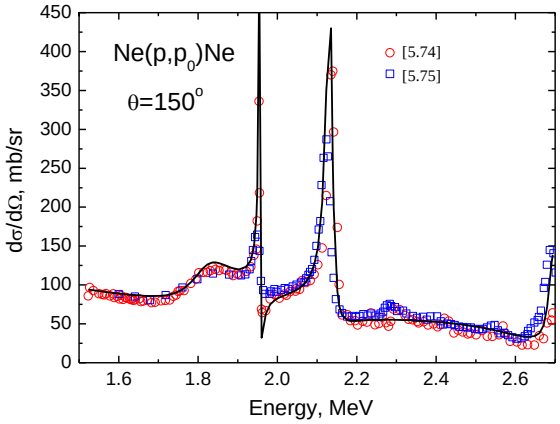

FIG. 5.16. The same as in Fig. 5.4 for Ne(p,p$_0$)Ne. Reproduced courtesy of Elsevier [5.106].

5.3.7. Sodium

The cross section for the elastic scattering of protons was measured in [5.70,5.76,5.77]. It is of complicated structure with many strong narrow resonances (see Fig. 5.17). The points measured in [5.70] are in obvious disagreement with the other two sets of the data and so they were discarded in the evaluation. The results of the evaluation are shown in Fig. 5.17 showing some inconsistencies between the data sets [5.76] and [5.77] exceeding the effect of slightly different scattering angles. Additional measurements are needed in order to resolve the observed discrepancies.

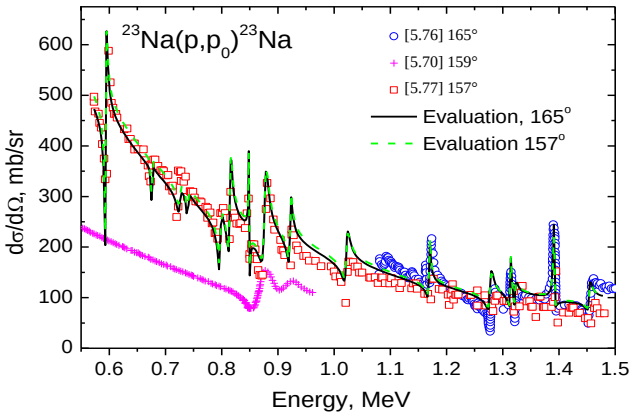

FIG. 5.17. The same as in Fig. 5.4 for ^{23}Na(p,p$_0$)^{23}Na. Reproduced courtesy of Elsevier [5.106].

5.3.8. Magnesium

The evaluated differential cross sections [5.78] are compared with the available experimental data for proton elastic scattering from ^{24}Mg [5.79] and from natural magnesium (78.99% of ^{24}Mg) [5.80,5.81] in Fig. 5.18. The cross section for natural magnesium was calculated as a sum of the cross sections for its three stable isotopes weighted by the relative abundance. A significant contribution of the proton resonance scattering from ^{26}Mg to the results obtained for natural magnesium was revealed. The benchmark experiment performed with a thick uniform natural magnesium target (see [5.78]) supported the results of the evaluation.

For alpha elastic scattering the evaluated curve is close to the data from [5.82, 5.83] whereas in the more recent measurements [5.84] the cross section structure is completely missed (Fig. 5.19).

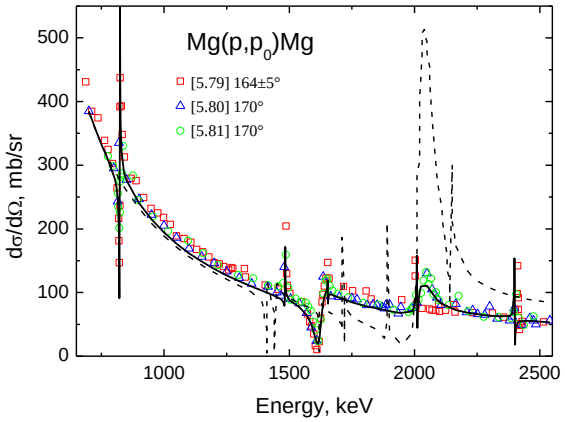

FIG. 5.18. The same as in Fig. 5.4 for Mg(p,p$_0$)Mg. The solid line is for natural magnesium, the dashed one shows the calculated cross section for ^{26}Mg. Reproduced courtesy of Elsevier [5.106].

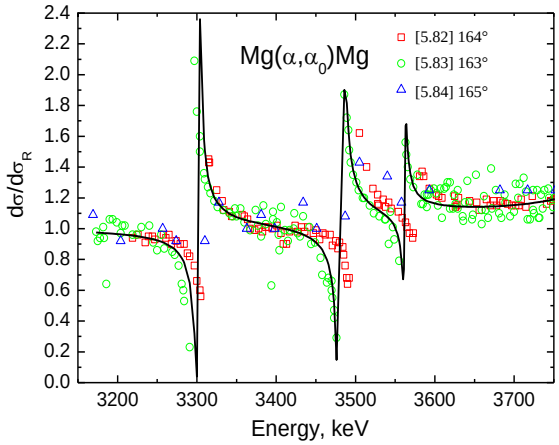

FIG. 5.19. The same as in Fig. 5.4 for Mg(α,α$_0$)Mg. Reproduced courtesy of Elsevier [5.106].

5.3.9. Aluminum

The proton elastic cross section has a lot of narrow resonances in the whole energy range of IBA interests. A typical width of the resonances is 1 to 10 keV. In order to obtain the detailed excitation function, the results of the high resolution proton resonance measurements published in [5.85] were used. In Fig. 5.20 the theory results are compared with the experimental data [5.86, 5.87]. The benchmark experiment reported in [5.88] confirmed both the consistency of the theoretical cross sections with the results of posterior measurements, and the necessity of the detailed knowledge of the cross section fine structure for the adequate simulation of backscattering spectra.

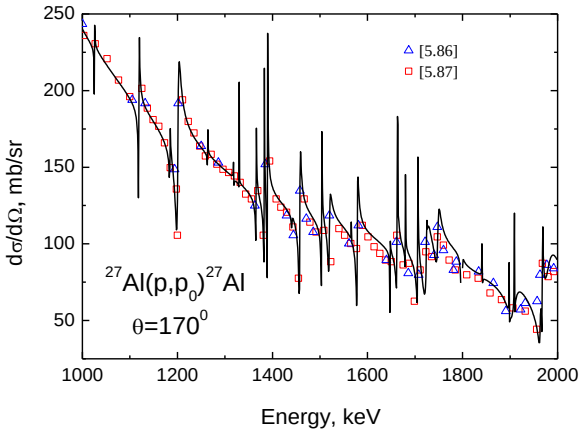

FIG. 5.20. The same as in Fig. 5.4 for ^{27}Al(p,p$_0$)^{27}Al. Reproduced courtesy of Elsevier [5.106].

5.3.10. Silicon

The cross section for natural silicon (92.2% of ^{28}Si, 4.7% of ^{29}Si, and 3.1% of ^{30}Si) was calculated as a sum of the cross sections for its three stable isotopes weighted by the relative abundance. The evaluation was described in [5.89]. The additional work to resolve discrepancies between theoretical and experimental data confirmed the results of the

evaluation [5.90]. The comparison with posterior measurements was reported in [5.30]. The results of the evaluation along with the experimental data are shown in Fig. 5.21. It is worth noting that the contribution of the minor silicon isotopes to the total cross section is significant when the ^{28}Si cross section is small. For instance, the ^{29}Si and ^{30}Si isotopes give in sum about a half of the observed cross section for 170° excitation function at the center of the broad dip near 2.8 MeV.

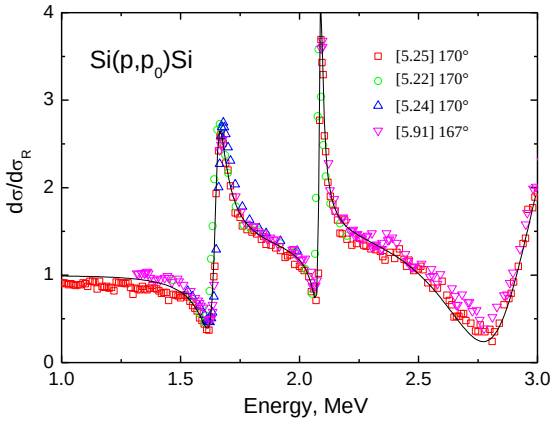

FIG. 5.21. The same as in Fig. 5.4 for Si(p,p$_0$)Si. Reproduced courtesy of Elsevier [5.106].

5.3.11. Phosphorus

The cross section for the elastic scattering of protons was measured in [5.92,5.93]. The resonance fine structure was investigated in [5.94]. Significant discrepancies are observed in the results of the measurements [5.92,5.93]. The data [5.92] show some dip at a proton energy of about 1.3 MeV whereas the data [5.93] reveal a bump centered at approximately 1.75 MeV. Besides, the results [5.93] are on average higher than Rutherford cross section whereas the points measured in [5.92] oscillate around Rutherford cross section at low energy. There are all reasons to believe that the cross section for proton elastic scattering from phosphorus should, on average, follow the Rutherford formula in the studied energy range. On the other hand, the information on resonance parameters taken from the NuDat 2.5 data base (http://www.nndc.bnl.gov/nudat2/), shows that some of the resonances are extremely narrow and so they could not be adequately reproduced in the measurements. In addition, no indication on the origin of the dip at 1.3 MeV or of the bump at 1.75 MeV was found in the nuclear structure data. The evaluated curve shown in Fig. 5.22 gives a theoretical prediction of the cross section behavior differing from the one derived from the experimental data.

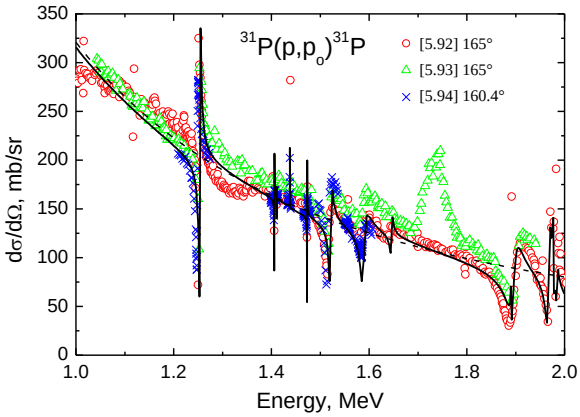

FIG. 5.22. The same as in Fig. 5.4 for $^{31}P(p,p_0)^{31}P$. The Rutherford cross section is shown by a dashed line. Reproduced courtesy of Elsevier [5.106].

5.3.12. Sulfur

The evaluated cross section is presented in Fig. 5.23. The results reported in [5.95] are reproduced fairly well. More recent measurements performed in the energy range of 1.5–2.7 MeV [5.80] are in a good agreement with the calculations.

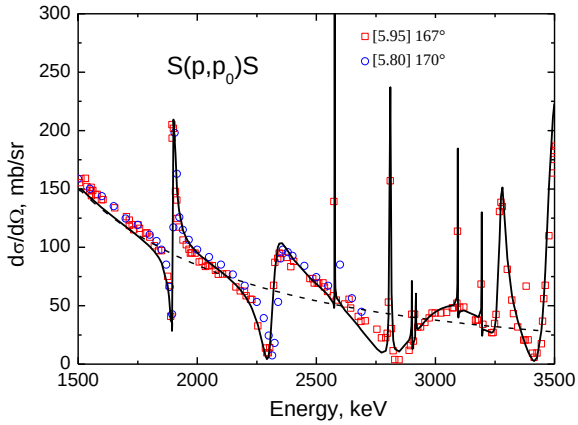

FIG. 5.23. The same as in Fig. 5.4 for S(p,p$_0$)S. The Rutherford cross section is shown by a dashed line. Reproduced courtesy of Elsevier [5.106].

5.3.13. Argon

Broad anomalies were observed in the experimental data for proton elastic scattering [5.96, 5.97,5.98] in the energy range from 1.72 to 2.75 MeV. The fine structure of the anomalies seen in the evaluated curve in Fig. 5.24 is based on the resonance parameters taken from the NuDat 2.5 data base. The evaluated curve closely reproduces the results of the high resolution measurements [5.99] made for the structure located around ~1.9 MeV (see Fig. 5.25). It should be noted that measured at sparse points, data [5.97,5.98,5.99] are inconsistent with the cross section even when it is averaged (see Fig. 5.25).

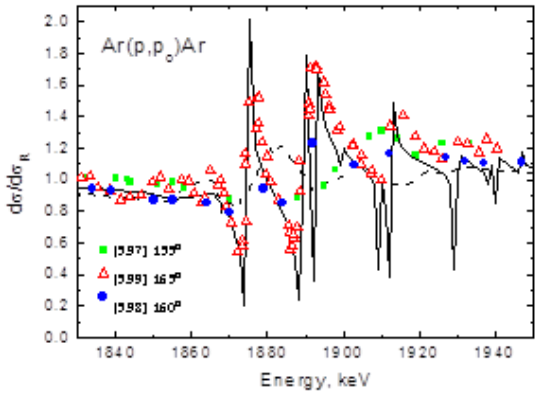

FIG. 5.24. The same as in Fig. 5.4 for Ar(p,p$_0$)Ar. Reproduced courtesy of Elsevier [5.106].

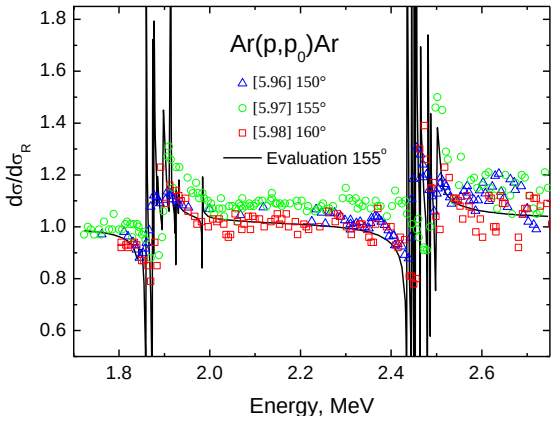

FIG. 5.25. The same as in Fig. 5.4 for Ar(p,p$_0$)Ar fine structure. The cross section averaged over 12 keV is shown by a dashed line. Reproduced courtesy of Elsevier [5.106].

5.3.14. Potassium

For potassium only one work was found [5.100] where the results of the cross section measurement for proton elastic scattering were presented in arbitrary units. In the process of the evaluation these data were normalized against theory. Some of the resonance parameters were taken from the NuDat 2.5 data base. Since the data [5.100] reveal a much more complicated structure than can be accounted for by the resonances listed in NuDat 2.5, additional resonances were added to improve the description of experimental data. As far as experimental data are available for one single angle the spin and parity values assigned to the added resonances may be incorrect.

Consequently the results of the evaluation are reliable in the vicinity of the scattering angle of 168°, for which experimental data were obtained. The results of the calculations are shown in Fig. 5.26.

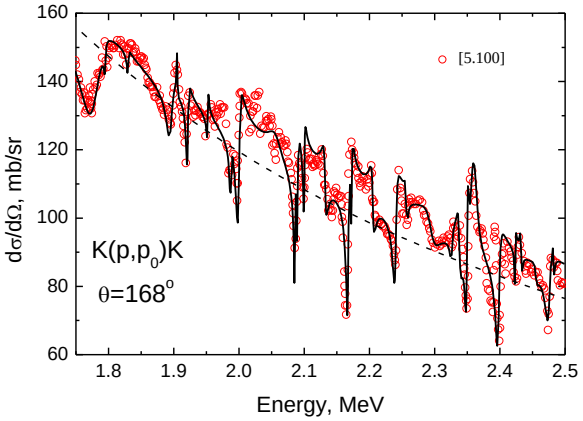

FIG. 5.26. The same as in Fig. 5.4 for K(p,p$_0$)K. The Rutherford cross section is shown by a dashed line. Reproduced courtesy of Elsevier [5.106].

5.3.15. Calcium

The theoretical differential cross section for elastic scattering of protons is in a good agreement with the experimental data [5.101,5.102] (see Fig. 5.27). The resonance parameters for the calculations were taken from the NuDat 2.5 data base. No physical reasons were found for the cross section to exceed the Rutherford value by 9% at 1800 keV as obtained in [5.101].

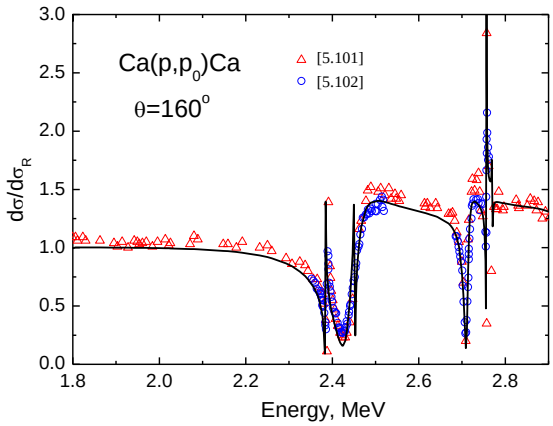

FIG. 5.27. The same as in Fig. 5.4 for Ca(p,p_0)Ca. Reproduced courtesy of Elsevier [5.106].

5.3.16. Titanium

The cross section for elastic scattering of protons from natural titanium is calculated as a sum of the cross sections for its stable isotopes weighted by the relative abundance. The evaluation (see Fig. 5.28) is based mainly on the work [5.103] where a table of the resonance parameters for Ti-48 is published. Only potential scattering (no resonances) was taken into account for minor titanium isotopes. The data [5.86] give an average cross section with no resonance structure. Some points at which the cross section was measured in [5.104] corresponded to the resonance energies and so the obtained excitation function has significant fluctuations. However, these fluctuations do not reproduce the actual resonance structure. The benchmark [5.105] demonstrated that the use of the cross section [5.104] in the simulation resulted in poor agreement with measured spectra.

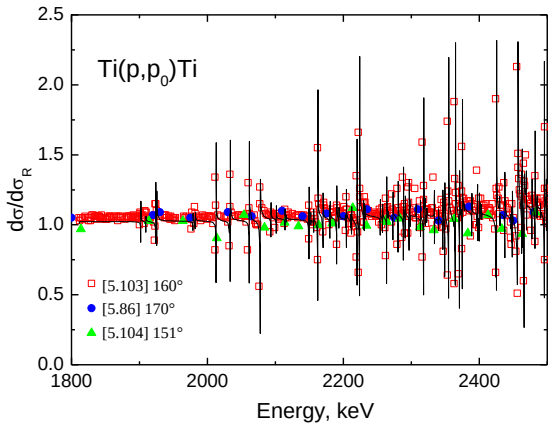

FIG. 5.28. The same as in Fig. 5.4 for Ti(p,p_0)Ti. Reproduced courtesy of Elsevier [5.106].

5.4. CONCLUSIONS

The evaluation provides the best possible cross sections on the basis of the theoretical analysis of the available experimental information. The evaluated cross sections can be retrieved for any scattering angle from the web site SigmaCalc (http://www-nds.iaea.org/sigmacalc/). They are also integrated into the web site IBANDL (http://www-nds.iaea.org/ibandl) where a comparison of the available experimental data with evaluation results can be easily made.

NOTE: The results and discussions included in this chapter have been published for the most part in [5.106].

REFERENCES

[5.1] GURBICH, A.F., Evaluation of non-Rutherford cross sections for IBA: Theory and results, Nucl. Instrum. Methods Phys. Res. B **261** (2007) 401.

[5.2] LANE, A.M., THOMAS, R.G., R-matrix theory of nuclear reactions, Rev. Mod. Phys. **30** (1958) 257.

[5.3] DODDER, D.C., HALE, G.M., JARMIE, N., et al., Elastic scattering of protons by helium 4: New experiments and analysis, Phys. Rev. C **15** (1977) 518.

[5.4] KIM, S.K., CHOI, H.D., Analysis of proton elastic recoil cross section by using R-matrix theory, Nucl. Instrum. Methods Phys. Res. B **174** (2001) 33.

[5.5] NURMELA, A., RÄISÄNEN, J., RAUHALA, E., Elastic scattering cross sections for the analysis of helium by ^{1}H backscattering and hydrogen by ^{4}He ERD, Nucl. Instrum. Methods Phys. Res. B **136-138** (1998) 77.

[5.6] PUSA, P., RAUHALA, E., GURBICH, A., et al., Alpha–proton elastic scattering cross sections for ERDA in the resonance region, Nucl. Instrum. Methods Phys. Res. B **222** (2004) 686.

[5.7] KEAY, J.C., INGRAM, D.C., Absolute cross section for forward recoiling hydrogen with 1.0–12.5 MeV ^{4}He, Nucl. Instrum. Methods Phys. Res. B **211** (2003) 305.

[5.8] QUILLET, V., ABEL, F., SCHOTT, M., Absolute cross section measurements for H and D elastic recoil using 1 to 2.5 MeV ^{4}He ions, and for the ^{12}C(d,p)^{13}C and ^{16}O(d,p$_1$)^{17}O nuclear reactions, Nucl. Instrum. Methods Phys. Res. B **83** (1993) 47.

[5.9] BOGDANOVIĆ-RADOVIĆ, I., BENKA, O., Determination of H recoil cross sections for He ions incident at 2.5 – 4.5 MeV and recoil angles from 30° to 60°, Nucl. Instrum. Methods Phys. Res. B **174** (2001) 25.

[5.10] BROWNING, J.F., BANKS, J.C., WAMPLER, W.R., et al., Cross sections for the elastic recoil of hydrogen isotopes for high energy helium ions, Nucl. Instrum. Methods Phys. Res. B **219 - 220** (2004) 317.

[5.11] WETTELEND, C.J., MAGGIORE, C.J., TESMER, J.R., et al., LANL report LA-UR-98-4867.

[5.12] BAGLIN, J.E.E., KELLOCK, A.J., CROCKETT, M.A., et al., Absolute cross section for hydrogen forward scattering, Nucl. Instrum. Methods Phys. Res. B **64** (1992) 469.

[5.13] KIM, C.-S., KIM, S.-K., CHOI, D., Proton elastic recoil cross sections for 0.6–5.0 MeV ^{4}He ions, Nucl. Instrum. Methods Phys. Res. B **155** (1999) 229.

[5.14] WANG, H., ZHOU, G., Measurement of ^{4}He-p recoil cross sections, Nucl. Instrum. Methods Phys. Res. B **34** (1988) 145.

[5.15] BARNARD, A.C.L., JONES, C.M., WEIL, J.L., Nucl. Phys. **50** (1964) 604.

[5.16] BROWNING, J., LANGLEY, R., DOYLE, B., et al., High accuracy, high energy He-ERD analysis of H, D and T, Nucl. Instrum. Methods Phys. Res. B **161-163** (2000) 211.
[5.17] SZILAGYI, E., PASZTI, F., MANUABA, A., Cross section measurements of the $^{1}H(^{4}He, ^{4}He)^{1}H$ elastic recoil reaction for ERD analysis, Nucl. Instrum. Methods Phys. Res. B **43** (1989) 502.
[5.18] YAMAGUCHI, S., FUJINO, Y., NAGATA, S., et al., Analysis of hydrogen in corrosion product films on amorphous alloy using the elastic recoil detection technique, Nucl. Instrum. Methods Phys. Res. B **218** (1983) 598.
[5.19] NAGATA, S., YAMAGUCHI, S., FUJINO, Y., et al., Depth resolution and recoil cross section for analyzing hydrogen in solids using elastic recoil detection with ^{4}He beam, Nucl. Instrum. Methods Phys. Res. B **6** (1985) 533.
[5.20] INGRAM, D., McCORMICK, A., PRONKO, P., Hydrogen analysis as a function of depth for hydrogenous films and polymers by proton recoil detection, Nucl. Instrum. Methods Phys. Res. B **6** (1985) 430.
[5.21] GURBICH, A.F., Evaluation of non-Rutherford proton elastic scattering cross section for carbon, Nucl. Instrum. Methods Phys. Res. B **136-138** (1998) 60.
[5.22] RAUHALA, E., Proton elastic scattering cross sections of carbon, nitrogen and silicon for backscattering analysis in the energy range 0.7 – 2.5 MeV, Nucl. Instrum. Methods Phys. Res. B **12** (1985) 447.
[5.23] LIU, Z., LI, B., DUAN, Z., et al., Cross section measurements for 170° backscattering of protons from carbon in the energy range 0.3 – 3.0 MeV, Nucl. Instrum. Methods Phys. Res. B **74** (1993) 439.
[5.24] SALOMONOVIC, R., Angular distribution of proton non-Rutherford elastic scattering cross section of carbon and silicon, Nucl. Instrum. Methods Phys. Res. B **82** (1993) 1.
[5.25] AMIRIKAS, R., JAMIESON, D.N., DOOLEY, S.P., Measurement of (p,p) elastic cross sections for C, O and Si in the energy range 1.0 – 3.5 MeV, Nucl. Instrum. Methods Phys. Res. B **77** (1993) 110.
[5.26] YANG, G., ZHU, D., XU, H., et al., Proton elastic scattering for light element cross section enhancement with $E_p > 2.5$ MeV, Nucl. Instrum. Methods Phys. Res. B **61** (1991) 175.
[5.27] JACKSON, H.L., GALONSKY, A.I., EPPLING, F.J., et al., The $C^{12}(p, p)C^{12}$ Differential Cross Section, Phys. Rev. **89** (1953) 365.
[5.28] MAZZONI, S., CHIARI, M., GIUNTINI, L., et al., Erratum to: Proton elastic scattering cross section on carbon from 350 keV to 3 MeV in: Nucl. Instrum. Methods Phys. Res. B 136–138 (1998) 86–90, Nucl. Instrum. Methods Phys. Res. B **159** (1999) 191.
[5.29] GURBICH, A.F., Proton elastic scattering cross section for carbon: confrontation of theory and experiment, Nucl. Instrum. Methods Phys. Res. B **152** (1999) 403.
[5.30] RAMOS, A.R.L., PAUL, A., RIJNIERS, L., et al., Measurement of (p,p) elastic differential cross sections for carbon, nitrogen, oxygen, aluminium and silicon in the 500 – 2500 keV range at 140° and 178° laboratory scattering angles, Nucl. Instrum. Methods Phys. Res.B **190** (2002) 95.
[5.31] AJZENBERG-SELOVE, F., Energy levels of light nuclei A = 13-15, Nucl. Phys. A **523** (1991) 46.
[5.32] GURBICH, A.F., Evaluation of the cross section for elastic scattering of ^{4}He from carbon, Nucl. Instrum. Methods Phys. Res.B **161-163** (2000) 125-129.

[5.33] LEAVITT, J.A., MCINTYRE JR., L.C., STOSS, P., et al., Cross sections for 170.5° backscattering of ^{4}He from carbon for ^{4}He energies between 1.6 and 5.0 MeV Nucl. Instrum. Methods Phys. Res. B **40/41** (1989) 776.
[5.34] FENG, Y., ZHOU, Z., ZHOU, C., et al., Cross sections for 165° backscattering of 2.0–9.0 MeV ^{4}He from carbon, Nucl. Instrum. Methods Phys. Res. B **86** (1994) 225.
[5.35] HILL, R.W., Elastic Scattering of Alpha-Particles by Carbon, Phys. Rev. **90** (1953) 845.
[5.36] GOSSETT, C.R., Non-Rutherford elastic backscattering for light element cross section enhancement, Nucl. Instrum. Methods Phys. Res. B **40/41** (1989) 813.
[5.37] BITTNER, J.W., MOFFAT, R.D., Elastic scattering of alpha particles by carbon, Phys. Rev. **96** (1954) 374.
[5.38] CHENG, H.-S., SHEN, H., TANG, F., et al., Acta Physica Sinica 43 (1994) 1569.
[5.39] DAVIES, J.A., ALMEIDA, F.J.D., HAUGEN, H.K., et al., Quantitative calibration of intense (α,α) elastic scattering resonances for ^{12}C at 5.50 – 5.80 MeV and for ^{16}O at 7.30 – 7.65 MeV, Nucl. Instrum. Methods Phys. Res. B **85** (1994) 28.
[5.40] SOMATRI, R., CHAILAN, J.F., CHEVARIER, A., et al., Alpha backscattering used in stoichiometry determination of thin SiC coatings on Si(100) wafers, Nucl. Instrum. Methods Phys. Res. B **113** (1996) 284.
[5.41] BOGDANOVIC RADOVIC, I., JAKSIC, M., BENKA, O., et al., Helium elastic scattering from carbon for 30° to 150° in the energy region from 2 to 4.8 MeV, Nucl. Instrum. Methods Phys. Res. B **190** (2002) 100.
[5.42] SATCHLER, G.R., An optical potential for deuteron scattering from carbon, Nucl. Phys. **85** (1966) 273.
[5.43] KIM, H.J., MILNER, W.T., McGOWAN, F.K., Nuclear Data Tables A **2** (1966) 353.
[5.44] KOKKORIS, M., MISAILIDES, P., KOSSIONIDES, S., et al., A detailed study of the ^{nat}C(d,d_0) reaction at detector angles between 145° and 170°, for the energy range $E_{d,\,lab}$ = 900–2000 keV, Nucl. Instrum. Methods Phys. Res. B **249** (2006) 81.
[5.45] KASHY, E., PERRY, R.R., RISSER, J.R., Excited States in N^{14} from C^{12}(d,d)C^{12}, C^{12}(d,p_0)C^{13}, and C^{12}(d,p_1)C^{13}, Phys. Rev. **117** (1960) 1289.
[5.46] A.P. KLYUCHAREV et al., Izv. Akad. Nauk **30** (1966) 224 (in Russian).
[5.47] PACHECO DE CARVALHO, J.A.R., REIS, A.D., Differential cross-section measurements for the ^{12}C(d,p_0)^{13}C reaction and applications to surface analysis of materials, Nucl. Instrum. Methods Phys. Res. B **266** (2008) 2263.
[5.48] BALIN, V.G., GURBICH, A.F., SHORIN, V.S., Preprint FEI-1341 (1982) Obninsk (in Russian).
[5.49] KOKKORIS, M., MISAELIDES, P., KONTOS, A., et al., A detailed study of the ^{12}C(d,p_0)^{13}C reaction at detector angles between 135° and 170°, for the energy range Ed, lab = 900–2000 keV, Nucl. Instrum. Methods Phys. Res. B **249** (2006) 77.
[5.50] GURBICH, A., Evaluation of non-Rutherford proton elastic scattering cross section for nitrogen, Nucl. Instrum. Methods Phys. Res. B **266** (2008) 1193.
[5.51] TAUTFEST, G.W., RUBIN, S., Elastic scattering of protons from B^{11} and N^{14}, Phys. Rev. **103** (1956) 196.
[5.52] FERGUSON, A.J., CLARKE, R.L., GOVE, H.E., Elastic scattering of protons by nitrogen, Phys. Rev. **115** (1959) 1655.
[5.53] HAGEDORN, F.B., MOZER, F.S., WEBB, T.S., et al., Elastic scattering of protons by N^{14}, Phys. Rev. **105** (1957) 219.
[5.54] JIANG, W., SHUTTHANANDAN, V., THEVUTHASAN, S., et al., Nitrogen analysis using energetic ion beams, Surf. Interface Anal. **37** (2005) 374.

[5.55] BOGDANOVIC RADOVIC, I., SIKETIC, Z., JAKSIC, M., Measurement parametrization of proton elastic scattering cross sections for nitrogen, J. Appl. Phys. **104** (2008) 074905.
[5.56] OLNESS, J.W., VORONA, J., LEWIS, H.W., Elastic and inelastic scattering of protons by N^{14}, Phys. Rev. **112** (1958) 475.
[5.57] HERRING, D.F., REN CHIBA, GASTEN, B.R., et al., $N^{14}(\alpha,\alpha)N^{14}$ and $N^{14}(\alpha,p)O^{17}$ differential cross sections, Phys. Rev. **112** (1958) 1210.
[5.58] BOGDANOVIC RADOVIC, I., et al., unpublished.
[5.59] TERWAGNE, G., GENARD, G., YEDJI, M., et al., Cross-section measurement of the $^{14}N(\alpha,p)^{17}O$ and $^{14}N(\alpha,\alpha)^{14}N$ reaction between 3.5 and 6 MeV, J. Appl. Phys. **104** (2008) 084909.
[5.60] FENG, Y., ZHOU, Z., ZHOU, G., et al., Cross sections for 165° backscattering of 2.0 – 9.0 MeV ^{4}He ions from nitrogen, Nucl. Instrum. Methods Phys. Res. B **94** (1994) 11.
[5.61] KASHY, E., MILLER, P.D., RISSER, J.R., Energy Levels in F^{18} from the $N^{14}(\alpha,\alpha)N^{14}$ and $N^{14}(\alpha,p)O^{17}$ Reactions, Phys. Rev. **112** (1958) 547.
[5.62] GURBICH, A.F. Evaluation of non-Rutherford proton elastic scattering cross section for oxygen, Nucl. Instrum. Methods Phys. Res. B **129** (1997) 311.
[5.63] LUOMAJARVI, M., RAUHALA, E., HAUTALA, M., Oxygen detection by non-Rutherford proton backscattering below 2.5 MeV, Nucl. Instrum. Methods Phys. Res. B **9** (1985) 255.
[5.64] CHOW, H.C., GRIFFITS, G.M., HALL, T.H., The $^{16}O(p,\gamma)^{15}F$ direct capture cross section with an extrapolation to astrophysical energies, Can. J. Phys. **53** (1975) 1672.
[5.65] EPPLING, F.J., CAMERON, J.R.,. DAVIS, R.H., et al., unpublished. Reproduced from graph published in J.W. Mayer and E. Rimini, eds., Ion Beam Handbook for Material Analysis (Academic Press, New York, 1977).
[5.66] LEAVITT, J.A., McINTYRE JR., L.C., ASHBAUGH, M.D., et al., Cross sections for 170.5° backscattering of ^{4}He from oxygen for ^{4}He energies between 1.8 and 5.0 MeV, Nucl. Instrum. Methods Phys. Res. B **44** (1990) 260.
[5.67] CHENG, H.-S., SHEN, H., TANG, J., et al, Cross sections for 170° backscattering of ^{4}He from oxygen in the energy range of 2.0 – 9.0 MeV, Nucl. Instrum. Methods Phys. Res. B **83** (1993) 449.
[5.68] DEMARCHE, J., TERWAGNE, G., Precise measurement of the differential cross section from the $^{16}O(\alpha,\alpha)^{16}O$ elastic scattering at 165° and 170° between 2.4 and 6 MeV, J. Appl. Phys. **100** (2006) 124909.
[5.69] JESUS, A.P., BRAIZINHA, B., CRUZ, J., et al., Influence of target thickness on resonant elastic scattering of protons by ^{19}F Nucl. Instrum. Methods Phys. Res. B **174** (2001) 229.
[5.70] DEARNALEY, G., The elastic scattering of protons by light elements, Phil. Mag. **8**/1 (1956) 821.
[5.71] KNOX, J.M., HARMON, J.F., Non-Rutherford elastic scattering in fluorine, Nucl. Instrum. Methods Phys. Res B **44** (1989) 40.
[5.72] WEBB, T.S., HAGEDORN, F.B., Fowler, W.A., et al., Elastic scattering of protons by F19, Phys. Rev. **99** (1955) 138.
[5.73] OUICHAOUI, S., BEAUMEVIEILLE, H., BENDJABALLAH, N., T=1 states in ^{20}Ne as compound resonances induced by the $p+^{19}F$ reactions, Nuovo Cim. A **94** (1986) 133.
[5.74] LAMBERT, M., MIDY, P., DRAIN, D., Study of ^{21}Na excited states, J. Phys. **33** (1972) 155.

[5.75] VALTER, A.K., DEINEKO, A.S., SOROKIN, P.V., et al., Izv. Acad. Nauk **24** (1960) 884 (in Russian).
[5.76] VANHOY, J.R., BILPUCH, E.G., WESTERFELDT, C.R., et al., Proton resonances in ^{24}Mg from Ex = 12.7 to 15.7 MeV, Phys. Rev. C **36** (1987) 920.
[5.77] BAUMANN, N.P., PROSSER, F.W., READ, G.W., et al., Elastic scattering of protons from ^{23}Na, Phys. Rev. **104** (1956) 376.
[5.78] GURBICH, A.F., JEYNES, C., Evaluation of non-Rutherford proton elastic scattering cross section for magnesium, Nucl. Instrum. Methods Phys. Res. B **265** (2007) 447.
[5.79] MOORING, F.P., KOSTER, L.J., GOLDBERG, E. et al., Elastic scattering of protons from ^{24}Mg, Phys. Rev. **84** (1951) 703.
[5.80] RAUHALA, E., LUOMAJÄRVI, M., Cross sections for 170° backscattering of 0.8 – 2.7 MeV protons from magnesium and sulfur, Nucl. Instrum. Methods Phys. Res. B **33** (1988) 628.
[5.81] ZHANG, X., LI, G., DING, B., et al., Non-Rutherford elastic scattering cross sections of natural magnesium for protons, Nucl. Instrum. Methods Phys. Res. B **201** (2003) 551.
[5.82] KAUFMANN, S., GOLDBERG, E., KOESTER, L.J., et al., Energy levels in ^{28}Si excited by alpha particles on ^{24}Mg, Phys. Rev. **88** (1952) 673.
[5.83] CSEH, J., KOLTAY, E., MATE, Z., et al., Nucl. Phys. A 385 (1982) 43.
[5.84] CHENG, H.-S., SHEN, H., YANG, F., et al., Cross sections for non-Rutherford backscattering of ^{4}He from five light elements, Nucl. Instrum. Methods Phys. Res. B **85** (1994) 47.
[5.85] NELSON, R.O., BILPUCH, E.G., WESTERFELDT, C.R., Proton resonances in ^{28}Si from Ex = 12.5 to 13.4 MeV, Phys. Rev. C **29** (1984) 1656.
[5.86] RAUHALA, E., Proton backscattering and computer data analysis in the non-Rutherford energy region, Nucl. Instrum. Methods Phys. Res. B **40/41** (1989) 790.
[5.87] CHIARI, M., GIUNTINI, L., MANDO, P.A., et al., Proton elastic scattering cross section on aluminium from 0.8 to 3 MeV, Nucl. Instrum. Methods Phys. Res. B **174** (2001) 259.
[5.88] GURBICH, A.F., BARRADAS, N.P., JEYNES, C., et al., Applying elastic backscattering spectrometry when the nuclear excitation function has a fine structure, Nucl. Instrum. Methods Phys. Res. B **190** (2002) 237.
[5.89] GURBICH, A.F., Evaluation of non-Rutherford proton elastic scattering cross section for silicon, Nucl. Instrum. Methods Phys. Res. B **145** (1998) 578.
[5.90] HEALY, M.J.F., GURBICH, A.F., New data on the proton elastic scattering cross section for silicon, Nucl. Instrum. Methods Phys. Res. B **161-163** (2000) 136.
[5.91] VORONA, J., OLNESS, J.W., HAEBERLI, W., et al., Levels of P^{29} from $Si^{28}(p,p)Si^{28}$ and $Si^{28}(p,p')Si^{28}$, Phys. Rev. **116** (1959) 1563.
[5.92] FANG, D.F., BILPUCH, E.G., WESTERFELDT, C.R., et al., Proton resonances in ^{32}S from Ex = 9.83 to 12.74 MeV, Phys. Rev. C **37** (1988) 28.
[5.93] COHEN-GANOUNA, J., LAMBERT, M., SCHMOUKER, J., Spin and parity of certain levels in ^{32}S by analysis of the scattering $P^{31}(p,p)P^{31}$, Nucl. Phys. **40** (1963) 67.
[5.94] VERNOTTE, J., GALES, S., LANGEVIN, M., et al., Research on isobaric analog resonances in ^{32}S by means of the reactions $^{31}P(p,\gamma)^{32}S$, $^{31}P(p,p)^{31}P$, and $^{31}P(p,\alpha_0)^{28}Si$, Nucl. Phys. A **212** (1973) 493.
[5.95] OLNESS, J.W., HAEBERLI, W., LEWIS, H.W., Levels of Cl^{33} from $S^{32}(p,p)S^{32}$ and $S^{32}(p,p'\gamma)S^{32}$, Phys. Rev. **112** (1958) 1702.

[5.96] VALTER, A.K., MALAKHOV, I.YA., SOROKIN, P.V., et al., Elastic Scattering of protons by Ar^{40}, Izv. Acad. Nauk **23** (1959) 846 (in Russian).
[5.97] FREIER, G.D., FAMULARO, K.F., ZIPOY, D.M., et al., Elastic scattering of protons by A40, Phys. Rev. **110** (1958) 446.
[5.98] BARNARD, A.C.L., KIM, C.C., Elastic scattering of protons by Argon-36, Nucl. Phys. **28** (1961) 428.
[5.99] COHEN-GANOUNA, J., LAMBERT, M., SCHMOUKER, J., Reactions $A^{40}(p,p)A^{40}$ and $A^{40}(p,\gamma)K^{41}$ determination and study of certain excited states of K^{41}, Nucl. Phys. **40** (1963) 82.
[5.100] DE MEIJER, R.J., SIEDERS, A.A., LANDMAN, H.A.A., et al., Investigation of proton induced resonance reactions on ^{39}K, Nucl. Phys. A **155** (1970) 109.
[5.101] WILSON JR., W.M., MOSES, J.D., BILPUCH, E.G., Thomas-Ehrman shifts in ^{41}Ca-^{41}Sc, Nucl. Phys. A **227** (1974) 277.
[5.102] KOLTAY, E., MESKO, L., VEGH, L., Levels of ^{41}Sc from the $^{40}Ca(p,p)^{40}Ca$ reaction, Nucl. Phys. A **249** (1975) 173.
[5.103] PROCHNOW, N.H., NEWSON, H.W., BILPUCH, E.G., et al., High-resolution proton scattering from ^{48}Ti, Nucl. Phys. A **194** (1972) 353.
[5.104] HU, P., ZHANG, J., JIN, Q., et al., Proton elastic scattering cross sections of titanium from 1.0 to 3.0 MeV at the laboratory angle of 151°, Nucl. Instrum. Methods Phys. Res. B **217** (2004) 551.
[5.105] BARRADAS, N.P., unpublished.
[5.106] GURBICH, A.F., Evaluated differential cross-sections for IBA, Nucl. Instrum. Methods Phys. Res. B **268** (2010) 1703.

6. BENCHMARKING CROSS-SECTION DATA

6.1. INTRODUCTION

The purpose of establishing high quality scattering cross sections for ion beam analysis is to be able to *accurately* analyse given samples. Accurate analysis is indispensable for every application depending on reliable metrology. That is, it pervades all modern thin film technology, and many other fields besides.

This section on *benchmarking* is intended to establish the present outside limits of verifiable knowledge of these scattering cross sections. If something is true, then it is true however you look at it. Benchmarking is a way of independently demonstrating the validity of specific parameters. One measurement of a quantity can be affected by an unknown bias: only when the quantity is re-measured using different and independent methods can we start to be sure that any unknown bias is not important.

In the summary presented to the Hyderabad IBA conference [6.1], it was pointed out that benchmarking is very valuable in establishing the validity of a set of cross sections. Cross sections are almost always measured using thin film samples: such measurements are difficult and errors can easily creep in. Benchmark experiments take the measured cross sections (which may also be evaluated) and apply them to the simulation of spectra from well known (usually thick) samples, thus demonstrating how internally consistent the cross-section data are.

The problem of correctly simulating the spectrum in the presence of resonances in the scattering cross-section function, where these resonances may be very sharp, has been solved explicitly [6.2]. This problem is not trivial: the different simulation codes are not equivalent and can give significantly different results (for an evaluation see [6.3]).

The value of benchmarks can be highlighted, as one example of many possible ones, by the $^{24}Mg(p,p_0)$ reaction for which there is an exceptionally strong and sharp resonance at 1483 keV [6.4]. Such sharp resonances in the scattering cross sections are not possible to measure explicitly, since the thin film used for the measurements must have some thickness over which the resonance is averaged. Even though this Mg(p,p) reaction had been evaluated, the nuclear data used to determine the height and width of the resonance left these parameters unknown in significant respects. In this case the benchmark measurements could both establish reasonable values for these resonance parameters, and also demonstrate that even such sharp resonances could be simulated correctly.

Benchmark experiments have been implicitly defined in the literature. [6.5] has: "*The final stage is to compare the calculated curves to the experimental points and analyze the revealed discrepancies. In dubious cases the measurement performed with a standard sample (benchmark) followed by spectrum simulation can help to clarify the reality.*" [6.1] has: "*In addition to the cross section measurements benchmark experiments consisting of measuring charged particle spectra from well characterized uniform thick targets are also planned within the CRP.*" This latter paper includes a comment on the use of inversion techniques (including Bayesian inference) to obtain cross sections directly from bulk sample spectra. Here we treat measurements using those techniques as effectively benchmarking experiments since "well characterized

uniform thick targets" are used, and the cross sections derived automatically fit the thick target spectra.

6.1.1. Methods

Several benchmarking methods are reported here. Most obviously, evaluated EBS cross-sections can simply be applied to the simulation of bulk spectra. If the simulation fits then the cross-section is valid. The difficulty in this case is in assigning the region of validity and the uncertainties with reasonable confidence.

Then, series of simulations for different beam energies can be made of a thin film sample, and (say) the film thickness can be derived which should of course be constant over the series. This is another way of checking the absolute value of the cross-section at different energies and was used for Mg.

A variant of this is shown in the case of depth profiling by PIGE, where the gamma yield from a known thin film is calculated directly from the differential cross sections. The fact that the correct film thickness is extracted (that is, the observed excitation is reproduced by the calculation) demonstrates the validity of the cross sections. We include PIGE results for protons on Al, even though the remit of this CRP is for particle scattering, since this is a very complicated case where the gamma rays often carry important complementary information.

A different and rather intricate possibility is the case where the cross-sections are extracted from bulk sample spectra by an inverse method, using ***Bayesian Inference*** techniques (BI). This can be demonstrated to work surprisingly well where the cross-section function is not too discontinuous. The method used for extracting the cross-section function automatically gives statistically robust estimates of the uncertainty for every point in the function. Such indirectly measured data always constitute an independent cross-section data-set; however, they are also interpreted as a benchmark for *other* cross-section data-sets, as we show below for C, N, Si (several of these results are reproduced from [6.6]: in turn some of these are published in [6.7] using an improved algorithm published in [6.8]).

Results similar to those of the BI method can also be obtained more simply, although a realistic value of the uncertainty is not easy to determine. Given an estimate of the cross-section function, each spectrum can be inverted to a depth profile ***point-by-point***. Then for each point, a correction to the cross-section function can be calculated. Results using this method are presented for Li and F.

Both of the Bayesian Inference and the point-by-point methods depend on the simultaneous evaluation of thick sample spectra collected at different beam energies. Whenever these or similar methods are used it is essential to use an absolute detector electronics calibration, where the spectra are interpreted on the basis of the actual energy deposited in the active region of the detector rather than the energy of the particle leaving the sample: that is, with the pulse height defect correction [6.9].

Finally, the questions arise: firstly, can the simulations be calculated correctly; and secondly, can (and in what circumstances can) cross-sections with many sharp resonances be simplified for practical purposes? This latter is desirable since correct calculation from highly structured cross-section functions (such as the Ti(p,p)

reaction) is extremely time consuming. We will show that present codes can indeed calculate correctly, although some tricky technical questions remain and further development is expected. However, most codes still use approximations that noticeably distort simulations (see [6.3] for details). We will also show some preliminary work suggesting that reasonable approximations to very highly structured cross-section functions may be available, although it is still not yet clear how to make these approximations reliably.

6.1.2. Estimation of Uncertainties in the Beam Energy

In the new edition of the *IBA Handbook* there are Tables (Tables 15.2, 15.3, 15.4 of [6.10]) of accelerator calibration points which significantly extend (and correct) the previous (1995) edition. A few (secondary) points from EBS resonances are included. Here we present further information. There are also *two* reference points for the $^{27}Al(p,\gamma)^{28}Si$ reaction, with a better reference for the standard 992 keV reaction than appears in the *Handbook*.

EBS spectra are interesting because, unlike RBS spectra, the spectrum tells you what the beam energy was. This is always useful as a check, and is often very valuable. We therefore present here a Table of resonances whose positions are validated. Even when a cross-section function is evaluated, and can be calculated by SigmaCalc, it is not easy to assign uncertainties from the evaluation. But a benchmark experiment can directly put uncertainties independently determined from the energy response of the system, noting that *positions of edges* in the spectra can be obtained with far greater precision than the experimental energy resolution [6.11].

A careful analysis of the energy uncertainty in pulse-height-defect-corrected sets of data over an energy range (see Section 6.11 below) shows that when this is done correctly an energy uncertainty of 0.2% can be assigned. Clearly, nuclear spectroscopy can do far better than this, but in the absence of evaluated uncertainties for values obtained by spectroscopy even this relatively large uncertainty may often be valuable.

We propose that in the absence of more detailed information, and where a benchmark experiment has been completed on evaluated (SigmaCalc) cross sections over an energy range, the evaluated (SigmaCalc) resonance energies are assigned a 0.2% uncertainty as an outside limit.

TABLE 6.1. RESONANCE ENERGIES

Energy		Reaction	Full-Width Half-Maximum	Reference
value	uncertainty			
keV	keV		keV	
991.90	0.04	$^{27}Al(p,\gamma)^{28}Si$	0.1	[6.12]
1799.75	0.09	$^{27}Al(p,\gamma)^{28}Si$		[6.13]
823	2	$^{24}Mg(p,p)^{24}Mg$		[6.4] interpreted here
1483	3	$^{24}Mg(p,p)^{24}Mg$	0.3	[6.4] interpreted here
1630	3	$^{24}Mg(p,p)^{24}Mg$		[6.4] interpreted here
1058	2	$^{14}N(p,p)^{14}N$	9	[6.7] interpreted here
1550	3	$^{14}N(p,p)^{14}N$	80	[6.7] interpreted here
1742	3	$^{14}N(p,p)^{14}N$	19	[6.7], interpreted here
2348	5	$^{14}N(p,p)^{14}N$	26	[6.14]
3198	7	$^{14}N(p,p)^{14}N$	7	[6.14]
1734	3	$^{12}C(p,p)^{12}C$		[6.7], interpreted here

6.2. LITHIUM

6.2.1. $^{nat}Li(p,p)^{nat}Li$

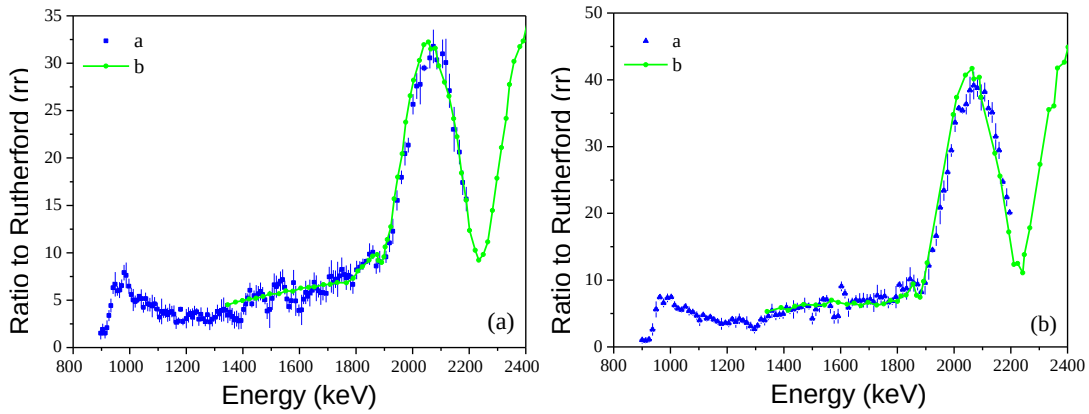

FIG. 6.1. (Fig. 12 in [6.6]) EBS cross sections derived from LiF bulk samples, data points from point-by-point inversion of spectra (blue); compare with cross sections from IBANDL [6.15] (green line): (a) data 140^0 (blue), [6.15] 145.3^0 (green), (b) data 160^0(blue), [6.15] 165^0 (green).

Li and F cross sections were extracted simultaneously by the point-by-point inverse technique applied to EBS spectra from single crystal LiF samples amorphised with a high fluence 300 keV Ar implant for two angles and 15 energies between 999─2200 keV. The F data is discussed below. Fig. 6.1 shows the extracted cross sections for Li, together with the (1σ) estimates of uncertainty per point that come naturally from the method. The new data extends the cross-section function down to the Rutherford region and broadly confirms Malmberg's 1956 data [6.15], except in the detail of the

2100 keV resonance, and except for the extra structure that appears to be there around 1600 keV.

The large resonance at about 2100 keV (30 times Rutherford even at 140^0 scattering angle) even makes the Li signal in $LiNbO_3$ visible, as shown in Fig. 6.2. Unfortunately, even for these very large cross sections, the signal: background ratio is poor for the Li signal; in Fig.2a for example the 1σ counting statistics uncertainty for the surface Li signal is only 5%. This experiment is low sensitivity: it certainly cannot discriminate Ramos data from [6.15] data at 2100 keV. However, it should be pointed out that the advantage of $LiNbO_3$ is that it has a very well defined stoichiometry, and an excellent surface quality. Perhaps these measurements could be repeated at higher precision?

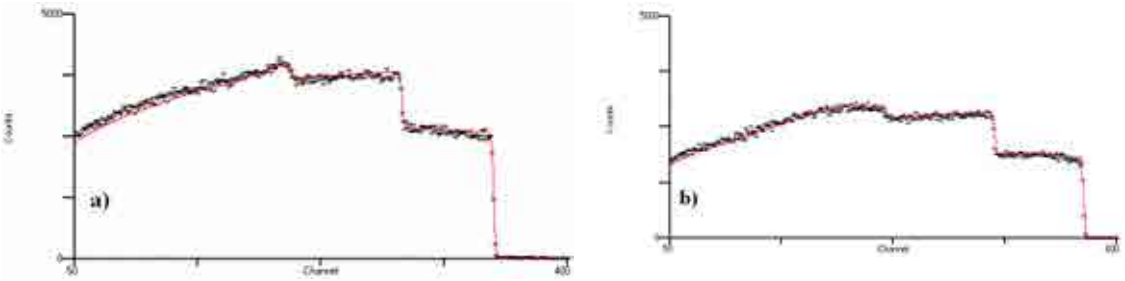

FIG. 6.2. (Figs.14b and 14e in [6.6]) Proton EBS spectra, with simulations, from lithium niobate ($LiNbO_3$) sample at 140^0 scattering angle. Similar spectra are available at 160^0 and at other energies between 1950─2200 keV. (a) 2000 keV, (b) 2150 keV.

6.3. BORON

6.3.1. $^{10}B(p,p)^{10}B$ & $^{11}B(p,p)^{11}B$

For the benchmark test measurements of the elastic scattering cross-sections of protons on ^{10}B and ^{11}B a thick target of high-purity B_4C was used (only surface contaminations of N and O at trace levels were found). The elastic backscattering measurements were performed with the 1.7 MV Tandetron accelerator of IMM in Bologna. Proton beams of 2.250 ± 2 MeV and 2.600 ± 3 MeV with a 2 × 1 mm^2 cross-section were used. The sample was mounted normal to the beam in an electrically insulated scattering chamber acting as a Faraday cup with and estimated uncertainty in the charge.solid-angle product of 2% [6.16]. Backscattered protons were collected by a ion-implanted Si detector (25 mm^2 area. 300 μm thickness) having 13 keV FWHM energy resolution and a dead-layer equivalent thickness of $250 \cdot 10^{15}$ Si/cm2. The detector was collimated by a circular aperture of 5.05 mm diameter set at 100.5 mm from the target. Scattering angles of 165°, 160°, 155° and 120° (with uncertainties estimated at 0.2°) were chosen to match available experimental data.

The proton beam current was 9 nA in order to have negligible dead time corrections; all the measurements were allowed to run until integrating a beam charge of 10 μC. The electronic gain of the detection system was determined from 2 MeV proton spectra of a thin ($40 \cdot 10^{15}$ at/cm^2) Pb-doped BiSCCO film, containing Bi, Pb, Sr, Cu, Ca and O, deposited on a carbon substrate. The pulse height defect correction was

applied, except for the effect of the non-ionising (nuclear) energy loss. The resulting uncertainty in the electronic gain (i.e. keV/channel) is below ±1%.

In the following figures the comparisons between the experimental spectra and the results of simulations using SIMNRAv6.05 with SRIM2003 stopping powers are shown, for the different scattering angles and proton beam energies. In the simulations the following $^{10}B(p,p)^{10}B$ cross-section data were compared with the benchmark spectra: Chiari *et al*. [6.17] at all measured angles, Overley & Whaling [6.18] at 155° and 120°. The following $^{11}B(p,p)^{11}B$ cross-section data were compared: Chiari *et al*. [6.17] again at all measured angles, Mayer *et al*. [6.19] at 165°, Segel *et al*. [6.20] at 160°, Symons & Treacey [6.21] at 155° and Mashkarov *et al*. [6.22] at 120°. The evaluated SigmaCalc cross-section for $^{12}C(p,p)^{12}C$ was used in all the simulations.

From this benchmark experiment it turns out that $^{10}B(p,p)^{10}B$ and $^{11}B(p,p)^{11}B$ cross-section data taken from the large measurements series done by Chiari *et al*. [6.17] are underestimated by a single systematic factor consistent with an error in the determination of the thickness of the target used for the cross-section measurements. This factor has a value of 1.1890 ± 0.0012, obtained from a overall fit of the simulated spectra to the experimental ones and using a single multiplicative factor for the partial spectra of both isotopes of B as free parameter, with the uncertainty from counting statistics.

The combined uncertainty of the benchmark spectrum height is about 3% (dominated by 2% for the charge.solid-angle product and 1% for the gain), where the combined uncertainty of the simulation itself is dominated by the uncertainty in the stopping power (~4%). The cross-section data in [6.17] have a declared combined uncertainty about 5%.

Both the absolute $^{11}B(p,p)^{11}B$ cross-section values measured by Mayer *et al*. [6.19] and the $^{10}B(p,p)^{10}B$ cross-section data from Overley & Whaling [6.18] are in good agreement with the corrected data from Chiari *et al* [6.17]. Spectra simulated from the other datasets (Segel *et al*. [6.20], Symons & Treacy [6.21] and Mashkarov *et al*. [6.22]), do not reproduce the benchmark spectra.

In conclusion, we recommend the corrected Chiari *et al*. dataset.

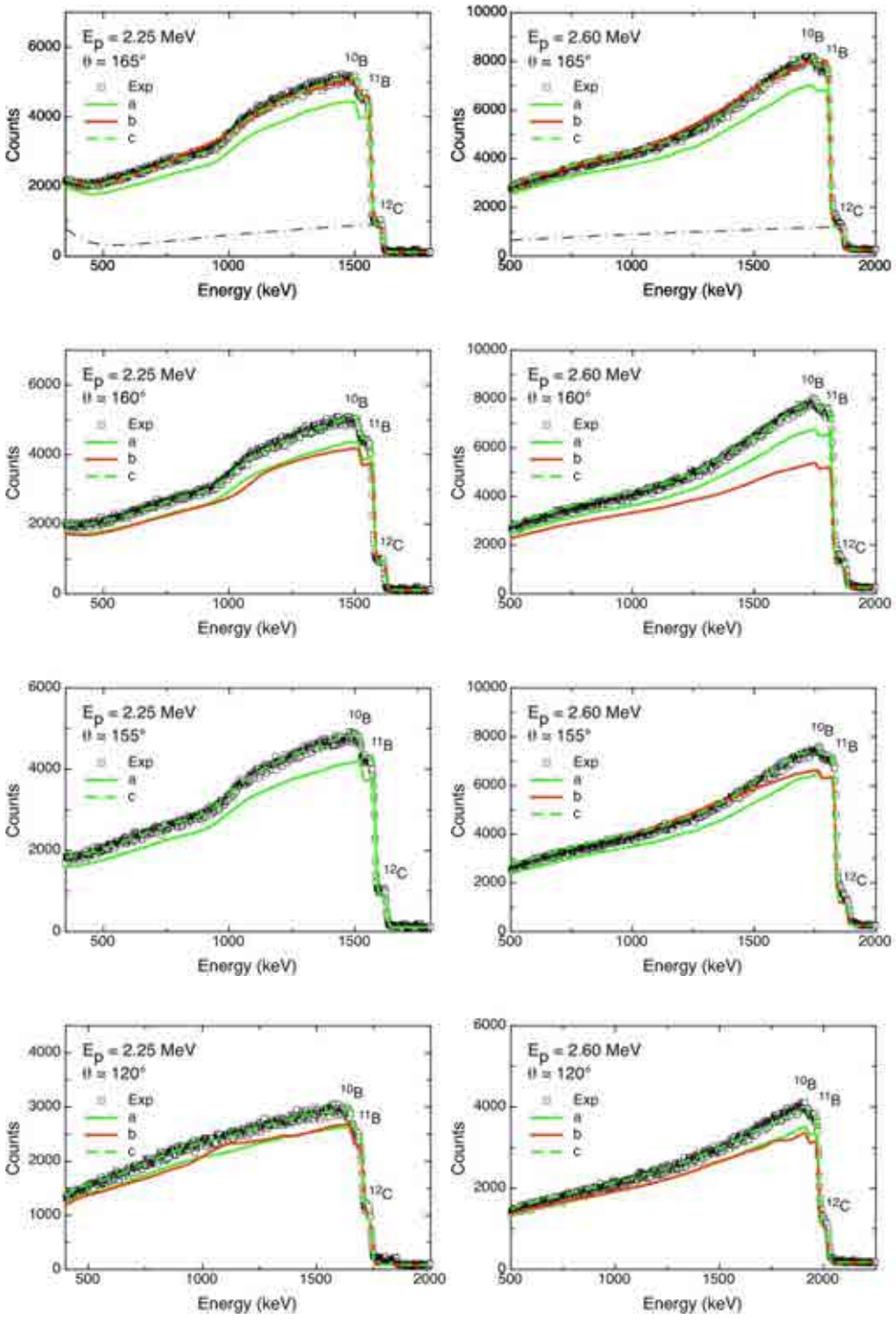

FIG. 6.3. Comparison between experimental and simulated spectra of B_4C target. The partial spectrum of C is shown as dash-dot line. Open squares represent experimental data, while SIMNRA simulations are shown as lines. a) Simulation using p+^{10,11}B elastic scattering cross-section values from [6.17]. b) Simulation using cross-section data for : (165°) ^{10}B(p,p)^{10}B from [6.17] and for ^{11}B(p,p)^{11}B from [6.19] ; (160°) ^{10}B(p,p)^{10}B from [6.17] and for ^{11}B(p,p)^{11}B from [6.20] ; (155°) ^{10}B(p,p)^{10}B from [6.18] and for ^{11}B(p,p)^{11}B from [6.21] (no data below 2.2 MeV) ; (120°) ^{10}B(p,p)^{10}B from [6.18] and for ^{11}B(p,p)^{11}B from [6.22]. c) same as a) but with the cross-section values scaled up by 19% (see text for details).

6.3.2. $^{10}B(d,p_2)^{11}B$ & $^{11}B(d,\alpha_0)^{9}Be$

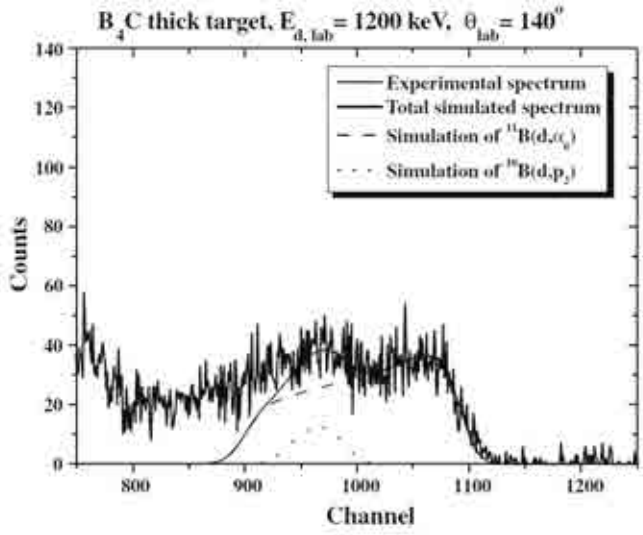

FIG. 6.4. Experimental NRA spectrum of a high purity B_4C target taken at 140^0 and deuterium energy of 1200 keV, along with the simulation, combining cross sections determined in the present work for the $^{11}B(d,\alpha_0)^9Be$ reaction, along with data from IBANDL [6.23] for the $^{10}B(d,p_2)^{11}B$ reaction. Reproduced courtesy of Elsevier [6.24].

Boron is frequently analysed by NRA since it is a light element important in many materials. However, natural B has 20% ^{10}B, so the situation can rapidly get very complicated. The Q value for the $^{10}B(d,p)$ reaction is 9.23 MeV and that for $^{11}B(d,\alpha)$ is 8.03 MeV. However, the fast protons from the d,p_0 reaction have strong interferences with $^{16}O(d,p_1)$ when O is present in the sample (the $^{16}O(d,p_1)$ reaction is much more likely than the $^{16}O(d,p_0)$ one). Although Q for $^{11}B(p,\alpha)^8Be$ is 8.59 MeV, these p,α reactions generate complicated spectra with many possible interferences. Therefore d-NRA gives useful possibilities.

Cross sections were measured directly with a thin film B target, and the benchmark made on an unpolished B_4C thick target. The part of the spectrum corresponding to alphas from the $^{11}B(d,\alpha_0)$ reaction also had the proton signal from the $^{10}B(d,p_2)$ reaction. The cross-section data was obtained for deuterium energies between 900 and 1200 keV (and a range of detector angles). Thus, the fit in Fig. 6.4 does not extend to the low energy part of the spectrum.

However, the accessible part of the data is well fitted by the simulation, even though the counting statistics are rather poor. This may be misleading, since the calculated data appears to be normalised to the measured data. No independently determined $Q\times\Omega$ factor is demonstrated. Thus, apparently the absolute value of the cross-section functions seems not to be benchmarked.

6.4. CARBON

6.4.1. $^{12}C(p,p)^{12}C$

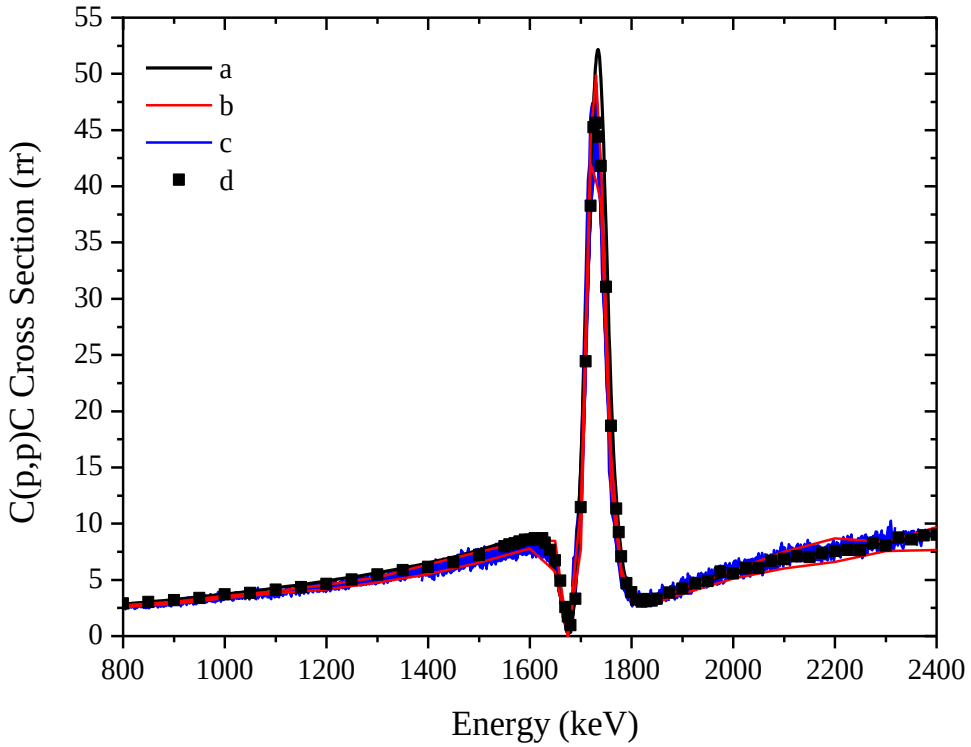

FIG. 6.5. (Fig. 8 in [6.6], compare Fig. 2 of [6.7]) Comparison of C(p,p$_0$)C cross section at 160º scattering angle using Bayesian inference, with SigmaCalc and literature from IBANDL. (a) SigmaCalc (this line is sometimes obscured by the other lines). (b) ±1 sigma variations on the average value calculated by the Bayesian algorithm. (c) point by point cross sections calculated by transforming the yield at each channel into a cross-section value. (d) experimental values from IBANDL [6.25]. SigmaCalc goes through all of these points.

This is an exercise using the well-known and evaluated C(p,p) cross sections to validate the use of the Bayesian method of inverting the spectra of bulk samples to generate the scattering cross-section function. The sample was an AlN thin film (with $(645 \pm 17).10^{15}$ N/cm^2) on a vitreous carbon substrate with $(43.7 \pm 0.5).10^{15}$ Au/cm^2 for an internal standard for $\Omega \times Q$, and spectra at four angles and some 60 energies were taken in the range 600─2500 keV.

This sample was used for determining the N(p,p) cross sections discussed in the next section, but the data from the thick carbon substrate was also used to re-validate the C cross sections. Of course, the SigmaCalc cross sections for C(p,p) are already well validated ([6.26] contains latest information), but this cross section is extraordinarily important and the new Bayesian inversion is not only a welcome confirmation of the SigmaCalc evaluated data, but also supplies evaluated uncertainties for this data set. It is therefore worth reporting.

6.4.2. $^{12}C(p,p)^{12}C$

For the benchmark test measurements of the elastic scattering cross-sections of protons on C in the high proton energy range (3-4.5 MeV), a thick target of polished Sigradur glassy carbon was used. The elastic backscattering measurements were performed with the 3 MV Tandetron accelerator of LABEC in Florence. Proton beams of different energies (2600 ± 3, 3000 ± 3, 3600 ± 4, 4100 ± 4 and 4500 ± 5 keV) with a 1.2 × 1.8 mm^2 cross-section were used. The sample was mounted at normal incidence in the scattering chamber. Backscattered protons were collected by a Si PIN diode (100 mm^2 area. 300 μm thickness) having 16 keV FWHM energy resolution and a dead-layer equivalent thickness of $1500 \cdot 10^{15}$ Si/cm2. The detector was collimated by a rectangular aperture 3 mm width × 6 mm set at 61 mm from the target. The measurements were performed placing the detector in IBM geometry at the fixed angle of 150° (estimated uncertainty ± 0.2°). The proton beam current was about 2-3 nA in order to have almost negligible dead time corrections (< 5%); all the measurements were allowed to run for 600 seconds. The accuracy of the measurement of the charge - solid angle product (± 3.0%) was checked by irradiating at different energies an Ag reference standard (1.2 mg/cm^2 thick).

The electronic gain of the detection system was determined from the energies and the positions of elastic and inelastic scattering peaks obtained from 3.6 MeV and 4.5 MeV proton spectra of a thin LiF target (30 $\mu g/cm^2$) evaporated on a C film. The pulse height defect correction was applied, except for the effect of the non-ionising (nuclear) energy loss. The resulting uncertainty in the electronic gain (i.e. keV/channel) is below ± 1%.

In the Fig. 6.6 the comparisons between the experimental spectra and the results of simulations using SIMNRAv6.05 with SRIM2003 stopping powers are shown, for the different proton beam energies. In the simulations the following C(p,p)C cross-section data were verified: SigmaCalc, Caciolli et al. [6.27] for the measurement at 3.60, 4.10 and 4.50 MeV, Jackson et al. [6.28] for the measurement at 3.60 and 4.10 MeV, and Reich et al. [6.29] for the measurement at 4.50 MeV alone. Note that data from [6.28] and [6.29] refer to a slightly different scattering angle, 146.2° and 146.8°, respectively (with a 3% change between 146° and 150°). For the cross-section values of $p+^{13}C$ elastic scattering the only available data from Kashy et al. [6.30] were used, even if referring to a different scattering angle (namely 163.8°). In the simulation of the thick target spectra pile-up effects were calculated using the model proposed in [6.31] and implemented in SIMNRA.

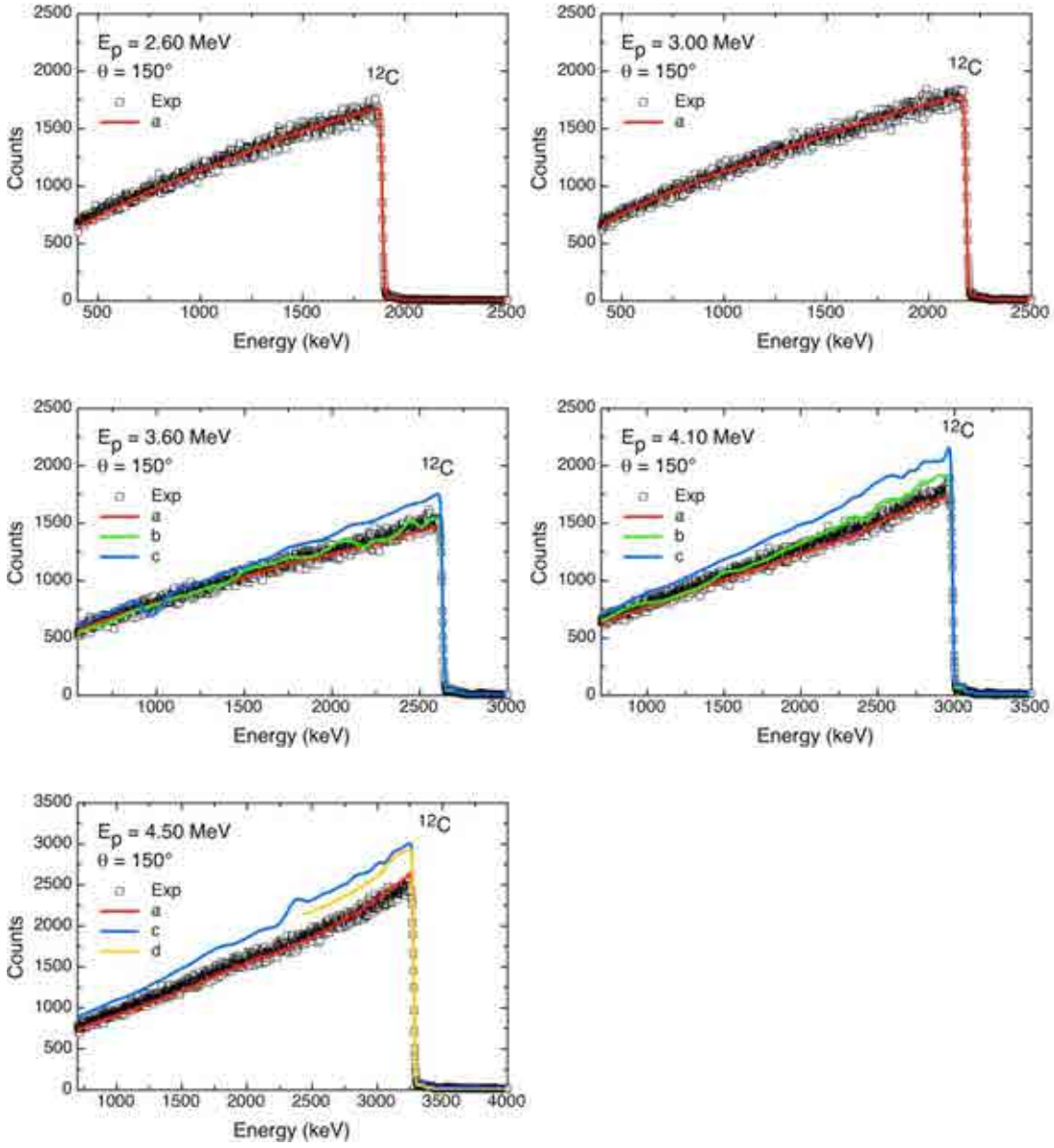

FIG. 6.6. Comparison between experimental and simulated spectra of a glassy C thick sample at 150° and different proton energies: 2.60, 3.00, 3.60, 4.10 and 4.50 MeV. Open squares represent experimental data, while SIMNRA simulations are shown as lines. a) Simulation using p+12C elastic scattering cross-section values calculated with SigmaCalc. b) Simulation using cross-section data from [6.28] at 146.2°. c) Simulation using cross-section data from [6.27]. d) Simulation using cross-section data from [6.29] at 146.8° (no data below 4.1 MeV).

From this benchmark experiment it turns out that simulations using the $^{12}C(p,p)^{12}C$ cross-section data calculated with SigmaCalc are in good agreement with experimental data within the overall estimated accuracy of ± 5.5% for these benchmark test measurements. The agreement is valid not only for proton energies below 3 MeV - as it has been confirmed by many other different experiments – but also at higher energies. Actually, the SigmaCalc cross-section data are indeed evaluated data up to 3 MeV energy, while for higher proton beam energies they are just extrapolated.

On the contrary, cross-section data from Reich et al. [6.29] and Caciolli et al. [6.27] appear to be overestimated by 15% and 8-20%, respectively (the maximum disagreement in the data of Caciolli is for energies above 4 MeV); these factors are greater than the quoted experimental uncertainties of ± 3.8% and ± 3.5%, respectively.

Finally, simulated spectra using the cross-section values taken from Jackson et al. [6.28] are in agreement with the experimental data within 5-6%, a fairly good agreement indeed, taking into account that the estimated uncertainties in the original paper are ± 5%.

6.5. NITROGEN

6.5.1. N(p,p)N

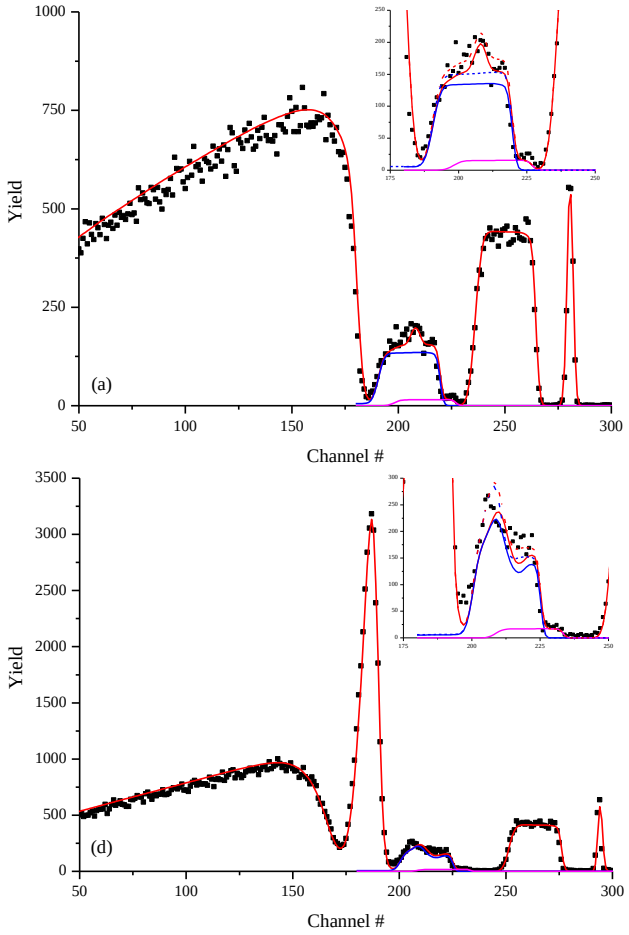

FIG. 6.7. (Figs.10a and 10d in [6.6]) EBS spectra of a 2.6 μm TiN film on vitreous carbon. The TiN had composition (Ti, N, O) = (47.6, 47.6, 4.8) mol% with some C contamination. There was (72.2±1.4).10^{15} Au/cm^2 for an internal standard of ΩxQ. Partial spectra are shown (see insets) for N, O and C, where the dotted blue lines are calculated from SigmaCalc [6.14] (a) 1718 keV, Φ=140º; (d) 1788 keV, Φ=160º.

Proton spectra were acquired at 140º scattering angle (movable detector) and 160º scattering angle (fixed detector) for 29 different beam energies in the 1030 keV─2370 keV interval. The movable detector angle was determined directly from the EBS C

signal, which is extremely sensitive to scattering angle. The spectra were interpreted using SigmaCalc cross sections for O and C.

All the data were consistent with the new (2007) SigmaCalc values for N(p,p) reported in [6.14]. Since this is a well characterised "thick" film sample (2.6 μm is quite thick), these measurements are equivalent to a benchmark experiment.

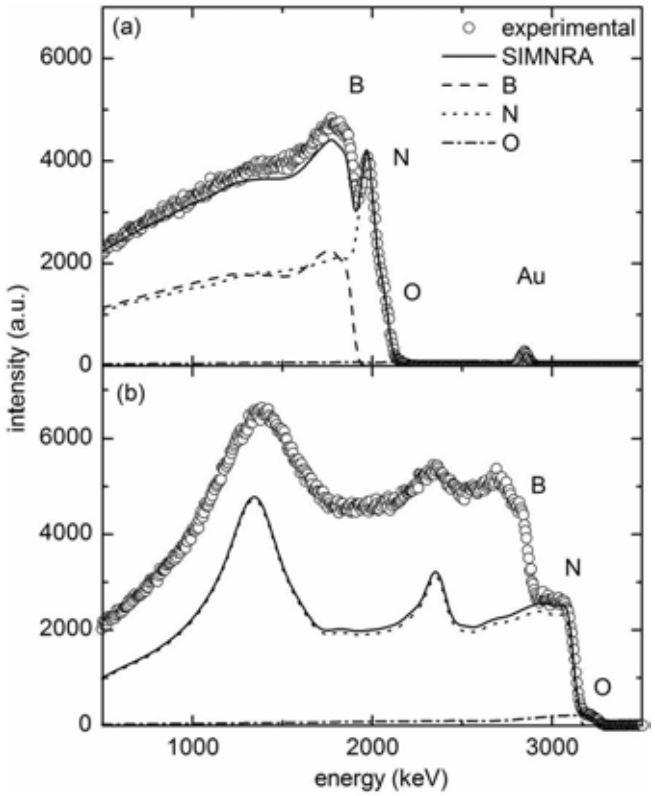

FIG. 6.8. (Fig.4 in [6.32]) Comparison between experimental and simulated spectra of BN target at 150° and two proton energies: (a) 3.24 MeV and (b) 4.50 MeV. Solid line is SIMNRA simulation and circles represent experimental data. B(p,p) data for 3.24 MeV is downloaded from IBANDL [6.33]. B(p,p) data are not available above 3.3 MeV. Reproduced courtesy of AIP Publishing [6.32].

A benchmark experiment was also attempted using a BN target ([6.32]: see Fig.6.6). For this, elastic cross sections for both ^{10}B and ^{11}B are needed, and downloaded from IBANDL, but are available only up to 3.3 MeV. This experiment must be regarded so far as indicative, but encouraging.

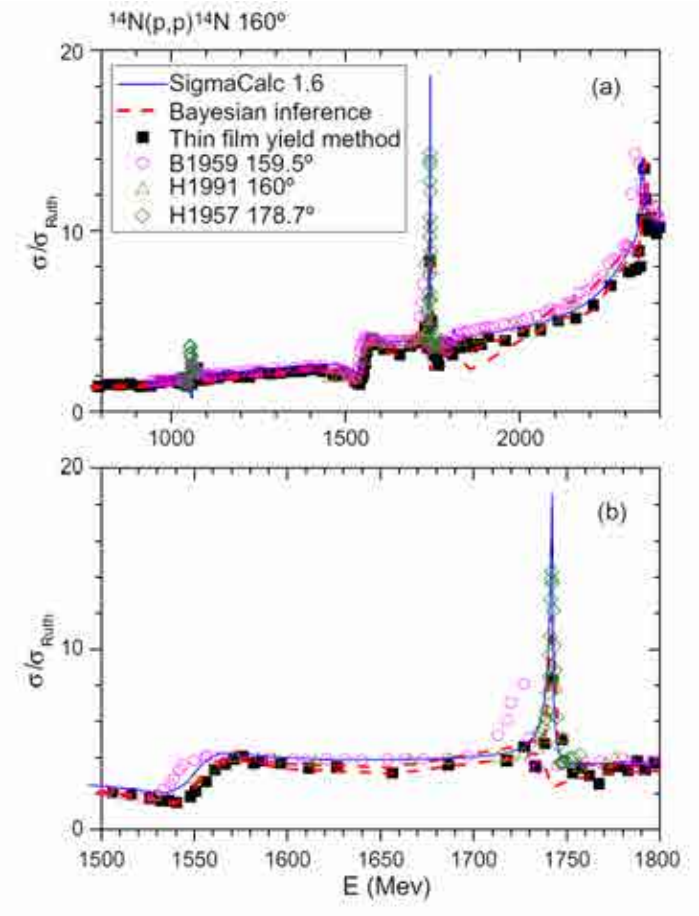

FIG. 6.9. Bayesian Inference extraction of $^{14}N(p,p)^{14}N$ elastic cross sections (double red line showing ± σ uncertainties) using an AlN/C sample, together with direct thin film measurements, SigmaCalc [6.14], and selected data from IBANDL (Hagedorn 1957 [6.34], Bashkin 1959 [6.35], Havranek 1991[6.36]) (a) full energy range measured, (b) detail. Reproduced courtesy of Elsevier [6.7].

Figure 6.9 shows data extracted by Bayesian Inference from the same AlN/C sample shown in Fig. 6.5 and reported in [6.7]. The Bayesian inference was done twice under different conditions for the C and N signals for technical reasons. The data were approximately consistent with SigmaCalc [6.14]. Since this is a well characterised thick film sample, these measurements are equivalent to a benchmark experiment. This experiment does suggest that the Bashkin data [6.35] mis-assigns the 1.55 MeV resonance energy and overestimates the cross section at 1.65 MeV by maybe 20%.

6.6. FLUORINE

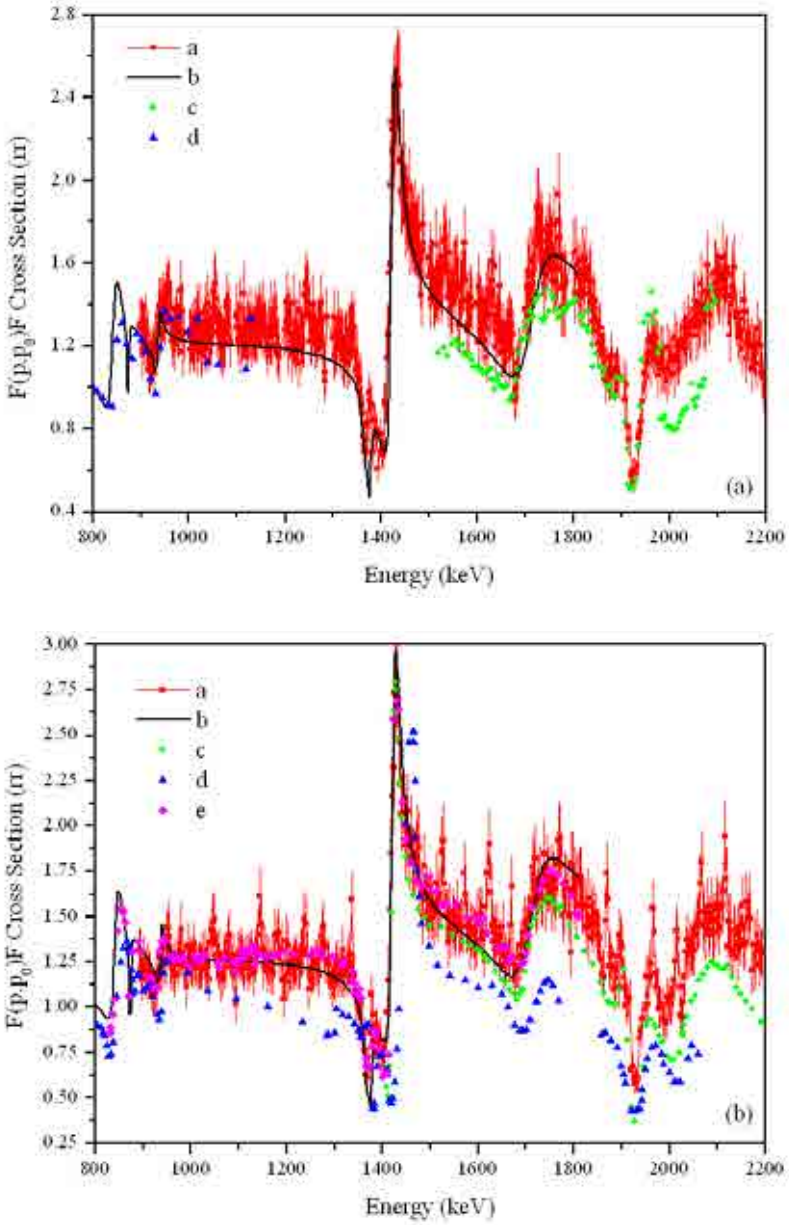

FIG. 6.10. (Fig.11 in [6.6]) EBS cross sections derived from LiF bulk samples, data points from point-by-point inversion of spectra shown in red (a), SigmaCalc is black line (b), and literature values from IBANDL. (a) 140º scattering angle, compare (c) Φ=137.75º Ouichaoui 1985 [6.37], (d) Φ=145º Caracciolo 1974 [6.38]; (b) 160º scattering angle, compare (c) Φ=165º Jesus 2001 [6.39], (d) Φ=159.8º Dearnaley 1956 [6.40], (e) Φ=158.7º Webb 1955 [6.41].

This data, deriving from the F signal above the Li edge measured at 15 energies at two angles on bulk LiF samples, was obtained by inverting all 30 spectra in turn to obtain the scattering cross-section function. The uncertainties are relatively large since (p,p') reactions were also present, since the LiF had substantial luminescence under the ion beam (ionoluminescence), and since very low beam currents were required due to the sensitivity of the sample to the beam.

In this work the Bayesian Inference step was not taken: only the raw cross-section inversion is shown. These data, being derived from thick film spectra, are equivalent to a benchmark, and are in agreement with the evaluated SigmaCalc cross sections up to 1.8 MeV, and also tend to confirm the data from Jesus *et al* [6.39] up to 2.1 MeV.

6.7. SODIUM

For the benchmark test measurements of the elastic scattering cross-sections of protons on Na a thick target of commercial glass (Ca 4%, Si 30%, Na 11%, O 55%) coated with thin Ti (75 nm) and Au (145 nm) layers was used. The target composition has been determined by several IBA measurements: RBS with 2 MeV alpha particles and 10 MeV ^{12}C ions, and PIXE with 3 MeV protons. The elastic backscattering measurements were performed with the 3 MV Tandetron accelerator of LABEC in Florence. Proton beams of different energies (3.20, 2.90, 2.50 and 1.47 MeV) with a 2 $\times$ 2 mm^2 cross-section were used. The sample was mounted at normal incidence in the scattering chamber. Backscattered protons were collected by a Si PIN diode (100 mm^2 area. 300 μm thickness) having 17 keV FWHM energy resolution and a dead-layer equivalent thickness of $1500 \cdot 10^{15}$ Si/cm2. The detector was collimated by a rectangular aperture 3 mm width $\times$ 6 mm set at 61 mm from the target. The measurements were performed placing the detector in IBM geometry at the fixed angle of 150°. The proton beam current was about 5 nA in order to have almost negligible dead time corrections (< 5%); all the measurements were allowed to run for 600–900 seconds. The Au layer acted as internal normalization standard for the charge - solid angle product.

In Fig. 6.11 the comparisons between the experimental spectra and the results of simulations using SIMNRAv6.05 with SRIM2003 stopping powers are shown, for the different proton beam energies. In the simulations the following Na(p,p)Na cross-section data were verified: Caciolli et al. [6.42] for the measurement at 3.20, 2.90 and 2.50 MeV, and SigmaCalc for the measurement at 1.47 MeV. The cross-section values for the elastic scattering of protons on the other target elements were calculated using SigmaCalc; for proton beam energies where no evaluated data exist the measured cross-section values were downloaded from IBANDL, as in the case of p+Si [6.43] and p+Ti [6.44]. For the measurement with 1.47 MeV protons the p+Ca and p+Ti elastic scattering cross-sections were assumed to be Rutherford.

The overall agreement between experimental and simulated spectra is good, although some discrepancies occur for Ca signal in the spectrum measured at 3.2 MeV proton energy due to the lack of evaluated or measured cross-section data in this energy range (the Rutherford value was assumed). The reliability of the measured and the evaluated p+Na elastic scattering cross-section data is thus verified.

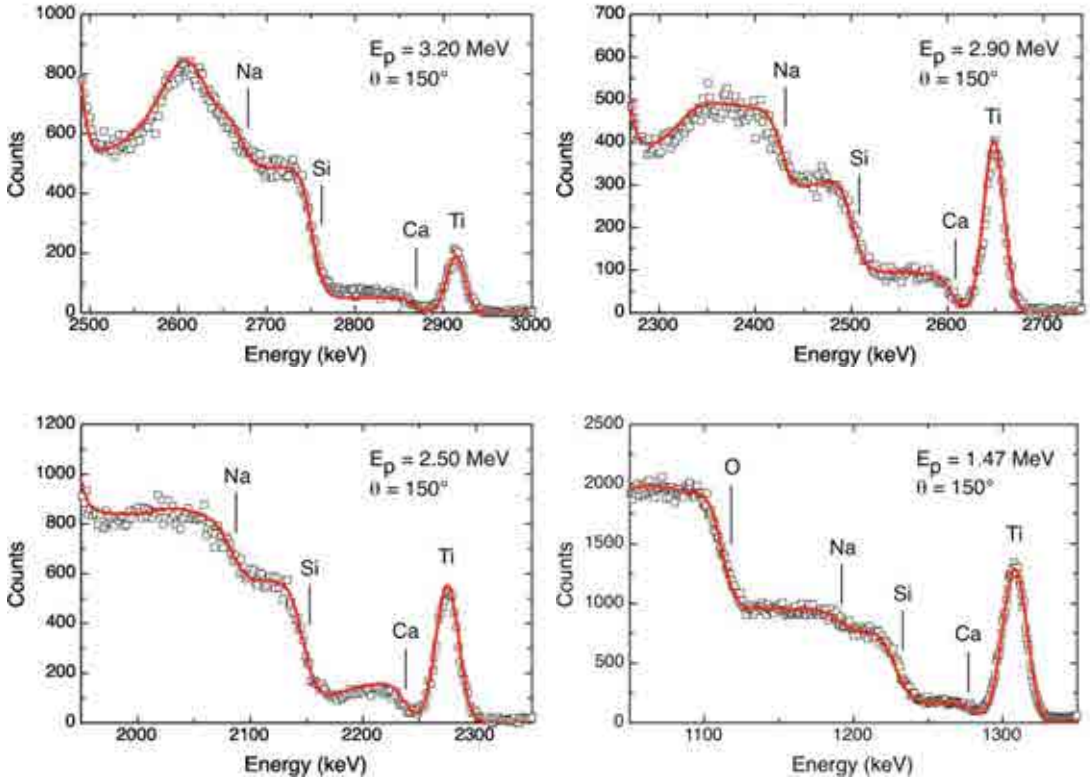

FIG. 6.11. (partly redrawn from Fig. 4 of [6.42]) Comparison between experimental and simulated spectra of Au/Ti/glass sample containing Na at 150° and different proton energies: 3.20, 2.90, 2.50 and 1.47 MeV. Open squares represent experimental data, while SIMNRA simulations are shown as lines. The Au signals (in some cases the O signals as well) are not shown purposely to better detail the spectra region around Na signal.

6.8. ALUMINIUM

6.8.1. $^{27}Al(p,p)^{27}Al$

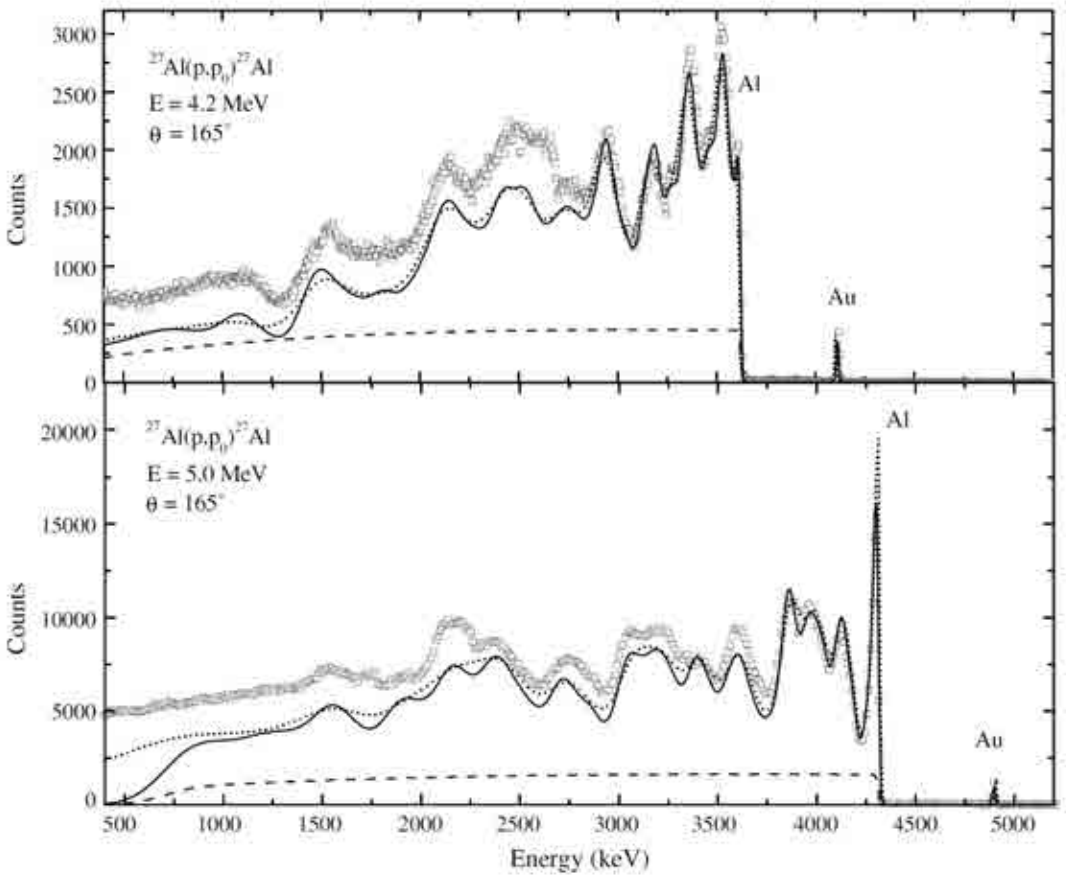

FIG. 6.12. The RBS spectrum simulated from the measured cross sections. Squares – measured spectrum, solid line – simulated spectrum using SIMNRA [6.46], dotted line – simulated spectrum using NDF [6.8], dashed line – Rutherford cross sections. Reproduced courtesy of Elsevier [6.45].

Figure 6.12 shows the benchmark bulk spectrum measurement with simulations using the *measured* cross sections reported in [6.45]. The Al(p,p) reaction is extraordinarily complicated, with a fine structure containing a very large number of resonances (22 main ones between 900 and 1800 keV, many of these multiple but with an average cross section which is still close to Rutherford: see the evaluation in [6.47] and Fig. 6.13). Clearly the main structure of the backscattering spectrum is reproduced well in both Figs 6.12 and 6.13, showing that even though the measured cross sections smeared out all the details of the fine structure, nevertheless they appear adequate for the purposes of this relatively low resolution EBS. The results do not change significantly if different stopping power data are used.

There is satisfactory agreement for the high energy part of the spectra but at lower energies simulated and experimental spectra disagree even more than in [6.47]. The simulations used both codes (SIMNRA and NDF) capable of simulating this challenging case. However, as discussed in [6.48], NDF is designed to simulate from the real cross-section function, and therefore will add the broadening of the experimental cross-section function to the simulation; but SIMNRA does not

convolute beam energy broadening into the effective cross section at each depth. Thus, where measured (and therefore broadened) cross sections are used, NDF will show smooth sharp features, whereas SIMNRA simulations may look more similar to the data.

We believe that at least part of the disagreement must come from the unknown contributions of cross sections for $^{27}Al(p,p_1)$, $^{27}Al(p,p_2)$, $^{27}Al(p,a_0)$ and $^{27}Al(p,a_1)$ reactions. There are measurements of these cross sections below 3 MeV but no attempt is made to account for them either in these simulations, or in those of [6.47] (Fig. 6.13) which also show the same effect. These other exit channels also explain why the same part of the excitation function provides satisfactory simulation for 4.2 MeV and fails to do so for 5.0 MeV.

A part of the disagreement must also be due to the incomplete knowledge of the fine resonant structure. For the low energy part of the spectra multiple and slit scattering can also contribute.

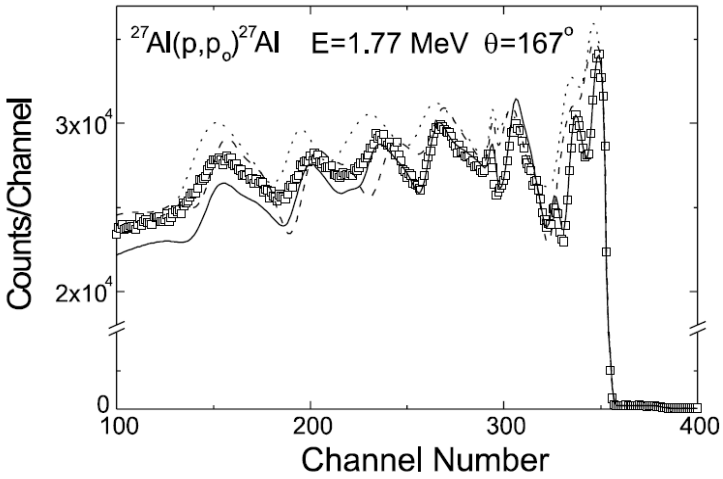

FIG. 6.13. Measured data with simulations. Solid line – SigmaCalc cross section, dotted and dashed lines – various cross sections from literature. Reproduced courtesy of Elsevier [6.47].

6.8.2. $^{27}Al(p,\gamma)^{28}Si$

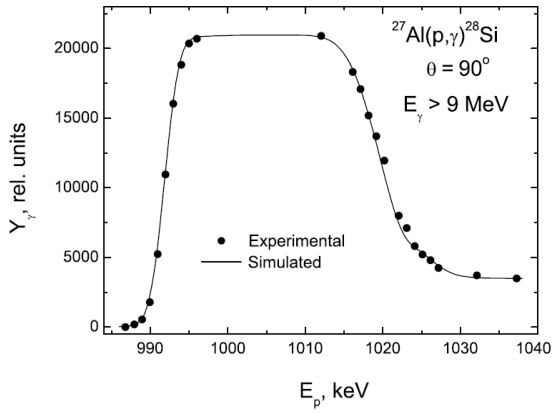

FIG. 6.14. Resonant PIGE depth profiling of free-standing 600 nm Al foil, with simulated curve from direct integration of the differential cross section. Reproduced courtesy of Elsevier [6.49].

In view of the importance of PIGE for the analysis of Al, these cross-section data are included here, even though it is not backscattering data since a proton beam used for EBS will also necessarily generate the gammas.

Fig. 6.14 shows the result of simulating the total yield in a large gamma detector with a known efficiency and geometrical correction from an Al foil whose thickness was measured directly with 1100 keV $^{27}Al(d,d)^{27}Al$ RBS.

6.8.3. $^{27}Al(d,p')^{28}Al$

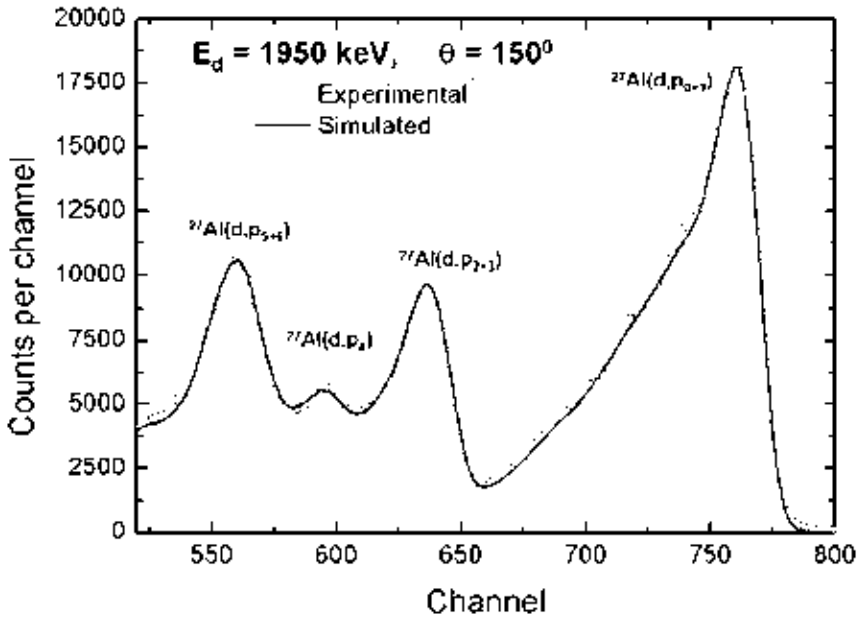

FIG. 6.15. (cf. Fig.11 in [6.49]) Measured data (circles) with simulations (line) [6.50]. Reproduced courtesy of Elsevier [6.49].

Fig. 6.15 shows the measured spectrum for this set of reactions on a thick target together with a SIMNRA simulation based on the measured cross sections. The maximum proton energy in Fig. 6.15 is about 6.3 MeV (Q = 5.5 MeV). The simulation incorporates all the IBANDL data ([6.49] and [6.51]).

This benchmark confirms IBANDL data up to 1.95 MeV D energy at 1─3% precision. Unfortunately there is no benchmark for the absolute values of the cross sections.

6.9. SILICON

6.9.1. $^{nat}Si(p,p)^{nat}Si$

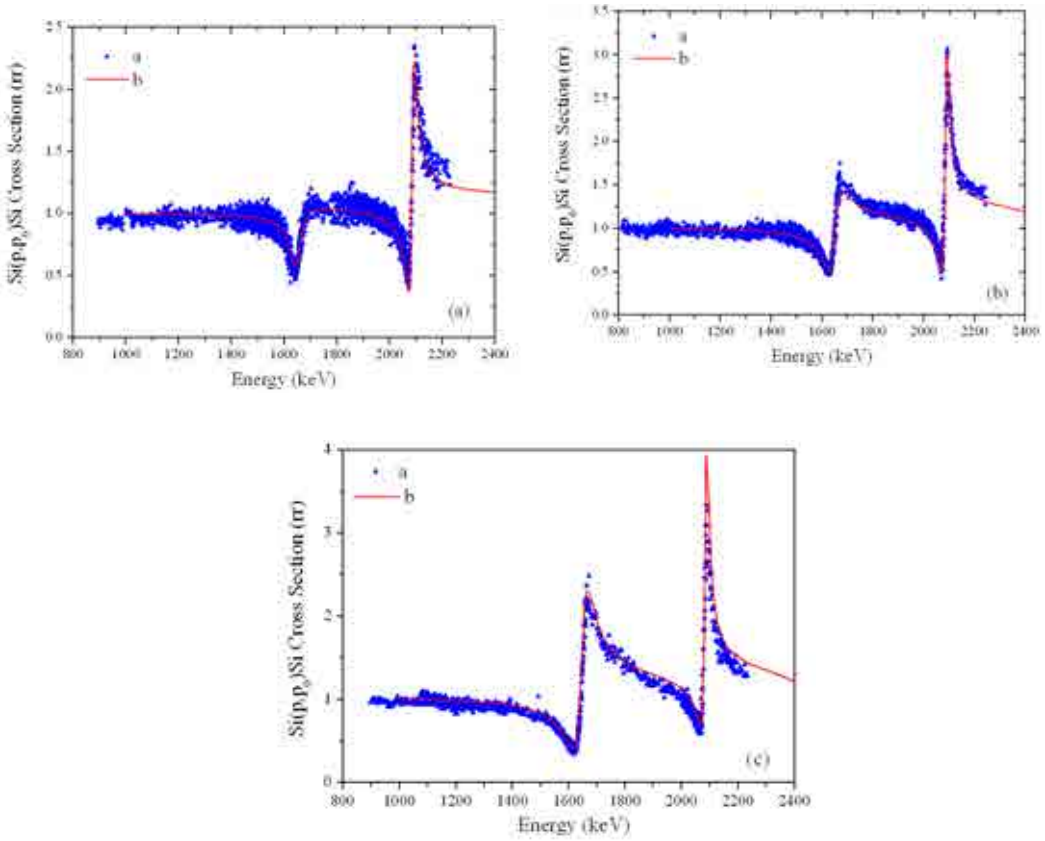

FIG. 6.16. (Fig.9 in [6.6]) Si(p,p0)Si cross sections calculated by transforming the yield at each channel (point-by-point) into a cross section value: red line "b" is SigmaCalc. (a) 125º scattering angle, 31 data sets. (b) 140º scattering angle: 29 data sets. (c) 160º scattering angle: 31 data sets.

For this thick target experiment (equivalent to a benchmark), the sample was a Si wafer implanted with $(26.6 \pm 0.6).10^{15}$ W/cm^2 at 150 keV. The implant provides an internal standard for $\Omega \times Q$ and also amorphises the Si thus avoiding channelling effects.

The stopping powers used were SRIM 2003. The demonstrable validity of SigmaCalc also shows that the SRIM03 stopping powers are valid over this energy range.

6.10. TITANIUM: ^{nat}Ti(p,p)

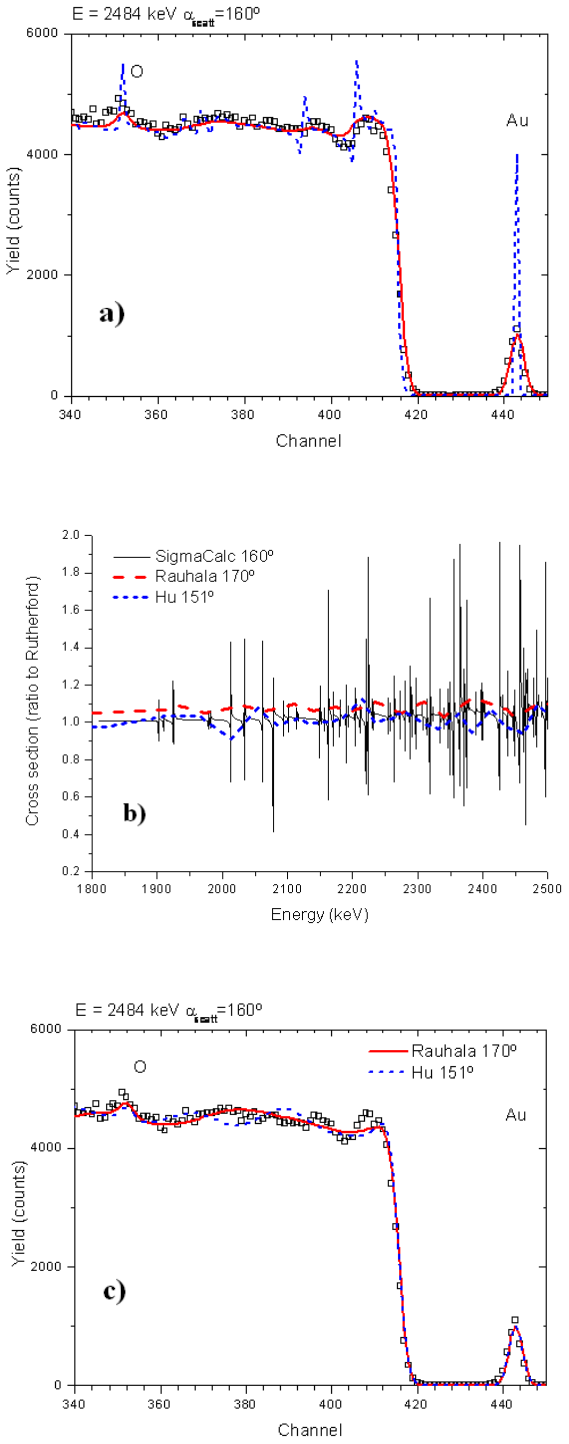

FIG. 6.17. 2484 keV H EBS with low resolution detector (ΔE=30 keV) with various simulations using NDFv9.2m. ***(a)*** *Data with NDF simulation from SigmaCalc for ΔE=30 keV (red) and ΔE=10 keV (blue).* ***(b)*** *SigmaCalc cross sections together with measurements by Rauhala (1989) [6.53] and Hu (2004) [6.54] downloaded from IBANDL.* ***(c)*** *Data with simulations from Rauhala and Hu data, shown as red and blue lines respectively in (b) and (c). Reproduced courtesy of Elsevier [6.52].*

Preliminary measurements using a rather poor detector were made on a polished bulk Ti sample for energies from 1400─2500 keV and compared to simulations from cross sections based on [6.55] evaluated by A.F.Gurbich (Fig. 6.17). All the EBS spectra were analysed with the same absolute electronics calibration, that is, with the pulse height defect correction. The Ti cross section is another example where there is an extraordinary number of extremely sharp resonances, in this case mostly rather weak. The spectra do not depart very far from Rutherford in most of the energy range.

Such a strong resonant structure is extremely time consuming to calculate, and two questions arise: can the simulations be done correctly in such a challenging case, and is there any way to simplify the cross-section function with operationally the same result.

The first question cannot be convincingly answered in this low resolution experiment, and further high resolution measurements are planned, using a magnetic spectrometer.

The second question is technically difficult: it is not at all obvious how to smooth the cross-section function in such a way as to locally conserve area. For standard EBS, with FWHM resolutions larger than 10 keV, perhaps a "simpler" cross section could be obtained by convoluting the calculated cross section with a Gaussian with around 2─3 keV FWHM. The convolution would need to be done carefully in order to preserve the total area. Fewer points in the cross section curve would be necessary. A 25 point FFT smoothing did not preserve the total area locally, so, although results were acceptable, they were not perfect in terms of reproducing the simulated curves with the full cross section.

The limitations of smoothing can be seen in Fig. 6.17c. Here, two experimental cross-section curves are used, neither of which show any resonances because of the thickness of the targets and the coarseness of the energy steps. Curiously, for all the energies, except the highest one shown in the figure, the simulations from a grossly simplified cross-section function fitted the data reasonably well. Only for the highest energy there is a large deviation. It should be noted however that this low resolution experiment is not a very stringent test of this idea.

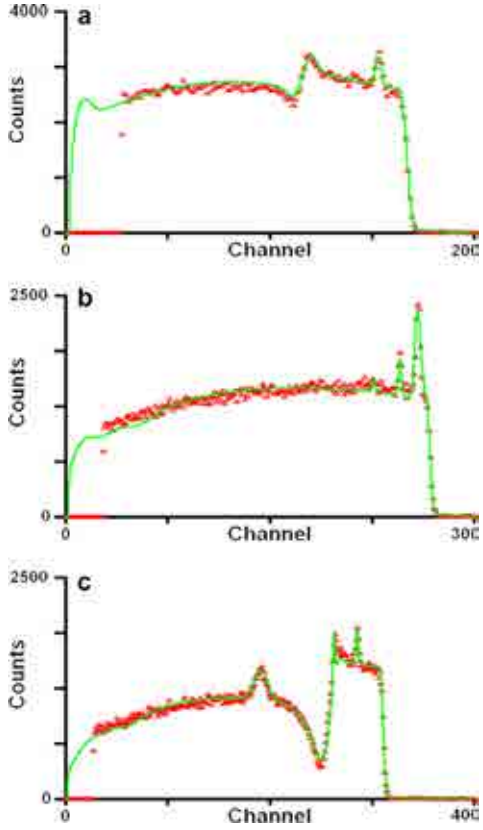

FIG. 6.18. Data and simulations for a bulk Mg sample near the (a) 823, (b) 1483 and (c) 1630 keV resonances. Scattering angle 172.8^0. Oxygen contamination is visible. Resonance shapes are fitted excellently, including the sharp 1483 keV resonance near the surface (b) and buried deep (c). Reproduced courtesy of Elsevier [6.4].

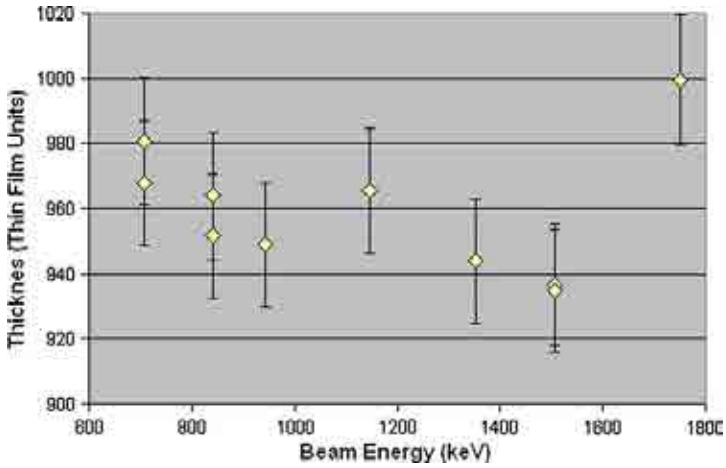

FIG. 6.19. Apparent Mg content of multilayer (thin film) Au/Mg/C sample (Mg = 958 TFU), normalised to the substrate carbon signal and assuming SigmaCalc cross sections. Mg(p,p) is Rutherford at 700 keV. The ordinate is in units of 10^{15} atoms/cm^2 (TFU). ± 2% uncertainty bars are shown. Reproduced courtesy of Elsevier [6.4].

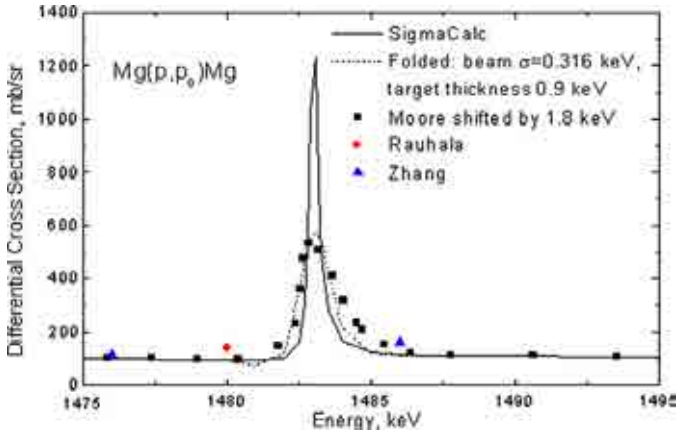

FIG. 6.20. 1483 keV resonance for evaluated (SigmaCalc, actual and folded) and experimental data from IBANDL [6.56] representation. Reproduced courtesy of Elsevier [6.4].

Gurbich and Jeynes [6.4] presented an evaluation of the Mg(p,p) reaction, together with a benchmark using both bulk and thin film samples. A series of EBS spectra were obtained at seven energies between 600 and 1800 keV and analysed using a uniform absolute detection electronics calibration, that is, correcting for the detector pulse height defect [6.9]. Bulk spectra are shown in Fig. 6.18, and processed results from the thin film sample shown in Fig. 6.19.

The absolute electronics calibration means that the energies of the three detected resonances are directly comparable over the dataset with a combined uncertainty better than 0.2% given by the relative uncertainty in the beam energy (much better than 0.1%), the uncertainty in the position of the Mg edge (better than about 0.1 channel or 0.1%, see [6.11]), and the uncertainty of the electronic gain (0.1%). This weak limit on the uncertainty of the resonance energies is useful where other information is not available. In particular it means that the SigmaCalc energies are consistent (to the uncertainty of the data in Fig. 6.18) with the independently determined machine energies over the whole data range.

In Fig. 6.19 the apparent thin film thickness is shown for all the energies at which EBS data is taken. Of course, the film is the same so the thickness should be constant, which it is to about 2% (4% for 1.8 MeV). The benchmark therefore confirms that the absolute SigmaCalc cross sections are correct (with an uncertainty of about 2%). This benchmark had the specific purpose of determining the validity of the published cross-section measurements just above the first resonance at 823 keV, which being about 4% higher than SigmaCalc were not consistent with it.

Figure 6.20 shows how direct cross-section measurements using thin films necessarily distort fine structure at resonances. Here the extraordinarily sharp and strong resonance at 1484 keV, whose parameters are determined from nuclear data, is convoluted (folded) with the energy loss in the thickness of the thin film used in the cited literature, resulting in the observed cross-section function. This figure is shown because there was initially some doubt about the nuclear parameters, but they were confirmed by the benchmark experiment, which shows this same resonance is fitted excellently (Fig. 6.18).

6.12. CONCLUSIONS

We have shown benchmarking experiments for a number of cases. Clearly, this is a work that will never be finished: many species remain to be evaluated and then benchmarked, and it is already known that the range of validity of existing evaluations could profitably be increased.

And there is likely to be a future need of enhanced accuracy. The accuracy of neither the absolute value of cross-sections nor the absolute positions of the resonances has yet been established unequivocally in most cases, even for evaluated resonances. The uncertainty of the results of evaluations is not easy to establish from the evaluation process, and probably must be established externally through well designed benchmarking experiments. We have here given a Table of resonance energies that can reasonably be assigned a definite uncertainty, and we anticipate that this Table will be extended greatly in the future.

In the many cases for which evaluated data is not available, benchmarks can give an indispensible corroboration of the validity of the data that do exist. However benchmarks are the most valuable on evaluated data, since it is only such data that are well understood, and since it is only well understood techniques that can be used for fundamentally traceable analysis.

We here list the conclusions for each nucleus studied.

1. Lithium: $^{nat}Li(p,p)^{nat}Li$. Data from a bulk LiF target was inverted using the point-by-point inversion (PPI) method. This can be interpreted as equivalent to a benchmark for the [6.15] data (from IBANDL) in the energy region 1.3-2.4 MeV. The [6.15] data does not show extra structure in the cross-section function at the two resonances near 1.6 and 2.1 MeV. LiF is beam sensitive, ionoluminescent, and contains light elements that give interfering NRA signals so is not an ideal benchmarking material. A second benchmark was attempted using $LiNbO_3$, but the sensitivity was too low to be useful.
2. Boron: $^{10}B(p,p)^{10}B$ & $^{11}B(p,p)^{11}B$. EBS data at 2.25 and 2.6 MeV from a B_4C target benchmarks the extensive cross-section measurements of [6.17] at 4 scattering angles. Apart from a normalisation constant consistent with a thickness error on the thin film sample used for the cross-section measurement, the data of [6.17] is validated at 4%.
3. Boron: $^{10}B(d,p_2)^{11}B$ & $^{11}B(d,\alpha_0)^{9}Be$. NRA on B using the d,α reaction will always also involve the interfering d.p_2 reaction. The measured cross-sections for both of these reactions [6.23] was benchmarked on a B_4C thick target in the measured energy range (0.9–1.2 MeV). This energy range is not wide enough to reproduce the spectrum, but otherwise the result looks satisfactory. However, the absolute values of the cross-section functions appear not to be benchmarked.
4. Carbon: $^{12}C(p,p)^{12}C$. The evaluated (SigmaCalc) carbon EBS cross-sections were compared with the results obtained using the Bayesian Inference (BI) technique (equivalent to a benchmark) on a bulk vitreous carbon sample in the energy range 0.8–2.4 MeV, with 60 separate energies and 4 angles. The evaluated cross-sections (SigmaCalc) fell within 1σ of the BI results over all this range. The same evaluated (SigmaCalc) cross-section function was benchmarked separately on a glassy carbon bulk target at 150° and energies up to 4.5 MeV and found consistent to the experimental accuracy of 5.5%.

5. Nitrogen: N(p,p)N. This experiment used a BI analysis of data from the same AlN/C sample as for the $^{12}C(p,p)^{12}C$ experiment (above). The BI analysis, equivalent to a benchmark experiment, suggests that the [6.34] data mis-assigns the 1.55 MeV resonance energy and overestimates the cross-section at 1.65 MeV by maybe 20%. An independent benchmark experiment was also carried out on a TiN/C sample (in the slightly smaller energy range 1.03–2.37 MeV) which was consistent in detail with the first experiment. A benchmark of cross-sections measured in the energy interval up to 4.5 MeV was also attempted using a BN sample. This was encouraging but not conclusive, since cross-sections for B were available only up to 3.3 MeV, and those are not evaluated.

6. Fluorine: $^{19}F(p,p)^{19}F$. The same sample and data-set was used as for Li (above), again with point-by-point extraction of the cross-sections interpreted as a benchmark for SigmaCalc (up to 1.8 MeV) and [6.38] to 2.1 MeV. This data is entirely consistent with SigmaCalc, but suggests that [6.38] is underestimated by about 25%.

7. Sodium: $^{nat}Na(p,p)^{nat}Na$. The benchmark was made with the data from Caciolli et al. [6.42] for the measurement at 3.20, 2.90 and 2.50 MeV, and SigmaCalc for the measurement at 1.47 MeV using a glass sample containing 11at% Na. The reliability of the measured and the evaluated EBS data was roughly verified.

8. Aluminium: $^{27}Al(p,p)^{27}Al$. Benchmarking Al EBS cross-sections is difficult since there are many competing NRA reactions which have not so far been taken into account. The EBS cross-section function is exceptionally complicated, and considerable work has gone to demonstrate that the SigmaCalc cross-sections (to 1.8 MeV) and the new cross-section measurements to 5 MeV [6.45] are consistent with thick film data. But it is not yet known how to interpret these spectra in detail.

9. Aluminium: $^{27}Al(p,\gamma)^{28}Si$. The thick target excitation function for 9 – 11 MeV γ rays and beam energies between 0.98 – 1.9 MeV was measured and benchmarked on a foil whose thickness (600 nm) was independently measured. The measured and simulated film thicknesses matched to about 2%, and the ratio of the simulated maximum yield (at 1 MeV) and the yield at high beam energy (1035 keV) matches experiment at about 4%.

10. Aluminium: $^{27}Al(d,p')^{28}Al$. IBANDL data for the four proton groups $p_{0,1}$, $p_{2,3}$, p_4, $p_{5,6}$ has been benchmarked at 1-3% precision to 1.95 MeV D energy. There is no benchmark for the absolute value of the cross-sections.

11. Silicon: $^{nat}Si(p,p)^{nat}Si$. SigmaCalc has been validated to 2.2 MeV incident proton energy using an amorphised Si wafer and three scattering angles at 31 energies. The point-by-point method was used to invert the bulk sample spectra. Realistic uncertainties cannot be obtained from this data-set.

12. Titanium: $^{nat}Ti(p,p)^{nat}Ti$. The Ti EBS cross-section function is similar to the Al one in its very high number of extremely sharp resonances. Preliminary experiments (at low resolution) show that spectra can be adequately simulated from the SigmaCalc evaluation with an advanced code, although this is time-consuming. Planned high resolution experiments will test the calculation capability of this code. An outstanding problem is whether this complex cross-section function can be adequately simplified so that the simulation of spectra can be speeded up. This work has demonstrated that a sparse data-set can certainly distort the simulated spectrum.

13. Magnesium: $^{nat}Mg(p,p)^{nat}Mg$. The SigmaCalc evaluation is validated at 2% to 1.5 MeV and 4% to 1.8 MeV. The benchmark also confirmed the parameters of the strong and sharp 1483 keV resonance, with is correctly simulated by an advanced code.

We have here described a variety of valid ways to complete a benchmarking exercise. The analytical community should be alive to these various possibilities, and in future take every opportunity to publish any well-found data that can act as a benchmark and increase our confidence in our scattering cross-section database.

Finally, we should point out that it is not yet clear what is the best way to formalise our knowledge of the various different uncertainties applicable to any particular reaction cross-section. This is an important topic that should be taken up by a future Coordinated Research Project at the same time that such a CRP revisits this database.

REFERENCES

[6.1] GURBICH, A.F., BOGDANOVIC-RADOVIĆ, I., CHIARI, M., et al., Status of the problem of nuclear cross section data for IBA, Nucl. Instrum. Methods Phys. Res. B **266** (2008) 1198.

[6.2] BARRADAS, N.P., ALVES, E., JEYNES, C., et al. (2006), Accurate simulation of backscattering spectra in the presence of sharp resonances, Nucl. Instrum. Methods Phys. Res. B **247** (2006) 381.

[6.3] BARRADAS, N.P., ARSTILA, K., BATTISTIG, G., et al., Summary of ''IAEA intercomparison of IBA software", Nucl. Instrum. Methods Phys. Res. B **266** (2008) 1338.

[6.4] GURBICH, A.F., JEYNES, C., Evaluation of non-Rutherford proton elastic scattering cross-section for magnesium, Nucl. Instrum. Methods Phys. Res. B **265** (2007) 447.

[6.5] GURBICH, A.F., Evaluation of non-Rutherford cross sections for IBA: Theory and results, Nucl. Instrum. Methods Phys. Res. B **261** (2007) 401.

[6.6] RAMOS, A.R., BARRADAS, N.P., ALVES, E., (2009), Final Report: Measurement of Proton Elastic Scattering Cross Sections for Light Elements – Validation of a "Bulk sample" Method, Contract Number: 13273/R0/Regular Budget Fund, Instituto Tecnológico e Nuclear, Sacavém, Portugal

[6.7] BARRADAS, N.P., RAMOS, A.R., ALVES, E., Determination of non-Rutherford cross-sections from simple RBS spectra using Bayesian inference data analysis, Nucl. Instrum. Methods Phys. Res. B **266** (2008) 1180.

[6.8] BARRADAS, N.P., JEYNES, C., Advanced physics and algorithms in the IBA Data Furnace, Nucl. Instrum. Methods Phys. Res. B **266** (2008) 1875.

[6.9] PASCUAL-IZARRA, C., BARRADAS, N.P., Introducing routine pulse height defect corrections in IBA, Nucl. Instrum. Methods Phys. Res. B **266** (2008) 1866.

[6.10] Handbook of Modern Ion Beam Materials Analysis, Y. Wang, M. Nastasi (Eds), Cambridge University Press, 2010.

[6.11] JEYNES, C., KIMBER, A.C. (1985), High accuracy data from Rutherford back-scattering spectra: measurements of the range and straggle of 60-400 keV as implants into Si, J. Phys. D: Appl. Phys. **18** (1985) L93.

[6.12] ROUSH, M.L., WEST, L.A., MARION, J.B., Precision determinations of nuclear reaction calibration energies by velocity measurements, Nucl. Phys. A **147** (1970) 235.

[6.13] MAAS, J.W., SOMORJAI, E., GRABER, H.D., et al., Investigation of ^{28}Si Levels with the (α,γ) and (p,γ) reactions, Nucl.Phys. A **301** (1978) 213.

[6.14] GURBICH, A.F., Evaluation of non-Rutherford proton elastic scattering cross section for nitrogen, Nucl. Instrum. Methods Phys. Res. B **266** (2008) 1193.

[6.15] MALMBERG, P.R., Phys. Rev. **101** (1956) 114.

[6.16] LULLI, G., ALBERTAZZI, E., BIANCONI, M., BENTINI, G.G., NIPOTI, R., LOTTI, R., Determination of He electronic energy loss in crystalline Si by Monte-Carlo simulation of Rutherford backscattering-channeling spectra, Nucl. Instrum. Methods Phys. Res. B **170** (2000) 1-9.

[6.17] CHIARI, M., GIUNTINI, L., MANDÒ, P.A., TACCETTI, N., Proton elastic scattering cross-section on boron from 0.5 to 3.3 MeV, Nucl. Instrum. Methods Phys. Res. B **184** (2001) 309-318.

[6.18] OVERLEY, J.C., AND WHALING, W., Highly Excited States in C^{11}. Elastic Scattering of Protons by B^{10}, Phys. Rev. **128** (1962) 315-324.

[6.19] MAYER, M., ANNEN, A., JACOB, W., GRIGULL, S., The $^{11}B(p,\alpha_0)^{8}Be$ nuclear reaction and $^{11}B(p,p)^{11}B$ backscattering cross sections for analytical purposes, Nucl. Instrum. Methods Phys. Res. B **143** (1998) 244-252.

[6.20] SEGEL, R.E., HANNA, S.S., ALLASET, R.G., States in C^{12} Between 16.4 and 19.6 MeV, Phys.Rev. B **139** (1965) 818-830.

[6.21] SYMONS, G.D., AND TREACY, P.B., The $B^{11}(p,\alpha)Be^{8}$ reaction and C^{12} states between 15 and 20 MeV, Nucl. Phys. **46** (1963) 93-107.

[6.22] MASHKAROV, JU.G., DEJNEKO, A.S., MALAKHOV, I.JA., SLOBOSPICKIJ, R.P., STORIZHKO, V.E., Investigation of the proton elastic scattering and the (p,α_0) reaction on the ^{11}B nucleus, Jour. Izv. Rossiiskoi Akademii Nauk, Ser.Fiz., **39** (1975) 1736.

[6.23] KOKKORIS, M., FOTEINOU, V., PROVATAS, G., et al, A detailed study of the d + ^{10}B system for nuclear reaction analysis – Part A: The $^{10}B(d,p)^{11}B$ reaction in the energy region $E_{d,lab}$ = 900–2000 keV, Nucl. Instrum. Methods Phys. Res. B **263** (2007) 357.

[6.24] KOKKORIS, M., DIAKAKI, M., MISAELIDES, P., et al., Study of the d + ^{11}B system differential cross-sections for NRA purposes, Nucl. Instrum. Methods Phys. Res. B **267** (2009) 1740.

[6.25] MAZZONI, S., CHIARI, M., GIUNTINI, L., MANDO, P.A., TACCETTI, N., Nucl. Instrum. Methods Phys. Res. B **136-138** (1998) 86.

[6.26] GURBICH, A.F., Comment on ‘‘Carbon analysis using energetic ion beams’’ in: Nucl. Instrum. Methods Phys. Res. B **222** (2004) 538, Nucl. Instrum. Methods Phys. Res. B **229** (2005) 157.

[6.27] CACIOLLI, A., CHIARI, M., CLIMENT-FONT, A., FERNÁNDEZ-JIMÉNEZ, M.T., GARCÍA-LÓPEZ, G., LUCARELLI, F., NAVA, S., ZUCCHIATTI, A., Proton elastic scattering cross-sections on F, C and Li from 3 to 7 MeV, Nucl. Instrum. Methods Phys. Res. B **249** (2006) 95-97.

[6.28] JACKSON, H.L., GALONSKY, A.I., EPPLING, F.J., HILL, R.W., GOLDBERG, E., CAMERON, J.R., The $C^{12}(p,p)C^{12}$ Differential Cross Section, Phys. Rev. **89** (1953) 365-369.

[6.29] REICH, C.W., PHILLIPS, G.C., RUSSELL JR., J.L., Scattering of Protons from C^{12}, Phys. Rev. **104** (1956) 143-153.

[6.30] KASHY, E., PERRY, R.R., STEELE, R.L., RISSER, J.R., Excited States in N^{14} from the Elastic Scattering of Protons by C^{13}, Phys. Rev. **122** (1961) 884-890.

[6.31] WIELOPOLSKI, L., GARDNER, R.P., The prediction of pulse-height spectral distortion caused by peak pile-up effect, Nucl. Instrum. Methods Phys. Res. B **133** (1976) 127-130.

[6.32] BOGDANOVIĆ RADOVIĆ, I., SIKETIĆ, Z., JAKŠIĆ, M., et al., Measurement and parametrization of proton elastic scattering cross sections for nitrogen, J. Appl. Phys. **104** (2008) 074905.

[6.33] CHIARI, M., GIUNTINI, L., MANDO, P.A., TACCETTI, N., Nucl. Instrum. Methods Phys. Res. B **184** (2001) 309.
[6.34] HAGEDORN, F.B., MOZER, F.S., WEBB, T.S., FOWLER, W.A., LAURITSEN, C.C., Phys. Rev. **105** (1957) 219.
[6.35] BASHKIN, S., CARLSON, R.R., DOUGLAS, R.I., Phys. Rev. **114** (1959) 1552.
[6.36] HAVRANEK, V., HNATOWICZ, V., KVITEK, J., Czech J. Phys. **41** (1991) 921.
[6.37] OUICHAOUI, S., BEAUMEVIEILLE, H., BENDJABALLAH, N., GENOUX-LUBAIN, A., Il Nuovo Cimento A **94** (1986) 133.
[6.38] CARACCIOLO, R., Lettere al Nuovo Cimento **11** (1974) 33.
[6.39] PEDRO DE JESUS, A., BRAIZINHA, B., CRUZ, J., RIBEIRO, J.P., Nucl. Instrum. Methods Phys. Res. B **174** (2001) 229.
[6.40] DEARNALEY, G., Philosophical Magazine ser. 8, 1 (1956) 821.
[6.41] WEBB, T.S., HAGEDORN, F.B., FOWLER, W.A., LAURITSEN, C.C. Phys. Rev. **99** (1955) 138.
[6.42] CACIOLLI, A., CALZOLAI, G., CHIARI, M., CLIMENT-FONT, A., GARCIA, G., LUCARELLI, F., NAVA, S., Proton elastic scattering and proton induced gamma-ray emission cross-sections on Na from 2 to 5 MeV, Nucl. Instrum. Methods Phys. Res. B **266** (2008) 1392-1396.
[6.43] AMIRIKAS, R., JAMIESON, D.N., DOOLEY, S.P., Measurement of (p,p) elastic scattering cross sections for C, O and Si in the energy range 1.0 - 3.5 MeV, Nucl. Instrum. Methods Phys. Res. B **77** (1993) 110-116.
[6.44] HU, P., ZHANG, J., JIN, Q., SHI, L., ZHOU, Z., Proton elastic scattering cross sections of titanium from 1.0 to 3.0 MeV at the laboratory angles of 151 degree, Nucl. Instrum. Methods Phys. Res. B **217** (2004) 551-554.
[6.45] SIKETIĆ, Z., BOGDANOVIĆ RADOVIĆ, I., SKUKAN, N., Proton elastic scattering from aluminum for 120^0, 150^0 and 165^0 in the energy interval from 2.4 to 5 MeV, Nucl. Instrum. Methods Phys. Res. B **261** (2007) 414.
[6.46] MAYER, M., *SIMNRA Manual*, Technical Report IPP 9/113, Max–Planck Institut für Plasmaphysik, Garching, Germany, 1997.
[6.47] GURBICH, A.F., BARRADAS, N.P., JEYNES, C., et al., Applying elastic backscattering spectrometry when the nuclear excitation function has a fine structure, Nucl. Instrum. Methods Phys. Res. B **190** (2002) 237.
[6.48] BARRADAS, N.P., ARSTILA, K., BATTISTIG, G., et al., International Atomic Energy Agency intercomparison of ion beam analysis software, Nucl. Instrum. Methods Phys. Res. B **262** (2007) 281.
[6.49] GURBICH, A.F., MOLODTSOV, S., Measurement of (d,p) and (d,a) differential cross-sections for aluminum, Nucl. Instrum. Methods Phys. Res. B **266** (2008) 3535.
[6.50] MOLODTSOV, S., GURBICH, A.F., Private Communication.
[6.51] PELLEGRINO, S., BECK, L., TROUSLARD, PH., TROCELLIER, P., Nucl. Instrum. Methods Phys. Res. B **266** (2008) 2268.
[6.52] BARRADAS, N.P., First experiments and calculations for a ^{nat}Ti(p,p)^{nat}Ti cross section benchmark, ITN report #38/2009, 2009.
[6.53] RAUHALA, E., Nucl. Instrum. Methods Phys. Res. B **40-41** (1989) 790.
[6.54] HU, P., ZHANG, J., JIN, Q., SHI, L., ZHOU, Z., Nucl. Instrum. Methods Phys. Res. B **217** (2004) 551.
[6.55] N.H. PROCHNOW, H.W. NEWSON, E.G. BILPUCH, et al., High-resolution proton scattering from ^{48}Ti, Nucl. Phys. A **194** (1972) 353.
[6.56] MOORING, F.P., KOESTLER, L.J.Jr., GOLDBERG, E., SAXON, D., KAUFMANN, S.G., Phys. Rev. **84** (1951) 703.

7. CONCLUSIONS

During the time of the implementation of the Coordinated Research Project (CRP) on Ion Beam Analysis (IBA) from 2005 to 2010, a large number of scattering cross sections were measured. Data existing in the literature were compiled and assessed, thus facilitating recommendations of elastic scattering cross sections for most wanted elements at selected scattering angles and moderate beam energies. Many cross sections have also been evaluated on the basis of nuclear physics models, allowing differential cross sections at any scattering angle to be calculated through the on-line calculator SigmaCalc.

Whereas IBANDL has virtually become the main source of cross-section data for IBA, some relevant data files have been compiled and stored independently only in EXFOR (http://www-nds.iaea.org/exfor/). The EXFOR format and database is used for many more data types than needed by the IBA community and was therefore developed to be extremely versatile. However, for over a decade the R33 format has been the accepted format for the communication and compilation of IBA cross-section data. For this reason, an additional option has been developed to facilitate retrieval of data from EXFOR. With this new option, EXFOR data are automatically recognized as relevant to IBA applications and are converted to the R33 format by a simple press of a button. Thus all the relevant EXFOR files can be easily imported into IBANDL.

There are a number of different IBA methods based either on the registration of elastically-scattered particles or the products of nuclear reactions. For all methods applied, a reliable source of cross-section data is needed except for Rutherford backscattering for which the cross section can be calculated according to the known formula. The requirements of analytical work favour the use of only those reactions for which adequate information already exists, irrespective of the actual needs. As far as IBA needs go, including differential cross sections for proton and ^{4}He non-Rutherford elastic scattering, and nuclear reactions for p, d, and ^{3}He with energy $E < 5.0$ MeV interacting with $A \leq 40$ nuclei, and in view of the number of possible exit reaction channels, it appears that the number of required data is tremendous. The work carried out in the framework of this CRP could only meet part of these requirements. Besides, there are still problems with some cross sections of primary importance to IBA applications (e.g. for elastic scattering of protons from boron, and alphas from silicon). Benchmarks for cross-section validation were only used in a limited number of cases as the evaluation still needs to be done for many cross sections.

After five years of significant efforts, IBANDL has been enriched with the results of the measurements, assessments, benchmarks and evaluations described in this report. Nonetheless, IBANDL remains an unfinished project since differential cross-section measurements and theoretical evaluations are a vast field of research and questions of accuracy, benchmarking experiments and use of alternate reactions including PIGE for light-element depth profiling need further investigation and remain to be solved by the coordinated efforts of the scientific community. The main output of this CRP is the IBANDL database. Its maintenance and upkeep is of utmost interest to the IBA community with the ultimate goal to finally cover all nuclear data needs of the IBA community.

LIST OF PARTICIPANTS

Barradas, N.P.	Nuclear and Technological Institute, Portugal
Bogdanović Radović, I.	Ruder Bošković Institute, Croatia
Chiari, M.	Istituto Nazionale Fisica Nucleare, Italy
Gurbich, A.	Institute of Physics and Power Engineering, Russian Federation
Jeynes, C.	University of Surrey, United Kingdom
Kokkoris, M.	National Technical University of Athens, Greece
Mayer, M.	Max-Planck-Institut fur Plasmaphysik-Garching, Germany
Lopes Ramos, A.R.	Nuclear and Technological Institute, Portugal
Rauhala, E.	University of Helsinki, Finland
Shi, L.	Fudan University, PR China
Vickridge, I.C.	Institut des Nano Sciences de Paris, France

Research Coordination Meetings

1st RCM, Vienna, Austria: 21-23 November 2006, INDC(NDS)-0481

2nd RCM, Vienna, Austria: 18-21 June 2007, INDC(NDS)-0511

3rd RCM, Vienna, Austria; 27-30 April 2009, INDC(NDS)-0555

LIST OF CONTRIBUTORS TO DRAFTING AND REVIEW

Barradas, N.P.	Nuclear and Technological Institute, Portugal
Bogdanović Radović, I.	Ruder Bošković Institute, Croatia
Chiari, M.	Istituto Nazionale Fisica Nucleare, Italy
Gurbich, A.	Institute of Physics and Power Engineering, Russian Federation
Jeynes, C.	University of Surrey, United Kingdom
Kokkoris, M.	National Technical University of Athens, Greece
Mayer, M.	Max-Planck-Institut fur Plasmaphysik-Garching, Germany
Lopes Ramos, A.R.	Nuclear and Technological Institute, Portugal
Rauhala, E.	University of Helsinki, Finland
Shi, L.	Fudan University, PR China

IAEA
International Atomic Energy Agency

No. 23

ORDERING LOCALLY

In the following countries, IAEA priced publications may be purchased from the sources listed below or from major local booksellers.

Orders for unpriced publications should be made directly to the IAEA. The contact details are given at the end of this list.

AUSTRALIA
DA Information Services
648 Whitehorse Road, Mitcham, VIC 3132, AUSTRALIA
Telephone: +61 3 9210 7777 • Fax: +61 3 9210 7788
Email: books@dadirect.com.au • Web site: http://www.dadirect.com.au

BELGIUM
Jean de Lannoy
Avenue du Roi 202, 1190 Brussels, BELGIUM
Telephone: +32 2 5384 308 • Fax: +32 2 5380 841
Email: jean.de.lannoy@euronet.be • Web site: http://www.jean-de-lannoy.be

CANADA
Renouf Publishing Co. Ltd.
5369 Canotek Road, Ottawa, ON K1J 9J3, CANADA
Telephone: +1 613 745 2665 • Fax: +1 643 745 7660
Email: order@renoufbooks.com • Web site: http://www.renoufbooks.com

Bernan Associates
4501 Forbes Blvd., Suite 200, Lanham, MD 20706-4391, USA
Telephone: +1 800 865 3457 • Fax: +1 800 865 3450
Email: orders@bernan.com • Web site: http://www.bernan.com

CZECH REPUBLIC
Suweco CZ, spol. S.r.o.
Klecakova 347, 180 21 Prague 9, CZECH REPUBLIC
Telephone: +420 242 459 202 • Fax: +420 242 459 203
Email: nakup@suweco.cz • Web site: http://www.suweco.cz

FINLAND
Akateeminen Kirjakauppa
PO Box 128 (Keskuskatu 1), 00101 Helsinki, FINLAND
Telephone: +358 9 121 41 • Fax: +358 9 121 4450
Email: akatilaus@akateeminen.com • Web site: http://www.akateeminen.com

FRANCE
Form-Edit
5 rue Janssen, PO Box 25, 75921 Paris CEDEX, FRANCE
Telephone: +33 1 42 01 49 49 • Fax: +33 1 42 01 90 90
Email: fabien.boucard@formedit.fr • Web site: http://www.formedit.fr

Lavoisier SAS
14 rue de Provigny, 94236 Cachan CEDEX, FRANCE
Telephone: +33 1 47 40 67 00 • Fax: +33 1 47 40 67 02
Email: livres@lavoisier.fr • Web site: http://www.lavoisier.fr

L'Appel du livre
99 rue de Charonne, 75011 Paris, FRANCE
Telephone: +33 1 43 07 50 80 • Fax: +33 1 43 07 50 80
Email: livres@appeldulivre.fr • Web site: http://www.appeldulivre.fr

GERMANY
Goethe Buchhandlung Teubig GmbH
Schweitzer Fachinformationen
Willstätterstrasse 15, 40549 Düsseldorf, GERMANY
Telephone: +49 (0) 211 49 8740 • Fax: +49 (0) 211 49 87428
Email: s.dehaan@schweitzer-online.de • Web site: http://www.goethebuch.de

HUNGARY
Librotade Ltd., Book Import
PF 126, 1656 Budapest, HUNGARY
Telephone: +36 1 257 7777 • Fax: +36 1 257 7472
Email: books@librotade.hu • Web site: http://www.librotade.hu

INDIA
Allied Publishers
1st Floor, Dubash House, 15, J.N. Heredi Marg, Ballard Estate, Mumbai 400001, INDIA
Telephone: +91 22 2261 7926/27 • Fax: +91 22 2261 7928
Email: alliedpl@vsnl.com • Web site: http://www.alliedpublishers.com

Bookwell
3/79 Nirankari, Delhi 110009, INDIA
Telephone: +91 11 2760 1283/4536
Email: bkwell@nde.vsnl.net.in • Web site: http://www.bookwellindia.com

ITALY
Libreria Scientifica "AEIOU"
Via Vincenzo Maria Coronelli 6, 20146 Milan, ITALY
Telephone: +39 02 48 95 45 52 • Fax: +39 02 48 95 45 48
Email: info@libreriaaeiou.eu • Web site: http://www.libreriaaeiou.eu

JAPAN
Maruzen Co., Ltd.
1-9-18 Kaigan, Minato-ku, Tokyo 105-0022, JAPAN
Telephone: +81 3 6367 6047 • Fax: +81 3 6367 6160
Email: journal@maruzen.co.jp • Web site: http://maruzen.co.jp

NETHERLANDS
Martinus Nijhoff International
Koraalrood 50, Postbus 1853, 2700 CZ Zoetermeer, NETHERLANDS
Telephone: +31 793 684 400 • Fax: +31 793 615 698
Email: info@nijhoff.nl • Web site: http://www.nijhoff.nl

Swets Information Services Ltd.
PO Box 26, 2300 AA Leiden
Dellaertweg 9b, 2316 WZ Leiden, NETHERLANDS
Telephone: +31 88 4679 387 • Fax: +31 88 4679 388
Email: tbeysens@nl.swets.com • Web site: http://www.swets.com

SLOVENIA
Cankarjeva Zalozba dd
Kopitarjeva 2, 1515 Ljubljana, SLOVENIA
Telephone: +386 1 432 31 44 • Fax: +386 1 230 14 35
Email: import.books@cankarjeva-z.si • Web site: http://www.mladinska.com/cankarjeva_zalozba

SPAIN
Diaz de Santos, S.A.
Librerias Bookshop • Departamento de pedidos
Calle Albasanz 2, esquina Hermanos Garcia Noblejas 21, 28037 Madrid, SPAIN
Telephone: +34 917 43 48 90 • Fax: +34 917 43 4023
Email: compras@diazdesantos.es • Web site: http://www.diazdesantos.es

UNITED KINGDOM
The Stationery Office Ltd. (TSO)
PO Box 29, Norwich, Norfolk, NR3 1PD, UNITED KINGDOM
Telephone: +44 870 600 5552
Email (orders): books.orders@tso.co.uk • (enquiries): book.enquiries@tso.co.uk • Web site: http://www.tso.co.uk

UNITED STATES OF AMERICA
Bernan Associates
4501 Forbes Blvd., Suite 200, Lanham, MD 20706-4391, USA
Telephone: +1 800 865 3457 • Fax: +1 800 865 3450
Email: orders@bernan.com • Web site: http://www.bernan.com

Renouf Publishing Co. Ltd.
812 Proctor Avenue, Ogdensburg, NY 13669, USA
Telephone: +1 888 551 7470 • Fax: +1 888 551 7471
Email: orders@renoufbooks.com • Web site: http://www.renoufbooks.com

United Nations
300 East 42nd Street, IN-919J, New York, NY 1001, USA
Telephone: +1 212 963 8302 • Fax: 1 212 963 3489
Email: publications@un.org • Web site: http://www.unp.un.org

Orders for both priced and unpriced publications may be addressed directly to:

IAEA Publishing Section, Marketing and Sales Unit, International Atomic Energy Agency
Vienna International Centre, PO Box 100, 1400 Vienna, Austria
Telephone: +43 1 2600 22529 or 22488 • Fax: +43 1 2600 29302
Email: sales.publications@iaea.org • Web site: http://www.iaea.org/books

15-46731

International Atomic Energy Agency
Vienna
ISBN 978–92–0–110515–8
ISSN 1011–4289